UNIVERSITY OF SOUTHAMPTON

FACULTY OF ENGINEERING AND THE ENVIRONMENT

Bioengineering Research Group

Volume 1 of 1

Novel Clay Gels as Regenerative Microenvironments for the Treatment of Diabetic Foot Ulcers

by

Daniel J. Page

Thesis for the degree of Doctor of Philosophy

Supervisor(s):

Dr Nicholas D. Evans

Dr Jonathan I. Dawson

Dr Claire E. Clarkin

Final Corrected Version

June 2018

UNIVERSITY OF SOUTHAMPTON

ABSTRACT

FACULTY OF ENGINEERING AND THE ENVIRONMENT

Bioengineering Research Group

Thesis for the degree of Doctor of Philosophy

NOVEL CLAY GELS AS REGENERATIVE MICROENVIRONMENTS FOR THE TREATMENT OF DIABETIC FOOT ULCERS

By Daniel Joseph Page

People that suffer with diabetes have an elevated risk of developing diabetic foot ulcers (DFUs), a type of chronic wound associated with hyperglycaemia. Current DFU treatments vary in their effectiveness and people that suffer with DFUs have an increased risk of eventual lower limb amputation. Biological agents including vascular endothelial growth factors (VEGF) and agonists of the Wnt signalling pathway have been investigated as agents that improve wound healing, yet delivery in an active economical form remains a significant clinical challenge.

In this project, we tested the hypothesis that Laponite, a synthetic smectite clay biomaterial, can be used to localise bioactive molecules to skin injury sites and can increase the rate and quality of wound healing.

Growth factor (VEGF) and small molecule (BIO, a Wnt pathway agonist) were incorporated in Laponite hydrogels, and their activity tested using cell-reporter assays. Laponite hydrogels were then administered subcutaneously and applied to circular wounds made on the dorsal skin of healthy and diabetic (*db/db*) mice. Bioactivity of localised VEGF by Laponite gels and its effect on wound healing was assessed by measuring the rate of wound closure and by histological analysis of blood vessel formation, the degree of cell invasion and the rate of re-epithelisation.

Human vein endothelial cell (HUVEC) tube formation was significantly increased when cultured on Laponite gels premixed with 1-5 µg/ml VEGF ($p = < 0.05$-< 0.0001). Successful adsorption of BIO by Laponite from aqueous media was measured at early time points. There was substantial retention of premixed BIO by Laponite over 7 days with the only evidence of BIO release (4.76%) into aqueous media measured at 24 hours ($p = < 0.01$). Laponite hydrogels were successfully retained *in vivo* up to 21 days (subcutaneously) and 18 days (wounds). There was a significant increase in blood vessel ingrowth into subcutaneously injected Laponite gels premixed with 10-40 µg/ml VEGF after 21 days in healthy mice ($p = < 0.05$-< 0.0001). Treatment of back skin wounds of *db/db* mice with vehicle Laponite gels exhibited a significant increase in the rate of re-epithelisation ($p = < 0.05$) and improvement to wound healing quality both visually and histologically. No further improvements to the rate of wound closure, re-epithelisation and appearance (e.g. reduced redness) was present when treated with Laponite gels containing 40 µg/ml VEGF; 1.1% alginate gel controls containing 40 µg/ml VEGF did exhibit improved wound closure suggesting that more rapid release of VEGF was more appropriate to a wound model that requires < 30 days recovery.

These results show the potential of Laponite hydrogels localising biologically active molecules to skin injury sites and improving the rate and quality of wound healing. However additional *in vitro* analysis and a modified murine model that would better characterise impaired wound healing in human DFUs, would be required to explore these findings in greater detail.

Contents

List of Figures

List of Tables

Declaration of Authorship

I, Daniel Page declare that this thesis entitled *Novel Clay Gels as Regenerative Microenvironments for the Treatment of Diabetic Foot Ulcers* and the work presented in the thesis are my own and has been generated by me as the result of my own original research. I confirm that:

1. This work was done wholly or mainly while in candidature for a research degree at this University;

2. Where any part of this thesis has previously been submitted for a degree or any other qualification at this University or any other institution, this has been clearly stated;

3. Where I have consulted the published work of others, this is always clearly attributed;

4. Where I have quoted from the work of others, the source is always given. With the exception of such quotations, this thesis is entirely my own work;

5. I have acknowledged all main sources of help;

6. Where the thesis is based on work done by myself jointly with others, I have made clear exactly what was done by others and what I have contributed myself;

7. None of this work has been published before submission.

Signed: .....

Date: .....

Acknowledgements

Wow, I honestly could not imagine getting to this point when I started this long road over 4 years ago! It has been a combination of an amazing, challenging, stressful, and fulfilling experience that I will always remember. To list everyone that I would like to thank would be impossible, but to everyone that I have worked with, chatted with, travelled with and had a laugh with I thank you.

Specifically, I'd like to give special thanks to my fantastic supervisor Nick Evans, whom without his love of Rush, many hours of dedication and witty sense of humour would have never challenged me to be the dedicated scientist that I am today. We have had an incredible 4 years and I will always fondly look back at our time in Cape Town when you rescued the wounded tortoise from becoming potential roadkill! I will forever be an avid listener of your infamous podcasts! To Jon Dawson, for all the support and guidance you have given me and, most importantly the love and passion you have for Laponite! And, also to Claire Clarkin who has given me support and supervision throughout my time at Southampton. I would also like to thank Raj Mani, Phillip Calder and Martin Feelisch for the supportive advice and comments during our group meetings.

Special mentions are to Richard Oreffo, Janos Kanczler, the supporting technical staff (Julia, Stef, Kate and Carol) and the whole Bone and Joint Department who have contributed immensely to my personal and professional time at University of Southampton.

I gratefully acknowledge the funding sources that made my PhD work possible. I was funded by The Grundy Education Trust, EPSRC and Novo Nordisk. Also to the wonderful team at the Biomedical Research Facility, for all your knowledge, time and care over the years of my study.

To Tsiloon, thank you for the doughnuts, promise of cooking Chinese (but never actually doing it) and countless lifts around Southampton. Janna, thank-you for helping me out during our time learning the wound healing model. Thanks also go to Roxanna for always replying to my hundreds of questions so quickly! To Agnieszka and Edo for all your precious time and help you gave to me during my initial training. To my desk neighbours Lisa and Shona, for all the banter and neighbourly love. To Susi for all the punches I endured. Thanks to Ravi for providing me with beautiful Auramine O staining, Dave Gibbs for early HUVEC training, Dan Tang for histology advice, Ewa and Yanghee for your patience teaching me how to do ELISAs, Emma Budd for my SET photoshoot and to anyone else who has helped me along the road.

Matt and Josh; thank you for our many evenings of procrastination. I must mention our addiction to binge watching Game of Thrones, The Walking Dead and Twin Peaks; without you I may have never left my desk!

To the semi colon; you magnificent piece of punctuation.

Lastly, but most importantly, I would like to thank my family for all their love and encouragement. To my dad, for making countless cups of tea and teaching me to be thorough. Mum, thank you for looking after me and always supporting me. Colin, thank you for being Facebook friends with my supervisor and passing his message on. Rachael, thank you for cheering me up with all the banter and jokes.

I dedicate this thesis to my wonderful, patient, supportive yet crazy partner in crime, Dominique. Without you I would have never got through these last four years as well as I have! You have been my rock as well as my financier, proof-reader and amazing illustrator, so thank you so much.

Definitions and Abbreviations

3-ITT	3-interval thixotropy test
+ve	Positive
-ve	Negative
AGEs	advanced glycation end-products
ANOVA	Analysis of variance
APC	Adenomatous polyposis coli
ATP	Adenosine triphosphate
Az	Azide
bFGF	basic fibroblast growth factor
BIO	6-Bromoindirubin-3'-oxime
BMP	Bone morphogenetic protein
CCL2	Chemokine ligand 2
CD31	Cluster of differentiation 31
CEC	Cation exchange capacity
CH	Chitosan hydrogel
CI	Confidence interval
CYS	Cysteine
CXCL	Chemokine (C-X-C motif) ligand
DAB	3,3′-Diaminobenzidine
DCCT	The Diabetes Control and Complications Trial
DFU	Diabetic Foot Ulcer
DKA	Diabetic ketoacidosis
DNA	Deoxyribonucleic acid
DVL	Dishevelled

ECGM	Endothelial cell growth medium
ECM	Extracellular matrix
EGF	Epidermal growth factor
ELISA	Enzyme-linked immunosorbent assay
EPCS	epithelial cells
FDA	Food and Drug Administration
FGF	Fibroblast growth factor
Flt-1	FMS-like tyrosine kinase-1
FLT-4	FMS-like tyrosine kinase-4
Fz	Frizzled
GM	Growth Medium
GSK-3	Glycogen synthase kinase-3 alpha/beta
H&E	Haematoxylin and eosin
HEPES	4-(2-hydroxyethyl)-1-piperazineethanesulfonic acid
HNC	Hyperosmolar non-ketotic coma
HPLC	High-performance liquid chromatography
HRP	Horseradish peroxidase
HUVEC	Human umbilical vascular endothelial cell
IDF	International Diabetes Federation
IGF	Insulin like growth factor
IL-1	Interleukin-1
IL-6	Interleukin-6
IL-8	Interleukin-8
IL-10	Interleukin-10
LA	Lactose
La	Lactic acidosis
Lap	Laponite

LEF	Lymphoid enhancer factor
LRP	Lipoprotein receptor related proteins
MIA	Multiplex immunoassays
MMP	Matrix metalloproteinase
MMP-8	Matrix metalloproteinase 8
MMT	Montmorillonite
MPO	Myeloperoxidase
mRNA	Messenger ribonucleic acid
MSD	Meso Scale Discovery
NO	Nitric oxide
NSAID	Non-steroidal anti-inflammatory drug
OCT	Optimal Cutting Temperature compound
PA	Plasminogen activator
PAH	Poly(allylamine) hydrochloride
PBS	Phosphate buffered saline
PDGF	Platelet-derived growth factor
PEG	Poly(ethylene glycol)
PFA	Paraformaldehyde
PGLA	Poly(lactic-co-glycolic) acid
pHEMA	Poly-hydroxyethyl methacrylate
pHPMAm	Poly(2-hydroxypropyl methacrylamide)
PIDF	Placental-derived growth factor
PKC	Protein kinase C
PSS	Poly(sodium styrene) sulfonate
PVA	Poly(vinyl alcohol)
RAGE	Receptor for AGE
RGB	Red, Green, Blue

rhPDGF	Recombinant PDGF
ROA	Region of interest
RTK	Receptor tyrosine kinase
SD	Standard deviation
SE	Standard error
SEM	Standard error of the mean
SLR	Single-lens reflex
TCF	T- Cell factor
TGF-β	Transforming growth factor-β
TIMP	Tissue inhibitor of metalloproteinase
TNF-α	Tumour necrosis factor
UV	Ultra-violet
V	Value
VE-Cadherin	Vascular endothelial-cadherin
VEGF	Vascular endothelial growth factor
VSI	Virtual slide image
WHO	World Health Organisation

Chapter 1:

Introduction

1.1 Preface: Chronic Wounds & Tissue Engineering Intervention

Chronic wounds are defined as skin injuries that fail to recover in an orderly and timely fashion. Restoration of anatomic and functional integrity of injured tissue is prolonged, requiring 4 weeks or more of recovery time (~3 months) [1]. In extreme cases, chronic wounds fail to fully recover and can result in the amputation of affected limbs [2].

The physical and mental burden that is imposed on individual sufferers can be huge [1]. There are also massive financial implications that result from treatment and care regimens, many of which are inefficient and lead to poor outcomes; this has been predicted to cost more than $10 billion globally each year [3]. The number of people suffering with chronic wounds will continue to rise due to an ageing population [4, 5] and from the impact of other chronic diseases [5].

More specifically, diabetes mellitus is a chronic condition that has a profound negative effect on an individual's overall health [6]. Amongst other associated complications, the developmental risk of chronic wounds in diabetic people are increased. These wounds usually develop in the lower legs and feet of an individual and are commonly known as diabetic foot ulcers (DFUs) [7].

In recent times, biomaterial and hydrogel-based wound interventions have been increasingly used as a method to treat serious chronic non-healing wounds to improve healing outcome [8]. These bioengineered strategies have additionally focused on the delivery of drugs or other exogenous bioactive molecules (e.g.

growth factors). This has become a huge area of interest as they have enormous potential for slow, sustained release of bioactive molecules to improve wound healing mechanisms in chronic wounds [9, 10]. However, delivery of these biomolecules in an economical and active form remains a significant challenge, often because of hostile proteinases that can degrade these molecules [10].

Suitable biomaterial delivery 'vehicles' to transport them in an economical and sustained fashion remains elusive, but over the years great strides have been made within the hydrogel and nanocomposite research fields [10-12]. A material of specific interest that comprises many nanocomposite biomaterials are clays. Their unique properties (e.g. highly sorptive and viscoelastic) can be incredibly useful for creating materials with high mechanical strength with a great capability of retaining bioactive molecules [13-16].

This chapter will address and compare current literature that documents recent biomaterial and hydrogel treatments that have shown potential at delivering bioactive molecules and improve DFU outcome. More specifically, it will:

- Summarise the potential of nanoclay gels as novel "carriers" of bioactive molecules appropriate to improve wound healing.

Prior to this however, a detailed summary of how diabetes increases the risk of chronic wounds will be explored. This will include:

- An overview of diabetes mellitus, chronic hyperglycaemia and associated complications;
- An overview of the major events associated with wound healing;

- The mechanisms behind chronic wound formation and persistence;
- An overview of key bioactive factors that could be used for DFU therapy.

1.2 Diabetes Mellitus

Diabetes mellitus is a disease that, as of 2014, affected 422 million people worldwide [17]. Between 1996 and 2015, the number of people in the UK with diabetes increased from 1.4 million to almost 3.5 million [18]; it has been estimated that the number of sufferers will increase to 4.5 million by the year 2030 [19].

Diabetes is characterised by a lack of insulin production, insulin function, or a combination of both that ultimately results in hyperglycaemia. Chronic hyperglycaemia can result in a multitude of long-term physiological complications including damage to various organs such as the nerves, kidneys, eyes, heart, and blood vessels [20].

The disease is usually categorised into two separate types: type 1 and type 2 diabetes mellitus. The incidence of type 2 is far higher than type 1, accounting for about 90% of all cases of diabetes [21].

1.2.1 Type 1 & Type 2 Diabetes Mellitus – A Brief Overview

Type 1 diabetes is caused by an autoimmune response that attacks and destroys the pancreatic insulin-secreting β-cells of the islets of Langerhans, leading to severe insulin deficiency [22]. The destruction of β-cells are thought to be caused by a complex ensemble of cellular immune responses [23], with evidence that genetic [24, 25] and environmental factors [26, 27] both play a role. The discovery

of insulin in 1921 by Sir Fredrick Banting, James Collip, Charles Best and John James Rickard Macleod was ground breaking. It revolutionised diabetic care and has saved the lives of many people suffering with type 1 diabetes [28, 29]. In more recent years, technological advancements in the form of blood glucose monitoring and insulin pump therapy have improved the control of type 1 diabetes. This has allowed sufferers of the disease to lead more normal lives and an increased life expectancy [30].

Type 2 diabetes is a heterogeneous disorder that is defined by a combination of insulin deficiency and insulin resistance leading to poor cellular uptake of glucose and elevated glucose concentrations in the bloodstream [31]. As with type 1 diabetes, an individual's susceptibility to type 2 diabetes is also determined by genetic and environmental factors. However, unlike type 1, deficiency and resistance to insulin are not caused by the complete destruction of β-cells by the host's immune system. Instead it is the combined effect of β-cell dysfunction, which leads to reduced insulin output [32, 33] and the host cells becoming desensitised to insulin. Genetic factors also play a significant role in an individual developing type 2 diabetes; recent research has identified various polymorphisms that may lead to increased susceptibility [34, 35].

1.2.2 Acute & Chronic Complications of Diabetes

People suffering with diabetes can exhibit acute and chronic complications during their lifetime. The risk of developing these complications depends on a variety of factors, with most of them linked to poor control of plasma glucose levels in the blood; this is known as hyperglycaemia or hypoglycaemia. Hyperglycaemia is defined as an individual who has a fasting plasma glucose level of ≥ 7.0 mmol/l (126 mg/dl) or a plasma glucose level ≥ 11.1 mmol/l (200 mg/dl) following

ingestion of a 75 g glucose load [36]. Lack of insulin released into the bloodstream (either full or partial deficiency) means that blood sugar rises uncontrollably as cells (particularly adipose and muscle cells) are not signalled to take up glucose. Acute complications of diabetes include diabetic ketoacidosis (DKA), hyperosmolar non-ketotic coma (HNC), lactic acidosis (La) and hypoglycaemia [37].

In addition to acute complications, people with diabetes also face a host of chronic, long-term problems that can cause increased morbidity and mortality. Chronic hyperglycaemia is considered the major causative factor behind many of these long-term issues. The most common include the reduced ability to heal, micro- and macrovascular problems, neuropathy, retinopathy and nephropathy [38, 39]. Many of these problems are interrelated, having an impact on one another that can result in further difficulties. This is very much the case with the formation of chronic wounds and foot ulcers.

1.2.3 The Role of Hyperglycaemia in Chronic Diabetic Complications

Over the past 50 years there has been a great deal of research that has enhanced our knowledge about hyperglycaemia and its negative long-term effects. It is generally understood that excessive levels of glucose within the blood stream lead to increased cellular uptake within specific types of cells, particularly vascular endothelial cells, neuronal cells and retinal cells [40].

Following excessive intracellular glucose uptake there are a variety of metabolic pathways that can become dysregulated, produce damaging metabolites. These

mechanisms include: (1) increased flux through the polyol pathway [41], (2) increased formation of advanced glycation end-products (AGEs) and receptor for AGEs (RAGE) [42], and (3) increased activation of protein kinase C (PKC) isoforms [43].

1.3 Chronic Wounds and the Diabetic Foot Ulcer Pathogenesis

The diabetic foot is defined as a pathological lower limb disorder that is either caused directly from diabetes or its associated long-term complications. Minor skin trauma to diabetic feet can potentially be disastrous, leading to a non-healing chronic wound often characterised as a diabetic foot ulcer (DFU). Individuals suffering with type 1 and type 2 diabetes are at risk of developing a DFU. The causes behind their formation and progression are multifactorial, however the risk of one forming is dictated by individual patient physiology as well as environmental factors [39].

DFUs are more prominent in people over the age of 60, with evidence that men develop ulcers more than women [44]. People that have suffered with diabetes for longer are more likely to develop an ulcer. In addition, patients with better blood glucose control are less likely to develop a DFU [45]. Studies have also shown that foot ulcer incidence is higher in Caucasian compared to Asian populations [46]. Other factors such as low socioeconomic status and poor education are also associated with increased risk [47]. However, diabetic individuals that already have a history of ulcers and lower extremity amputations are more likely to develop further DFUs [48].

The causative pathway of DFU formation is very complex. It is best summarised as a complication resulting from neuropathy, ischaemia and trauma. One of these aetiologies alone may not cause formation of ulcerative tissue, it is only when neuropathy, ischaemia or both occur in combination with trauma that problems can arise (e.g. callus formation, damage from walking bare foot and infection). These factors also impact on the healing of an existing ulcer that can (in some circumstances) never fully recover.

Therefore, DFUs are often characterised as chronic non-healing wounds. A review by Mustoe [49] suggested that chronic wounds can be broadly divided into 4 major casual groups: (1) cellular and metabolic changes associated with ageing (2), underlying disease state, (3) repeated reperfusion injury events and (4) bacterial infection that results in prolonged state of inflammation.

1.4 Normal Wound Healing

The skin is the largest organ of the integumentary system. It is a truly multifunctional organ that not only serves as the outer covering that protects the body from external stimuli (e.g. damage, pathogens and water loss), but is essential for the regulation of body temperature, sensation, and vitamin D synthesis. It is broadly separated into three different layers; the epidermis, dermis and hypodermis (subcutaneous layer) [50].

After skin tissue becomes damaged, underlying tissue may become exposed to various unwanted environmental factors. Swift action to repair skin breakage is essential so that normal physiological functions can be restored in the shortest time possible. This can be described as acute wound healing; an uncomplicated,

elegant and infection-free tissue recovery process that exhibits minimal scarring and negligible loss of physiological function [51].

The process of wound healing is complex and is initiated almost immediately following skin trauma. It can be categorised into four distinctive, yet overlapping events known as: haemostasis, inflammation, proliferation and remodelling. Both illustrations shown in Figure 1.1 and Figure 1.2, in addition to the following subchapters, breakdown and explain each stage in detail.

1.4.1 Haemostasis

Immediately following damage to skin and its underlying blood vessels, platelets within the blood plasma are exposed to various extracellular proteins (e.g. fibrillar collagen). Platelets that bind to these proteins undergo a change in morphology and become activated [52], which causes them to congregate at the wound site to form a 'platelet clot' (Figure 1.1. i).

Following platelet adhesion, activation and aggregation, the clotting cascade/ coagulation is the next stage in haemostasis, also known as secondary haemostasis. There are two coagulation pathways; the intrinsic and extrinsic pathways. Although each pathway is distinct and initiated in an unique way, both share commonalities that ultimately leads to the production of a stable fibrin clot [53].

The fibrin clot that is created by the coagulation cascade at the wound site acts as temporary shield against environmental factors. It also generates a suitable microenvironment for inflammatory cellular migration, initiates the tissue movements of re-epithelialisation and connective tissue contraction, and stimulates the production of new blood vessels. This is supported by the

production of cytokines and cell signalling molecules by activated platelets (Figure 1.1. i) [54].

1.4.2 Inflammatory Stage

Following haemostasis, inflammatory cells are recruited to the wound site and remove cell debris, prevent infection and begin to produce various cytokines to orchestrate cell movement and proliferation [55]. Immediately following fibrin clot formation, chemical mediators secreted by platelets initiate the recruitment of neutrophils (occurs within minutes to an hour). It has been shown that neutrophils engage with activated platelets during the initial stages of inflammation through a process of tethering; as neutrophils pass by immobilised platelets, which are attached to the blood vessel wall, they tether to p-selectin on platelets. This in turn promotes neutrophils to adhere to endothelial cells [56].

The high concentration of inflammatory mediators and the presence of prostaglandins causes blood vessels at the site of the wound to vasodilate, allowing more inflammatory cells to aggregate and become activated. Increasing numbers of neutrophils may be found within the wound due to a concentration gradient of chemical mediators, including interleukin-8 (IL-8) [57], transforming growth factor-β (TGF-β), IL-1 and tumour necrosis factor TNF-α [58] (Figure 1.1. ii). The number of neutrophils reaches its peak 24 to 48 hours after skin injury [59]. Neutrophils primarily phagocytose bacteria and cell debris, however they can also destroy bacterial cells through degranulation (the release of bactericidal substances). In addition, research has shown that they release chromatin and protease 'traps' as a way of inhibiting bacterial cells [60].

Circulating monocytes in the blood stream differentiate into macrophages following recruitment to the site of the wound (Figure 1.1. ii). Macrophages are present in small numbers after initial skin trauma, but following early inflammation, neutrophils are increasingly replaced with macrophages. Providing that there are minimal infectious cells present at the wound site, neutrophils undergo apoptosis. This process releases a huge burst of cytokines and a resultant of increased chemotaxis of macrophages. This is an important aspect of macrophage recruitment during wound healing; it has been shown to be responsible for the massive influx of macrophage cells 48 hours post injury [61].

Macrophages are responsible for phagocytosing any remaining bacterial cells and cell debris, which include the remnants of neutrophils following apoptosis. They are responsible for secreting an assortment of pro-inflammatory cytokines (IL-1 and IL-6) and growth factors (TGF-β, epidermal growth factor (EGF), fibroblast growth factor (FGF), TNF-α, platelet-derived growth factor (PDGF) and vascular endothelial growth factor (VEGF) (Figure 1.1. ii). The arrival of these growth factors acts as a cue for the wound healing process to move forward towards final stages by stimulating proliferative and regenerative cells [62].

1.4.3 Proliferation Stage

As the inflammatory response begins to subside there is a distinct shift towards tissue repair. During this stage, there are three important distinct phases that occur; (1) formation of granulation tissue and the extracellular matrix (ECM), (2) neovascularisation and (3) re-epithelialisation (see Figure 1.1. iii) [60].

At around three days following injury, fibroblasts begin to proliferate at the wound site [63]. They are responsible for laying down key components of the extracellular matrix (ECM) including: hyaluronan, proeteoglycans, fibronectin

and type 1 and type 3 collagen. ECM is an essential component of healing skin tissue providing a suitable environment for cells to grow, divide and differentiate [64].

Collagens are the most abundant protein within the ECM and are important for many of the ECM functions listed above [65]. Type 3 collagen is secreted by fibroblasts in greater quantities during wound healing than in skin homeostasis (30-40% compared to the 20% present in unwounded skin) [66]. During the latter stages of healing type 3 collagen is replaced with type 1 collagen [67], marking the transition into the remodelling stage. Importantly, after a substantial increase in collagen deposition within the first three weeks the rate stabilises after around 21 days; this is due to the reduction in proliferation of fibroblasts [68].

TGF-β, PDGF, TNF-α, FGF, and VEGF secreted during the inflammatory stage by platelets and macrophages stimulate angiogenesis (Figure 1.1. i-iii) [69-74]. This is essential because proliferating cells like fibroblasts, epithelial cells, keratinocytes and plasma B cells all require constant delivery of oxygen, nutrients and cytokines/growth factors supplied by blood [75].

Nearby endothelial cells respond to proangiogenic factors by activating mitosis, cell movement and secretion of molecules that initiate host cells to further secrete proangiogenic factors. More specifically the angiogenic cascade includes: protease-dependent degradation of the basal membrane facilitating endothelial cell movement through the extravascular space, chemotaxis and increase in vascular permeability, endothelial proliferation, remodelling and differentiation [76, 77]. The most dominant angiogenic factors that initiate this cascade of events are FGF and VEGF (Figure 1.1. iii) [78-80]; *in vitro* and *in vivo* studies have shown that they work in a synergistic manner [75].

After stimulation of growth factors, endothelial cells proliferate and traverse towards the site of the wound, also known as 'sprouting' [76, 77]. Matrix metalloproteinases (MMPs) and serine proteases (particularly the plasminogen activator (PA)–plasmin system) are enzymes that are commonly associated with angiogenic-dependent ECM degradation. Following degradation, endothelial cell junctions become relaxed and pericytes dissociate. Exposed endothelial 'tips' are able to extend into the degraded extravascular space and chemotactically respond to proangiogenic growth factors. The destruction of the ECM, which acts as a storage cytokine 'pool', leads to an increase in local proangiogenic cytokine concentration [76, 77].

As endothelial cells migrate, plasma proteins (e.g. fibronectin and fibrin) within the existing vessel leak out into the extravascular space providing a provisional matrix. This gives cells a supporting structure which enables tube formation. Eventually, vascular endothelial-cadherin (VE-cadherin) tight junctions form between adjacent endothelial cells creating vessels with lumens [76, 77].

Following the establishment of the ECM, vascular supply and mitogenic cytokine pool, various cell types undergo rapid proliferation. It is at this stage that the wound site will appear pink and fibrous in nature and it is commonly known as granulation tissue. Fibroblasts differentiate into myofibroblasts where they organise themselves along the edge of the ECM and generate a constrictive force; this aids in contraction and closure of the wound [81].

Neighbouring keratinocytes at the wound edge and epithelial stem cells from the hair follicles or sweat glands are responsible for the re-epithelialisation process [82]. Keratinocytes can re-epithelialise the wound bed in one of two ways: either by moving across the matrix proteins covering the wound bed in a 'rolling' [83]

or 'sliding' motion [84], undergoing mitosis and differentiation. Cell migration ceases once opposite keratinocytes meet each other due to contact inhibition [85]. The 'rolling' or 'sliding' motion remains controversial and is still currently unknown which one is more accurate at describing re-epithelisation. This is still an area of intense research with various updated models suggested in recent years [86, 87].

1.4.4 Remodelling Stage

Remodelling is the final stage of wound healing. It is a lengthy process that can take up to two years to complete and involves the maturation of the wound bed, and the cessation of the proliferation in the previous stage (see Figure 1.2 A) [88]. Over the course of this stage the ECM gradually transforms to a more stable structure, mainly due to a shift in collagen deposition where type 3 fibres are substituted with type 1 [67] (Figure 1.1. iv). This recreates a structure that is comparable to unwounded tissue yet is almost always physiologically inferior. Collagen deposited by fibroblasts is not uniformly organised and this results in reduced tensile strength and elasticity (the maximal strength that is usually achieved is approximately 80%) [89]. Sweat glands and hair follicles are also usually absent. The resulting structure that replaces the wound is characterised as a scar (Figure 1.1. iv). Over time a newly formed scar will show signs of maturity by exhibiting a distinct change in colour from red to pink to grey [60].

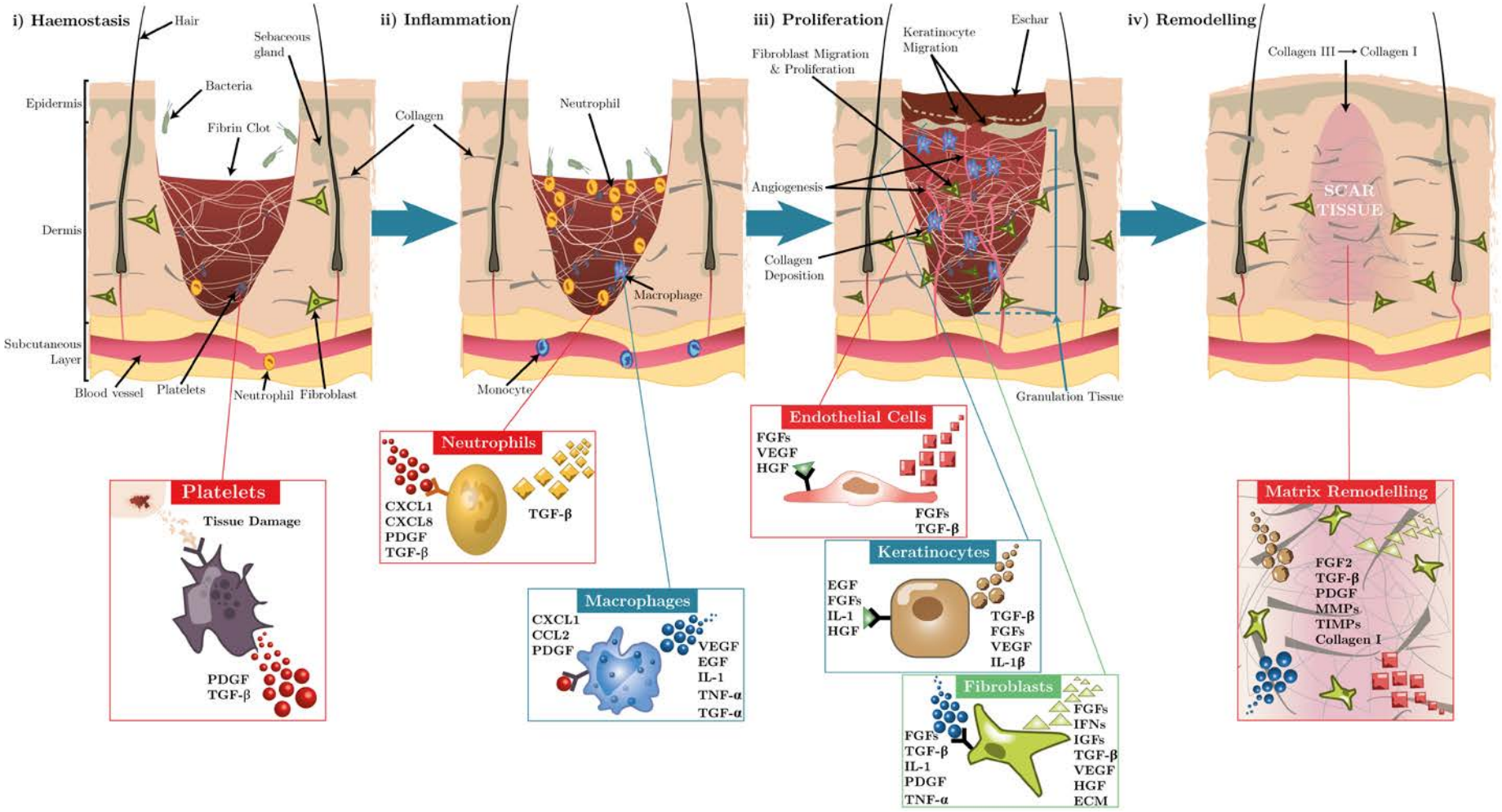

Figure 1.1. Phases of normal wound healing(adapted from [90], see main text for details). (i) Haemostasis: Platelets react to tissue damage and form a stable clot. (ii) Inflammation: Neutrophils initially phagocytose bacteria. They are subsequently replaced by macrophages, secreting an array of cytokines. (iii) Proliferation: Cell growth increases, granulation tissue, angiogenesis and re-epithelialisation occurs; many cell types/cytokines involved. (iv) Remodelling: Tissue remodelled to form a fibrous scar.

1.4.5 Impaired Wound Healing in Diabetes

Individuals suffering with diabetes have an increased risk of wound healing complications, mainly due to having a suppressed immune system. In addition, they are also susceptible to neuropathy and vascular problems. These factors have collectively been described as the triad of issues that cause ulceration of the foot. This however, is a very crude generalisation as the triad does not incorporate the risk of infection as a potential cause. Nor does it describe the domino effect that one pathogenic problem can cause leading to another, which in turn creates a wound that can never properly heal [39].

Wound healing deficiencies in people with diabetes are characterised by a variety of physiological deficiencies. Some of the major factors include impaired cytokine and growth factor production [91, 92], impaired macrophage function [93, 94] and failure to provide an adequate blood supply to the wound.

One vital difference that occurs in a diabetic wound compared to a non-diabetic wound is the abnormal extension in time of inflammation (refer to Figure 1.2 B) [95]. This can progress to a state where inflammatory cells, such as neutrophils, are always present and prevents the normal cascade of healing to occur [95, 96]. In turn, this can affect the overall environment of the wound; various cell types do not become activated, inhibiting the production of essential cytokines [95, 96]. In addition, increased presence of neutrophils in chronic wounds leads to more degradative enzymes and include, MMPs (specifically MMP-8) and neutrophil-derived elastase [97-99].

Microcirculatory defects due to endothelial cell dysfunction lead to a reduction in a thickening of the capillary size, basement membrane and reduction of blood supply to the wound bed; consequently, nutrient, cytokine and cellular delivery is compromised. In addition, vascular synthesis is inhibited, a situation negatively affecting both vasculogenesis and angiogenesis. AGEs have been suggested to play a pivotal role in reducing vasculogenesis; they have been shown to decrease nitric oxide (NO) bioavailability in late epithelial cells (EPCs) that negatively affects their migratory, adhesive and secretory action [100]. Impaired angiogenesis is caused by poor production of important angiogenic growth factors, namely vascular endothelial growth factor (VEGF) [101], platelet derived growth factor (PDGF) [102, 103], insulin like growth factor (IGF-1) [104], epidermal growth factor (EGF) [105] and interleukin 8 (IL-8) [106].

The bioactivity of secreted growth factors is hindered further by uncontrolled proteomic degradation. Amongst others (e.g. PDGF-BB, TGF-β [99]) VEGF has been shown to be susceptible as a study by Lauer *et al* [107] documented that plasmin can unwantedly facilitate its degradation. They also showed that in a chronic wound setting that VEGF transcription is likely to be increased, however this study was not specific to diabetic wounds. This further highlights the negative impact that diabetes has on a chronic wound environment and the many ways DFUs can arise.

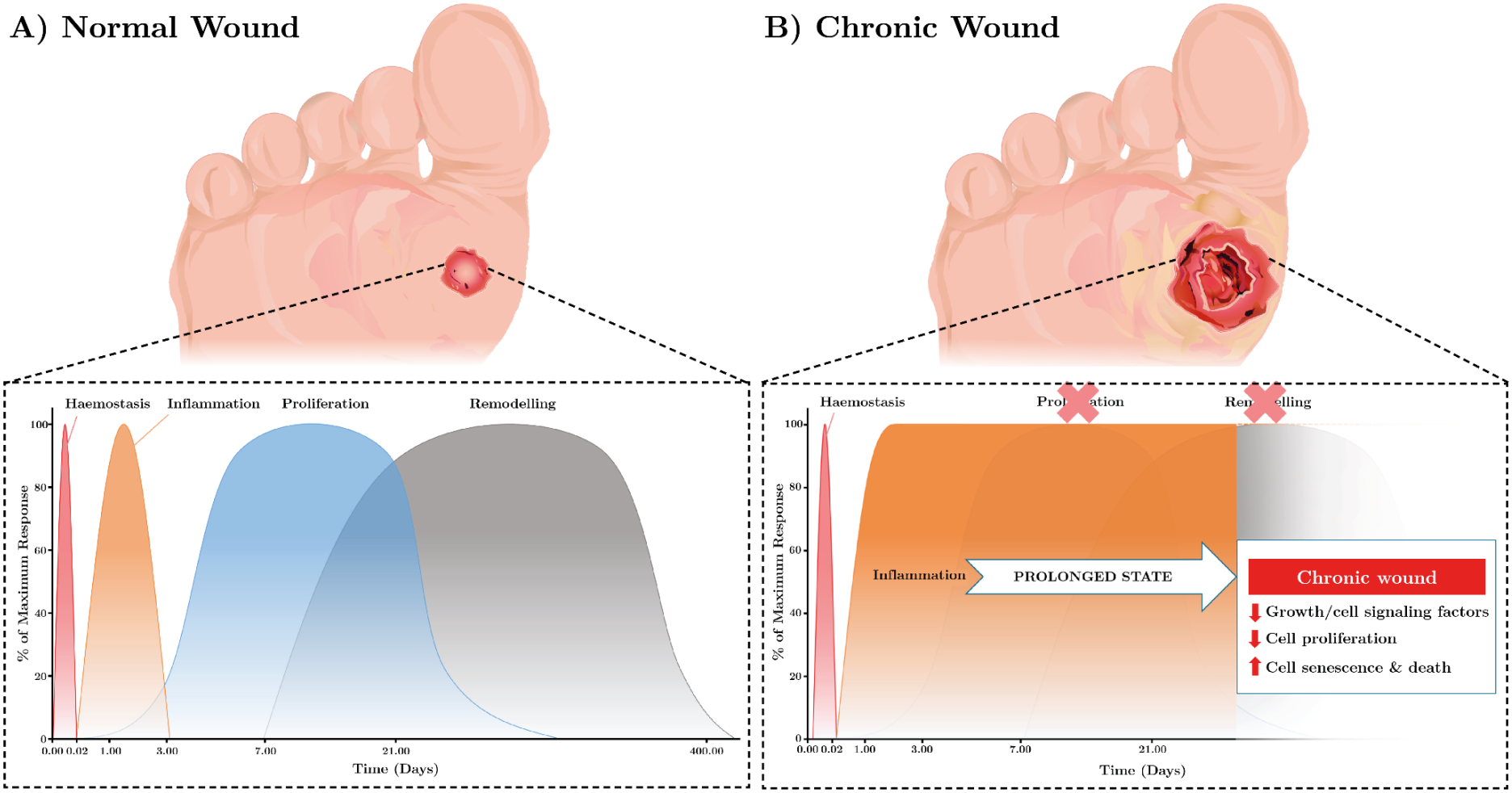

Figure 1.2. Normal vs chronic wound healing timeline (see main text for further details). (A) Normal wound: The overlapping stages of wound healing occur in a timely manner. (B) Chronic wound: Inflammation stage of wound healing is prolonged due to excessive proteinases and inflammatory signal molecules. This impacts on cytokine production and cell growth which results in an increase in cell senescence and death; proliferation and matrix remodelling is inhibited.

Aberrant cell signalling in DFUs, overproduction of proteases and response to bacterial invasion can cause fibroblasts and keratinocytes to enter a senescent state. Senescence is displayed when metabolically active cells are unable to undergo any further mitotic divisions. Although this is common in aged cells that have shortened telomeres, senescent cells in DFUs are commonly associated with stressful stimuli (e.g. Deoxyribonucleic acid (DNA) damage, oxidative stress) mimicking the effects of ageing [108]. These events are dependent on blood glucose control, duration of suffering with diabetes, environmental factors (e.g. repeated trauma events) and age.

1.5 Diabetic Foot Ulcer Prevention & Treatment

1.5.1 DFU Classification

Preventing formation in the first place the most desirable approach and can be achieved by good blood glucose control. Ensuring that hyperglycaemia is kept to a minimum there is an emphasis to educate individuals with diabetes to maintain strict blood glucose control; a comprehensive study carried by The Diabetes Control and Complications Trial (DCCT) in 1993 showed that by implementing an intensive glucose control regimen, the progression and effects of diabetes-related complications can be significantly reduced in those suffering with type 1 diabetes [109].

Sufferers of diabetes are also made aware of potential complications that an individual may endure as the disease progresses. To minimise foot complications, it is recommended that individuals with diabetes regularly check their feet for

signs of diminished sensitivity, pain, vascular problems and trauma. On a positive note, it is thought that 69% of the adult population with diabetes are at low risk of ulcer formation [110]. People in this group have no symptoms of neuropathy and ischaemia; 99.6% of them will not develop an ulcer in a 2-year period [110]. In the UK, these people are not expected to have routine podiatry care, however it is still recommended that they have an annual check-up [111].

1.5.2 Current DFU Treatments and Their Limitations

The standard practice for DFU treatment includes: wound debridement, infection control, revascularisation procedures and ulcer offloading. This approach can be successful depending on the progression of an ulcer and the physiological and environmental state of the patient [112].

Wound debridement involves the removal of necrotic tissue and wound debris that (both of which inhibit the healing process of a chronic wound). It also significantly decreases the risk of infection because it removes a source of bacterial nutrition at the wound site. Devitalised necrotic tissue can look yellow, wet and stringy in appearance and is often known as slough [113]. Importantly, necrosis and debris can cause dysregulation of the wound healing cascade, marked by increased inflammation. Overproduction of inflammatory cytokines from neutrophils and macrophages up-regulate secretion of matrix metalloproteinases (MMPs) during the proliferation stage. Although MMPs are required for natural wound debridement during normal wound healing, their overproduction is thought to be hallmark of DFU pathogenesis [114].

Various forms of debridement are currently used during DFU care in the UK. These include: autolytic, mechanical, larval therapy (biosurgical), ultrasonic, hydrosurgical, sharp and surgical debridement [102]. Sharp debridement is considered the 'gold standard' for DFU care, however it is not necessarily more effective than the other debridement methods listed and there is not conclusive evidence that any single method of debridement is the best [103]. Sharp debridement involves surgical removal of dead tissue using scalpel or forceps until a healthy bleeding ulcer site is created; care and attention to not disrupt healthy granulation tissue must be undertaken for this method to be successful [115].

When the lower limb is affected by severe ischaemia then revascularisation procedures can be carried out. A revascularisation procedure will either involve a bypass or an endovascular technique (e.g. transluminal angioplasty, subintimal recanalisation or a hybrid of both) [116]. The goal is to re-establish adequate perfusion of the lower limb and in extreme cases salvage the limb from amputation [117].

Offloading techniques can be used as both a preventative method and as a treatment. If sensitivity examinations indicate diminished sensitivity, specialised footwear can be recommended to inhibit the pressure on high risk areas of the foot. If there is an existing ulcer, offloading is essential because it improves the healing capacity of the wound and reduces repeated trauma [112].

While standard diabetic foot care does improve the recovery of chronic wounds, in many cases it is not effective enough; current statistical data suggests that up to 84% of amputations would have been preceded with a DFU [2]. In the UK, it is suggested that the amputation rate is increasing and could be as high as 7000

per year by 2015 [118]. Also, many of these standard treatments are invasive and rather extreme and usually require the expertise of highly trained doctors or podiatrists.

The choice of dressing is another key aspect of standard DFU wound care. It has been known for many years that a moist environment improves the rate of epithelisation during healing [119, 120]. This type of environment can be maintained by using suitable occlusion dressings [121]. However, the application of moist dressings to chronic diabetic ulcers requires careful consideration because they sometimes negatively impact wound recovery (e.g. excess production of exudate leading to skin tissue maceration) [122].

Many of the standard care procedures described above are reliant on the natural healing process. Therefore, the chance of an ulcer progressing to the latter stages and ultimately requiring amputation of lower limbs remains high. As impaired wound healing is a core feature of DFU progression there has been a great focus in recent years to try and investigate the mechanisms that cause disruptions in the wound healing cascade.

1.6 Factors That Could Improve Chronic Wound Healing and DFUs

An area of significant interest is delivery of essential growth factors or biological active molecules directly to the wound site to improve cell signalling, differentiation and proliferation. In addition, cell therapy based approaches attempting to replace expired or senescent cells to achieve tissue regeneration would be advantageous [123].

However, the regeneration potential of adult tissue during wound healing is limited, where original tissue is replaced with physiologically inferior fibrous tissue. The formation of fibrous 'scar' tissue is partly due to inefficient collagen deposited by fibroblasts [123]. Furthermore, cutaneous adult healing does not recover through a regenerative process even though it has been shown that multipotent epidermal stem cells exist within hair follicle bulb [124, 125] and undifferentiated mesenchymal cells are present within the dermis [126]. Activation of these stem cells may provoke cell regeneration and could restore cell integrity and reverse senescence in a chronic wound [123].

The rationale for use of growth factors as a DFU therapy was based on early animal studies. These investigated important growth factors (PDGF-BB, TGF-β, EDF, and FGF-2) and showed that PDGF-BB had the potential to increase granulation, tissue formation and re-epithelisation in chronic wounds [127, 128]. To date, only recombinant PDGF-BB (rhPDGF) (Becaplermin, trade name is Regranex) has been approved in the UK for the treatment of chronic wounds and diabetic ulcers that are $\leq$ 5cm^2 in size [129]. Its positive stimulation of macrophages, fibroblasts and vascular endothelial cells means that it can promote healthy granulation tissue formation and angiogenesis [130]. The approval to use rhPDGF-BB treatment was based off several randomised control trials (measuring its efficacy and cost-effectiveness), and since has become available globally [131-133].

A double-blinded study by Steed [132] indicated that administration of Becaplermin gel to DFUs achieved complete wound healing in 48% of patients compared to 25% of patients treated with a placebo ($p = 0.01$). A subsequent study by Wieman, Smiell and Su [134] also showed a significant difference with

administration of Becaplermin gel however only at a higher concentration (50% Becaplermin-treated vs 35% placebo-treated, $p = 0.01$). Two other studies compared classical treatment therapies with Becaplermin gel therapy [131, 133]. The results were contradictory and indicated that there was no significant benefit with using PDGF treatment compared to classical therapy [131].

The limitations of growth factor therapy are often attributed to poorly controlled delivery and excessive growth factor degradation within chronic wounds [135]. Therefore, alternative strategies to alter the milieu of a chronic wound could be investigated. A possible approach could be to exploit the highly conserved Wnt signalling pathway to stimulate differentiation of stem cells and test if it promotes skin regeneration [136]. As for a possible growth factor, exogenous VEGF could be introduced to promote angiogenesis and potentially restore a functional vascular network. Such approaches will require effective delivery methods to ensure that biologically active proteins or molecules are not degraded. Furthermore, it should be accessible to cells so that a suitable regenerative microenvironment is established.

1.6.1 Vascular Endothelial Growth Factor (VEGF)

VEGF is a well-documented growth factor that is responsible for increasing vascular permeability, endothelial cell signalling and proliferation to stimulate angiogenesis [137].

VEGF exists as a family of proteins with a total of five members: VEGF-A, VEGF-B, VEGF-C, VEGF-D and placental-derived growth factor (PlGF). The most important and most characterised member is VEGF-A, especially in wound healing [79]. It was the first member of VEGF family to be discovered and

extensively researched, so for this reason it is often referred as VEGF. It is a homodimeric glycoprotein that exists in many different isoforms.

In humans, there have been shown to be several VEGF-A isoforms, all named $VEGF_{xxx}$. The $_{xxx}$ refers to the number of amino acid residues the variant consists of, all of which is achieved by alternative splicing of pre-Messenger ribonucleic acid (pre-mRNA) from a single gene [138]. The most biologically understood spliced variants are $VEGF_{121}$, $VEGF_{165}$, and $VEGF_{189}$ [139-142].

$VEGF_{164}$ ($_{165}$) is described as the perfectly 'balanced' isoform *in vivo*, as it is biologically more available than $VEGF_{189}$, yet exhibits a similar mitogenic potency. Conversely it is less diffusible than $VEGF_{121}$, but its impact is for angiogenic signalling is vastly more effective [143, 144]. This is supported by the fact $VEGF_{121}$ exerts a 100-fold less mitogenic effect on vascular endothelial cells and in turn, produces a more disordered pattern of vessel growth [145]. The slight functional differences present between VEGF isoforms suggests that $VEGF_{165}$ is the most promising candidate for ectopic application of VEGF for therapeutic benefit.

1.6.1.1 VEGF Application to Improve Chronic Wound Healing

Numerous studies have assessed $VEGF_{165}$-based treatments to improve wound healing outcome in chronic wounds. A study by Peppe *et al* [140] showed that adenovirus-mediated transfer of the human $VEGF_{165}$ gene into CD1 streptozotocin-induced diabetic mice wounds improved wound recovery compared to saline-treated controls; encouragingly, the rate of recovery was comparable to normal healing in healthy CD1 mice.

Another study by Galiano *et al* [146] topically applied recombinant $VEGF_{165}$ to full-thickness wounds on *db/db* mice; they documented a significant improvement in wound closure size in VEGF-treated wounds compared to phosphate buffered saline (PBS) controls ($p = < 0.05$) 5 days post wounding. After 10 days, there was a 225% increase in granulation tissue area ($p = < 0.05$) and a 3.4-fold increase ($p = < 0.001$) in CD31 antigen staining; the former showed that the proliferation stage occurred much sooner during healing, whereas the latter was a good indicator that there were more blood vessels present.

Although these studies have shown some promising data, a VEGF-based therapy for DFUs has yet to reach the clinic. The drawback with topical-based VEGF treatment is that frequent applications are required to ensure sustained delivery occurs, which has an impact on cost and safety of the treatment. Furthermore, the biological stability of VEGF has also been questioned due to having a short half-life *in vivo* ($\leq$ 30 minutes in blood plasma) [147]. This means a more effective delivery vehicle is required that ensures controlled, sustained and protected delivery of VEGF to the wound site.

1.6.2 The Wnt Signalling Pathways

Wnt based strategies have also been explored as an alternative to VEGF. Wnt signalling is formed by a group of signal transduction pathways that are controlled by a group of secreted Cys-rich proteins that are evolutionarily conserved. These have been conventionally divided into two subclass pathways: the canonical (β-catenin dependent) and the non-canonical pathway (β-catenin independent). These subclasses should only be used as a general guide as there are many upstream pathways that interact between the two [148].

1.6.2.1 The Canonical (β-catenin dependent) Pathway

The canonical pathway is the most understood Wnt signalling pathway. It is defined by the cytosolic accumulation of β-catenin that subsequently translocates into the nucleus where it activates Wnt target gene expression [149].

Figure 1.3 illustrates the two main pathways of the canonical pathway. Following Wnt ligand binding to Fz and LRP5 and 6, a member of the Dishevelled (Dvl) proteins is recruited to the Fz receptor through its PDZ domain and oligomerisation of its DIX domain. Subsequently, Axin and GSK-3 associate with Dvl, disrupting the β-catenin destruction complex. Stable β-catenin translocates to the nucleus where it interacts with T-cell factor/lymphoid enhancer factors (TCF/LEF transcription factors) and initiates gene expression (Figure 1.3 A) [149].

β-catenin production by cells is regulated through a degradation mechanism which is controlled via binding of Wnt ligands to an appropriate Wnt receptor. Thus, in the absence of a Wnt ligand the β-catenin population is targeted by a protein complex and ultimately degraded [150] (Figure 1.3 B).

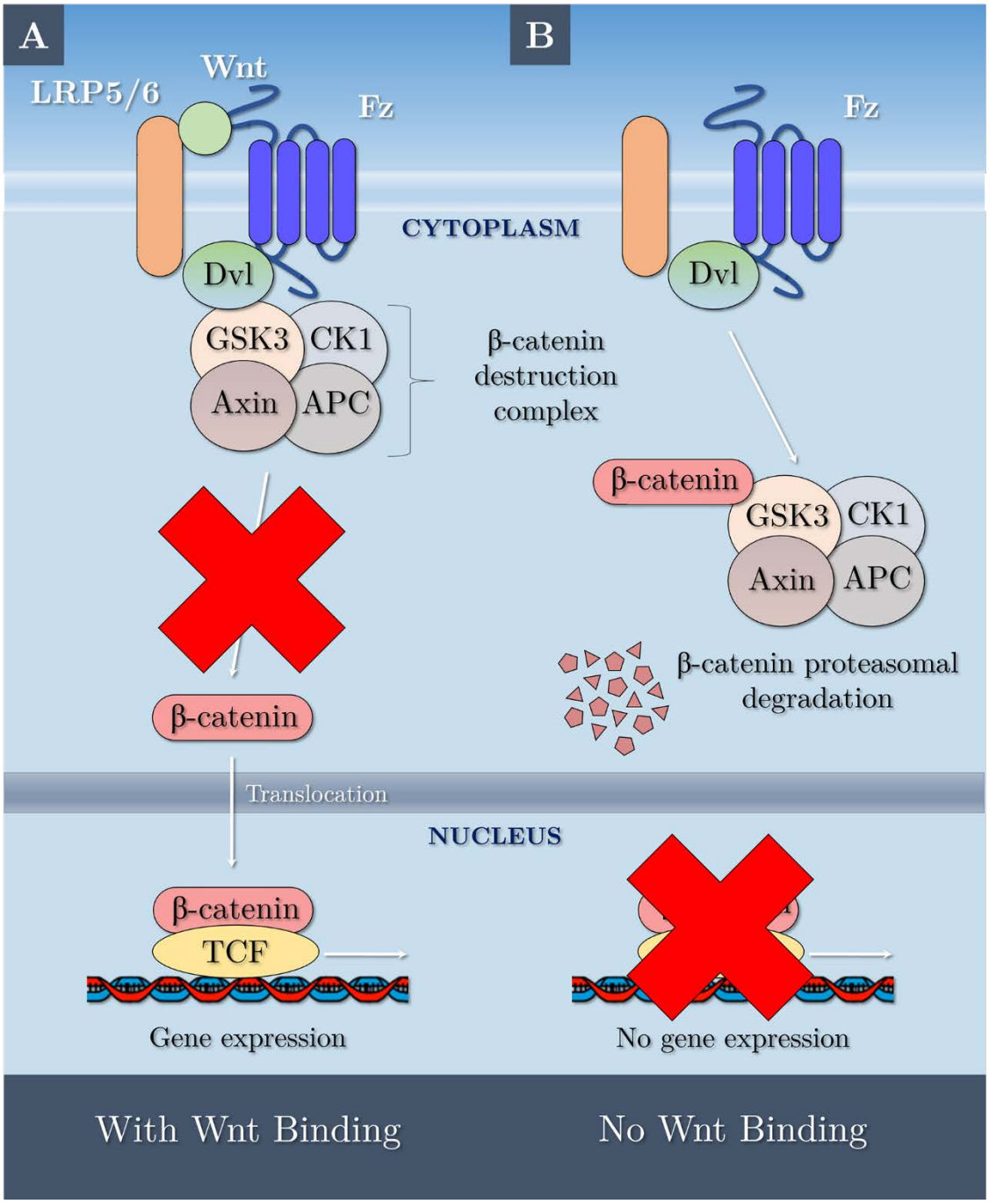

Figure 1.3. Diagram representing the canonical (β-catenin dependent) Wnt pathway (figure adapted from Behrens [151]). (A) The presence of Wnt protein binding to Fz causes Dishevelled (Dvl) to associate with GSK3 that inhibits the β-catenin destruction complex from phosphorylating β-catenin for proteasomal destruction. β-catenin can then translocate to the nucleus and activate gene expression of key regulatory genes. (B) When there is absence of Wnt protein binding the Frizzled (Fz) receptor, β-catenin is degraded by the β-catenin destruction complex and is unable to activate Wnt-related gene expression.

1.6.2.2 The Role of Wnt Signalling for Skin Homeostasis and Wound Healing

Wnt signalling is known to be essential for the regulation, maintenance, self-renewal and differentiation of stem cells in adult mammalian tissue. It has been shown that interfollicular stem cells require autocrine signalling to maintain self-renewal [152]. Stem cells that reside within the hair follicle bulge have also been documented to be in direct control by Wnts [153]. These stem cells are important for cutaneous wound repair [154, 155] and recent evidence has shown that stimulating the canonical Wnt pathway can augment the healing process [136]. Thus, treatment of non-healing wounds using Wnts or Wnt agonists may offer significant benefits that improve wound recovery.

1.7 Biomaterial Hydrogels, Drug Delivery and Nano-clay for Wound Healing Therapy

The earliest evidence showing benefits of hydrogels in biomedical applications was provided by Wicherle and Lim in 1960; they had developed a synthetic polymer hydrogel, poly(hydroxyethyl methacrylate) (pHEMA), that was used as a material for soft contact lenses [156]. Since then, hydrogels have played an essential role within the biomedical field. Their applications as biomaterials to treat various diseases and defects has had an important impact on improving human health. This includes products that are used for hygiene purposes, tissue engineering, wound dressings and drug delivery [9].

The primary reason why hydrogels are suitable for biomedical applications are due to their unique structural properties. They consist of three-dimensional, hydrophilic, polymeric networks capable of retaining copious quantities of water or biological fluids. Their high-water content and flexible structure allows them to integrate well with biological tissue, with minimal risk of host rejection [157]. Traditional hydrogels consist of synthetic or natural polymers, exist as homopolymers or copolymers and can be cross-linked by chemical or physical means [158].

Though hydrogels alone can improve wound healing outcome [159, 160], their capabilities as drug carriers [161] has provided further opportunities in the fields of wound care and tissue engineering [10]. Reflecting this, there is a large field of ongoing research that is attempting to deliver small or large molecular weight drugs and other bioactive agents in a time-controlled, site-specific manner using hydrogels [10, 162-165].

The specific benefits that hydrogel-based materials can offer to wound healing was first demonstrated by a landmark paper published in 1962 by George D. Winter [119]. This research provided evidence against the notion that skin wounds healed more quickly when exposed to air (promoting the formation of a scab). A moist environment was shown to double the rate of re-epithelisation, which the author attributed to greater migration of leucocytes and epithelial cells into the surrounding wound exudate.

Shortly after this publication, medical researchers were curious to develop better ways to promote moist wound healing. Naturally, hydrogels were of significant interest due to the hydrophilicity and biocompatibility that had been documented

two years earlier [156]. The pHEMA hydrogel was subsequently patented manufactured under its trade name, Hydron [166] and was investigated early on as a dressing to help treat burn wounds [159, 160].

In the decades that followed, the development of advanced wound dressings containing hydrogels had increased significantly; these include ActiFormCool® (Activa), Aquaflo® (Covidien) and can be applied to an array of different cutaneous wound types [167, 168]. Hydrogels within these dressings are either amorphous gels or sheet gels; amorphous hydrogels are flexible and soft that reduce in viscosity as they absorb fluid whereas sheet hydrogels are less flexible and swell when fluid is absorbed, yet retain their structural integrity [167, 168].

Many hydrogel-based drug delivery systems are now more sophisticated and are formed from composite materials. These materials attempt to address the inherent problems of many hydrogel systems or augment their capabilities further. These include; improving mechanical strength [169, 170], enhancing biomolecule release kinetics [171, 172], improving gel porosity [173] and creating self-assembling gels with stimulus-specific properties [174].

One group of materials of significant interest that have been used as additives for hydrogel enhancement are clays [175, 176]. Clay minerals exhibit unique sorptive properties due to their charged structure and small size (nanometre particulate crystals), which can aid in improving gel strength [177] and improve retention of bioactive molecules for drug delivery [14]. Clay minerals alone can even be formulated into hydrogel-like materials, formed by electrostatic interactions between clay particles, inter-clay cations and water molecules [14, 178]. Whilst these nano-clay gels are not created by any form of polymer-based crosslinking,

they exhibit many of the beneficial properties that hydrogels can offer in a wound healing milieu. A definition that better describes materials that deviate from standard hydrogel formulations (like those containing nano-clays) could be classed as hydrocolloids [179, 180]. The true definition of a hydrocolloid would be a colloidal suspension of nanoparticles (the biomaterial) in gel phase which consists primarily of water [179].

As the technologies into biomaterial drug delivery and production of advanced wound dressings evolved, various derivatives of hydrogels have been formulated. There are now hydrogel-based films that have the potential to coat materials and deliver drugs [181]. As mentioned previously, many different composite materials can create hydrogel formulations described as hydrocolloids. Some hydrogel technologies now involve the use of 3D-printing [182] and production of electrospun nano-fibres [183] for increased strength, durability, compatibility with biological tissues and drug delivery.

Combining all current knowledge on the benefits of hydrogels for improving wound healing and drug delivery, there are many opportunities for better, novel treatments to be formulated. Desirable outcomes for successful novel drug delivery treatments are that they are simple, cheap and easy to administer within the clinic [184]. Sustained, slow-releasing delivery of bioactive factors would be essential as this ensures that beneficial effects are translated in a safe manner [185]. Furthermore, many bioactive factors are produced at considerable expense so economical delivery is also important for future-proofed therapies [184]. The use of clay-based hydrogels address many of these requirements and therefore offer great promise towards a novel DFU therapy.

1.7.1 Current Biological Applications of Clays

Clay is defined as a fine-grained material consisting primarily of phyllosilicate minerals (i.e. any silicates with a crystal structure of parallel sheets of silicate tetrahedra with Si_2O_5 or 2:5 ratio [186]) with traces of organic matter that is malleable in the presence of water and becomes hardened when dried or fired [187]. The use of clay medicinally has occurred since prehistoric times; it is believed that *Homo erectus* and *Homo neanderthalensis* used soil and various earth minerals (e.g. ochre) mixed with water to clean and treat wounds. There is even evidence that the ancient Egyptians would topically apply clay on their skin for therapeutic purposes. Furthermore, they also were known to ingest clay to aid digestion and treat gastrointestinal problems [188]. The practice of using clay in this manner is believed to be instinctive and many animals also exhibit similar behaviour, especially through the ingestion of clay and soils (termed as geophagy) [189].

Since then the use of clay for therapeutic benefits has continued as well as being used to solve various environmental problems. It has only been within the last 100 years that the true capabilities of clay have been elucidated, namely their high adsorption properties and small particle size (nanometre to micrometre). Our knowledge of chemistry has improved over this time and there have also been huge technological advances. We now have a more detailed understanding about the structure of clays and the reasoning behind their unique properties [188].

The high sorptive capacity, low toxicity, rheological properties and high cation exchange capacity (CEC) of clays (particularly those from the smectite group, for instance montmorillonite) have made them of interest for drug delivery and other medical applications. Conventionally they have been used as antacids, often

prescribed following prolonged use of non-steroidal anti-inflammatory (NSAIDs) drugs. They are also present within many gastrointestinal drugs for the treatment of diarrhoea. Their ability to treat gastrointestinal problems is due to their high proton adsorption and water swelling properties, which neutralises stomach acid and solidifies faecal matter [188]. Kaolinite and smectite clay minerals are a large component within many cosmetic-based products, especially topical skin products that serve as a protective barrier and remove excess skin secretions [188]. Talc is also found in cosmetic products with a similar function (e.g. talcum powder), and is also useful as a lubricant in baby powder to prevent nappy rash [190].

There has been a focus on more innovative ways to use clay medically in recent years especially in areas of antibiotic resistance, drug delivery and tissue regeneration [191]. Due to the great capacity for bioactive molecules and drugs to adsorb to the surface of smectite crystal particles, they have been identified as a suitable "carrier" material for biological systems. The nature of how smectite particles interact within a biological system to promote tissue regeneration is also of interest [14].

Although natural clays and clay minerals are ubiquitous in nature there can be a high degree of structural heterogeneity when they are extracted. This can limit the potential benefits they offer for specific applications. Furthermore, some natural clays can be difficult to obtain in adequate quantities, so as a solution to these draw-backs, synthetically-produced alternatives are now available [192]. Through the recent development of nanotechnology and nanoscience there is ever increasing interest for synthetically-produced and naturally-enhanced clay minerals.

1.7.1.1 Overview of Clay Minerals & Structural Properties

Clay minerals are layered hydrous phyllosilicates that are either formed naturally through the process of weathering, or that can be created synthetically. They all contain a silica tetrahedral sheet where four oxygen atoms are covalently bonded to a single silicon atom. Each tetrahedron are associated by three adjacent tetrahedra through covalent bonding with three basal oxygen atoms. The fourth apical oxygen atom within a single tetrahedron are all orientated in the same direction as neighbouring tetrahedra, which point away from the basal oxygen atoms (i.e. like the 'tip' of a pyramid) [193]. Repeating tetrahedron units that are bonded in this way form the silicon tetrahedral sheet within clays. Clay mineral layers also consist of an octahedral sheet where a metal cation (often aluminium) is surrounded by six oxygen atoms. Two of these are shared from apical oxygen atoms presented in the tetrahedral sheet, given by two tetrahedra. Any remaining oxygen atoms within the octahedral sheet that are not shared by either the adjacent octahedron or tetrahedral sheet become hydrated (form –OH groups through covalent bonding with a hydrogen atom). An illustrative example showing the arrangement of atoms within the tetrahedral/octahedral sheets is shown in a later subchapter discussing in detail about the structure a synthetic clay named Laponite (Figure 1.5 B).

The tetrahedral/octahedral sheets exist in either a 1:1 or 2:1 crystal lattice arrangement depending on the number of tetrahedral sheets that 'fuse' to an octahedral sheet. So, a 1:1 layered silicate consists of one tetrahedral sheet and one octahedral sheet whereas a 2:1 layered silicate consists of two-dimensional layers where a central octahedral sheet is sandwiched in-between two tetrahedral sheets [194].

Depending on the type of metal cation that forms the octahedral sheet, either a dioctahedral or trioctahedral sheet silicate is created. A trioctahedral sheet is formed when divalent cations, like Mg^{2+} or Fe^{2+}, occupy all available (3/3) octahedral cation sites. Conversely, a dioctahedral sheet is formed when trivalent cations (usually Al^{3+}) occupy only two of every three octahedral cation sites [195].

A single crystal particle can associate with another and this interaction occurs via interlayer counter-ions, however this depends if the crystal particle exhibits a net layer charge or is neutral. By understanding their layer arrangement, the magnitude of net layer charge (x) per formula unit, and the type of interlayer species that resolves the net layer charge, clays can be categorised into seven groups: (1) serpentine-kaoline, (2) talc-pyrophyllite, (3) smectite, (4) vermiculite, (5) mica, (6) chlorite and (7) interstratified clay minerals [196].

The structural differences that exist between the natural clay minerals can yield varying negative-unit charges. This determines how strongly they interact with interlayer cations and how tightly each silicate layer associate with one another Of particular interest in this regard are smectite clays which have a net negative unit charge of 0.2-0.6 (vermiculite and mica range from 0.6-1.0) [196, 197]. This allows the layers of smectite clays can fully delaminate when hydrated in excess [14]. Some clays like the synthetic smectite Laponite can form complex networks when hydrated due to the relatively weak association between layer particles. This occurs because water molecules that interact within the layers cause the particles to "swell" (Figure 1.4 A).

The weak negative-face charge in smectites also allows substitution of interlayer cations with other positively charged molecules, for instance proteins and other

biologically active molecules. This high adsorption capacity, along with their rheological properties are why smectites are of particular interest therapeutically [14].

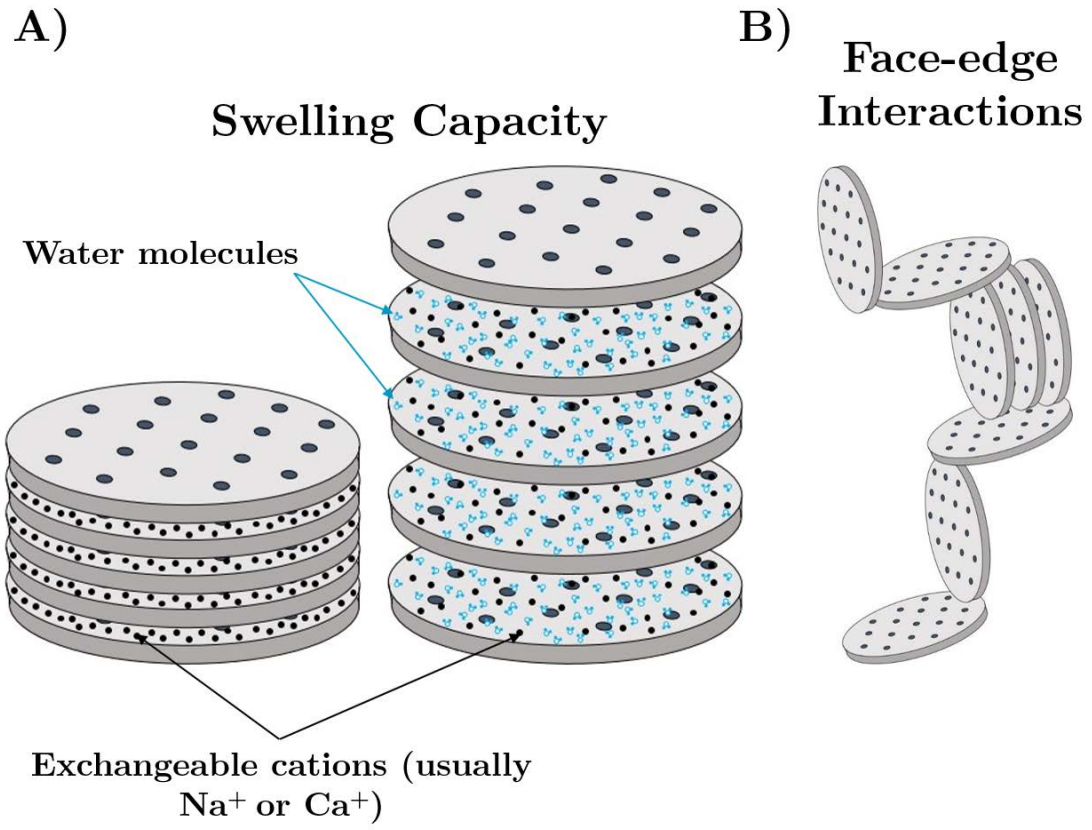

Figure 1.4. Illustration of the several types of interactions of seen in smectite clays (specifically Laponite) (A) Depicts how clays can swell in the presence of water molecules. (B) Face-edge interactions leading a "house-of-cards" type of structure.

Another important structural property of many of the phyllosilicates is that they exhibit a weak pH-dependent charge at the edge of crystal particles. This plays an important role in the colloidal aspect of clay mineral suspensions as crystal particles often arrange in a face-edge manner (Figure 1.4 B) [194]. This can be seen with hydrated smectite clays where following crystal particle delamination, a "house-of-cards" structure is created [198]. This type of suspension generates a low viscosity hydrogel that can occur at low clay particle concentrations (2-3%).

What is remarkable about this structure is that it can be easily disrupted due to the weak Van der Waal forces that hold the face-edge interactions in place. Hence, clay hydrogels have a unique shear thinning property (thixotropy), which means gel suspensions can become less viscous upon agitation. Furthermore, the interlayer cations and crystal particle face-edge association can be exploited in the form of clay-biomolecule, clay-polymer and clay-clay interactions, all of which allow clays to be used to in a beneficial manner [14].

1.7.2 Overview of Hydrogel-Based Drug Delivery for Wound Healing

1.7.2.1 Synthetic Polymers

Synthetic polymers such as poly(ethylene glycol) (PEG), poly(lactic-co-glycolic acid) (PLGA), poly(2-hydroxypropyl methacrylamide) (pHPMAm), poly(vinyl alcohol) (PVA) and poly(hydroxyethyl methacrylate) (pHEMA) provide great chemical and architectural versatility when used to formulate drug delivery hydrogels. They can be tailored in combination with different synthetic and natural polymers to improve hydrogel structure, site-specific formation (e.g. *in situ* formation) and controlling the release of drugs and biological factors [199].

A non-biodegradable and highly biocompatible polymer widely adopted in many hydrogel systems is PEG. It is also one of the most well-known and well-characterised synthetic polymers in use today. Each monomer unit can exist as a linear or branched (multi-armed or star) structure and can be polymerised to any length via ethylene glycol or ethylene oxide in aqueous solution [200]. PEG is highly hydrophilic, making it excellent at sequestering water and other biological fluids and an ideal prerequisite for hydrogel synthesis. Crosslinking between PEG

monomer units can be achieved in three ways: (1) through specific chemical reactions (e.g. Michael-type addition, click chemistry, condensation), (2) radiation (e.g. gamma) and (3) free radical polymerisation. The latter crosslinking method is one of the most popular as it can be easily achieved via photo-polymerisation; this allows the use of natural or UV light to generate hydrogels quickly, efficiently and in an environment, that is alike human tissue [201, 202].

One of the earliest reports of the use of PEG as a biomaterial for skin wounds was during the development of a novel pHEMA-PEG film in the mid-1970s [160]. Shortly afterwards research into PEG for various biomedical applications increased dramatically. Throughout the 1990s, PEG was formulated into various hydrogel systems with increasing popularity; more was known about the potential benefits of PEG-based hydrogels with an emphasis to development a biomaterial capable of controlled drug delivery [203].

PEG and other synthetic polymers are often formulated into hydrogel systems as co-polymers with other synthetic and/or natural polymers (composite hydrogels). A recent publication by Zhu *et al* [204] developed a star-shaped amphiphilic block copolymer comprising poly(ethylene glycol) and poly (propylene sulfide) to aid the delivery of hydrophobic agents such BRAF inhibitors. This hydrogel system allowed for injectable *in situ* delivery of these agents and was found to improve wound recovery in diabetic mice.

Another example of PEGylated hydrogel system was the creation of a porogen-free injectable gel as a scaffold for cell invasion [205]. Whilst this published work was not directly focusing on drug delivery, they showed in a robust way how

tuneable gels can be formulated using a combination of PEG, RDG binding domains and MMP substrates.

PLGA is another widely used biodegradable polymer used in hydrogel formulations, often in accordance with PEG. Lee *et al* [206] showed that an acceleration in re-epithelialisation rates when PEG-PLGA-PEG hydrogels were loaded with a TGF-β1 encoding plasmid in diabetic mice.

There are many more examples of synthetic polymers being used for wound applications to improve hydrogel strength, formation, cell adhesion and drug delivery [207-209], many of which are out of the scope of this introduction. However, this subchapter emphasises the importance of synthetic polymers used in hydrogel drug delivery systems.

1.7.2.2 Natural Materials

Collagens

There has been widespread use of collagens in drug delivery and tissue engineering for many years due to their biocompatibility with cells and tissues and convenient properties; these properties include visco-elasticity (free-flowing when under stress but are semi-solid when resting), self-assembly of polymeric networks under physiological conditions and interaction with bioactive proteins/small molecules [210]. The simplicity and convenience of collagens also have several drawbacks including poor mechanical properties and limited control of gelation. To overcome many of these restrictions, collagens are often used within composite or more advanced gelation systems [211]. Nevertheless, there has been successful reports within the literature of collagen-based, drug delivery hydrogels that have been used for wound healing applications.

Ono et al., [212] documented reduced contraction and increased re-epithelisation of full-thickness dorsal wounds on rabbits when treated with basic fibroblast growth factor (bFGF) incorporated within collagen hydrogels; bFGF is a potent mitogen that promotes angiogenesis and stimulates the proliferation of fibroblasts [213]. These cells are essential for modulating wound contraction and deposition of matrix proteins (e.g. hyaluronan, proeteoglycans, fibronectin and collagens) [64]. Furthermore, knockout studies have showed that bFGF-/- mice exhibited wound healing impairment [214]. This study documented more efficient matrix deposition and increased wound granulation which boosted the quality of healing. A similar effect was noticeable in mice treated with aqueous bFGF. Crucially, bFGF delivery via collagen gels enhanced its positive effect when compared to bFGF administered aqueously. Furthermore, high doses of aqueous bFGF (10 µg) was required to yield a positive effect that was significantly different to controls; this response was akin to bFGF-collagen gels that contained only 1 µg of bFGF. Similar reports of increased reduction in wound size have been documented with bFGF using other biomaterial delivery systems [215, 216].

The same group later investigated the delivery of prostaglandin E1 to skin wounds using the same hydrogel and rabbit model [217]. Similarly, in their previous study, collagen hydrogels alone had positive effect on wound contraction. The use of high concentrations of prostaglandin E1 also had a minor positive effect on contraction. However, when prostaglandin E1 was combined with their collagen gel formulation, there was a huge increase in wound contraction at both 3 and 5 weeks post wounding.

Gelatin is a denatured form of collagen and has frequently been used as a biomaterial hydrogel for drug delivery. Extensive research into gelatin-based

hydrogels have also been successful at delivering bFGF to promote wound healing. Most of these hydrogels are based on gelatin microspheres; in brief, these are micro/nano-particles of gelatin hydrogels (± biomolecules) that are formed by emulsification of crosslinked gelatin in oil phase, followed by recovery and purification of microspheres and freeze-dried until use. Treatment of bFGF-gelatin microspheres has shown increased fibroblast proliferation, angiogenesis [218] and improved wound healing in both healthy wounds and a diabetic model of impaired wound healing.

Chitosan/Chitin

Chitin is one of most abundant natural polysaccharides available with an annual global availability of over 10 gigatons (1×10^{13} kg) [219]. It is largely derived from crustacean shell wastes but it can also be extracted from fungi and bacteria [219]. Chitin and its derivatives are known to harbour unique structure and chemical properties. These are specifically beneficial for biological applications including therapeutic benefits (e.g. anti-inflammatory, antimicrobial, immunity-enhancing, anti-cancer and antioxidant effects) and as biomaterials in the form of scaffolds or drug carriers for localised delivery [220].

Chitin and chitosan are both linear polysaccharides that are comprised of two monomer units; N-acetyl-glucosamine (N-acetylated groups) and N-glucosamine (N-deacetylated groups) units. Chitosan is the most well-known derivative of chitin; a deacylated analogue that contains lower amounts of N-acetylated groups than chitin [221]. Importantly, the conversion of chitin into chitosan creates a polymer that is water soluble in acidic media (it is possible for chitosan be soluble at neutral pH, but only when under specifically designed conditions). This allows

for greater flexibility when used for biological purposes, namely hydrogels and drug delivery [221].

Chitin and chitosan were proposed back in the 1970s as a potential biomaterial to accelerate the rate of wound healing [222-224]. In the following decades, chitin and chitosan were formulated into a commercially-available treatment for wounds, although most of these were in the form of filaments, powders, granules and sponges [225, 226]. More recently there have been an array of hydrogel systems that incorporate chitin/chitosan to aid in drug delivery for wound repair. Many of these exist alongside other biomaterial as composites, although there have been reports of a few simple chitosan-based gels.

Ono et al., [227] formulated a novel photo-crosslinkable chitosan hydrogel that could be useful as a biological adhesive. They incorporated azide (Az) and lactose (LA) moieties within chitosan molecules via a two-step condensation reaction using lactobionic acid and p-azidebenzoic acid, to form Az-CH-LA monomers. The Az groups attached to CH-LA monomers are photoreactive, meaning that they are susceptible to forming insoluble hydrogels when irradiated with UV radiation. These gels were reported to be soft, flexible and capable of offering biological adhesion properties with sealant strengths comparable to fibrin glue. In addition, they exhibited great biocompatibility with dermal fibroblasts with no measurable cytotoxicity. This hydrogel was later shown to exert positive effects on wound healing when applied as a wound occlusive dressing [228].

A study by Alemdaroğlu et al., [165] also investigated the effects of a chitosan hydrogel on wound healing in burn wounds; this gel was polymerised in the presence of glacial acid and incorporated with epidermal growth factor (EGF). It

is also an example of chitosan hydrogels being adapted and used as a vehicle for biomolecule delivery. They documented a significant increase in *in vivo* cell proliferation within rat wounds when treated when alone and as chitosan-EGF gels. Importantly, the proliferation rate was enhanced in chitosan-EGF gels which suggested that delivery of EGF from chitosan gels was positive.

Alginate

Alginate is an anionic polysaccharide that is classically derived from brown algae [229, 230], these include (but are not exclusive to): *Laminaria hyperborean, Laminaria digitata, Laminaria japonica, Ascophyllum nodosum* and *Macrocystis pyrifera* [231]. This biomaterial has been widely used for many biomedical applications due to its excellent biocompatibility, low toxicity and cost. It can form a hydrogel through the process of cross-linking with divalent cations (e.g. Ca^{2+}). Cross-linking occurs between linear co-polymers that consist of blocks of (1,4)-linked β-d-mannuronate and α-l-guluronate. These co-polymers will naturally contain cations that are associated with side-groups. When a divalent cation like Ca^{2+} is presented (usually in the form of $CaCl_2$) it displaces the endogenous cations and forms a stronger linkage between two-polymer blocks [232, 233]. Cross-linking between Ca^{2+} is the most conventional ionic method, but there have been other methods that include: covalent linkages with synthetic polymers (e.g. PEG) and through photo-crosslinking [231].

Alginate gels have been shown to deliver bioactive molecules for wound healing application. A paper by Tellechea *et al* [234] investigated the delivery of alginate gels encapsulating VEGF, neuropeptides, endothelial cells and a combination of the three and their effect on diabetic wounds healing. They showed that gels that

contained the combination of VEGF and endothelial cells and VEGF, cells and neuropeptides accelerated wound healing. Unfortunately, the authors did not include histological data for alginate-based treatments to support these claims, which would have improved the robustness of the data. They also showed that the release kinetics of Substance-P and Neurotensin exhibited a burst release from alginate gels. Another previous report by Dawson *et al* [235] also demonstrated that alginate gels delivering proteins result in a burst release. This may be useful in certain circumstances but the consensus within the drug delivery field is that slow, sustained delivery is more advantageous [236]. Furthermore, whilst the paper by Tellechea *et al* [234] exhibited positive changes within wound recovery using a delayed wound healing model, its release kinetics may not be suitable for chronic wounds exhibited in humans. This is because chronic DFUs can exhibit lengthy recovery times (months to years) [237], often due to a wound environment that can degrade bioactive molecules and inhibit cell growth [39]. However, alginate still exhibits important characteristics for drug delivery and wound healing, with extensive investigation within advanced, composite hydrogel systems [238-240].

1.7.2.3 Composites Using Natural Clays for Wound Care and Drug Delivery

Clay nanocomposite biomaterials may also have clinical potential in wound healing. A study by Kokabi *et al* [11] formulated a polymer-clay (Na-montmorillonite) nanocomposite poly(vinyl alcohol) (PVA) hydrogel for wound dressing application; they discovered that the proportion of clay that was added to nanocomposite hydrogel had a direct effect on the wound dressing properties. Specifically, higher quantities of clay led to gels with greater resistance to

mechanical strain, whilst not significantly impacting on the ability of the dressing to absorb moisture or wound exudate.

Nano-reinforced composite films consisting of cellulose and different montmorillonite analogues were investigated for their potential antimicrobial benefits [241]. The clay analogues were distinguished by slight variances in cation content (Na^{+}, Ca^{2+} and Cu^{2+}) and it was hypothesised that exposure to these cations would inhibit bacterial growth. They showed that Cu^{2+}-montmorillonite cellulose films offered superior reduction in bacterial growth than all the other test groups. Furthermore, the greater the content of clay, the stronger the antimicrobial effect. Antimicrobial natural clays have been shown to have positive effects on wound healing in rats; in one study, a clay emulsion was used rather than a composite gel, however its relevance is still important as it highlights the benefits that clays naturally induce on wound healing [242].

Many of the recent drug delivery systems containing clay minerals for wound healing applications have focused on antimicrobial and antibiotic delivery. Combining the antimicrobial properties that clays already exhibit, this is a logical progression that could have even greater benefits for wound care (e.g. novel wound dressings).

Again, many of these systems incorporate similar natural-based clays such as montmorillonite; a study by Saha *et al* [183] formulated an electrospun polymer fibres containing montmorillonite loaded with a cationic antiseptic (chlorahexidine acetate) showing positive *in vitro* effects against bacteria. Intercalation of antimicrobial silver sulfadiazine with chitosan/montmorillonite nanocomposites was successful in another study [243]. This research suggested

this novel composite would be applicable for burn wounds; however further study would be required to prove if their formulated composite has any benefits because only characterisation of intercalation was proven.

1.7.2.4 Synthetic Nanoclay (Laponite) for Wound Care and Drug Delivery

The commercially available, Laponite is produced by BYK Additives & Instruments [244] and is a synthetic nanoclay that overcomes the limitations of natural clays as discussed in section 1.7.2.3. It is structurally similar to the natural clay mineral hectorite and has a 2:1 layered structure with an empirical formula of $Na^{+}_{0.7}[(Si_8Mg_{5.5}Li_{3.3})O_{20}(OH)_4]^{-0.7}$ [245]. It is manufactured into different grades with slightly varying properties. Like natural smectite clays, it is classed as a 2:1 layered phyllosilicate that can form crystal particles 25 nm in diameter and approximately 1 nm in depth. Laponite has a high cation exchange capacity (CEC) within its interlayer due to hydrated sodium ions that weakly interact with the tetrahedral layer of individual crystal particles. This weak interaction is caused by a relatively low negative unit surface charge due to random isomorphic cation substitutions in the octahedral sheet [14] (see Figure 1.5).

Due to its purity, small particle size and charged structure, Laponite forms clear colloidal dispersions when added to water at low concentrations. These dispersions resemble a hydrogel in appearance yet offer greater benefits in mechanical strength and viscoelasticity. Laponite gels are strongly thixotropic - under shear stress the viscosity of Laponite gels decreases rapidly. Upon removal of the applied stress, these gels can regain their original viscosity rapidly [14].

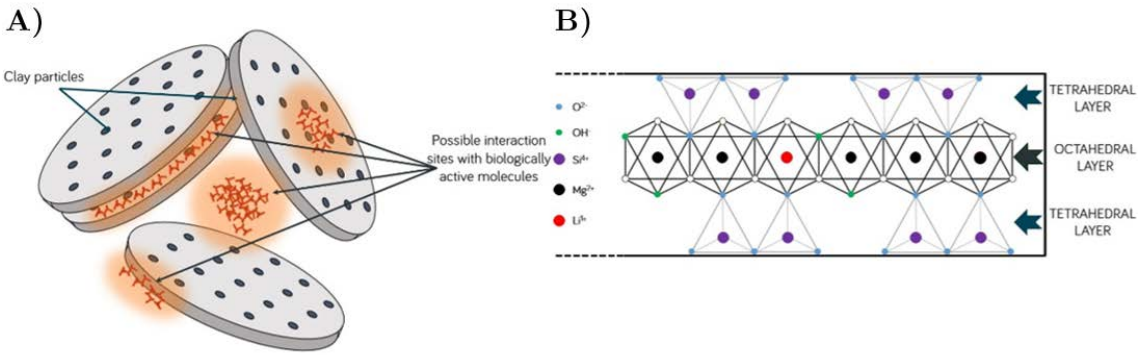

Figure 1.5. Structural properties of Laponite clay particles (figure adapted from Dawson and Oreffo [14]. (A) Indicating the possible functional binding sites available for proteins or other biologically active molecules. (B) Simplified diagram showing Laponite's structural layers within each nano-sized disc.

The charged structure of Laponite particles and the interlayer cations that allow interaction with water molecules also promotes strong association with other charged molecules such as proteins and bioactive molecules. The combination of gel-forming, thixotropic and sorptive properties make it an attractive biomaterial for drug delivery and wound healing therapy [14].

Research published by Wang *et al* [246] successfully intercalated a broad spectrum anti-cancer drug (doxorubicin) with Laponite particles. They showed that the cytotoxic effect of the drug was significantly greater when intercalated with Laponite. Further research into this area also documented Laponite's potential to be further enhanced when formulated into nanocomposite biomaterials with synthetic polymers; coating Laponite-doxorubicin with charged poly(allylamine) hydrochloride (PAH) and negatively charged poly(sodium styrene) sulfonate (PSS) led to more effective drug release at neutral and acidic pH levels [247]. Laponite has also been used as part of a nanocomposite in conjunction with alginate [248].

Other research groups have focused their attention to developing Laponite biomaterial gels/films that is specifically targeted for wound healing application.

Ghadiri *et al* [249] have investigated Laponite-amino acid functionalised gels at improving wound healing rates. Certain amino acids (e.g. arginine, lysine and leucine) are thought to be essential for wound healing recovery [250]; the authors showed that gels functionalised with these amino acids resulted in greater proliferation of human fibroblasts, with the most effective amino acid released (determined via release profiles) being Laponite-lysine gels. The same group also investigated delivery of the antibiotic, mafenide (a common antibiotic used to treat infections against *Pseudomonas aeruginosa* in burn wounds) with a Laponite gels and films [251]. They concluded that the use of Laponite-antibiotic combinations for wound infections could be beneficial due to the combination of antibiotic delivery, the soothing effect that Laponite offers (relieving pain) and release of Mg^{2+} ions into the wound from Laponite (these ions can offer further antimicrobial effects). Both functionalised Laponite gels/films investigated by this group would require further research, more specifically direct application within a suitable *in vivo* model.

VEGF offers potential therapeutic benefits to chronic wounds, but only when delivered in a controlled fashion, as explained in section 1.6.1.1. Encouragingly, Laponite has been shown by Dawson *et al* [235] to adsorb and localise $VEGF_{165}$; when testing VEGF-Laponite hydrogel capsules in an *in vitro* release/uptake human umbilical vascular endothelial cell (HUVEC) culture, they witnessed significant microtubule network formation between neighbouring cells. The extent of the tubule network was akin to HUVECs cultured in media containing VEGF. In the same paper, Laponite-VEGF suspensions were tested in an *in vivo* bone defect model using mice; it was discovered that VEGF could be delivered from Laponite-VEGF suspensions, improving the vasculature and recovery of the bone

defect. Nevertheless, the use of Laponite as a growth factor delivery vehicle in skin wounds remains untested.

1.8 Hypothesis and Objectives

Several properties of Laponite clays make it an attractive material for use in treating skin wounds. Laponite exhibits specific rheological characteristics, high CEC and adsorption properties.

The broad aim of this thesis is to test the hypothesis that Laponite clays can be used to deliver bioactive molecules to skin injury sites and to increase the rate and degree of healing in chronic wounds.

To test the above hypothesis, this thesis has been separated into distinct chapters investigating the following specific aims:

- To investigate the bioactive delivery of $VEGF_{165}$ by:
    - Encapsulating VEGF within 3% Laponite hydrogel suspensions
    - Determining the concentration of encapsulated VEGF that can exert a bioactive effect of human umbilical vein endothelial cell 2D tubule formation using Laponite-VEGF suspensions.
    - The adsorption and retention of small molecule Wnt signalling agonist 6-bromoindirubin-3'-oxime (BIO) by Laponite
- To determine if the bioactive effect of encapsulated VEGF within Laponite is translated *in vivo* by:

- Using an *in vivo* subcutaneous injection model to measure angiogenic effects over 21 days.

- Characterisation of an *in vivo* full-thickness wound healing mouse model to investigate:

  - The effect of Laponite suspensions on wound recovery in healthy and diabetic mice

  - Localising bioactive $VEGF_{165}$ at skin injury sites to stimulate angiogenesis within granulation tissue and improve wound recovery

Chapter 2:

Methods

2.1 General

2.1.1 Laponite Preparation

Suspensions of Laponite XLG (BYK Additives, Widnes, UK; product:) were prepared by slowly adding Laponite powder to distilled water under rapid agitation until a vortex was achieved. Suspensions were stirred 1-2 hours until a clear suspension was formed and then sterilised via autoclaving (Figure 2.1). Suspensions were weighed pre- and post-sterilisation to calculate water evaporation and % concentrations adjusted accordingly. 3% Laponite gel suspensions were used in all experiments; where an additive was required (e.g. growth factor), the dilution factor was always considered. Vehicle controls were always substituted with diluent (i.e. distilled water) to ensure Laponite concentrations were consistent.

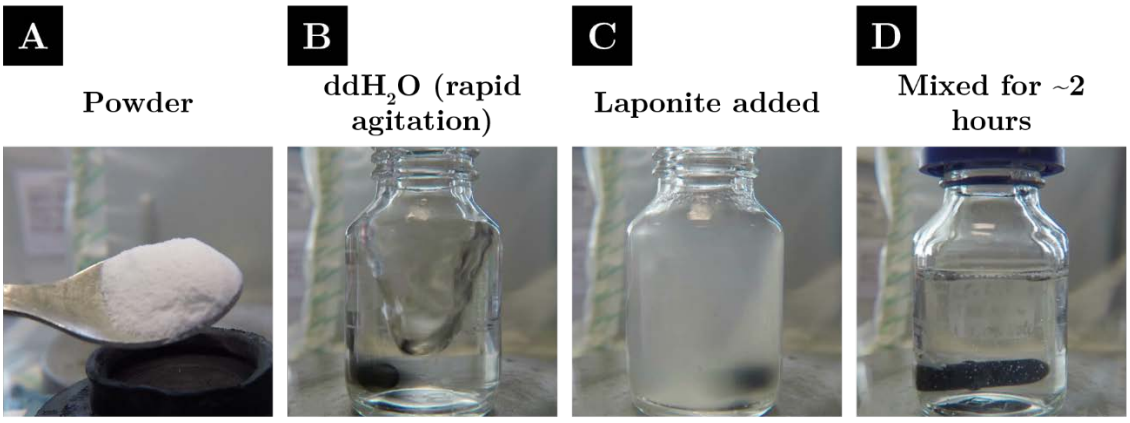

Figure 2.1. Preparation of Laponite Hydrogels. Anhydrous Laponite (A) was added slowly to distilled water under rapid agitation (B, C). Suspensions were stirred 1-2 hours until a clear suspension was formed then sterilised via autoclaving (D).

2.1.2 Alginate Preparation

2.1.2.1 Calcium Chloride ($CaCl_2$) Cross-linker Preparation

$CaCl_2$ stock: A 10% (w/v) $CaCl_2$ stock solution was created by dissolving $CaCl_2$ powder (Merck/Sigma-Aldrich, Gillingham, UK, product: 449709) in ddH_2O. A 1M 4-(2-hydroxyethyl)-1-piperazineethanesulfonic acid (HEPES) stock solution was also created by dissolving HEPES powder (Merck/Sigma-Aldrich, product: PHG0001) in ddH_2O.

$CaCl_2$ working solution: A final $CaCl_2$ working solution that contained $CaCl_2$ (1.1%), HEPES (20 mM) and Tween 20 (0.1 %) was created by diluting $CaCl_2$, HEPES stock solutions (as outlined above) and Tween 20 (Merck/Sigma-Aldrich, product: P1379) in ddH_2O. This was adjusted to pH 7.0 and filter sterilised using a 0.22 µm syringe filter.

2.1.2.2 Alginate Hydrogel Preparation

Anhydrous ultra-pure alginate (NovaMatrix, Sandvika, Norway) was UV sterilised for 30-60 minutes prior to preparation. Suspensions of alginate were prepared by slowly adding alginate powder to sterile PBS under rapid agitation until a vortex was achieved. Suspensions were stirred 30-60 minutes until a clear suspension was formed. 1.1% alginate gel suspensions were used in all experiments; where an additive was required (e.g. growth factor), the dilution factor was always considered. Vehicle controls were always substituted with diluent (i.e. 1x phosphate buffered saline (PBS); Thermo Fisher Scientific Oxoid Ltd, Basingstoke, UK; product: BR0014G) to ensure alginate concentrations were consistent. To crosslink the alginate gel suspensions, $CaCl_2$ was added as a 10%

fraction and mixed thoroughly (this step was always performed after the incorporation of additives).

2.2 *In vitro* Studies

2.2.1 2D Tubule Studies

2.2.1.1 Human Vein Endothelial Cell (HUVEC) Isolation and Culture

HUVECs were isolated from umbilical cords collected from the Princess Anne Hospital, Southampton, UK, with the approval of Southampton and South West Hampshire Local Research Ethics Committee (Ref:05/Q1702/102) by Stefanie Inglis. HUVECs were isolated and cultured as described by Jaffe *et al* [252] and Dawson *et al* [235] with some minor modifications.

The umbilical cord was cut at both ends; to one end, a cannula was inserted into an exposed vein and secured with ties. A syringe was then attached to the cannula and sterile PBS (Lonza, Castleford, UK; product: BE17-516F) was flushed through the cord until the waste PBS collected at the other end was clear. The umbilical cord was then fastened at the other end and umbilical cord vein filled with 5 mg/ml sterile collagenase B (Sigma-Aldrich/Merck; product: 11088807001) using a clean syringe. The syringe was left attached to the cord and the vein incubated with collagenase at room temperature for 1 hour. Following incubation, the collagenase was gently aspirated and then retracted back into the syringe. The collagenase containing detached cells was centrifuged at 1100 RPM for 4 minutes and the supernatant discarded. Cells were re-suspended in endothelial cell growth medium (ECGM), which consisted of: Medium 199 (Lonza; product:

LZBE12-117E), 10% foetal bovine (calf) serum (FCS; Life Technologies, Paisley, UK; product: 10270106, batch: 41Q4297P), penicillin-100U/ml-streptomycin-100U/ml (Sigma-Aldrich/Merck; product: P4333) and endothelial cell growth supplement (Promocell GmbH, Heidelberg, Germany; product: C-30120). Re-suspended cells were cultured at 37°C/5% CO_2 in humidified conditions. Following incubation, cells were sub-cultured using ECGM and passages of 1-4 were used in all experiments.

2.2.1.2 HUVEC 2D Tubule Formation on Laponite

This protocol was documented previously by Dawson *et al* [235] and adapted with a few modifications. HUVECs were cultured in ECGM as described above. Laponite was premixed with human fibronectin (Merck-Millipore, Watford, UK; product: FC010) as a 5% fraction to create a final concentration of 50 µg/ml. To create vascular endothelial growth factor subunit-165-Laponite suspensions (VEGF-Laponite), reconstituted human recombinant $VEGF_{165}$ (from this point on this will be referred to as VEGF) (PeproTech, London, UK; product: 100-20) was added as 10% fraction. A concentration range of 1-5 µg/ml VEGF was used for VEGF-Laponite gels in this study.

150 µl of Laponite or VEGF-Laponite was added to the base of 48-well plate, briefly centrifuged to ensure an even Laponite layer was formed and then incubated for 1 hour at 37°C to allow gelation (Figure 2.2 iii). The 'Bound VEGF' treatment involved adding ECGM that contained 40 ng/ml VEGF to Laponite coated wells and then ECGM alone to all other Laponite coated wells ('No VEGF Control'). Following a 2-hour incubation at 37°C, the 'Bound VEGF' treatment (Figure 2.2 ii) and ECGM alone treatment were removed and all wells were washed twice with sterile PBS. HUVECs were re-suspended in ECGM containing

10% FCS and 40 ng/ml of basic fibroblastic growth factor (bFGF; Thermo Fisher Scientific-Invitrogen, UK; product: 13256029) (present in all treatments) and 40 ng/ml VEGF (VEGF in media control, Figure 2.2 i) and seeded at 5 x 10^4 cells/well (n=6). 'Mixed VEGF' involved the same procedure as the 'No VEGF Control' but ECGM was added to wells containing VEGF-Laponite (Figure 2.2 iii). Seeded cells were incubated at 37°C/5% CO_2 for 18 hours and then microscope images were taken to assess HUVEC tubule formation.

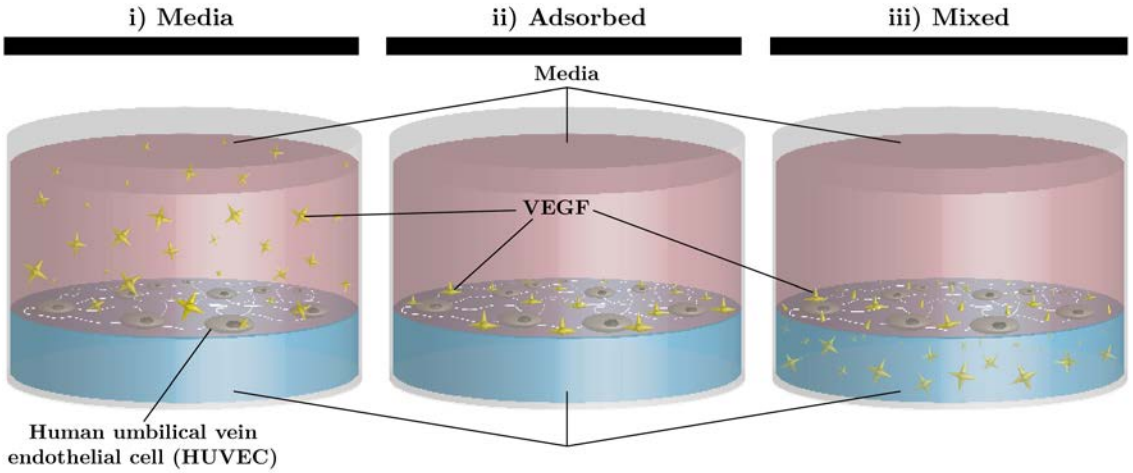

Figure 2.2. Human umbilical vein endothelial cell (HUVEC) 2D Tubule Formation Assay Schematic. HUVECs were seeded on top of Laponite gels that either contained: (1) VEGF in the growth medium, (ii) VEGF-bound to Laponite gels via surface-adsorption or (iii) VEGF pre-mixed within Laponite gels. Refer to main text for details.

2.2.1.3 Image Analysis of HUVEC 2D Tubule Network

A freely available macro for ImageJ called 'Angiogenesis Analyzer' by Gilles Carpentier (Gilles Carpentier. Contribution: Angiogenesis Analyzer, ImageJ News, 5 October 2012, http://image.bio.methods.free.fr/ImageJ/?Angiogenesis-Analyzer-for-ImageJ#nb1 for NIH Image J 1.47v Program was used to automatically quantify HUVEC 2D tubule network. The settings that were applied to compare tube networks were as follows: *Show maps of elements (single analysis)*, *show segments*, *Show nodes and junctions*, *Show meshes*, *Analyse*

master tree, Show extremities, Show branches, Show master segments and *Show supressed isolated elements* was all checked. Default sizes were used but an *Iteration number* of 2 was applied. Phase contrast images were first converted to 8-bit by using the *Image/Type* module and then finally converted to red, green, blue (RGB) (Macro requires 8-bit RGB image for phase contrast analysis. The *Batch Image Treatment Tool* was used to analyse a batch of captured images using the phase contrast module. The macro generates a network overlay of each analysed imaged where it has identified the HUVEC network and an output data file; the *Tot. branching length* (pixels) was used to determine network organisation. A total of 6 wells per test group were analysed. 3-6 images were taken from each well and the mean calculated; these individual means were then used to calculate an over mean for that test group.

2.2.2 3T3 Mouse Fibroblast Cell Culture

3T3 mouse fibroblast cells were grown using reagents from the Leading Light™ Wnt Reporter Assay Kit (Enzo Life Sciences, Exeter, UK; product: ENZ-61001-0001). Cells were grown in *Growth Medium* provided by the kit at 37°C/5% CO_2 in humidified conditions and passaged twice using the kit *Assay Medium* before use in assays. Cells were used at passages 5-9 at a maximum confluence of 60% for assay tests.

2.2.3 BIO-Laponite Hydrogel Uptake/Release Assay

2.2.3.1 Validation of Wnt Signalling Pathway of Reporter Cell Line with BIO

The 3T3 mouse fibroblast cell line has been genetically engineered to express the firefly luciferase reporter gene under the control of Wnt-responsive promoters (TCF/LEF). Luciferase activity in this cell line can be stimulated with the addition of exogenous Wnt proteins/Wnt agonists in a dose-dependent way. The small molecule 6-Bromoindirubin-3′-oxime (abbreviated as BIO; Sigma-Aldrich/Merck; product: B1686, molecular formula: $C_{16}H_{10}BrN_3O_2$, molecular weight: 356.179 g/mol [253]) is a potent agonist of Wnt signalling (it acts as a selective, Adenosine triphosphate (ATP)-competitive inhibitor of GSK-3α and GSK-3β) [254], which can be used to up-regulate the activity of luciferase. Enzyme activity is measured by changes in chemiluminescent output following cell treatment with an exogenous luciferin substrate.

To validate the dose-dependent relationship of exogenous BIO on 3T3 cell luciferase activity, 3T3 cells were seeded in a 96 well plate with assay medium at 25,000 cells/well. Cells were incubated overnight at 37℃/5% CO_2 in humidified conditions. BIO was added to cells 100 µl/well to support a range of concentrations from 0.5 µM to 5 µM. Cells containing BIO were incubated overnight in the same conditions as described above. Following incubation, culture medium was removed and the Steady-GLO® Luciferase Assay System (Promega, Southampton, UK; product: E2510) was added to cells (100 µl/well) and incubated for 10 minutes at room temperature. The chemiluminescent signal

was then measured using a VarioSkan Flash (ThermoElectron) fluorescence reader (0.1 seconds/well).

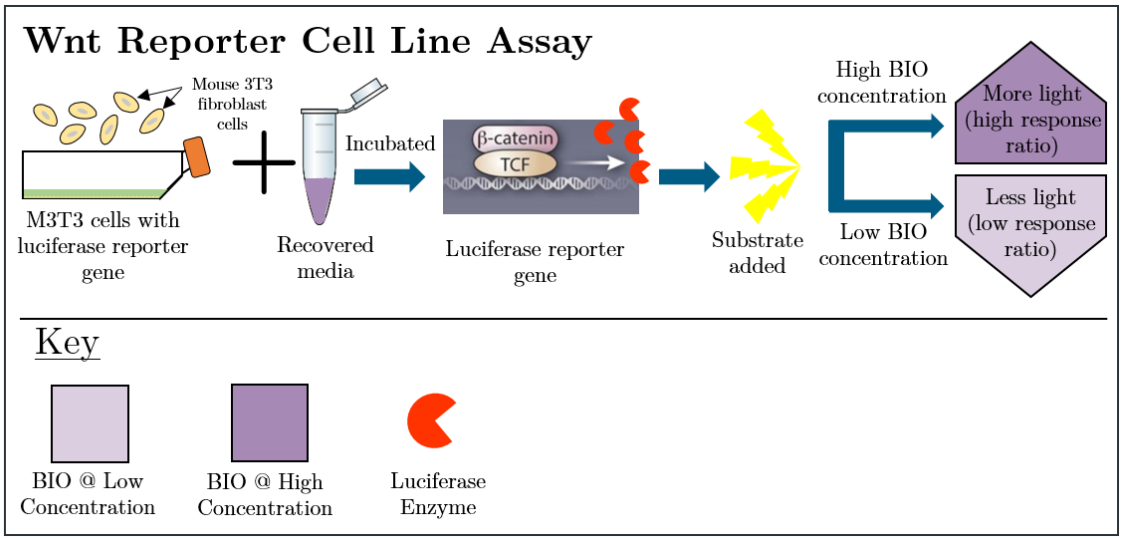

Figure 2.3. Validation of Wnt reporter cell line assay with BIO. Media recovered from assays were added to sub-cultured 3T3 Mouse fibroblast cells. An overnight incubation followed to allow for luciferase production. A fluorescently labelled substrate was added to cells and the change in light absorbance measured to determine the activity of luciferase. The addition of a BIO agonist will up-regulate luciferase production and changes in this activity was measured.

Fold changes in chemiluminescent activity was calculated by dividing the baseline signal by the test signal (refer to schematic in Figure 2.3). Response ratios were plotted against increasing BIO concentration to determine the dose-response relationship of BIO.

2.2.3.2 Validation of Adsorption of Assay Media Components by Laponite Hydrogels

To test whether adsorption of components from the growth medium by Laponite could interfere with the reporter cell line read-out, assay medium was incubated with Laponite hydrogel capsules for various periods of time up to 60 minutes and up to 168 hours (7 days) (Figure 2.4).

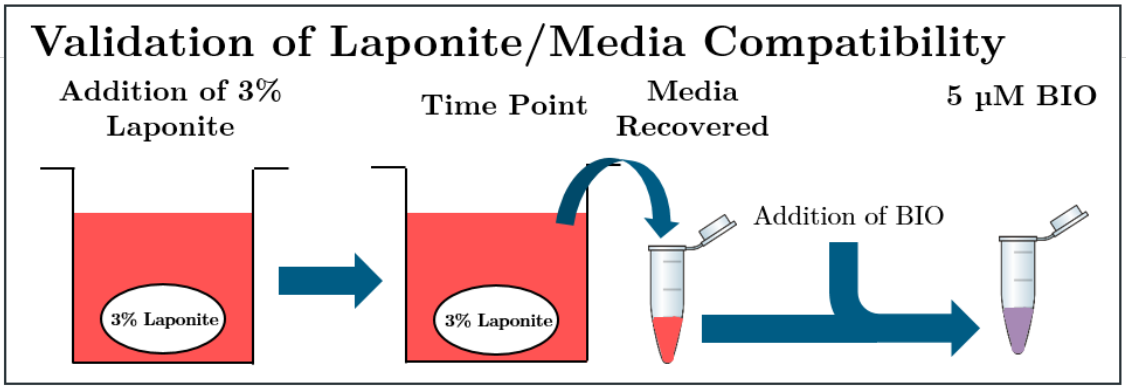

Figure 2.4. Validation of adsorption of assay media components by Laponite assay schematic. Following the addition and incubation of Laponite capsules with assay medium, samples of assay medium were taken combined with BIO (5 µM).

The 60-minute test involved the transfer of 1 x 50 µl Laponite hydrogel aliquots to 250 µl assay medium, whereas the 7-day test involved the transfer of 5 x 50 µl Laponite hydrogel aliquots into 500 µl assay medium. Assay medium was incubated at 37°C/5% CO_2 in humidified conditions and then samples taken at various time points over the stated time frame. BIO was added to recovered media samples (5 µM final concentration) prior to using with the Wnt reporter cell line as discussed in section 2.2.3.1.

2.2.3.3 Adsorption of BIO by Laponite Hydrogels

To assess potential uptake of BIO by Laponite, an assay was performed to measure potential decrease in BIO concentration in aqueous medium following incubation with Laponite. In this assay, BIO was mixed with 3T3 fibroblast assay medium to create a final 5 µM concentration. 1 x 50 µl Laponite hydrogel aliquots were transferred into wells containing 250 µl of BIO media to test for BIO adsorption. Media was incubated at 37°C/5% CO_2 in humidified conditions and then recovered at various time points up to 60.0 minutes for later assay of concentration using a reporter cell line (see Figure 2.5 A).

2.2.3.4 Release of BIO by Laponite Hydrogels

To assess the release of BIO by Laponite hydrogels, an assay was performed to measure the release of BIO encapsulated in Laponite into aqueous medium (Figure 2.5 B). To do this, BIO was premixed with Laponite at high concentrations of either 50 µM or 80 µM.

In an initial study, 1 x 50 µl aliquots of Laponite-BIO (50 µM) were transferred into wells containing 250 µl assay diluent. Media was incubated at 37℃/5% CO_2 in humidified conditions and then recovered at various time points up to 60 minutes. In a revised study, 5 x 50 µl aliquots of BIO-Laponite (80 µM) were added to wells as a single layer to 500 µl assay medium. 5 x 50 µl aliquots of Laponite alone was also added to media to serve as a negative control test. Media was recovered at various time points up to 168.0 hours (7 days) and stored at -20℃ until required for analysis.

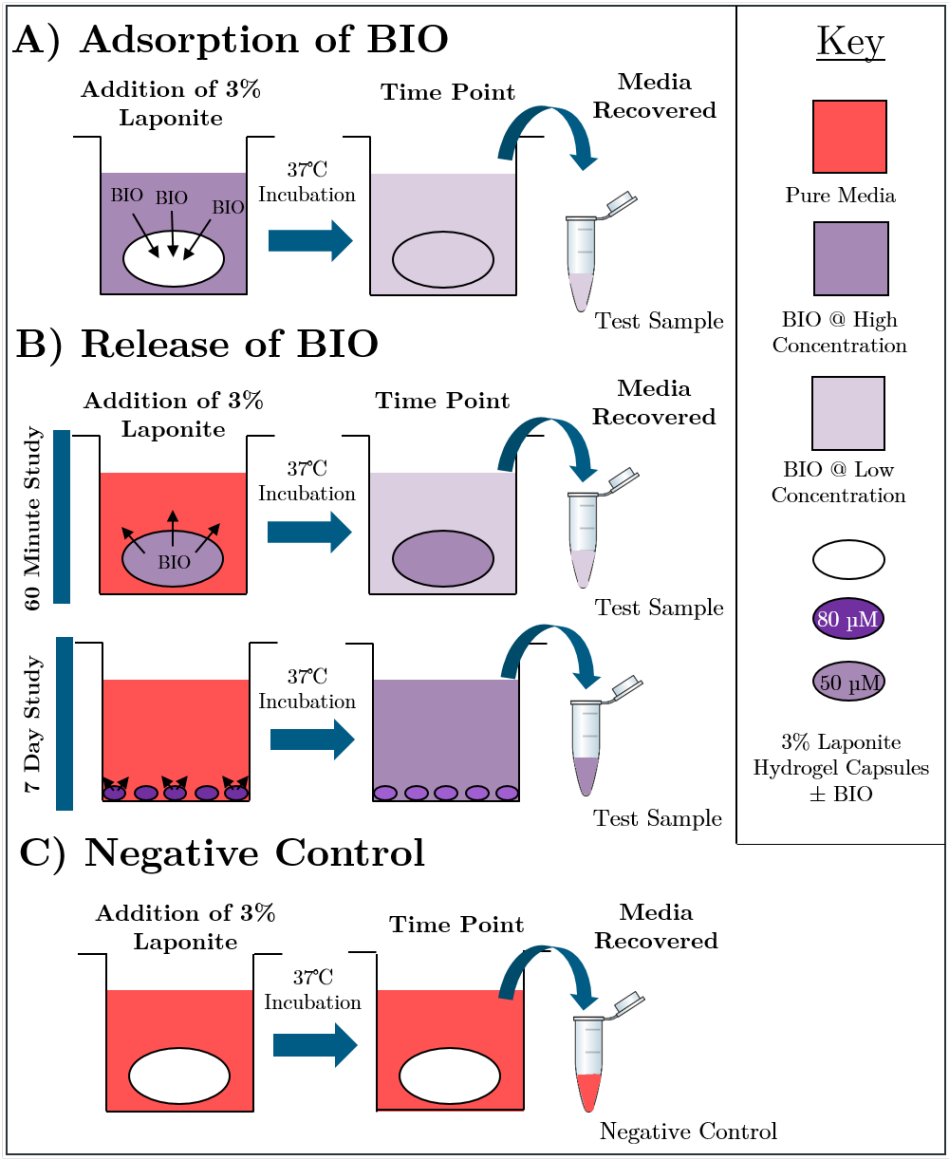

Figure 2.5. Adsorption/release of BIO by Laponite hydrogels assay schematic. (A) Adsorption of BIO by Laponite. Laponite capsules were added to assay medium containing 5 µM BIO and incubated for >60 minutes. Samples of assay medium were taken and later assayed with a 3T3 reporter cell line to determine the proportion of BIO adsorbed. (B) Release of BIO by Laponite. Aliquots of BIO encapsulated in Laponite were added to assay medium and incubated for >60 minutes or >7 days; the 60-minute study involved the addition of a single 50 µM BIO-Laponite capsule whereas the 7-day study involved the addition of multiple (n=5) 80 µM capsules. At various time points, samples of assay medium were taken and later assayed as previously described and determine BIO released. (C) Negative Control; aliquots of Laponite (single and multiple capsules) absent of BIO was added to assay medium and media recovered/analysed as previously described.

In both studies, media samples recovered were tested to determine BIO concentration using a Wnt reporter cell line as discussed in section 2.2.1.1.

2.2.3.5 Luciferase Data Analysis

Data were analysed using Microsoft Excel 2013 to calculate the response ratio (background divided by test reading) and graphs were generated using GraphPad Prism v6.6.2. Please refer to Appendix A for calculations and raw data.

The statistical analysis used on the test assay response ratio data was a two-way ANOVA (parametric). Sidak's multiple comparison test was used to calculate individual p values.

2.2.4 Release of VEGF by Laponite and Alginate Hydrogels

To assess the release of VEGF by Laponite and alginate hydrogels, an assay was performed to measure the release of VEGF encapsulated in Laponite and alginate into aqueous medium. To do this, VEGF was premixed with each biomaterial at a concentration of 40 µg/ml. 10 µl aliquots of biomaterial-VEGF were transferred into low-protein binding tubes (Eppendorf® LoBind) containing 90 µl assay diluent. Biomaterials containing no VEGF and media with aqueous VEGF added served as negative and positive controls respectively. Media was incubated at 37℃/5% CO_2 in humidified conditions and then recovered at various time points up to 3 weeks and stored at -20℃ until required for protein analysis.

To analyse the protein content from the supernatant recovered from biomaterial tubes, an enzyme-linked immunosorbent assay (ELISA) (R&D Systems, Abingdon, UK; product: DVE00) was performed. Manufacturer instructions were followed specifically *For Cell Culture Supernate Samples.*

2.2.5 Rheometry

2.2.5.1 Equipment and General Test Conditions

Rheological measurements for the biomaterial samples hydrated at 25°C and 37°C were performed using stress or strain controlled rheometer (Anton Paar, MCR 302, St Albans, UK) equipped with a parallel plate configuration (diameter 50 mm, gap 0.5 mm). Samples were applied on the rheometer stage with a spatula (enough to cover the stage) and equilibrated at 25 °C for 5 minutes before starting analysis. Data was recorded using the Rheoplus 32 software, version 3.62 (Anton Paar, Germany GmbH).

After loading and equilibrating gel samples on the rheometer stage, a 3-interval thixotropy test (3-ITT) was chosen within the software package (please refer to Appendix A.2 for background about 3-ITT).

2.3 *In vivo* Studies

2.3.1 Project Licence

All *in vivo* experiments were strictly performed in accordance to procedures outlined in Project Licence (PPL) 30/2971.

2.3.2 Subcutaneous VEGF-Biomaterial Angiogenesis Model

2.3.2.1 Animals

18 male MF1 mice (Biomedical Research Facility, University of Southampton) aged between 8-10 weeks old were used to investigate localisation of VEGF using Laponite hydrogels. All animals were bred and maintained at the Biomedical Research Facility, Southampton in a temperature controlled environment (20℃-22℃) with a 12-hour light/dark cycle (lights on at 06:00). Food and water was provided ad libitum both pre- and post-injection.

2.3.2.2 Subcutaneous VEGF-Biomaterial Treatments

VEGF-Laponite treatment: Mice were anesthetised using inhaled anaesthetic (isoflurane; product from Centaur, Castle Cary, UK) and the whole dorsal region shaved. On the left side of the dorsum, pre-prepared Laponite-VEGF hydrogels were administered subcutaneously at three separate locations (rostral to caudal) with three different VEGF doses (0.1, 1.0 and 4.0 µg total VEGF) ($n = 6$ mice). On the contralateral side 3 vehicle Laponite treatments were administered (negative control). A control biomaterial hydrogel, alginate was administered in the same way ($n = 3$ mice).

2.3.2.3 Tissue-Biomaterial Harvest

Mice were killed by CO_2 asphyxiation for 3-5 minutes followed by cervical dislocation. Biomaterial and surrounding cutaneous tissue was surgically removed after 21 days and fixed in 4% paraformaldehyde (PFA) (Thermo Fisher Scientific; product: 10131580) for 18 hours. Tissue samples were then transferred to 70%

ethanol (Thermo Fisher Scientific; product: 10437341) and kept in the fridge until required for processing.

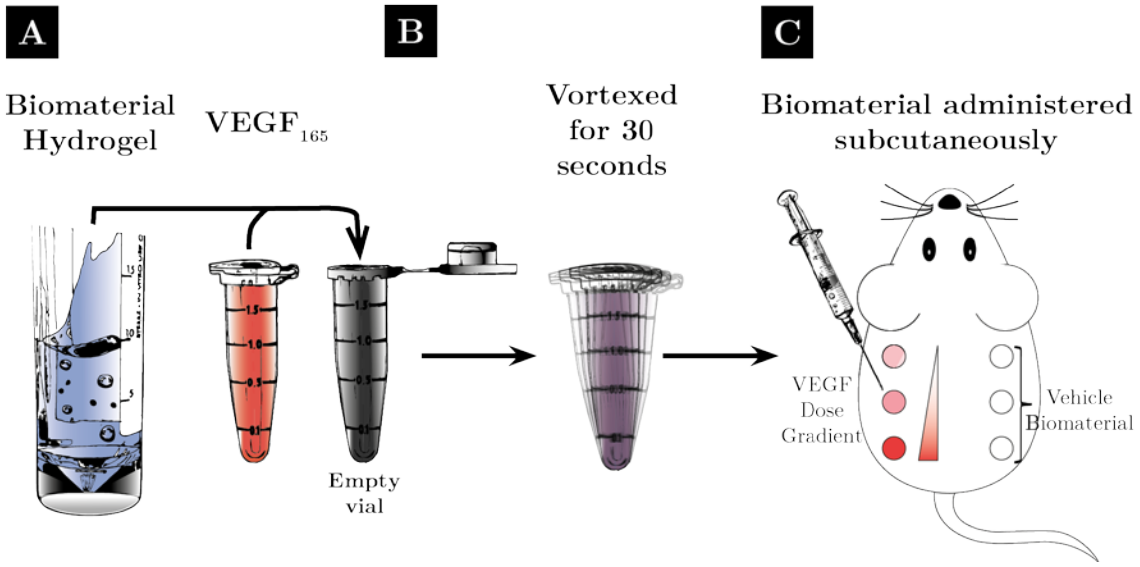

Figure 2.6. Subcutaneous VEGF-Biomaterial Injection Study. (A) Pre-prepared Laponite/alginate hydrogels are combined with VEGF and (B) mixed thoroughly. (C) VEGF-biomaterial suspensions are administered by subcutaneous injection using a 25G hypodermic needle on the dorsum of mice at 0.1, 1.0 and 4.0 µg VEGF doses. Contralaterally, biomaterial containing no VEGF (diluent added instead) serves as the vehicle control.

2.3.2.4 Macroscopic Angiogenic Scoring

Upon tissue harvest, photographs of each biomaterial treatment and dose were captured using a Nikon D3200 digital single-lens reflex (SLR) camera. A scaled ruler was present for all images captured. All images were then labelled (biomaterial treatment, VEGF concentration, time point). Using the *Measure* module within ImageJ, the assigned label was 'measured' using the *Batch* command in order to generate a list of all the image names with a corresponding number. This data was imported into Microsoft Excel (2016 version).

Within Excel, a column was inserted adjacent to the label data set. In the first cell of this column the *=RAND()* command was entered, and then copied into every cell; this command created a list of random numbers which then allowed

the label data set to be sorted to this random list. The images were then arranged on blank page (no label included). The sheets that contained these randomised images were used as the basis of a randomised blinded questionnaire used to measure the degree in which angiogenesis had occurred. Please refer to Appendix A.1 for a copy of the questionnaire that was designed for this study.

2.3.3 Experimental Wound Model

2.3.3.1 Animals

Healthy mice:

(1st Study): 12 male MF1 mice (Biomedical Research Facility, University of Southampton) aged between 8-10 weeks old were used to investigate the localisation and effect of Laponite hydrogels vs a saline control on normal wound healing. (2nd study): 18 male C57BL/6 mice (Biomedical Research Facility, University of Southampton) aged between 8-10 weeks old were used to investigate localisation of VEGF using Laponite hydrogels.

Diabetic mice:

21 male BKS. CG-+$Lepr^{db}$/+$Lepr^{db}$ mice (Envigo, Huntingdon, UK) aged between 8-10 weeks old were used to investigate localisation of VEGF using Laponite hydrogels.

All animals were bred and maintained at the Biomedical Research Facility, Southampton in a temperature controlled environment (20℃-22℃) with a 12-hour light/dark cycle (lights on at 06:00). Food and water was provided ad libitum both pre- and post-injection.

2.3.3.2 Wounding Procedure

General Procedure:

Mice were anesthetized intraperitoneally with 0.4 mg/kg fentanyl citrate and 12.5 mg/kg fluanisone (Hypnorm; VetaPharma Ltd, Leeds, UK; product: Vm41760/4000) and 12.5 mg/kg midazolam chloride (Hypnovel; Roche, Welwyn, UK; product: 10161105) (Figure 2.7 A, I). The whole dorsal region of mice was depilated (shaved followed by Nair™ hair removal cream) prior to wounding (Figure 2.7 A, II). Two areas on either side of the upper and lower dorsum were inked using a 6-mm diameter biopsy punch. Skin was excised using surgical scissors through all skin layers (full-thickness) to create a wound approximately 0.50cm^2 in size; this created a total of four symmetrical 6 mm wounds (two towards the rostral region and two towards the caudal region) (Figure 2.7 A, III). Following surgery, a Tegaderm™ dressing was applied over the dorsal region to cover all wounds (dressing was cut to size) (Figure 2.7 A, IV). Following the procedure, mice were transferred to a pre-warmed (25-30°C) incubator for 2-3 hours for recovery. Following this recovery period, they were removed to room temperature conditions for the remainder of the study. Dressings were changed at day 7 post-wounding using inhaled anaesthetic (isoflurane) and then subsequently changed as and when required.

Treatment groups:

db/db mice: Rostral left side wounds were treated with 50 µl Laponite hydrogel containing 40 µg/ml VEGF (2 µg total VEGF). Both rostral and caudal right-side wounds were treated with vehicle Laponite hydrogel (negative control). In a

separate treatment group, vehicle Laponite was treated to left side wounds and sterile PBS to right side wounds. All treatments were administered by injection underneath Tegaderm™ dressing using a 25G hypodermic needle (Figure 2.7 B).

Healthy mice:

(1st study): The same general procedure as *db/db* mice above but only two wounds were surgically created. Left side wounds were treated with 3% Laponite gels and right-side wounds with PBS control. (2nd study): The same general procedure as *db/db* mice but left side wounds were treated with 50 µl Laponite hydrogel containing 1 µg/ml VEGF. Right side wounds were treated with Laponite vehicle.

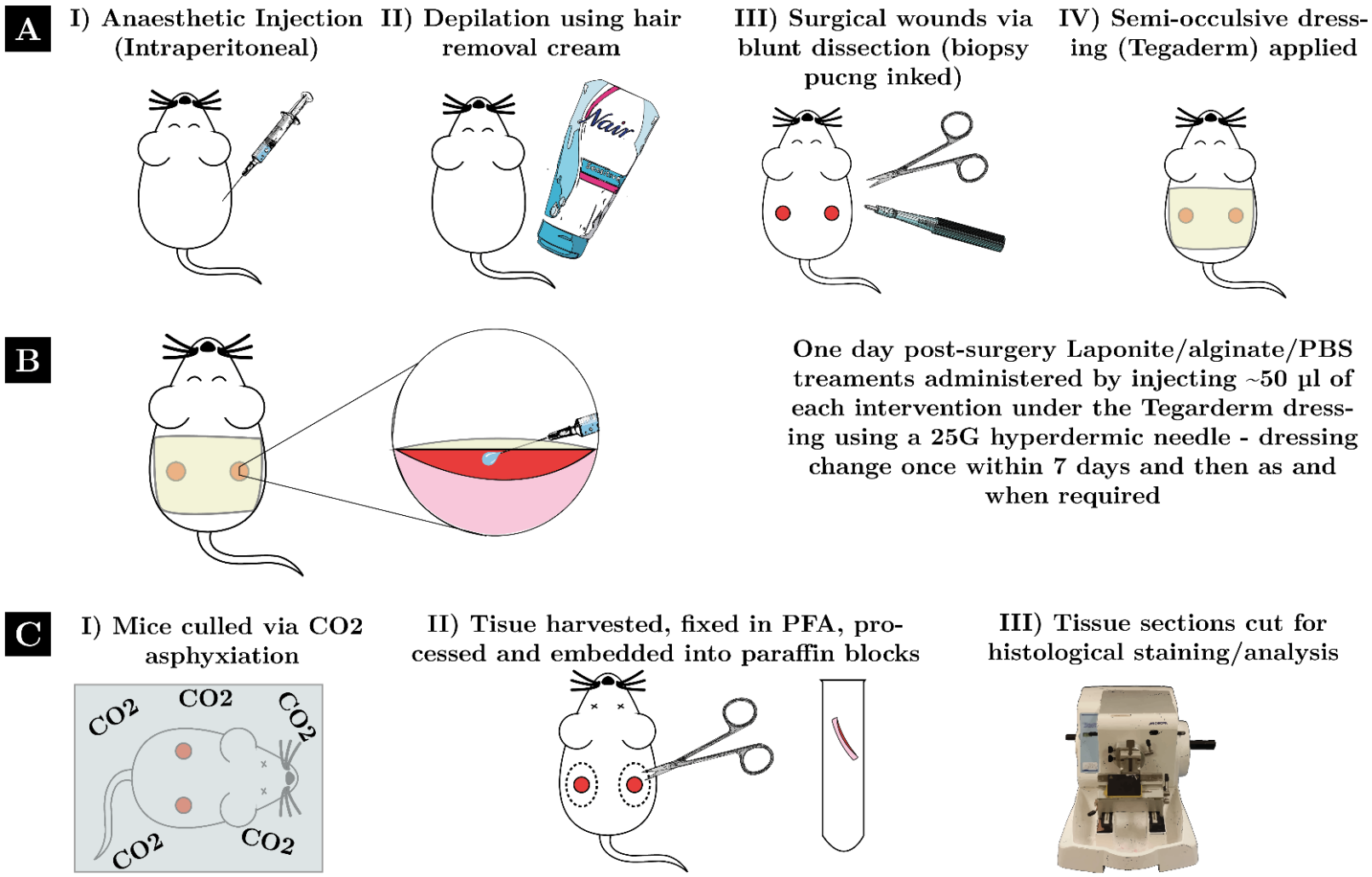

Figure 2.7. Illustration showing the protocol used for all the wound healing studies. Refer to main text for details (PBS = phosphate buffered saline; PFA = 4% paraformaldehyde).

2.3.4 Blood Glucose Measurements

Non-fasting and fasting blood glucose levels were measured using the Accu-Chek® Aviva Expert Bolus Advisor System (Roche, Burgess Hill, UK) and compatible Accu-Chek® Aviva testing strips (Roche; product: 317-1253). Blood samples were taken from the tail vein after pricking with a 25G needle whilst under anaesthetic.

2.3.5 Macroscopic Analysis of Wound Area and Closure Rates

Wound photographs were captured using a Nikon D3200 digital SLR camera and a GoPro Hero 4; a calibrated ruler was included for scaling purposes. To calculate wound area, captured images were analysed using Fiji ImageJ (version 1.50b). This involved setting a common scale by measuring the ruler scale within each image and using the *Analyse* function. The wound edge within each image was measured using the *Freehand selection tool* and wound area measured using the *Analyse* function.

The closure rate was then measured using the following calculation:

$$\% \text{ change of wound area from time } 0 = \frac{\text{area at } t_0 - \text{area at } t_x}{\text{area at } t_0} \times 100$$

Where: t_0 = area at time 0; t_x = specific time point

2.3.6 Tissue Harvest

Mice were killed by CO_2 asphyxiation for 3-5 minutes followed by cervical dislocation. Wound tissue was surgically removed, and fixed in 4 % PFA for 18

hours. Tissue samples were then transferred to 70% Ethanol and kept in the fridge until required for processing (Figure 2.7 C, I-II).

2.3.7 Histology

2.3.7.1 Sample Preparation and Sectioning

Cryo-Embedding and Sectioning: Fixed samples were washed in PBS prior to incubation with 30% sucrose (Sigma-Aldrich/Merck: product: S7903) in non-sterile PBS overnight at 4°C. The samples were then briefly washed in Optimal Cutting Temperature compound (OCT) (CellPath, Newtown, UK; product: KMA-0100-00A) to remove excess sucrose and then immersed with OCT in a cryo-mould. Cryo-moulds were placed into a solution of pre-cooled (-80°C) isopropanol (dry ice was added to isopropanol) to allow controlled sample freezing. Moulds were stored at -80°C until required for sectioning. Sequential sections were cut at 10 µm thickness using a cryotome (maintained at -25°C to -30°C) and mounted on charged glass slides and placed on a warming rack (37°C) for 30 minutes and then stored at -80°C.

OCT-Embedded Slide Staining Preparation: When required for histological and immunohistological staining, cryo-sections were thawed at room temperature for 10 minutes and washed in PBS for 10 minutes to remove OCT.

Paraffin Embedding and Sectioning: Fixed tissue samples were processed in a series of graded alcohols (70%-100%) and then cleared with Histoclear (National Diagnostics, Atlanta, USA; product: HS-200) before being embedded in paraffin wax (Thermo Fisher Scientific; product: 8002-74-2). The duration of time that tissue samples were processed in each solvent are listed in Table 2.1 below:

Processing Stage	**Solvent & Concentration**	**Time (Minutes)**
1	70% Ethanol	30
2	90% Ethanol	45
3	95% Ethanol	45
4	100% Ethanol	45
5	100% Ethanol	45
6	Histoclear	45
7	Histoclear	45
8	Molten Paraffin Wax	30
9	Molten Paraffin Wax	30
10	Molten Paraffin Wax Under Vacuum Conditions	30

Table 2.1. Stage of tissue processing prior to tissue embedding showing solvent type used and the duration.

After stage 10, individual tissue samples were embedded into blocks using an embedding machine.

Paraffin-Embedded Slide Staining Preparation: When required for histological and immunohistological staining, slides were deparaffinised in Histoclear (2 x 7 minutes) and then rehydrated by submerging slides in graded ethanols (100% to 50%) followed by running tap water (2 minutes each).

2.3.7.2 Haematoxylin and Eosin (H&E) Staining

Histological sections were deparaffinised and rehydrated (cryo-sections were incubated in PBS) as previously described (see page 74). Slides were then flooded with haematoxylin for 3 minutes and then washed in tap water for 5 minutes Haematoxylin was prepared by mixing Weigerts haematoxylin A and B solutions 1:1 (Haematoxylin A was prepared by adding haematoxylin powder (Thermo Fisher Scientific; product: H9627) to hydrochloric acid (HCl) (VWR, Leicester,

UK; product: 101256J) (1% w/v) and left to mature for 4 weeks at room temperature. Haematoxylin B was prepared by adding 1.2 % (w/v) iron(III) chloride ($FeCl_3$) powder (Sigma-Aldrich/Merck: product: 451649) and 1% (v/v) HCl to distilled water).

Slides were then treated 10 dips of acid alcohol for ~2 seconds per dip (1% (v/v) concentrated in 70% (v/v) ethanol) and then washed again in tap water for 2 minutes. Slides were then flooded with 1% Eosin Y (w/v) (Sigma-Aldrich/Merck; product: E4009) for 30-60 seconds and then washed in tap water for 2 minutes. Following this last water wash, tissue samples were dehydrated using graded alcohols (50%-100%) for 30 seconds each and then cleared in Histoclear. Slides were then mounted with coverslips using DPX mounting medium (Thermo Fisher; product: 10050080).

2.3.7.3 Diarylmethane Fluorescent Staining (Auramine O)

Histological sections were deparaffinised and rehydrated (cryo-sections were incubated in PBS) as previously described (see page 74). Slides were then flooded with pre-prepared Auramine O (Auramine O 0.3 g, phenol 3.0 g, distilled water 100 ml) (Sigma-Aldrich/Merck; product: 05151-1KT-F) for 15 minutes at room temperature in the dark. Excess Auramine O solution was discarded and slides washed in distilled water (2 x 2-minute washes). Slides were immediately mounted with coverslips using Fluoromount™ (Sigma-Aldrich/Merck; product: F4680-25ML) and sealed with nail varnish. Slides were stored in the dark until required for microscopy (note, that imaging was done within 3 days of staining due to poor stability of the stain.

2.3.7.4 Immunohistochemistry Staining

General Immunohistochemistry Method: Slide sections were deparaffinised/OCT removed as previously described on page 74. They were then submerged in distilled water for 2 minutes. Endogenous peroxidase activity was blocked using 0.3% H_2O_2 (Sigma-Aldrich/Merck; product: H1009)) in absolute methanol (Thermo Fisher Scientific; product: 10284580) and then rinsed with wash buffer (0.05% Tween 20 in PBS) 3 times for 2 minutes each. The appropriate antigen retrieval method was then performed (refer below for details of antigen retrieval methods). Sections were then washed in wash buffer for 5 minutes, drained and then incubated with normal goat serum (Vector Laboratories, Peterborough, UK; product: PK-6101) (blocking step) for 20 minutes at room temperature. Slides were then washed in wash buffer 3 times, 2 minutes each. Sections were then incubated with avidin solution (Vector Laboratories; product: SP-2001) for 20 minutes at room temperature. Slides were then washed in wash buffer 3 times, 2 minutes each. Sections were then incubated with biotin solution (Vector Laboratories; product: SP-2001) for 20 minutes at room temperature. Slides were then washed in wash buffer 3 times, 2 minutes each. Sections were incubated with the appropriate primary antibodies (see below for details and dilutions) for 12-18 hours at 4°C. Slides were washed in wash buffer 3 times, 5 minutes each and then incubated with the appropriate secondary antibody for 30 minutes at room temperature. This was followed by 3 x 5-minute washes with wash buffer. Then, VECTASTAIN *Elite* ABC reagent (Vector Laboratories; product: SP-2001) was applied to sections following manufacturer's instructions and incubated for 30 minutes at room temperature. Slides sections were then washed in wash buffer 3 times, 5 minutes each and then submerged with distilled water. 3,3'-diaminobenzidine (DAB) chromogen substrate (Steady DAB/Plus)

(Abcam, Cambridge, UK; product: ab103723) was prepared as described by the manufacturer's instructions and was added to sections; the formation of the reddish-brown precipitate linked between DAB and peroxidase activity was visualised (up to 5 minutes). Negative controls (omission of the primary antisera) were included in all immunohistochemistry procedures; no staining was observed in all negative control sections. Following DAB reaction, sections were washed in deionised water. Following this last water wash, sections were dehydrated using graded alcohols (50%-100%) for 30 seconds each and then cleared in Histoclear. Slides were then mounted with coverslips using DPX mounting medium.

Anti-CD31 (for OCT sections, used in Chapter 4.2.3.4): The endothelial cell marker, anti-CD31, was chosen to identify blood vessel structures within cryo-sectioned tissue sections. A rat detection kit for anti-mouse CD31 (MenaPath, Menarini Diagnostics, Winnersh, UK; product: MP-517-RTK6) was used in combination with an anti-CD31 antibody (rat monoclonal, MenaPath, Menarini Diagnostics, product: MP-303-CM01) following manufacturer's instructions with minor modifications:

Following removal of OCT described previously, slide sections were submerged in distilled water for 2 minutes. Endogenous peroxidase activity was blocked using MenaPath Peroxide Block for 5 minutes and then rinsed with wash buffer (0.05% Tween 20 in PBS). Sections were then incubated with Mouse Background Blocker for 30 minutes at room temperature and then rinsed with wash buffer. Sections were then incubated with an anti-CD31 primary antibody (1:100 dilution) at 4°C overnight. This was followed by two 3-minute washes in wash buffer. Sections were then incubated at room temperature with the Rat Probe for 15 minutes, followed by two 3-minute washes in wash buffer. Sections were then treated with

Rat-on-Mouse Horseradish peroxidase (HRP) Polymer for 15 minutes at room temperature followed by two 3-minute washes in wash buffer. 3,3'-diaminobenzidine (DAB) Chromagen substrate from the MenaPath kit (1 drop/ml deionised water) was added to sections and the formation of the reddish-brown precipitate linked between DAB and peroxidase activity was visualised (up to 5 minutes). Refer to *General Immunohistochemistry Method* on page 77 for remaining steps.

Anti-CD31 (for paraffin sections, used in Chapter 4.2.3.6): Please refer to *General Immunohistochemistry Method* section on page 77 for general staining protocol. Please find below a list of deviations/additions to this protocol that was specific to this antibody stain:

Antigen retrieval: Proteinase K (QIAGE, Hilden, Germany; product: 19133) was diluted in TE-$CaCl_2$ buffer (50 mM Tris Base, 1 mM EDTA, 5 mM $CaCl_2$, 0.5% Triton X-100, adjusted to pH 8.0) to form 20 µg/ml concentration. Slide sections were covered and incubated with proteinase K-TE-$CaCl_2$ buffer solution for 20 minutes at 37°C in a humidified chamber. Sections were then allowed to cool at room temperature for 10 minutes prior to washing off the proteinase K-TE-$CaCl_2$ buffer solution. Slide sections were then washed in wash buffer 3 times, 2 minutes each and then proceeded with next steps outlined in the *General Immunohistochemistry Method* section on page 77.

Primary antibody: Anti-CD31 (Abcam; product: ab56299, 1:100 dilution) was applied at the primary antibody step.

Secondary antibody: Goat F(ab')2 Anti-Rat IgG H&L Biotin (Abcam; product: ab98357, 1:500 dilution) was applied at the secondary antibody step.

Anti-Ki67 (proliferation marker): Please refer to *General Immunohistochemistry Method* section on page 77 for general staining protocol. Please find below a list of deviations/additions to this protocol that was specific to this antibody stain:

Antigen retrieval: Slide sections were immersed in sodium citrate buffer (10 mM sodium citrate, 0.05% Tween 20 and adjusted to pH 6.0) that had been pre-heated to 95-100°C. Sections were incubated at this temperature for 30 minutes and then removed from the heat and cooled at room temperature for 20 minutes. Slide sections were then washed in wash buffer 3 times, 2 minutes each and then proceeded with next steps outlined in the *General Immunohistochemistry Method* section on page 77.

Primary antibody: Anti-Ki67 (Abcam; product: ab15580; 1:500 dilution) was applied at the primary antibody step.

Secondary antibody: Goat Anti-Rabbit IgG biotinylated from the VECTASTAIN Elite ABC kit (Vector Laboratories, SP-2001, 1:500 dilution) was applied at the secondary antibody step.

Anti-Myeloperoxidase (anti-MPO; neutrophil marker): Please refer to *General Immunohistochemistry Method* section on page 77 for general staining protocol. Please find below a list of deviations/additions to this protocol that was specific to this antibody stain:

Antigen retrieval: Applied the same antigen retrieval method that was used for anti-Ki-67 staining (see page 80)

Primary antibody: Anti-MPO (Abcam; product: ab9535; 1:100 dilution) was applied at the primary antibody step.

Secondary antibody: Applied the same secondary antibody (and dilution factor) that was used for anti-Ki-67 staining (see page 80).

2.3.8 Microscopy

2.3.8.1 Standard Microscopy

General: Cell/histological samples were imaged using the Carl Zeiss AxioVert 200 inverted fluorescence microscope. The capture software used was AxioVision (ver. 4.9.1); images saved as a .zvi file format with a pixel size of 1388 x 1040 (16-bit).

Cell imaging: Images of cells were captured using Fluar 5.0x/0.12 objective, HAL 100 halogen illuminator as the light source transmitted via Bright-field. The capture device used was an AxioCam MRm (monochromatic) camera.

Fluorescent histological sections (Auramine O): Images of cells were captured using Fluar 2.5x-20x objectives (sample dependent), a wide-field fluorescence excitation light source (X-Cite® 120Q, Excelitas Technologies, Southampton, UK) and a AxioCam HR (colour) camera. Please refer to Table 2.2 for the fluorescent filter sets used with all relevant spectra information.

Spectra Information	**Filter Set**	
	2	**16**
Excitation (nm)	G 365	BP 485/20
Beam splitter (nm)	FT 395	FT 510
Emission (nm)	LP 420	LP 515
Assigned identifer (fluorophore)	DAPI	FITC

Table 2.2. Filter set spectra information.

2.3.8.2 dotSlide Virtual Slide Microscopy

Histological sections were imaged using the Olympus BX 51 dotSlide virtual slide microscope system (Olympus Life Science, Southend-on-Sea, UK). Captured images were extracted and analysed using Fuji ImageJ v1.50b, BIOP PT VSI plugin and Olympus Virtual Slide Desktop 2.4 software.

2.3.9 Analysis of CD31 Staining by Chalkley Count

The Chalkley point-overlap morphometric technique (more simply referred to as "Chalkley method") is a relative area estimate method to measure the abundance of microvessels in a immunohistochemical sample [256, 257]. It works in accordance to the theoretical assumptions of systematic random sampling and has eliminated many of the problems associated with blood microvessel counting. More specifically, it removes the decision for an observer to define adjacent structures as single or two separate blood vessels. In a cross-sectional histology sample this can be difficult to define as it relies on counting structures in 2D rather than considering their existence in a 3D system [258].

Conventionally this analysis requires the use of a "Chalkley point array graticule" which is a fitted onto the eyepiece of a microscope. This graticule consists of a grid that contain 25 random dots which can be rotated 360°. An observer can then overlay these dots over structures that have stained positively with a blood vessel marker (e.g. anti-CD31). The rotational position with the most dots that land on positively stained structures is described as the 'Chalkley count' and

samples that have higher counts are considered to contain a greater abundance of blood vessels [258].

More recently, this method has been adapted on digital images of histological sections stained with a blood vessel marker by using a digital "Chalkley point array graticule overlay" [259]. This author managed to automate the process of counting using this method, although the use of this automation was not freely available.

Therefore, the idea of a digital Chalkley overlay was adopted and manual counting (akin to conventional Chalkley counting) was used instead. A digital Chalkley grid overlay was applied to a x20 magnification image at 3-5 different "hot-spot" regions (Figure 2.8).

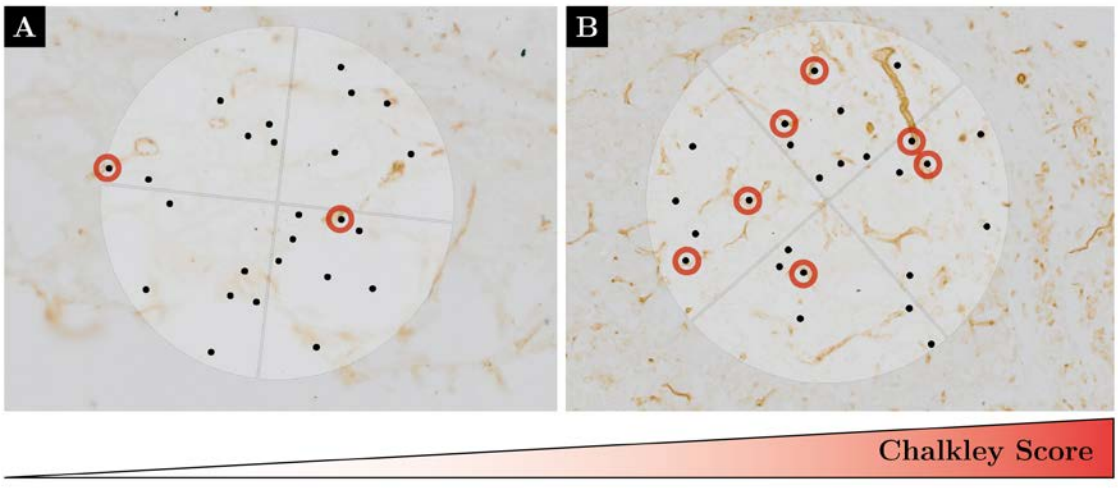

Figure 2.8. Quantification of blood vessel example by Chalkley count using a digital overlay. A digital grid that contained 25 random dots was aligned in 3-5 "hotspot" ROIs (areas that harbour the most vessels in the sample tissue). The digital grid was rotated until the maximum number of dots land on positively stained vessels. The left panel (A) shows an example of a low Chalkley count (n=2) and the right panel (B) an example of a high count (n=7) (shown by the red circles).

Counts of these 3-5 regions that landed on the most positively stained structures through rotating the digital overlay were averaged. An example of a high Chalkley count is shown in Figure 2.8 A and a low count in in Figure 2.8 B.

2.3.10 Measurement of Wound Closure and Rate of Re-epithelisation Using Histological Samples

H&E-stained tissue sections scanned by the dotSlide microscope were used to measure the thickness of the wound epithelium. Images were imported within the Olympus Virtual Slide Desktop 2.4 software. Within the *Measure→Measurement and ROI* window, the *Arbitrary* line or *Polyline* tool was selected. Using *Arbitrary* line tool, the length of the defect was measured from the edge of the wound margin, left to right (black arrow, Figure 2.9). Using either *Arbitrary* line or *Polyline* tool, the length of epithelisation was then measured (the length of both sides were combined when full re-epithelisation had not occurred) (blue arrows, Figure 2.9). The size of the remaining defect (minus the closure by re-epithelisation) was measured from edge-to-edge of the migrating epithelium (white arrow, Figure 2.9).

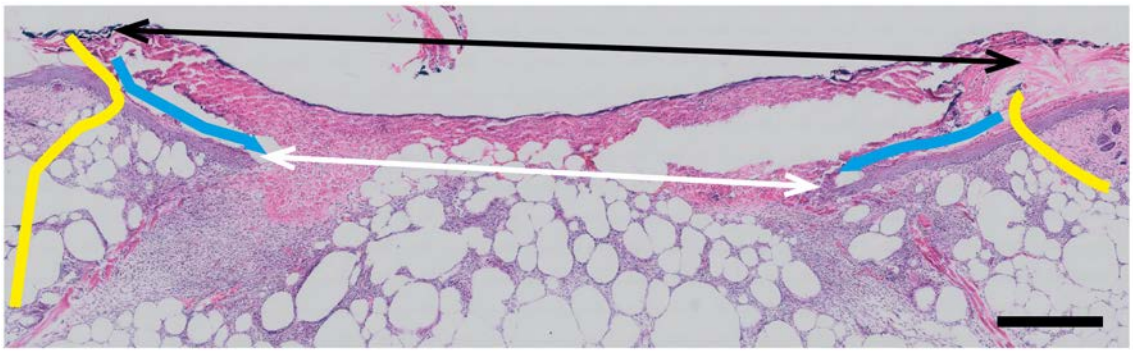

Figure 2.9. An example of how wound measurement data was collected. Yellow lines = wound edge/margin; Black arrow = total defect size; Blue arrows = length of epithelial migration; White arrow = Current defect size. Scale bar = 500 µm. See main text for details.

Histology wound closure rate calculation:

To calculate the change in wound closure rates as a percentage from day 0, the following calculation was used:

$$\frac{dt_0 - dt_x}{dt_0} \times 100$$

Where: dt_0 = average defect size at day 0*;*

dt_x = average remaining defect size at specific time

% re-epithelisation rate calculation:

To calculate the rate of re-epithelisation as a percentage increase, this calculation was used:

$$\frac{ODt_x}{Ept_x} \times 100$$

Where: ODt_x = length of the defect measured from the edge of the wound margin;

Ept_x = total length of epithelium

2.3.11 Analysis of Wound Epithelial Thickness

DotSlide-scanned images were imported and measurement tool selected as described in 2.3.10. Using *Arbitrary* line tool, the epithelial thickness was measured by drawing a perpendicular line from the surface to the bottom of the epithelium. The number of thickness measurements that were taken across the epithelium was governed by the total length of epithelial tissue present. This number of measurement points were defined as follows: ≤ 1 mm: 3 points; 1-2 mm: 4 points; 2-3 mm: 5 points and > 4 mm 6 points (please refer to the

subchapter 2.3.10 above for the details on how the length of epithelium was measured).

2.3.12 Analysis of Cellularity

H&E-stained image samples were imported into a free open-source software program called Orbit Image Analysis (revision 2.67; http://www.orbit.bio/download/). This software was used to isolate/segment haematoxylin-stained (nucleated) cells and measure and compare the % area of pixels. Please refer to Appendix A.3 for software configuration settings.

2.3.13 Statistical Analysis

A one-way analysis of variance (ANOVA) (parametric) was used for statistical analysis of blood glucose level data and mouse weight data Tukey's multiple comparison test was used to determine individual p values. A two-way ANOVA (parametric) was used for statistical analysis of wound closure rate data and Tukey's multiple comparison test was used to determine individual p values. A student's t-test (unpaired) was used for statistical analysis of CD31 staining data.

Chapter 3:

Delivery of Bioactive Factors Using Laponite Hydrogels: An *In Vitro* Approach

3.1 Introduction

The biocompatibility, hydrophilicity and ability for rapid diffusion of molecules makes hydrogels exceptional candidates for drug delivery in the field of regenerative medicine. Their highly porous structure can be tailored to mimic three-dimensional matrices that are found in nature (e.g. extracellular matrix) whilst being able to associate with bioactive molecules that can be used for cell signalling and proliferation (as explained in Chapter 1.6). Although the hydrophilic nature of hydrogels can be a useful platform for drug delivery it also can be a hindrance. The most common limitations are: poor retention of bioactive molecules, low tensile strength and restrictive assembly and cross-linking of gels for site-specific treatments [260];

The poor retention of biomolecules is associated with the high-water content and large pore size of many hydrogel systems [236]. This can result in the undesirable and rapid release of biomolecules that remain active for short periods of time (e.g. hours or days). This can also be further exacerbated if the biomolecules being loaded are hydrophobic, thus relying on more complex hydrogel systems to ensure controlled release [261, 262]. Rapid diffusion can be particularly problematic for therapies that require sustained and localised delivery of bioactive molecules, such as topical or injectable-based administration routes. This is applicable for DFU treatments as the simplest and most effective methods are using a topical route such as a cream/gel or advance [132, 263, 264]. Thus, sustained and controlled delivery within the local wound environment via these delivery methods is essential [10].

Recent drug delivery hydrogel systems have tried to reduce these limitations and improve their drug delivery capabilities by creating more advanced formulations (refer to Chapter 1.7.2). This can create drug delivery systems that are overly-complex and difficult to implement when applied clinically, for example many crosslinking parameters can require specific conditions (e.g. UV, chemical, time and temperature-based). Furthermore, most systems attempt to control the release of biomolecules which can be challenging to translate and measure *in vivo* due to the complexities of a biological environment (refer to Chapter 1.7.2).

An alternative approach would be to use a simple system that also exhibits all the positive properties of conventional hydrogels. There has been recent interest in clay minerals as vectors for drug delivery. Certain cationic clays have shown the ability to adsorb biologically active molecules through ionic, hydrogen and Van der Waal interactions between molecules and charged clay particles. They are typically used within the pharmaceutical industry as excipients or active molecules to help improve drug delivery formulations [265].

As mentioned in Chapter 1.7.1.1 Laponite, a synthetic smectite that can form highly pure dispersions in water at low concentrations. Laponite's nano-sized particles exhibit a permanent surface negative charge due to cationic substitutions within the metal cation structural layer. They also harness a pH-dependent rim charge that can allow for self-organisation between particles (face-edge interactions) and formation of a gel network that offers great porosity and reversibility [14] (refer to Chapter 1.7.2.4).

Dawson *et al* [235] demonstrated the *in situ* self-assembling ability of Laponite via shear force (thixotropy) and the addition of physiological saline. They also demonstrated the rapid adsorption and sustained retention of proangiogenic

VEGF that was biologically active in both *in vitro* and *in vivo*. To show VEGF-Laponite interaction and bioavailability *in vitro*, they assayed 2D tubule formation of HUVECs exposed to VEGF that was tethered to Laponite dispersions.

Currently, most bioactive molecules that are associated with cationic clays for regenerative strategies involve clay-protein interactions. This is largely because the charge structure of proteins and peptides exhibit a dynamic array of potential interaction sites with cationic clays as previously mentioned [14]. In contrast, less is known whether smaller bioactive molecules of low molecular weight, can associate with cationic clays for cellular manipulation.

As a potential therapy for wound healing, stimulation of the Wnt signal cascade is of interest as it has been shown to increase the potential of wounds recovering via regeneration (e.g. control of stem cell turnover, stimulates cell proliferation) [136]. However, augmenting this signal cascade is controversial as it has been shown to exert serious side-effects. Thus, delivery in a localised or slow release form would be required for effective utilisation by stem cells present within the wound environment [136, 266].

The eventual aim is to use Laponite as a vehicle to localise bioactive factors to chronic skin wounds and increase the rate and degree of wound healing. Based on what has been discussed above, there is limited knowledge within the literature that defines the potential of Laponite to incorporate bioactive factors (as opposed to surface adsorption) as a method to 'deliver' them to a defect of interest. Seeing that previous work has successfully delivered surface-bound VEGF *in vitro* [235], it seems logical to investigate this further with regards to delivery of incorporated VEGF. In contrast, current knowledge on retention of small molecules is poorly

understood, often requiring complex hydrogel systems and would be another interesting avenue to investigate [260, 267].

Seeing that agonists of Wnt signalling with low molecular weights have been discovered [254, 268], it was decided that investigating the potential retention and delivery of said molecules by Laponite gels would be suitable option. A viable candidate is 6-bromoindirubin-3'-oxime (BIO); it is a potent, reversible and ATP-competitive inhibitor for GSK-3α/β that inhibits the β-catenin destruction complex from instructing the proteasomal degradation of β-catenin during Wnt signalling (refer to Chapter 1.6.2 for details). It has a molecular mass of 356.17 g/mol, which by comparison with a protein such as $VEGF_{165}$, is approximately 126-times smaller in mass (refer to Chapters 1.6.2 2.2.3 for details).

Therefore, it is hypothesised that Laponite will deliver bioactive factors (VEGF and BIO) when premixed into 3% gels. Delivery of VEGF using this approach will predictably require much greater concentration of VEGF then surface bound as previously documented by Dawson *et al* [235]. Regarding small molecule interaction, it is hypnotised that Laponite will be able to retain BIO as well as allowing adsorption over a suitable time frame.

To test the above set of hypotheses, a set of studies were carried out. These included:

a) Testing the retention of and bioactivity of premixed VEGF to stimulate *in vitro* 2D tube formation of human umbilical vein endothelial cells (HUVECs).

b) Testing the retention and release of small molecule agonists of Wnt signalling (BIO) by measuring:
   i) The release of BIO from Laponite gels overtime using a Luciferase reporter system
   ii) The uptake of BIO from exogenous media to Laponite gels using a Luciferase reporter system.

c) Testing the thixotropic properties of 3% Laponite gels using a rheological 3-interval thixotropy test (3-ITT).

3.2 2D HUVEC Tubule Assay Results

The formation of HUVEC tubules *in vitro* is a well-documented method of assessing the response to proangiogenic biomolecules (refer to Chapter 2.2.1.2). In brief, endothelial cells form tube-like structures that link with adjacent cells creating a 'network'. Tubule formation can be stimulated with the addition of proangiogenic factors like VEGF and FGF2. Thus, if there is a more extensive network between cells (i.e. more tubules) in the presence of a proangiogenic growth factor (either aqueously in growth medium or within the growth surface) compare to a control it can be deduced that the growth factor has had a stimulatory effect.

3.2.1.1 Tubule Network Identification and Analysis

Phase contrast images were captured and the tubule network analysed with a software using image analysis software (refer to Chapter 2.2.1.3). Individual HUVECs (Figure 3.1 A, black arrows) with extensions that linked with adjacent cells to form a continuous network between many cells (Figure 3.1 A, purple arrows). These have been successfully identified with image analysis software, depicted by different coloured interconnecting lines that correspond to a specific aspect of a network (Figure 3.1 B).

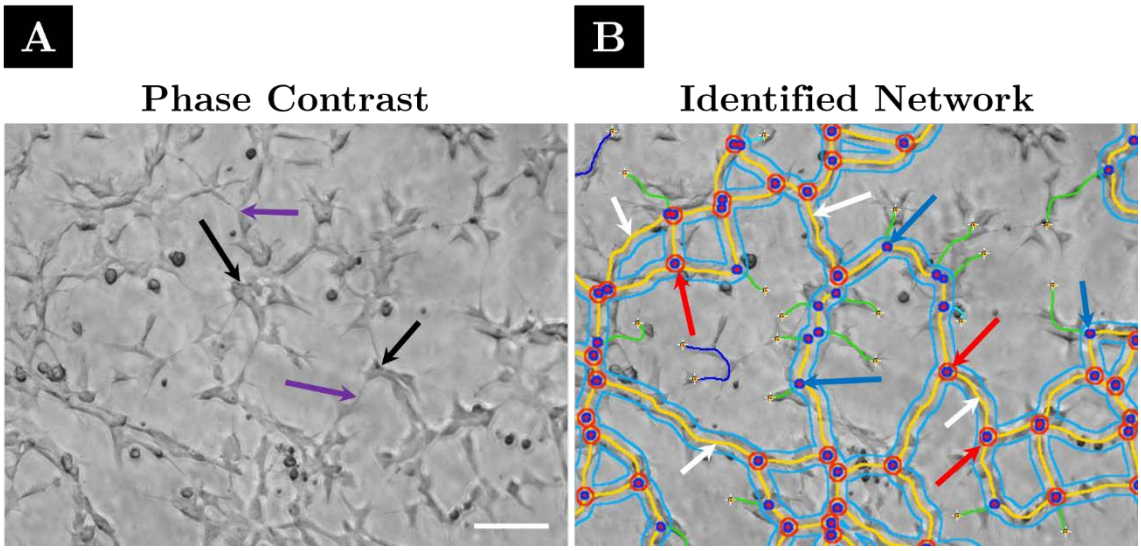

Figure 3.1. Identified HUVEC Tubule Network by Image Analysis. (A) Image shows HUVECs cultured with 0.04 µg/ml VEGF in aqueous growth medium. Original phase contrast image shows individual HUVECs (black arrows) and tube extensions formed between adjacent cells (purple arrows). (B) Identified network using ImageJ 'Angiogenesis Analyser' plugin. Yellow lines depict 'master segments of a continuous network (white arrows), with junctions ('nodes) between cells identified by a red dot surrounded by blue circle (blue arrows). 'Master junctions' are 'nodes' surrounded by a red circle; these are major junction points that link 3 or more 'master segments' (red arrows). Green lines depict branch points of the network with terminal ends (extremities) and the light blue lines that surround 'master segments' are defined as mesh regions ('loops' of a network). Scale bars = 200 µm.

Yellow lines identify the 'master segments', which are the regions of a continuous tube network that link adjacent cells together (white arrows). The junction points, or 'nodes', are identified by pixels that have at least 3 neighbouring pixels. These are shown as a red dot surrounded by blue circle (blue arrows). Nodes that form as part of a 'master junction' are surrounded by a red circle (red arrows), 'master junctions' are defined as regions that link 3 or more 'master segments'. Green lines indicate 'terminal branching points' of the network and blue lines are isolated elements that are not part of a network (e.g. individual cells that are not connected with another cell). Light blue lines that surround 'master segments' (black arrows) are mesh regions that can determine 'loops' within a network.

Identified network regions can be quantitatively measured by the number of pixels covered. All quantitative measurements reported in this subchapter are as 'mean

tubule branching points'. This measured the total number of pixels of 'master segments' and 'terminal branching points' of identified tubule networks (excluded isolated regions).

3.2.2 Effect of VEGF Concentration on HUVEC Tubule Formation

To confirm that 3% Laponite hydrogel surfaces can be used to successfully culture HUVECs and assess tubule formation, cells were seeded in the presence of different concentrations of VEGF premixed within growth medium.

An increase in tubule network organisation was present with HUVECs grown in all VEGF concentrations (0.01, 0.02, 0.04 and 0.100 µg/ml) when compared to the no VEGF control group (Figure 3.2). Quantitative analysis of identified networks determined that the response to 0.01 and 0.02 µg/ml VEGF was similar (0.01 µg/ml mean branch pixels was 10966 ± 2248 pixels, 0.02 µg/ml mean branch pixels was 11223 ± 2287; Figure 3.3 A); however, only 0.02 µg/ml VEGF was statistically greater than the no VEGF control, with a 276 ± 48 % increase in identified HUVEC tubule network (Figure 3.3 B and C, $p = < 0.05$, error = standard deviation (SD)). An even greater tubule network was established at the highest VEGF concentrations (0.04 and 0.1 µg/ml) with an increase of 432 ± 59 % and 472 ± 171 % mean tubule branching length respectively (Figure 3.3 B and C, $p = < 0.0001$, error = SD).

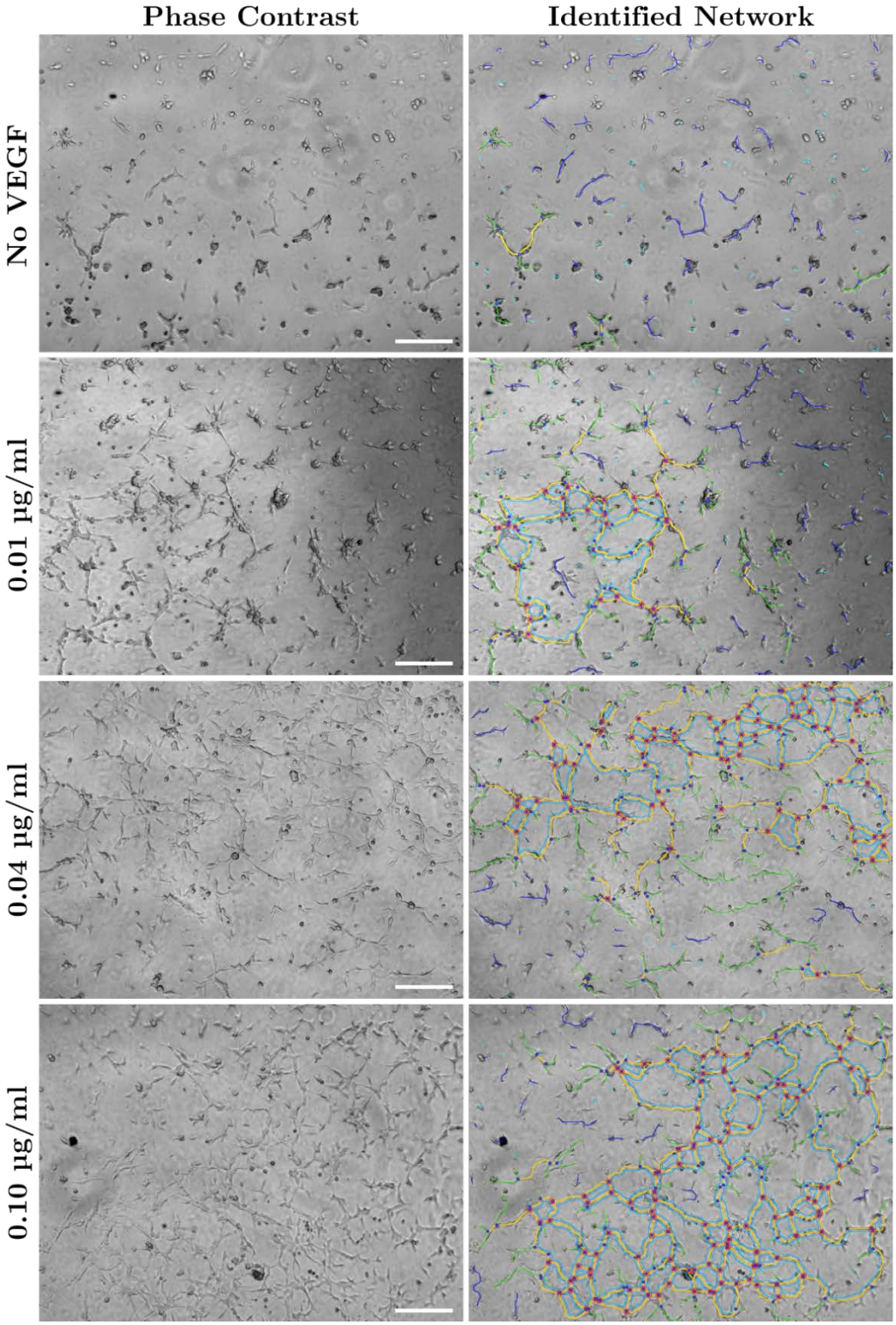

Figure 3.2. 2D tubule formation of human vein endothelial cells (HUVECs) on Laponite hydrogels cultured using different VEGF aqueous concentrations. Image analysis showing that increasing concentrations of VEGF mixed with growth medium can stimulate tubule formation between adjacent HUVECs. Formation of tubes were similarly present at 0.01 µg/ml and 0.02 µg/ml VEGF concentrations. A more defined network was established when HUVECs, were grown the highest VEGF concentrations (0.04 µg/ml and 0.10 µg/ml). Scale bars = 500 µm.

A

Descriptive Statistics			
Group Statistics			
VEGF Test Group	*n*	Mean & SD (Pixels)	95% CI (Pixels)
No VEGF	3	2984 ± 1548	-861 - 6828
0.01 µg	2	10966 ± 2248	-9229 - 31160
0.02 µg	2	11223 ± 2287	-9327 - 31773
0.04 µg	3	15866 ± 2464	9745 - 21986
0.10 µg	3	17062 ± 4196	6638 - 27468

B

Descriptive Statistics					
Differences Between VEGF Groups and No VEGF Control					
VEGF Test Group	Mean & SE (Pixels)		95% CI (Pixels)	% Difference	*p*
0.01 µg	7982	2046	52 - 16016	267	ns
0.02 µg	8239	2046	205 - 16274	276	0.0411
0.04 µg	12882	1830	5696 - 20068	432	< 0.0001
0.10 µg	14078	1830	6892 - 21264	472	< 0.0001

C

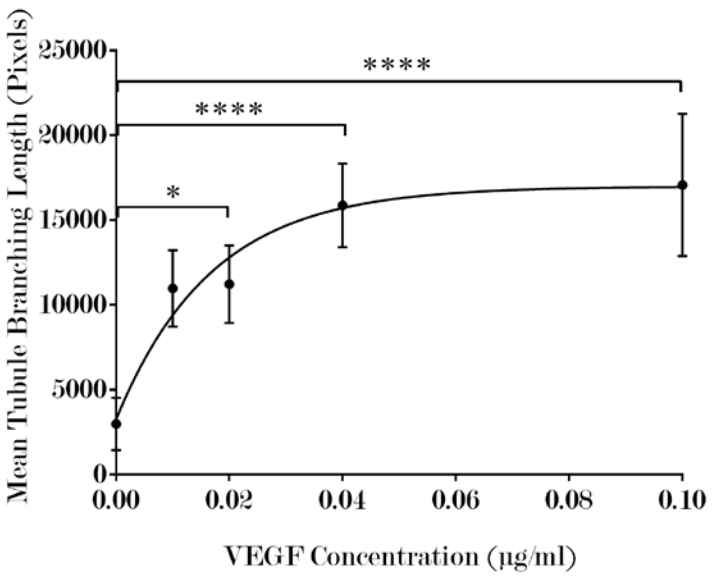

Figure 3.3. Quantitative analysis of HUVEC 2D tubule formation on Laponite hydrogels in response to VEGF growth media. (A) The total network length was quantified by total pixel number and the mean, standard deviation (SD) and confidence interval (CI) calculated. The mean difference between groups were calculated stating exact p numbers. (B) Comparison of the mean tubule branch length between different VEGF concentrations showed that there was a significant increase in tubule formation in all groups, except 0.01 µg/ml. 0.04 µg/ml and 0.100 µg/ml VEGF stimulated the most significant increase in mean tubule branching length (432% and 472%). (C) Quantitative data shown graphically with relevant statistical significance. Error bars = SD, n = 2/3 (an n of 4 was used but some of the Laponite surfaces were damaged and HUVEC networks disrupted - these could not be included), one-way ANOVA analysis performed with Tukey's post-hoc test applied for multiple comparisons; * denotes < 0.05; **** denotes p = < 0.0001.

3.2.3 Localisation of Bioactive VEGF by Adsorption to Laponite Hydrogels

Results showed an increased organisation of tube networks in the VEGF "bound" group when compared to HUVECs grown on Laponite with no VEGF (Figure 3.4). Quantitative data confirmed there was significantly greater tubule network in the Laponite-"bound" VEGF group than the no VEGF group (Figure 3.5 A & B). The extent of the tubule network in the Laponite-"bound" group was significantly different, like VEGF that was available to HUVECs in the media (1827 $\pm$ 1866 pixel difference, $p = < 0.49$, error = SD). These results further highlight that 3% Laponite hydrogels can associate with VEGF effectively and localise it in an active form *in vitro*.

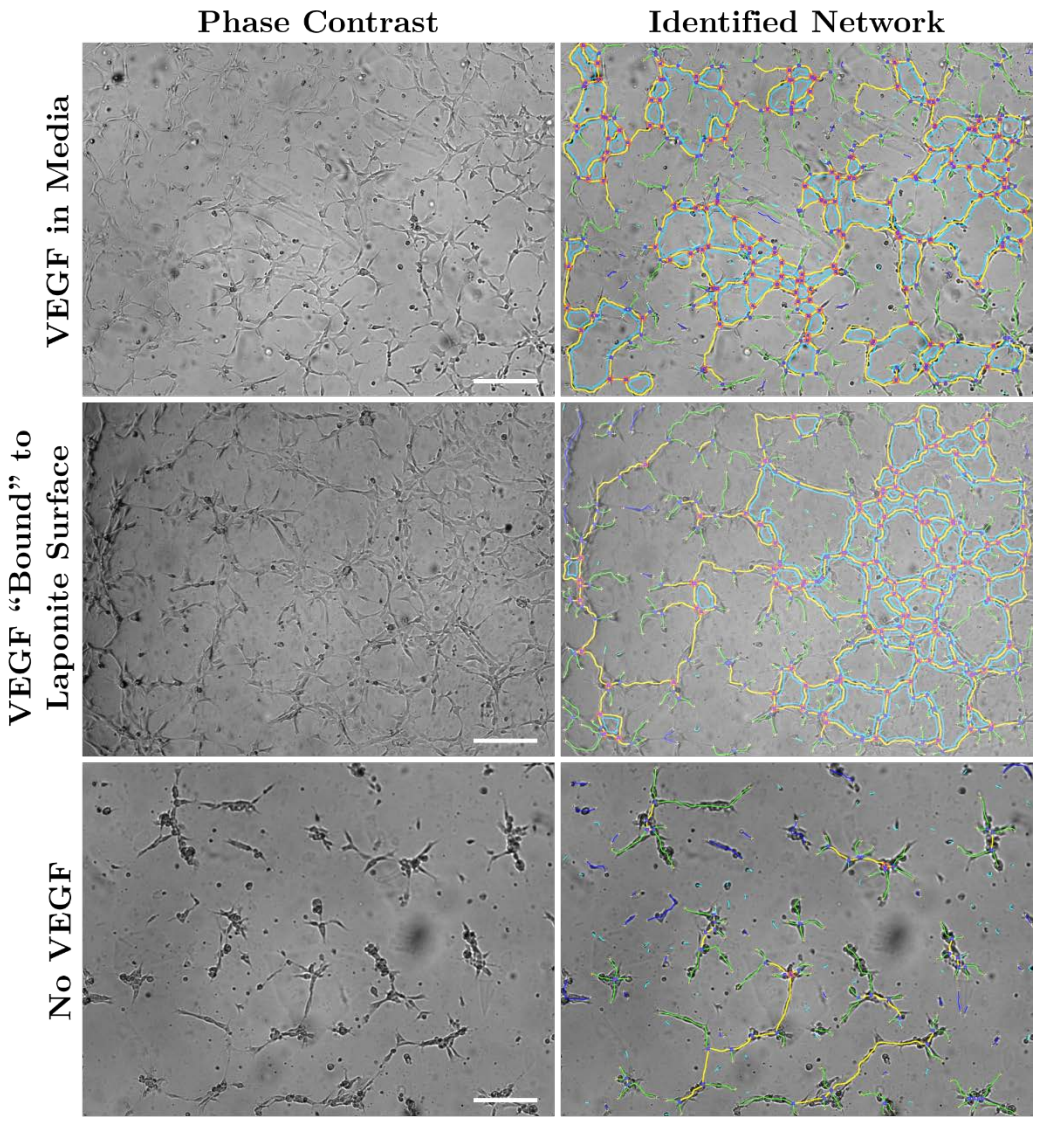

Figure 3.4. 2D tubule formation of human vein endothelial cells (HUVECs) on Laponite hydrogels in different VEGF conditions. Image analysis showing that VEGF "bound" to 3% Laponite surfaces (VEGF in aqueous medium pre-incubated with Laponite for 2 hours and washed) exhibited similar tubule network formation to VEGF that was present in aqueous medium. Scale bars = 500 µm.

A

Descriptive Statistics

Group Statistics				Differences Between Groups				
VEGF Test Group	*n*	Mean & SD (Pixels)	95% CI (Pixels)	VEGF Test Group	Mean & SE (Pixels)	95% CI (Pixels)	% Diff	*p*
VEGF "Bound" to Laponite	6	16271 ± 2668	13470 - 19071	VEGF in Media - No VEGF	11781 ± 1573	7684 - 15868	186	<0.0001
No VEGF	6	6317 ± 1176	5083 - 7551	VEGF "Bound" to Laponite - No VEGF	9954 ± 1573	5866 - 14041	158	<0.0001
VEGF in Media	6	18098 ± 3712	14202 - 21994	VEGF in Media - VEGF "Bound" to Laponite	1827 ± 1573	-2260 - 5914	11	0.4931

B

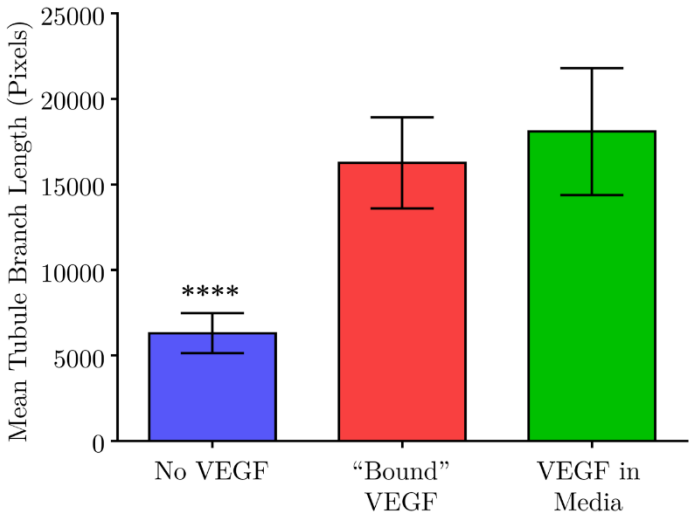

Figure 3.5. Quantitative analysis of HUVEC 2D tubule formation on Laponite hydrogels in different VEGF conditions. (A) The total network length was quantified by total pixel number and the mean, standard deviation (SD) and confidence interval (CI) calculated. The mean difference between groups were calculated stating exact p numbers. (B) Comparison of the mean tubule branch length between sample groups showed that Laponite hydrogels pre-incubated with VEGF ("bound") exhibited similar tubule network organisation to VEGF present in aqueous media. HUVECs cultured on Laponite hydrogels absent of VEGF exhibited significantly less formation than the other two groups. Error bars = SD, n = 6, one-way ANOVA analysis performed with Tukey's post-hoc test applied for multiple comparisons; **** denotes p = < 0.0001.

3.2.4 Incorporation of VEGF within Laponite Hydrogels and its Effect on HUVEC Tubule Formation

To determine whether incorporation of VEGF within Laponite hydrogels could evoke a similar increase in tubule formation compared with that achieved with VEGF mixed into growth medium, different concentrations of VEGF were premixed into 3% Laponite hydrogels. A concentration range of 0.04 µg/ml to 5.00 µg/ml VEGF was chosen. This range was significantly higher than concentrations of VEGF present in aqueous solution and were chosen to maximise the chance of measuring a HUVEC response.

Establishment of a well-formed HUVEC network at the low VEGF concentrations (0.04 µg/ml and 0.10 µg/ml) was not successful with a mean tubule branching length no greater than the control group (Figure 3.6 and Figure 3.8 A). Evidence of tubules forming between HUVECs was detected at 0.50 µg/ml VEGF (Figure 3.6). However, once a concentration of 1.00 µg/ml was reached a significant HUVEC network was established (Figure 3.7) with a mean tubule branching length increase of 279 ± 73 % (8331 ± 2019 pixels, $p = < 0.01$, error = SD). Further increases in network organisation was measured at higher VEGF concentrations (2.00 µg/ml and 5.00 µg/ml) with a 320 ± 111 % and 463 ± 26 % rise in tubule branching length when compared to the no VEGF control (Figure 3.8 B and C, error = SD, $p = < 0.001$ and < 0.0001 respectively).

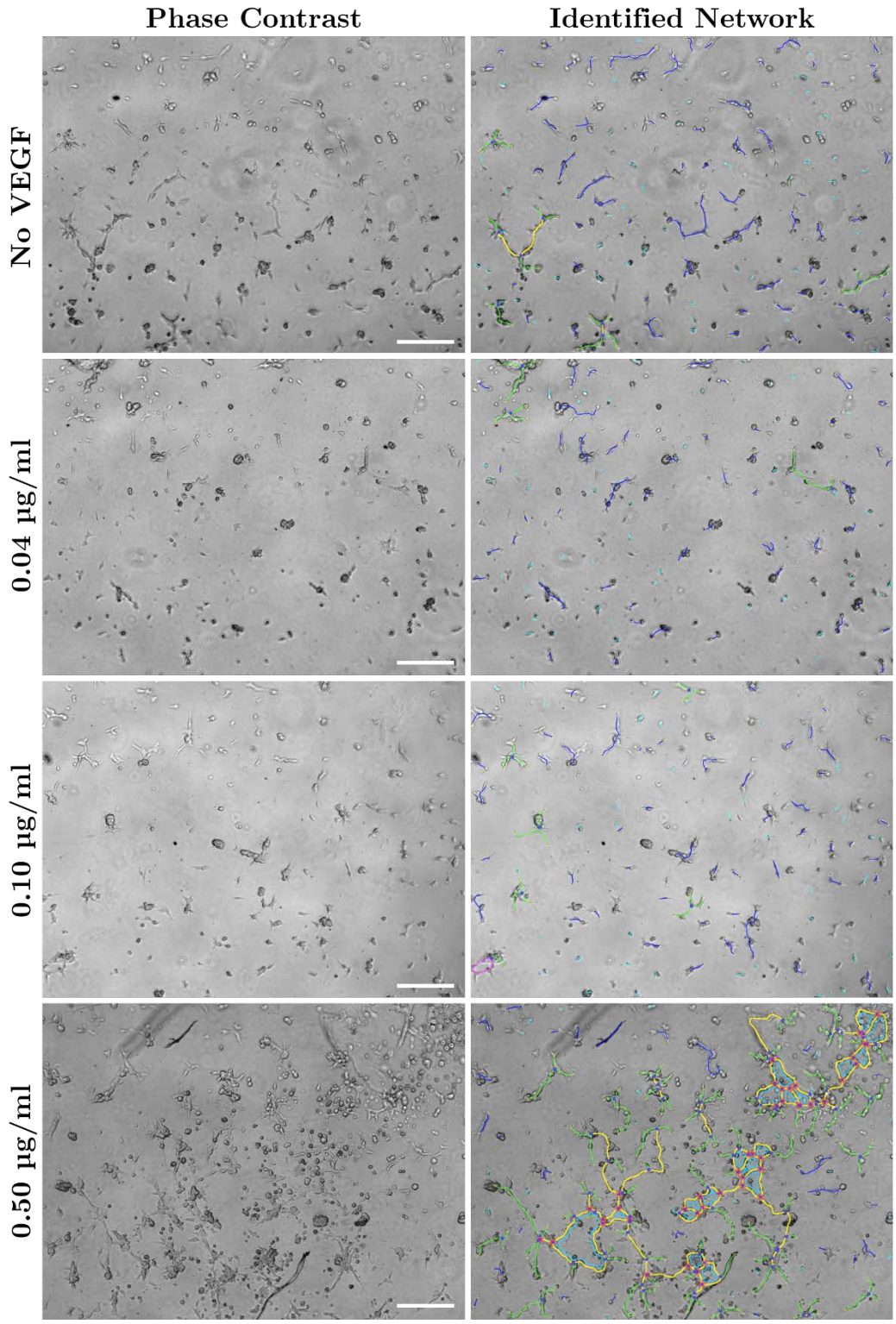

Figure 3.6. 2D tubule formation of human vein endothelial cells (HUVECs) on Laponite hydrogels containing low premixed VEGF concentrations. There was no evidence of tubule formation at the two lowest Laponite-VEGF concentrations (0.04 µg/ml and 0.01 µg/ml). There was an indication that HUVEC organisation was present at 0.50 µg/ml as the identified network image shows. Scale bars = 500 µm.

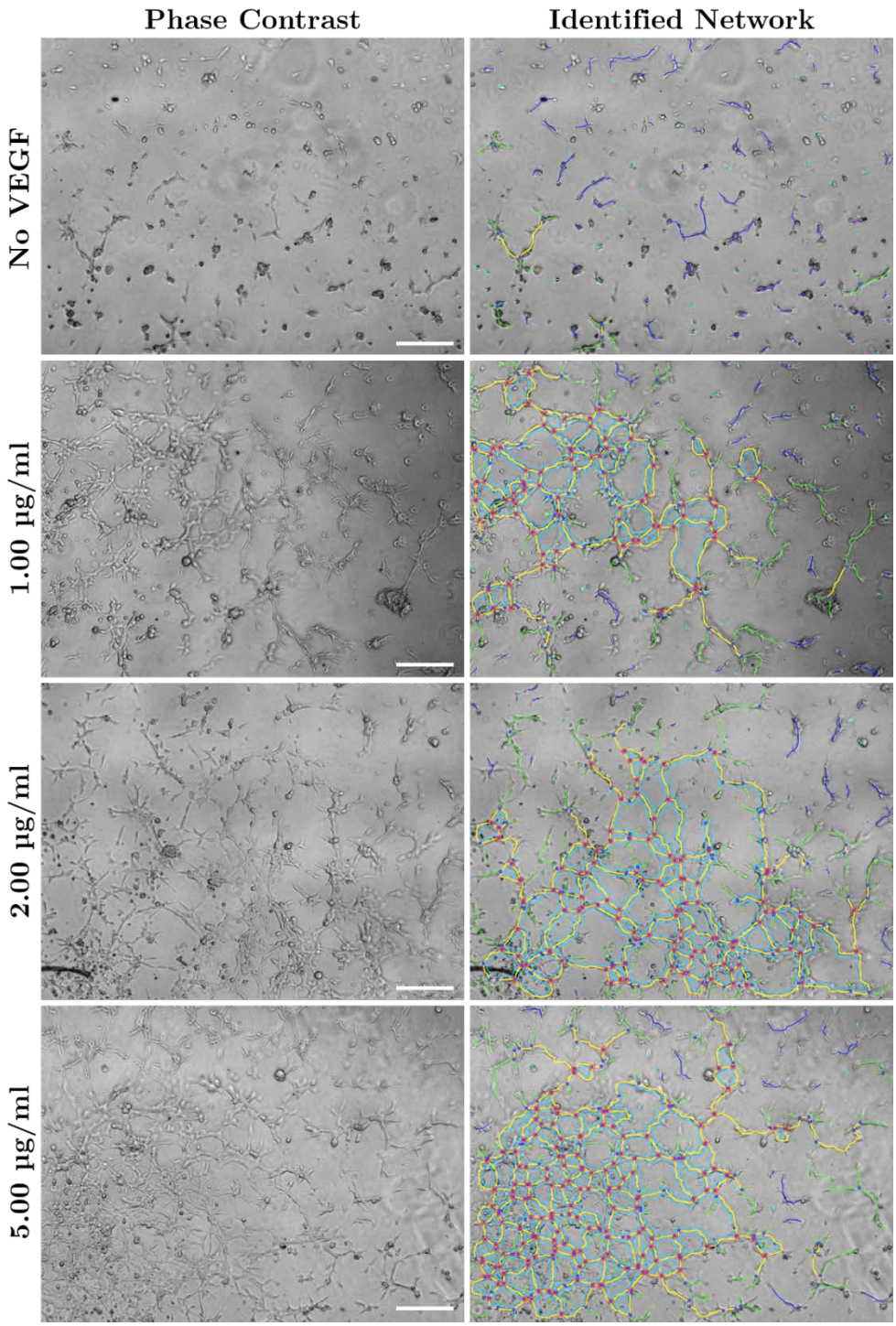

Figure 3.7. 2D tubule formation of human vein endothelial cells (HUVECs) on Laponite hydrogels containing high premixed VEGF concentrations. Organised network between HUVECs were present in all Laponite-VEGF test groups. Tubule formation was seen to increase with increasing VEGF concentrations from 1.00 µg/ml to 5.00 µg/ml. Scale bars = 500 µm.

A

Descriptive Statistics			
Group Statistics			
VEGF Test Group	*n*	Mean & SD (Pixels)	95% CI (Pixels)
No VEGF	3	2984 ± 1548	-861.2 - 6828
0.04 µg	4	1704 ± 1200	-205.2 - 3613
0.10 µg	4	2859 ± 2215	-665.4 - 6384
0.50 µg	3	6165 ± 2275	512.1 - 11817
1.00 µg	3	11315 ± 2671	4679 - 17951
2.00 µg	4	12546 ± 3262	7355 - 17737
5.00 µg	3	16788 ± 1151	13929 - 19647

B

Descriptive Statistics				
Differences Between VEGF Groups and No VEGF Control				
VEGF Test Group	Mean & SE (Pixels)	95% CI (Pixels)	% Difference	*p*
0.04 µg	-1280 ± 1889	-6895 - 4336	-43	0.9861
0.10 µg	-124.4 ± 1889	-5740 - 5491	-4	> 0.9999
0.50 µg	3181 ± 2019	-2822 - 9184	107	0.5873
1.00 µg	8331 ± 2019	2328 - 14334	279	0.0037
2.00 µg	9563 ± 1889	3947 - 15178	320	0.0005
5.00 µg	13805 ± 2019	7802 - 19808	463	< 0.0001

C

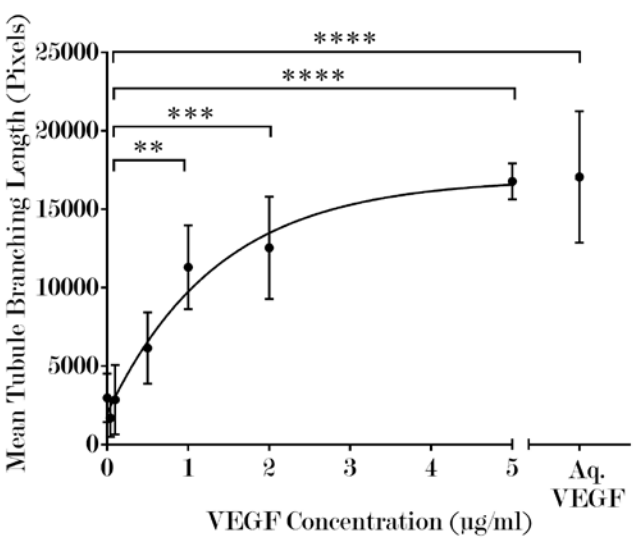

Figure 3.8. Quantitative analysis of HUVEC 2D tubule formation on Laponite hydrogels in different VEGF concentrations. (A) The total network length was quantified by total pixel number and the mean, standard deviation (SD) and confidence interval (CI) calculated. The mean difference between groups were calculated stating exact p numbers. (B) Comparison of the mean tubule branch length between different VEGF concentrations premixed within Laponite showed that there was a significant increase in tubule formation at 1.00-5.00 µg/ml (279-463% pixel increase), indicating that 1.00 µg/ml was the threshold concentration. (C) Quantitative data shown graphically with relevant statistical significance. Error bars = SD, n = 3/4 (an n of 4 was used but some of the Laponite surfaces were damaged and HUVEC networks disrupted – these could not be included), one-way ANOVA analysis performed with Tukey's post-hoc test applied for multiple comparisons; ** denotes $p = < 0.01$; *** denotes $p = < 0.001$; **** denotes $p = < 0.0001$.

3.2.4.1 Differences between VEGF Mixed into Laponite, Adsorbed to Laponite and VEGF Present in Aqueous Solution

VEGF premixed within Laponite hydrogels at a concentration of 1.00-5.00 µg/ml stimulated a HUVEC tubule response that was comparable to VEGF mixed into growth medium (Table 3.1).

Descriptive Statistics						
Differences Between VEGF in Laponite and VEGF in Media						
VEGF in Laponite		VEGF in Growth Medium	Mean & SE (Pixels)	95% CI (Pixels)	% Diff	p
1.00 µg	vs	0.01 µg	349.3 ± 2046	-6856 - 7555	3	> 0.9999
		0.02 µg	92 ± 2046	-7113 - 7297	1	> 0.9999
		0.04 µg	-4551 ± 1830	-10995 - 1894	-40	0.3289
2.00 µg	vs	0.01 µg	1581 ± 1581	-5255 - 8416	13	0.9975
		0.02 µg	1323 ± 1323	-5512 - 8159	11	0.9994
		0.04 µg	-3319 ± -3319	-9348 - 2709	-26	0.6452
5.00 µg	vs	0.01 µg	5822 ± 5822	-1383 - 13028	35	0.1835
		0.02 µg	5565 ± 5565	-1640 - 12770	33	0.2275
		0.04 µg	922.6 ± 922.6	-5522 - 7367	5	> 0.9999

Table 3.1. Differences of mean tubule branching length between HUVECs grown with 1.00-5.00 µg/ml VEGF in Laponite and 0.01-0.04 µg/ml VEGF in growth medium. 1.00 µg/ml of VEGF premixed within 3% Laponite stimulated a mean tubule branching length akin to 0.01 µg/ml and 0.02 µg/ml of VEGF in growth medium (1-3 % difference). When 2.00 µg/ml of VEGF was premixed within Laponite, tubule formation was slightly greater (11%) than 0.02 µg/ml VEGF mixed within growth medium; this was less than 0.04 µg/ml VEGF in growth medium (-26% difference). A 5.00 µg/ml concentration premixed in Laponite stimulated a tubule response that was equivalent to 0.04 µg/ml of VEGF in the growth medium.

VEGF at 1.00 µg/ml stimulated a mean tubule branching length that was comparable to 0.01 µg/ml and 0.02 µg/ml of VEGF in growth medium (1-3 % difference). 2.00 µg/ml of VEGF in Laponite had a response slightly greater (11%) than 0.02 µg/ml of VEGF in growth medium but a response that was less than 0.04 µg/ml in growth medium (-26% difference). However, at 5.00 µg/ml, the

concentration of VEGF within Laponite hydrogels was great enough to stimulate a tubule response that was equivalent to 0.04 µg/ml of VEGF in the growth medium (Table 3.1). These results clearly demonstrate that by premixing VEGF within Laponite hydrogels at sufficiently high concentrations (> 1.00 µg/ml) can induce a proangiogenic effect that is comparable to VEGF in an aqueous solution.

Based on previous work by Dawson *et al* [235], it was shown that the release of proteins from Laponite gels was negligible. Thus, it could be assumed that the biological response exhibited by HUVECs at these higher concentrations of pre-mixed VEGF would have occurred via sustained localisation of VEGF. This means that HUVECs would have required a degree of penetration within the Laponite gels to gain access to biological quantities of VEGF. To test this hypothesis and determine the depth of gel required to stimulate a biological effect a set of calculations were performed based on assumptions gained from the data in this subchapter. These assumptions were mainly based on the VEGF adsorption data (40 ng/ml) and the concentration of VEGF within Laponite that exhibited the greatest biological response (5 µg/ml). All subsequent calculations have been illustrated in Figure 3.9.

Assuming that 100% of VEGF had adsorbed to Laponite when pre-incubated with 0.04 µg/ml, the total VEGF bound to the surface would have been 12 ng (Figure 3.9 A). Therefore, this quantity of VEGF could be considered the amount required to exhibit a maximal biological response.

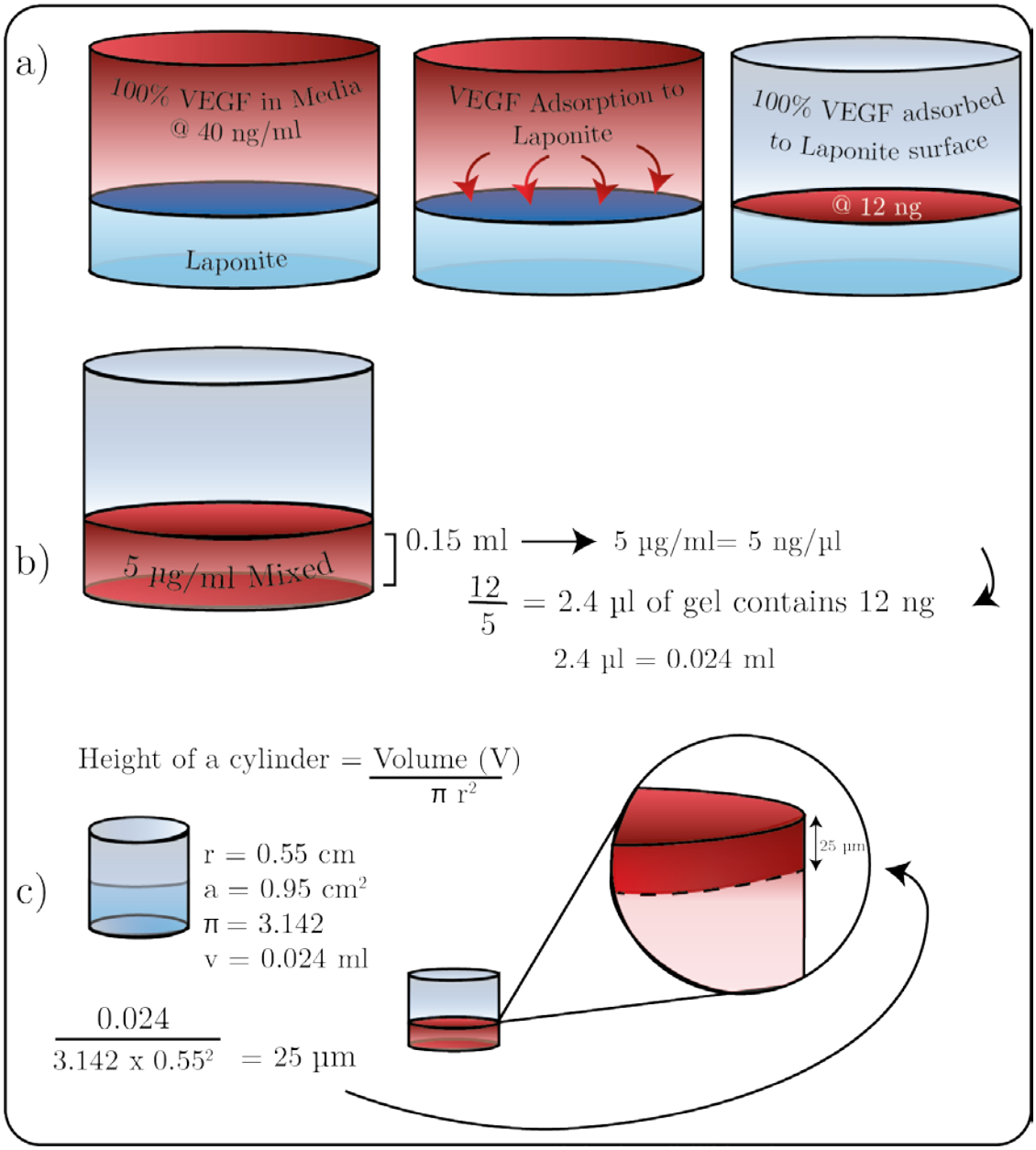

Figure 3.9. Calculation of the theoretical depth in a Laponite VEGF gel that is bioactive to HUVECs. A) Shows that if 100% of VEGF had adsorbed to Laponite gels when pre-incubated with 0.04 µg/ml, the total of VEGF bound to the surface would have been 12 ng. B) Based on the maximal pre-mixed VEGF concentration (5 µg/ml) and the volume of gel used (0.15 ml) the concentration of VEGF per µl would have been 5 ng. By dividing the concentration required to have a bioactive effect when adsorbed (shown in A = 12 ng) with concentration of VEGF that existed within 1 µl of pre-mixed gel this calculates the volume that would have been required to exert the same biological (12 ng) effect; this was calculated to be 0.024 ml. C) Using the calculated data from A and B in the equation that calculates the height of a cylinder, a depth of 25 µm was calculated; this is the depth of gel that would have been required for cells to penetrate in order to exhibit a successful biological response.

As demonstrated in Figure 3.9, the maximal pre-mixed VEGF concentration (5 µg/ml), the gel volume used (0.15 ml), the gel volume required to stimulate a

biological response (0.024 ml, calculated in Figure 3.9 B) and a well area of 0.95 cm^2 it was calculated that a depth of 25 µm was required for HUVEC penetration (Figure 3.9 C).

3.3 BIO Uptake/Release Assay Results

3.3.1 Validation of Wnt Signalling Pathway Reporter Cell Line Response to BIO

The activity of the canonical Wnt signalling pathway was measured using a 3T3 mouse fibroblast cell line. This cell line has been genetically engineered to express the firefly luciferase reporter gene under the control of Wnt-responsive promoters (TCF/LEF). Luciferase activity in this cell line can be stimulated with the addition of exogenous Wnt proteins/Wnt agonists in a dose-dependent way. This enzyme activity is measured by changes in chemiluminescent output following cell treatment with an exogenous luciferin substrate.

BIO is a potent yet reversible agonist of Wnt signalling; it behaves as a selective, ATP-competitive inhibitor of GSK-3α and GSK-3β. To validate the dose-dependent relationship of exogenous BIO on 3T3 cell luciferase activity, cells were incubated in culture medium containing BIO at different concentrations (0-5 µM) and the chemiluminescent signal measured.

Negligible production of luciferase was measured in media containing > 1 µM, however a rapid increase in enzyme activity was observed between 1 µM and 3 µM. No further increase in luciferase production was measured > 5 µM, indicating that this concentration of BIO is saturating (Figure 3.10). All subsequent

luciferase reporter gene data up-regulated by BIO was normalised to maximal enzyme activity at 5 µM.

A Descriptive Statistics

BIO Concentration (µM)	Mean Luciferase Activity and SD (%)			*n*
0.00	5.7	±	5.2	8
0.50	6.2	±	4.9	8
1.00	8.5	±	3.7	8
1.50	16.8	±	4.2	8
2.00	32.4	±	12.0	8
3.00	75.7	±	13.1	8
5.00	93.0	±	8.7	7

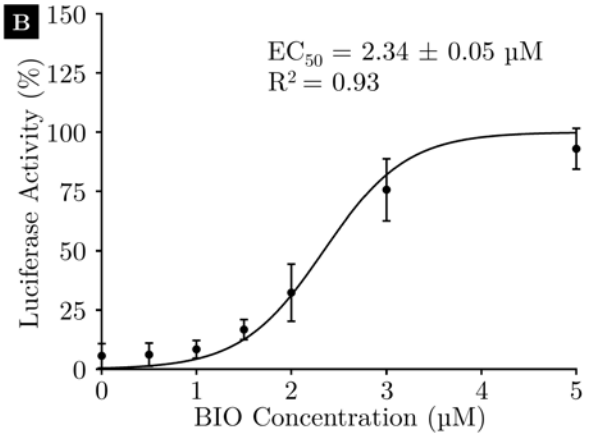

Figure 3.10. Dose-response control curve of BIO. (A) Descriptive statistics that represents mean normalised % activity of luciferase produced by a 3T3 fibroblast cell line that is controlled by a TCF/LEF Wnt reporter. (B) Luciferase assay data plotted against BIO concentration; this confirmed that luciferase activity responds in a dose-response manner with negligible activity at < 1 µM and a rapid increase in activity between 1-3 µM. Luciferase response to BIO reaches a steady-state at 5 µM indicating that this concentration is saturating. Error bars = S.D. n = 8 (except for 5.00 µM which had 7).

3.3.2 Validation of Adsorption of Assay Media Components by Laponite Hydrogels

To test whether adsorption of components from the growth medium by Laponite could interfere with the reporter cell line read-out, assay medium was incubated with Laponite hydrogel capsules for various periods of time (up to 60 minutes and up to 7 days). Following incubation, media was recovered and mixed with BIO (5 µM). This was then incubated with 3T3 fibroblast cell culture and the activity of luciferase measured.

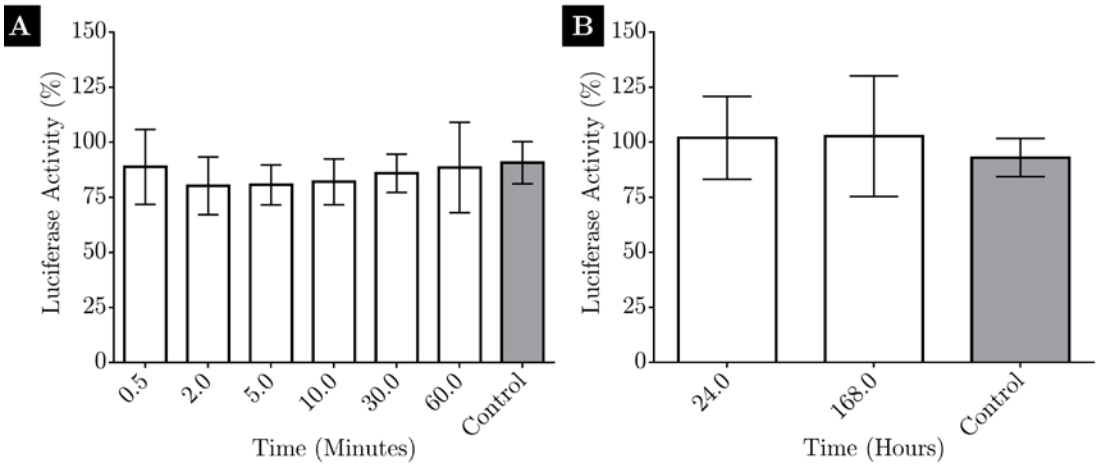

Figure 3.11. Validation that Laponite hydrogels have no impact on media components. Media was incubated with Laponite capsules prior to addition of BIO at saturation concentration (5 µM). Confirmation of BIO was determined by 3T3 cell luciferase production. Activity was compared to the 5 µM dose-response control; no significant reduction in luciferase activity was measured when Laponite capsules were incubated with media up to 60 minutes (A) or up to 168 hours (B). This confirmed that culture medium efficacy was unaffected when incubated with Laponite capsules. Error bars = S.D. N = 3 (10 and 30-minute samples), 6 (all remaining samples). One-way ANOVA statistical analysis was performed.

Supporting the hypothesis that Laponite does not interfere with a constituent of growth medium, no significant decrease in the response to 5 µM BIO was observed when compared to the control at any time point up to 7 days (see Figure 3.11 A and B, $p = > 0.85$).

3.3.3 Adsorption of BIO by Laponite Hydrogels

To test whether Laponite could adsorb BIO from growth medium, the luciferase activity of assay medium at the saturation concentration of BIO (5 µM) was measured following incubation with Laponite capsules at various time points (up to 60 minutes). A decline in activity would thus indicate BIO uptake.

A significant reduction in mean luciferase activity was measured between 0.0 and 0.5 minutes (Figure 3.12 A, 87.5 ± 15.8% reduced to 51.5 ± 11.9%, $p = < 0.05$). Although there was a reduction in luciferase active after 30 seconds, there was

inconsistency to support this adsorption at the remaining time points. This is best seen between 30 seconds and 60 minutes where there was a gradual rise in luciferase activity. After 60 minutes the difference between time 0 was only ~12%. Without further study it is difficult to conclude that Laponite gels could offer significant absorption of BIO over a 60-minute period.

A Descriptive Statistics

Media Removal Time (Minutes)	Mean Luciferase Activity and SD (%)			n
0.0	87.5	±	15.8	3
0.5	51.5	±	11.9	3
2.0	57.2	±	7.6	3
5.0	62.2	±	7.1	3
10.0	67.5	±	8.5	3
30.0	59.5	±	19.1	3
60.0	78.8	±	13.8	3

B

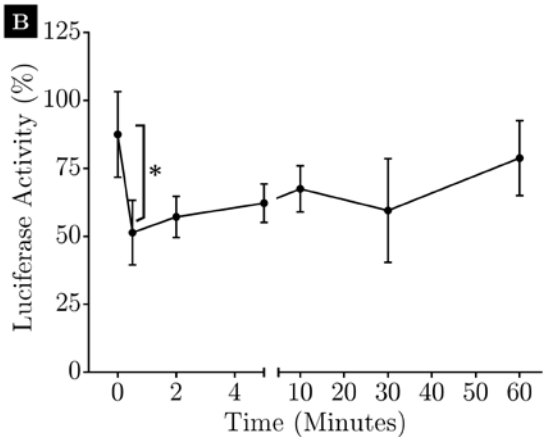

Figure 3.12. Investigating the adsorption of BIO by Laponite hydrogels. (A) Laponite hydrogel capsules were incubated with medium containing BIO (5 μM) up to 60 minutes. Recovered media at different time points was cultured with 3T3 fibroblast cells and the mean luciferase activity measured. (B) There was a significant reduction in luciferase activity after 30 seconds; no other time points were deemed significantly reduced (* denotes that $p = < 0.05$). Error bars = S.D, n = 3. One-way ANOVA test was performed.

3.3.4 Release of BIO by Laponite Hydrogels

To test whether Laponite would release BIO into the assay medium, Laponite capsules were premixed with a high concentration of BIO (50 μM or 80 μM, refer to 2.2.5.4) and incubated with assay medium at various time points. Like the adsorption study, the luciferase activity of 3T3 fibroblast cells was measured, however in this case any increase in activity would indicate BIO release.

In the initial study, no increase in luciferase activity was detected at any time point up to 60 minutes, thus indicating no release of BIO (Figure 3.13).

A Descriptive Statistics

Media Removal Time (Minutes)	Mean Luciferase Activity and SD (%)			n
0.0	3.3	±	1.0	3
0.5	3.6	±	1.5	3
2.0	3.4	±	1.0	3
5.0	3.0	±	0.8	3
20.0	2.6	±	0.6	3
60.0	2.9	±	0.7	3

B

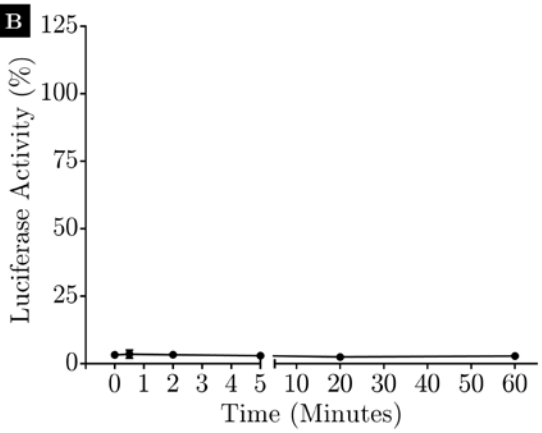

Figure 3.13. Investigating the release of BIO from Laponite hydrogels up to 60 minutes. (A) Laponite hydrogel capsules containing 50 μM were incubated with growth for up to 60 minutes. Recovered media at different time points was cultured with 3T3 fibroblast cells and the mean luciferase activity measured. (B) There was negligible activity of luciferase measured over the 60-minute time course indicating that no detectable BIO was released from Laponite. Error bars = S.D, n = 3. One-way ANOVA test was performed.

To increase the sensitivity of the release assay, a revised protocol was employed (see methods chapter 2.2.5.4). In brief, 5 Laponite capsules were incubated with assay medium at different time points up to 168 hours (7 days). In parallel, assay medium was also incubated with Laponite capsules absent of BIO; no BIO was added to this assay medium at any stage during the study and served as a baseline for luciferase activity (negative control). Like before, luciferase activity was measured following addition of media to 3T3 fibroblast cell culture. No increase in luciferase activity was detected with cells cultured with negative control media (Figure 3.14 A and B). In contrast, small increases in luciferase activity was observed in media incubated with BIO-Laponite capsules at all time points. However, only the activity of media incubated with BIO-Laponite capsules at 24 hours was significantly different from the negative control (Figure 3.14, 10.2 ± 2.7 % difference $p = < 0.01$).

3.3.4.1 Quantification of BIO Released from Laponite

As there was evidence of significant BIO released into assay medium at 24 hours, it was thought necessary to quantify the estimated concentration. To calculate

this, the luciferase activity data measured at 24 hours was used with the equation derived from the dose-response curve (Fig. 3.9) to interpolate the concentration of BIO (see appendix A.6). It was calculated that 1.3 µM of BIO was released into the assay medium at 24 hours (Fig. 3.14 A and B).

A

Descriptive Statistics									
	Negative Control				Test Release				
Media Removal Time (Hours)	Mean Luciferase Activity and SD (%)			n	Mean Luciferase Activity and SD (%)			n	p
0.0	2.1	±	0.3	6	1.8	±	0.4	6	> 0.9999
0.5	2.0	±	0.1	3	7.7	±	5.9	3	0.5312
1.0	2.0	±	0.0	3	5.0	±	2.1	3	0.9445
24.0	1.8	±	0.1	6	12.1	±	8.7	6	0.0022
168.0	2.0	±	0.1	3	6.7	±	7.7	6	0.5667

B

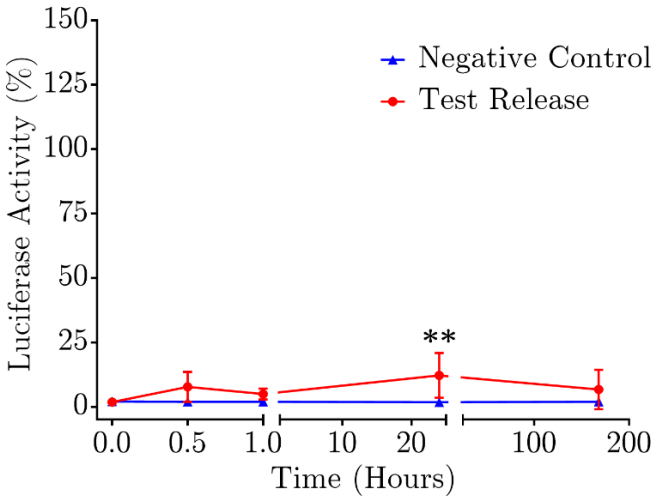

Figure 3.14. Investigation the release of BIO from Laponite hydrogels up to 168 hours (7 days). (A) Laponite hydrogel capsules premixed with BIO (80 µM) were incubated with growth medium up to 60 minutes. Recovered media at different time points was cultured with 3T3 fibroblast cells and the mean luciferase activity measured. (B) There was a significant increase in luciferase activity by 24 hours, indicative of BIO release; no other significant increase was measured at other time points (** denotes that p = < 0.01). Error bars = S.D, n = refer to table. Two-way ANOVA statistical analysis was performed with Sidak's multiple comparison post-hoc test applied.

A

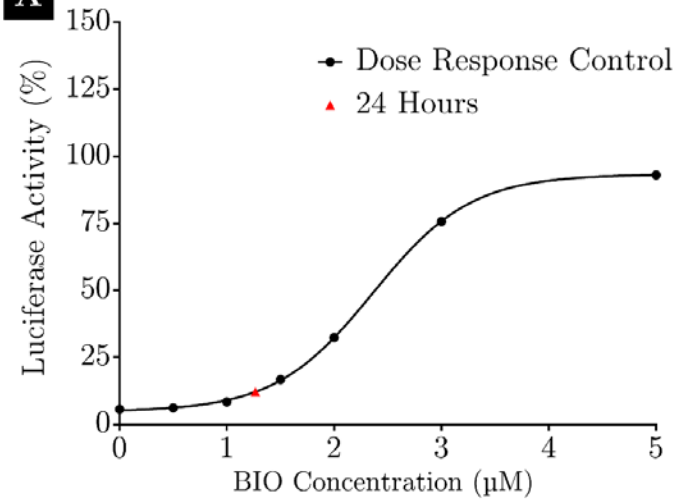

B

BIO Concentration Release/Retained by Laponite at 24 Hours	
Mean luciferase activity (%)	12.2
Standard deviation (%)	8.7
Interpolated BIO concentration (µM)	1.3
Maximum BIO if 100% released (µM)	26.7
% of BIO released into assay medium	4.8
% of BIO retained by Laponite capsules	95.2

Figure 3.15. Amount of BIO release/retained by Laponite hydrogel capsules after 24 hours during 7-day study. (A) Interpolated luciferase activity calculated using the dose-response control data. (B) Data table showing the mean luciferase activity after 24 hours was 12.2 ± 8.7% and the interpolated BIO concentration as 1.3 µM; approximately 4.8% was released into the growth medium and that > 95% was successfully retained.

To determine the proportion of BIO released from Laponite capsules, the theoretical maximum concentration of BIO was calculated by assuming the total BIO release. This was calculated to be approximately 26.7 µM (see appendix A.6). By using this concentration, it was calculated that there was 4.8% released at 24 hours (Figure 3.15 B). Whilst these results show evidence of BIO release, Laponite hydrogels retained BIO very effectively under these test conditions.

3.4 Discussion

The primary aim of this thesis is to develop Laponite gels as a carrier biomaterial to localise bioactive molecules to promote wound healing. It was considered that incorporation of bioactive factors within the bulk hydrogel, rather than by surface adsorption [235], would have advantages for wound treatment as it would enable topical administration like other growth factor gels or dressings [264, 269]. Surface adsorption has been shown previously to preserve VEGF activity, but it is unknown whether mixing molecules within the hydrogel bulk may compromise activity, by sequestering the molecule away from the cells or inactivating it. The main findings from these studies showed:

- Laponite premixed with ≥ 1 µg/ml VEGF stimulated significant tube formation of HUVECs.

- Higher concentrations are required when encapsulated *in vivo* which is likely due to VEGF being entrapped within the bulk Laponite gels.

- Following encapsulation BIO was retained in Laponite gels for up to a 7-day period.

- Preliminary adsorption data showed that BIO does not interact as well as VEGF.

3.4.1 Incorporated VEGF in Laponite gels stimulates *in vitro* angiogenesis

A VEGF titration in growth medium was performed to determine its dose response in promoting tubule formation on 3% (w/v) Laponite surfaces. Similar to Dawson *et al*, who studied 2.5% (w/v) Laponite gels, it was shown that tubule growth was stimulated when Laponite was pre-adsorbed with 0.04 µg/ml. This indicates that there is unlikely to be a difference in the activity or bioavailability of the VEGF related to this minor change in the proportion of Laponite.

In contrast to adsorption of VEGF, it was found that much higher concentrations mixed into Laponite was necessary to induce tubule formation compared to that delivered in the medium (maximal response at total 12 ng laponite dose (growth medium) vs 750 µg total laponite dose (bulk inclusion)). It was considered that this was likely due to the dispersion of the VEGF throughout the bulk of the Laponite, where it may be unavailable to the cells. Therefore, only a proportion of encapsulated VEGF is 'exposed' to cells on the surface is bioavailable; for simplicity, this can be named the 'bioactive fraction'.

To test the validity of this theory, a calculation was performed to predict the depth of the 'bioactive fraction'. This comprised approximately 25 µm of the uppermost portion of the gel. The mean diameter of HUVECs have been documented to be ~19 µm [247], although these cells are likely to penetrate beneath the surface of viscoelastic laponite gels. Nevertheless, assuming that cells do not penetrate much more than 25 µm in depth, it is reasonable to assume that the primary reason why the dose response curves differ is sequestration of VEGF away from the cells, rather than inactivation of the protein. To confirm the

presence of the 'bioactive fraction' an additional study could be performed testing the hypothesis that a gel thickness below 25 µm would result in reduced bioactivity. If this hypothesis was proven, it would be predicted that fewer tubules would form between adjacent cells as gel thickness decreases. To determine and control gel thickness, confocal microscopy could be used as a potential technique [270].

Future work could investigate the stability of VEGF *in vitro*, with regards to temperature and storage. The biological half-life of VEGF has been shown to be ≤ 30 mins *in vivo* [147] and 90 minutes *in vitro* [271]. The importance of this information relates to the potential shelf life of a VEGF-Laponite encapsulated therapy. It could be hypothesised that when VEGF is incorporated within Laponite gels, it is less exposed to negative environmental stimuli and is thus bioactivity is improved. To test this, Laponite-VEGF could be exposed to various environmental factors that can exert adverse effects (e.g. temperature, UV light) over time. Post-exposure, the bioactivity of VEGF within these gels would be assessed using the HUVEC tubule assay.

Another area of interest would be to determine whether premixed VEGF can be released from Laponite gels into its surrounding environment. Due to Laponite's sorptive properties minimal release from Laponite gels would be highly predictable, however a suitable study would need to be designed to prove this. To test this, Laponite gels premixed with VEGF could be added dropwise to PBS, and samples of PBS recovered overtime. Then, using an enzyme-linked immunosorbent assay (ELISA), release of VEGF could be measured from recovered PBS samples. This was documented in a forthcoming chapter (Chapter 4.2.4) but was tested using higher premixed VEGF concentrations than

investigated in this chapter; this concentration deviation was based on findings discovered by accompanying *in vivo* data presented in this chapter (please refer to Chapter 4.2.3.5).

Most importantly, these results have robustly proved that Laponite-VEGF gels ≥ 1 μg/ml can exert a bioactive effect *in vitro*. The most logical step would be to test these gels containing this concentration of VEGF in a murine-based wound healing model. This would aim to accept the hypothesis that Laponite gels containing bioactive VEGF can increase the rate and quality of wound healing.

3.4.2 Laponite Uptake and Release of Small Molecule BIO

Investigating the interaction (via adsorption and release) of small molecules was considered important because it is unknown if these molecules could be retained by Laponite gels. Evidence of small molecule adsorption and retention by Laponite is limited, although there has been evidence of successful antibiotic intercalation (mafenide and tetracycline) within Laponite clay particles [251]. They also successfully showed that sustained release was successful over a 72-hour period, although mafenide release did exhibit a burst release of 60-80% within the first 2 hours. Although a burst release that was seen in this study may be clinically sufficient for antibiotic delivery, this is less desirable for bioactive molecules whereby is essential [10, 14]. In addition, the release profiles between these two antibiotics were different (tetracycline did not exhibit the same level of burst release). Therefore, understanding the release kinetics of specific molecules are essential.

More specifically, smaller molecules, such as agonists of Wnt signalling like BIO, that exhibit poor solubility [272] may have the reduced capability to form electrostatic interactions between individual molecules and clay particles. Therefore, it was chosen to investigate the uptake/release profiles of BIO with Laponite gels using a luciferase gene reporter cell system.

Preliminary adsorption data suggested that rapid adsorption of BIO occurred within the initial moments of the study yet no further uptake occurred. Speculatively this could have been due to saturation of Laponite gel capsules. Developing this study further by decreasing the volume of Laponite and increasing the number of droplets would potentially increase the saturation time (greater surface area to volume ratio).

Overall, incorporation of BIO led to minimal release over a 7-day period. However, minor proportion of release was detected ($\geq$ 12%, the greatest being 24 hours post exposure) which can be considered advantageous. Many hydrogel-based therapies strive to deliver bioactive molecules in a slow-release and sustained manner [260]; these results suggest that with small molecules Laponite can meet these standards. However, further study that involved longer time frames would be required to test the hypothesis that Laponite releases small molecules slowly.

A possible concern are the concentrations that were adopted in for these uptake/release studies (50-80 µM). However, due to the preliminary data (see 3.3.4.1) suggesting limited release, any negative effects via excessive dosage would be predicted to be minimal.

The BIO uptake/release studies do not demonstrate the direct bioactive potential of BIO's interaction with Laponite gels. It would be interesting to mix BIO within

Laponite and attempt to grow 3T3 cells on Laponite. If feasible, it would be a huge benefit to know whether BIO can exert activity when localised by Laponite. If this was proven *in vitro* then the possibility to localise Laponite-BIO at wound sites could be investigated.

Based on the results discussed in the chapter, both VEGF and BIO could potentially be a useful strategy for improving cutaneous wound healing in chronic wounds by stimulating key cell progenitors for differentiation and proliferation. It was decided however, that the incorporation of VEGF would only be taken further in forthcoming chapters for more detailed investigation and analysis. The discovery that VEGF premixed within Laponite gels retained its bioactivity led to this decision with the rationale that Laponite-VEGF gels would translate its bioactivity in an *in vivo* wound healing model. Nevertheless, the potential therapeutic benefits of BIO and other small biomolecules via Laponite gels is not discredited by this choice. More specifically, this avenue would require significant *in vitro* work to prove direct bioactivity before any *in vivo* testing could go ahead. This in combination with limited time and resources meant that these set of studies could not be realistically undertaken.

Chapter 4:

Laponite Hydrogels Localise Bioactive VEGF and Induce Angiogenesis in Healthy Mouse Wounds

4.1 Introduction

There has been significant interest in the last 20 years to use natural bioactive molecules to improve the rate of wound healing for non-healing ulcers. Chronic diabetic wounds exhibit a pro-inflammatory state that is less geared towards to cell proliferation with a significant imbalance in cellular signalling due to reduced cytokine secretion and cell response to growth factors [92]. There are a wide array of dysregulated cytokine/growth factors that could potentially be used to improve wound healing including: PDGF, VEGF, IGF-1, TGF-β1, and EGF [91, 101, 102]. Only recombinant human PDGF-BB (rhPDGF) has been clinically approved, although control trials have proven that PDGF-BB offers varying efficacy for the treatment of DFUs [132, 134].

Growth factors are often unstable in chronic wounds due to elevated protease production. This makes growth factor delivery a significant challenge which is often overcome by administering the growth-factor therapy multiple times to exert a therapeutic effect. Adverse toxic effects that occur locally due to excessive growth factor applications has been suggested [273].

Whilst the incorporation of PDGF-BB into Laponite hydrogels would be an interesting prospect, current knowledge of Laponite-growth factor interactions has been documented in previous studies using VEGF [235]. More importantly, the conclusions obtained from the HUVEC tubule study in Chapter 3 have demonstrated further the potential of Laponite to localise bioactive VEGF *in vitro*.

However, based on previous work it is unknown if incorporation of VEGF would still yield a bioactive effect [235]. As the release of pre-encapsulated proteins from Laponite gels have been shown to be negligible any bioactive effect exerted would be through sustained localisation rather than 'delivery'.

Other researchers have tested the ability for hydrogels and other drug delivery systems to improve skin healing by using a full thickness murine model [146]. Testing a chronic wound model will provide an insight into bioactive molecules effect on delayed wound healing; refining and optimising a model using healthy mice is important. This will provide a baseline control and an understanding of any potential improvements.

Previous reports have shown that the chemical properties of Laponite allow the biomaterial to form reversible hydrated gel networks at low concentrations [14, 235]. In brief, when a high shear force is applied to Laponite gels, and a specific threshold is met, the viscosity rapidly decreases. Upon immediate removal of the applied shear force, the viscosity of the gel is re-established to a state that is akin to a pre-sheared gel. This unique property is defined as thixotropy [14, 274] and was deemed attractive for the potential of easy yet robust application to a skin wounds [275].

Many conventional biomaterial gel systems, like hydrogels, require a two-step process of gelation (e.g. biomaterial & addition of a crosslinker) [231]. Thus, in their pre-gelled state these hydrogels will often have low viscosity and structural properties. This can be beneficial with regards to handling before treatment and allow easy incorporation of bioactive molecules [275]. However, upon addition to a defect, like a skin wound, the addition of a crosslinker can cause application

difficulties due to gelation and rapid increase in viscosity. A variety of hydrogel systems attempt to negate this issue by forming a cross-linked hydrogel *in situ* [275, 276]. Using thixotropic gels such as Laponite may provide an alternative solution to this issue as its thixotropy may allow for lower viscosity pre-administration following a shear force (e.g. mixing or during extrusion via injection). Whilst *in situ*, its structural integrity would be restored automatically ensuring that its strength is maximised for suitable localisation at a wound site.

However, the time that is required for 3% Laponite gels to regain its original viscosity after high shear is not known. This is important to determine as thixotropic properties that are too high may cause gels to regain stiffness more quickly than desired for skin wound application (e.g. via injection under a wound dressing). In contrast, thixotropy that is too low could lead to poor localisation and persistence at the wound site, inhibiting its effectiveness at sustained biomolecule delivery. Determining the specifics of these properties would be advantageous to ensure that it would be fit-for-purpose as an injectable/topical gel.

Based on the questions raised above, the following hypotheses were tested:

- Laponite can be retained within a wound site for a minimum of 7 days.
- Encapsulated VEGF will increase the rate of wound closure and recovery.
- Encapsulated VEGF is required to initiate a proangiogenic response *in vivo*.
- Delivery of VEGF will occur via localisation rather than release (protein release kinetics)

4.2 Results

4.2.1 Rheology

Rheological testing using 3-interval-thioxtropy test (3-ITT; this is where gels were subjected to three oscillatory intervals and their viscosities/recovery measured during these intervals) showed that Laponite gels exhibited good thixotropic behaviour, with up to 70% recovery after 4 seconds upon removal of a shear force (please refer to Appendix C.1). In contrast, ~70% viscosity was slower than alginate gels which recovered at an overall greater rate than Laponite (2 seconds). This coupled with alginate's significantly greater pre-shear viscosity (Appendix C1, Figure 6.8; 18.85 ± 0.08 x 10^5 vs 3.22 ± 0.02 x 10^5 mPa· s at 25°C, error = SD, $p = < 0.0001$), proved that Laponite gels were far easier to manipulate during sample handling. These results support why application of Laponite via an injection was less prone to blockage when in the syringe, although both gels were successfully injected via a 25G hypodermic needle. These results show the advantages of using a clay based gel material over a crosslinked hydrogel like alginate.

4.2.2 The Effect of Laponite Hydrogels on Wound Closure in Healthy Mice

To test the biocompatibility of topical 3% Laponite at wound sites, a pilot study was initially performed. The aim of this pilot study was to test whether a single application of Laponite gel administered 1-day post-surgery would remain at the wound site for a minimum period of 7 days. It would also elucidate any beneficial effects that Laponite could exert on the wound healing process when compared to a PBS control wound.

Laponite and PBS-treated wounds exhibited a reduction in wound closure over the 7-day study period, with significant closure measured by day-5 (Figure 4.1 C, $p = < 0.05$).

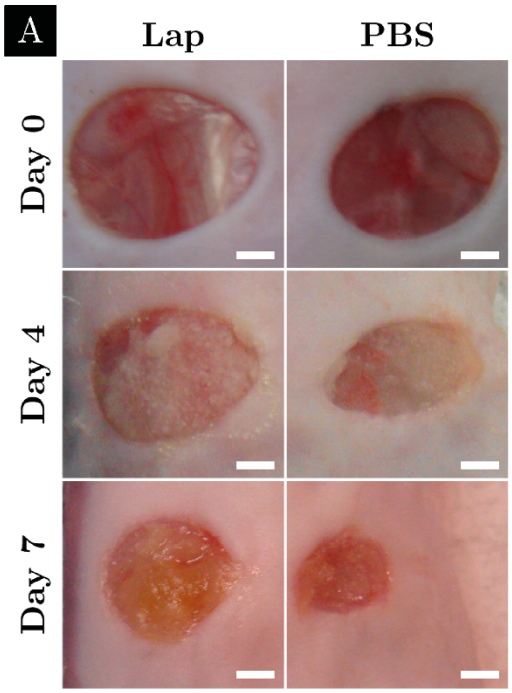

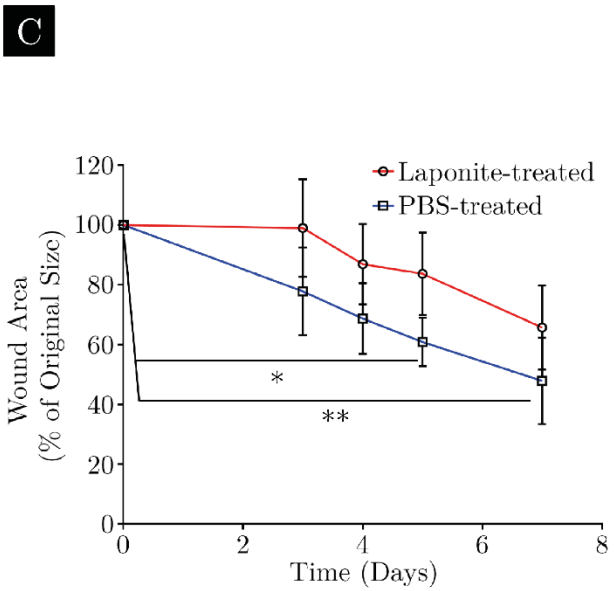

B

Descriptive Statistics

Time (Days)	3% Laponite Hydrogel Treated Wound		PBS Treated Wound		p
	Mean Size and SD (%)	n	Mean Size and SD (%)	n	
3	99.0 ± 16.4	3	77.8 ± 14.7	3	0.5155
4	86.9 ± 13.4	2	68.7 ± 11.8	2	0.8716
5	83.7 ± 13.8	3	60.9 ± 8.1	3	0.4212
7	65.7 ± 14.0	3	47.9 ± 14.4	3	0.7184

Figure 4.1. Laponite reduced the rate of wound closure up to 7 days in healthy mice. (A) Wound photographs were taken over time to assess the change in wound size and determine the average closure rate. An overall reduction in wound size was evident in both treatments but PBS-treated wounds exhibited greater closure. Scale bars = 2 mm. (B) Data table and (C) graph showing wound area measured from tracing around each wound. This data confirmed that there was a greater reduction in area in PBS-treated wounds with significant closure by day 5 when compared to day 0 wounds. Two-way ANOVA analysis was performed using Tukey's multiple comparison post-hoc test. * and ** denotes that p = < 0.05 and < 0.01 respectively. Number of mice (n) in all treatment groups was 3 (except day 4 where results were from 2 mice).

Wound tissue was next harvested at day 3, 5 and 7 post-surgery and serially sectioned. Haematoxylin and eosin stained tissue showed evidence of increased cell invasion into the wound bed at earlier time points, stimulated by the presence of Laponite (Figure 4.2 a-d, images ii-iii).

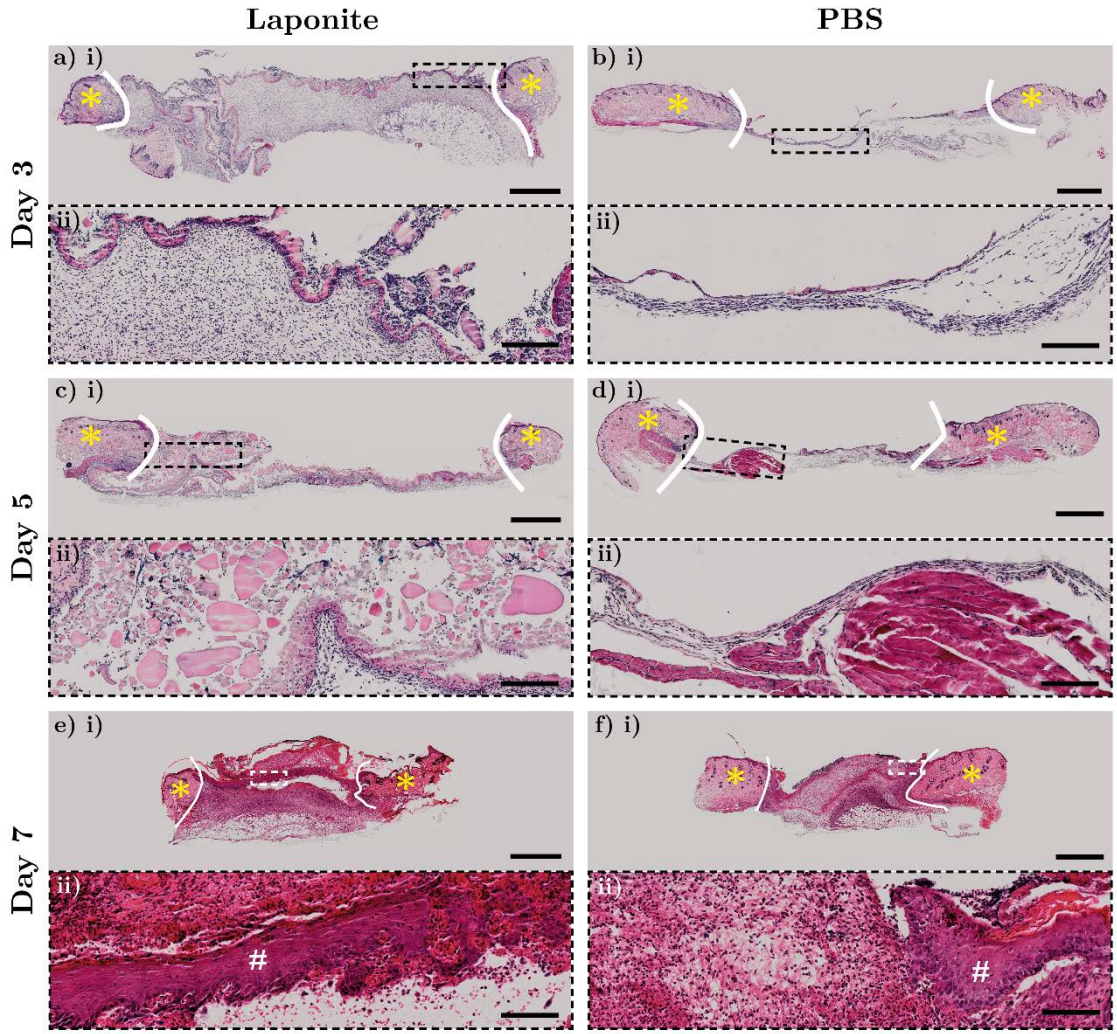

Figure 4.2. Laponite gels remain present within wound area for at least 7 days. Haematoxylin and eosin stained tissue sections; top image pane shows wound tissue overview; * shows healthy tissue and white lines depict wound margins; scale = 1 mm. Bottom left pane (ii) = higher magnification image of a region of interest (ROI) of upper image. Early evidence showed that Laponite-treated wounds retained Laponite for the duration of the 7-day study, demonstrating its biocompatibility as a topical treatment. There was also evidence of increased cell invasion into the wound bed at earlier time points, stimulated by the presence of Laponite (refer to images a-d, bottom image panes (ii-iii)). Increased cell invasion earlier within the wound healing cascade may have stimulated greater growth and migration of keratinocytes by day 7; epithelial tongue has extended further than PBS treated wound in this example (indicated by # in e-f, images ii).

Increased cell invasion earlier within the wound healing cascade may have stimulated greater growth and migration of keratinocytes by day 7; this may explain why the epithelial tongue had extended further than PBS treated wound in Figure 4.2 e and f, images ii.

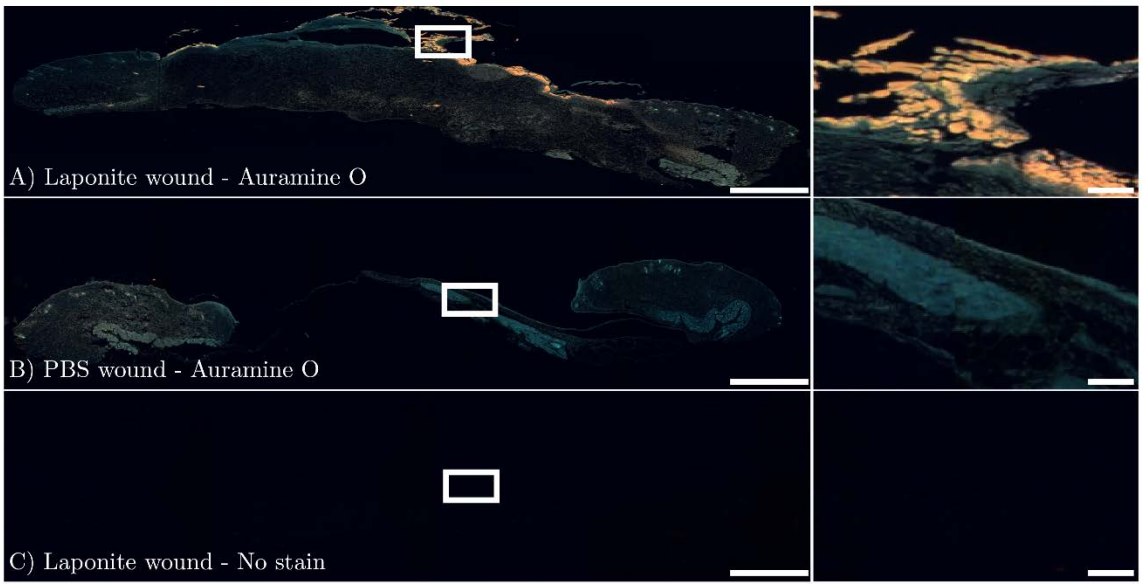

Figure 4.3. Wound tissue stained with a diarylmethane fluorescent stain (Auramine O) - a selective marker for Laponite. (A) Wound tissue that had been treated with Laponite hydrogel selectively stained with Auramine O; right panel clearly shows the fluorescent orange stain indicating the presence of Laponite within the wound bed. (B) PBS-treated wound stained with Auramine O; no fluorescent stain present due to the absence of Laponite. **(C)** Laponite-treated wound with no stain applied used as a control sample. Left panel scale bars = 1 mm, right panel scale bars = 100 µm. Filter set 2 (DAPI) used (please refer to Chapter 2.3.8.1, Table 2.2 for filter details).

To identify and track the presence of Laponite within the wound bed within the wound study tissue sections were stained using a diarylmethane fluorescent stain (Auramine O), a selective marker for Laponite. A control example demonstrating the ability of Auramine O to successfully identify Laponite (yellow-orange fluorescence) can be seen in Figure 4.3 A. In contrast, PBS-treated wound shows no signs of the fluorescent marker supporting the selective nature for Laponite.

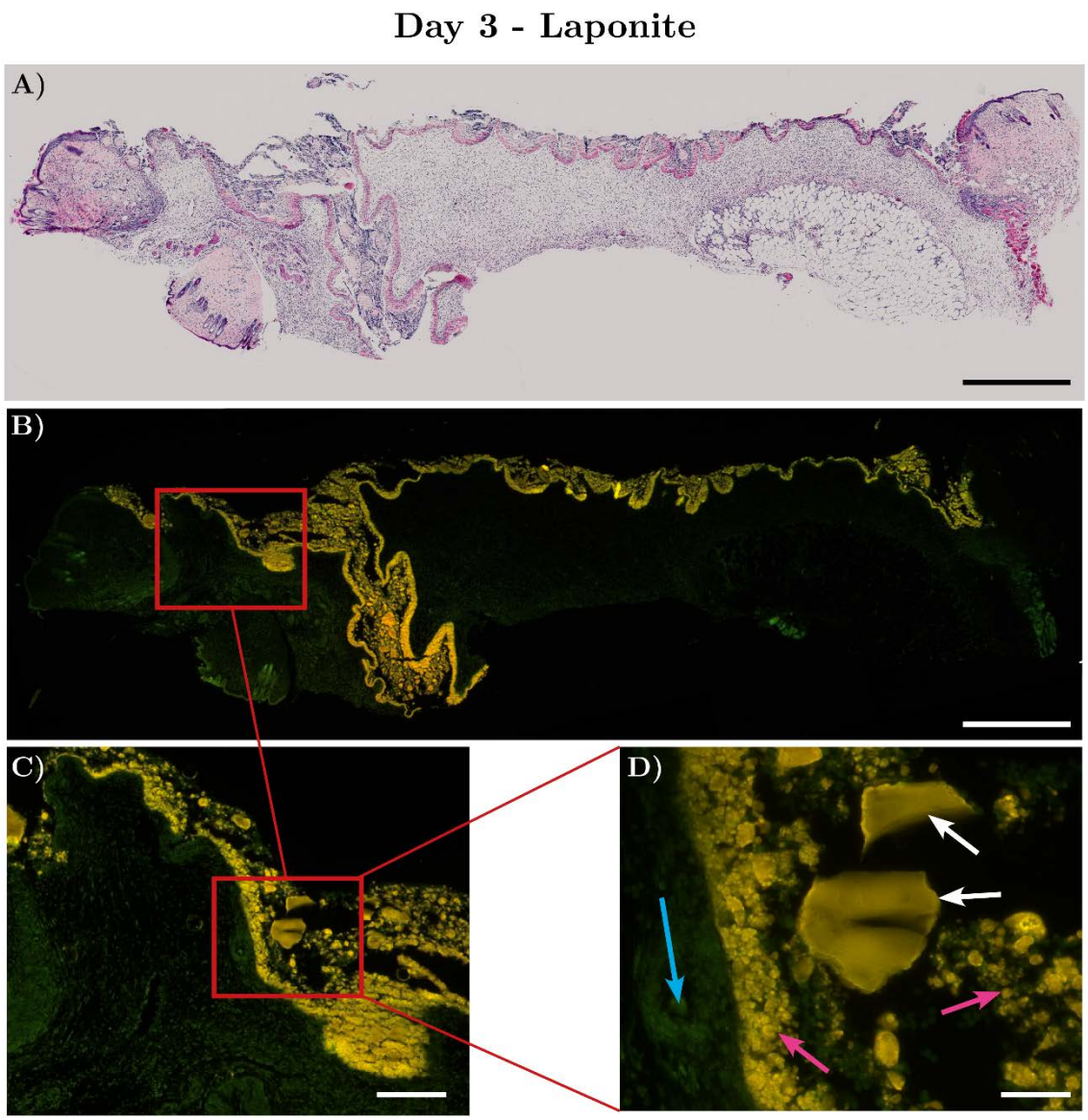

Figure 4.4. Laponite-treated wound 3-days post-surgery stained with Auramine O. (A) Haematoxylin & eosin stain; scale = 1 mm. (B) A parallel section stained with Auramine O stain, scale = 1 mm; (C-D) Higher magnification images taken from a region of interest in image (B); scale = 200 µm and 50 µm respectively. These image panels show that a large quantity of Laponite is present at day-3 post surgery (2 days after Laponite intervention). Laponite appears to have integrated well with wound tissue (e.g. cellular content, pink arrows), with larger pieces of Laponite (white arrows) in some areas devoid of cellular material. Areas of cellular content absent of Laponite are indicated with blue arrows. Filter set 2 (DAPI) used (please refer to Chapter 2.3.8.1, Table 2.2 for filter details).

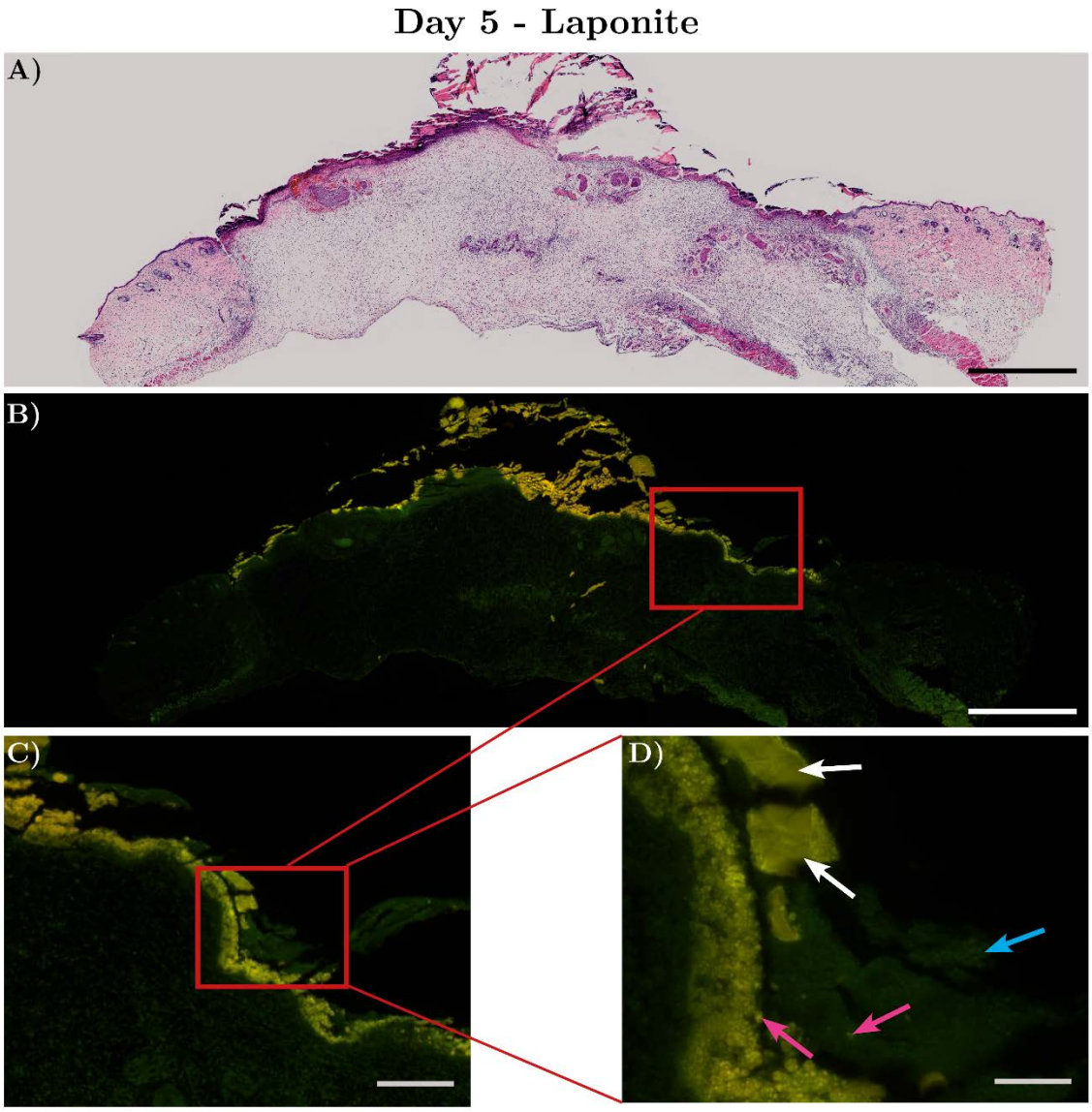

Figure 4.5. Laponite-treated wound 5-days post-surgery stained with Auramine O. (A) Haematoxylin & eosin stain, scale = 1 mm (B) A parallel section stained with Auramine O stain, scale = 1 mm; (C-D) Higher magnification images taken from a region of interest in image (B); scale = 200 µm and 50 µm respectively. These image panels show that a large quantity of Laponite is present at day-5 post surgery (4 days after Laponite intervention). Laponite appears to have integrated well with wound tissue (e.g. cellular content, pink arrows), with larger pieces of Laponite (white arrows) in some areas devoid of cellular material. Areas of cellular content absent of Laponite are indicated with blue arrows. Filter set 2 (DAPI) used (please refer to Chapter 2.3.8.1, Table 2.2 for filter details).

It was confirmed with the Auramine O stain that Laponite was present in the wound bed up to a period of seven days (Figure 4.4, Figure 4.5, Figure 4.6). Interestingly, at all three-time points, evidence of the integration of Laponite material within the wound bed is vivid. Speculatively this could suggest that cells had endocytosed Laponite or they may have simply infiltrated deeper within this

area of fragmented Laponite (Figure 4.6 pink arrows). To differentiate between these two possible events further investigation would be required.

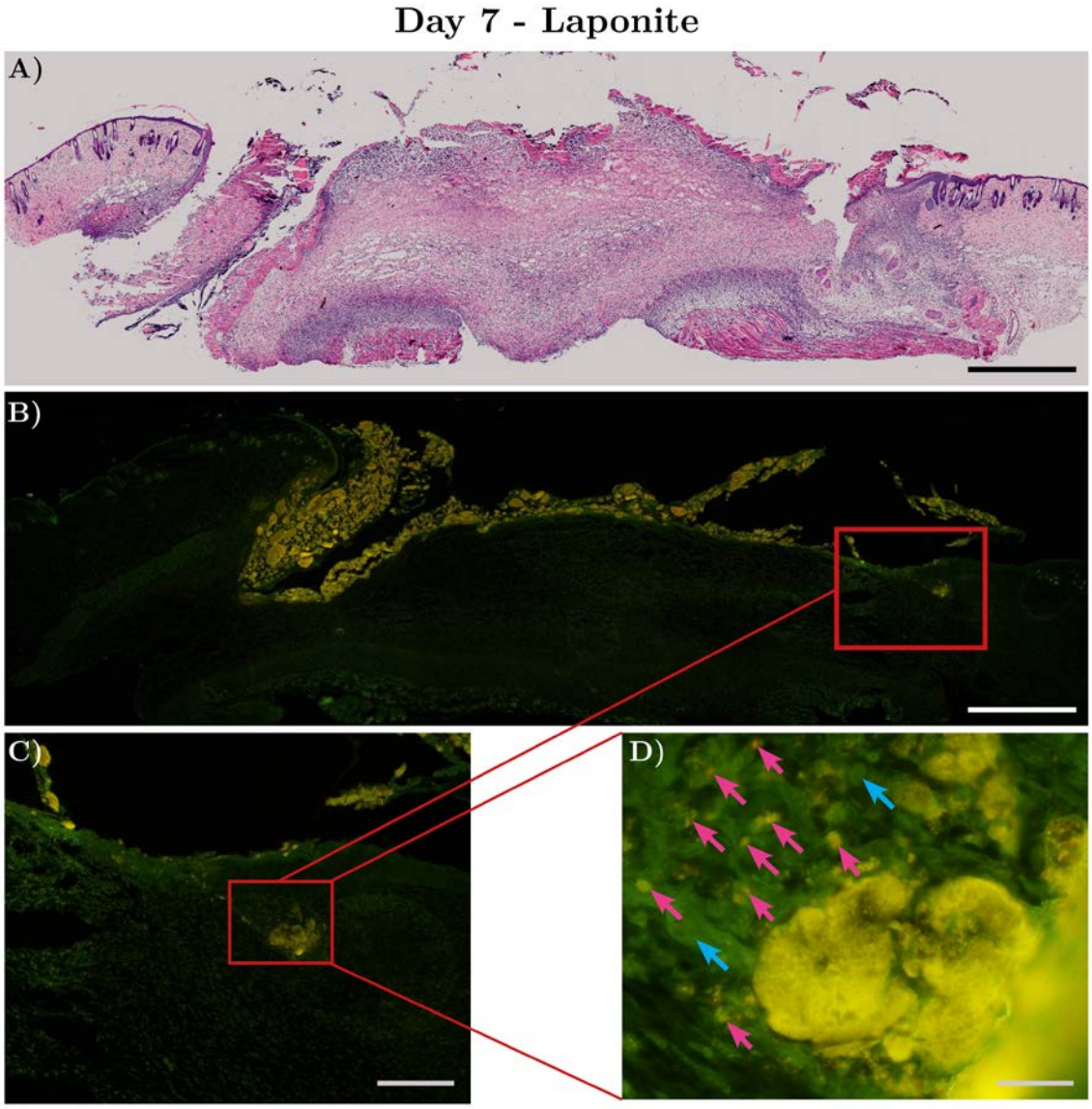

Figure 4.6. Laponite-treated wound 7-days post-surgery stained with Auramine O. (A) Haematoxylin & eosin stain, scale = 1 mm. (B) A parallel section stained with Auramine O stain, scale = 1 mm; (C-D) Higher magnification images taken from a region of interest in image (B); scale = 200 µm and 20 µm respectively. These image panels show that a large quantity of Laponite is present at day-7 post surgery (6 days after Laponite intervention). Laponite appears to have integrated well with wound tissue, potentially showing signs of endocytosed Laponite by cells or just greater cell infiltration (pink arrows). Cellular content absent of Laponite are indicated with blue arrows. Filter set 2 (DAPI) used (please refer to Chapter 2.3.8.1, Table 2.2 for filter details).

4.2.3 The Effects of Localised Laponite-VEGF Hydrogels on Skin Wounds in Healthy Mice

Effective localisation of Laponite hydrogels at skin injury sites led to the next stage in investigation; to test whether recombinant growth factors could be delivered to wounds using Laponite and improve wound recovery. Specifically, the proangiogenic factor VEGF was investigated as expected changes would lead to increase blood vessel formation within wound granulation and accelerate wound closure.

Four dorsal wounds were created per mouse; two rostral and two caudal regions. The use of multiple wounds was employed to increase data output and reduce the number of animals used. Two concentrations of Laponite-VEGF hydrogels were initially investigated. Rostral wounds were treated with a high VEGF concentration (1.0 µg/ml) whereas caudal wounds were treated with a lower VEGF concentration (0.1 µg/ml) (contralateral wounds were treated with a vehicle Laponite as a control). Wound tissue was harvested at various time points up to 11 days and photographs taken to measure wound closure.

4.2.3.1 Analysis of Blood Glucose

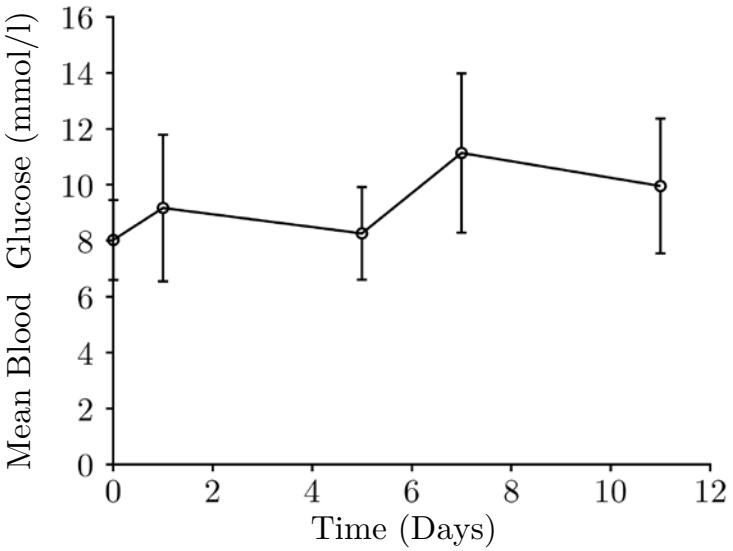

Figure 4.7. Blood Glucose levels monitored over 11 days. There were no significant changes of blood glucose levels over time, with an average reading of 9.3 ± 1.3 mmol/l. One-way ANOVA analysis was performed using Tukey's multiple comparison post-hoc test. Error bars = SD.

Blood glucose was tested prior to surgery (day 0 value) and subsequently throughout the study. It was found that the average glucose level was 9.3 ± 1.3 mmol/l.

4.2.3.2 Analysis of Murine Weight

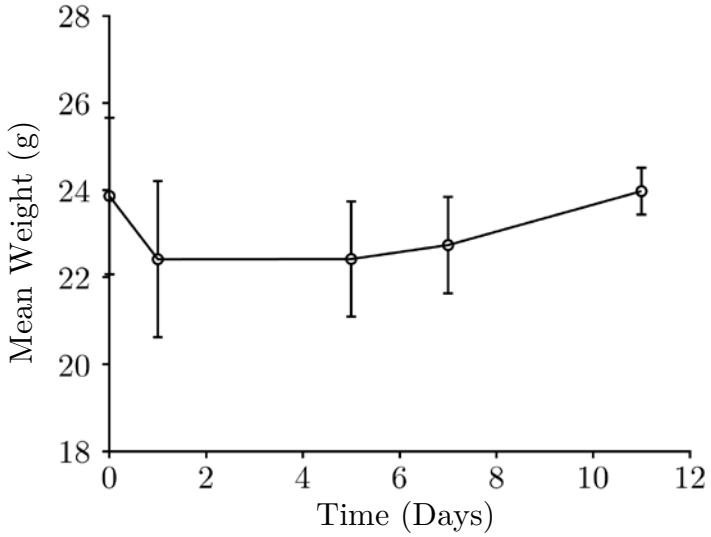

Figure 4.8. Weight of Mice monitored over 11 days. There were no significant changes of weight over time, with an average reading of 23.1 ± 0.8 g. One-way ANOVA analysis was performed using Tukey's multiple comparison post-hoc test. Error bars = SD.

Weight was measured prior to surgery (day 0 value) and also measured throughout the study. It was found that the average weight was 23.1 ± 0.8 g.

4.2.3.3 Analysis of Wound Closure

No significant differences in wound closure as a function of location (dorsal vs rostral; left vs. right) were observed between these two regions when compared (Figure 4.9, $p = > 0.99$).

Photographs of wounds over time showed that all treatment groups exhibited a similar reduction in wound size over time. By day 11 wounds treated with Laponite + 0.1 µg /ml VEGF did show a greater reduction than the other treatments, although this was minor (Figure 4.10 A).

Measurements of wound area over time did not show any significant differences in either the 0.1 µg /ml or 1.0 µg /ml treated wounds when compared with the control wounds (Figure 4.10 B -D, $p = > 0.85$).

A

Descriptive Statistics

Time (Days)	Rostral CL Treated Wound			Caudal CL Treated Wound			p
	Mean Size and SD (%)		n	Mean Size and SD (%)		n	
1	79.0	± 18.5	12	79.5	± 15.8	12	> 0.9999
5	61.4	± 16.8	12	62.0	± 14.7	12	> 0.9999
7	45.9	± 15.7	11	45.1	± 16.4	9	> 0.9999
11	13.0	± 4.9	8	10.3	± 8.7	8	> 0.9999

B

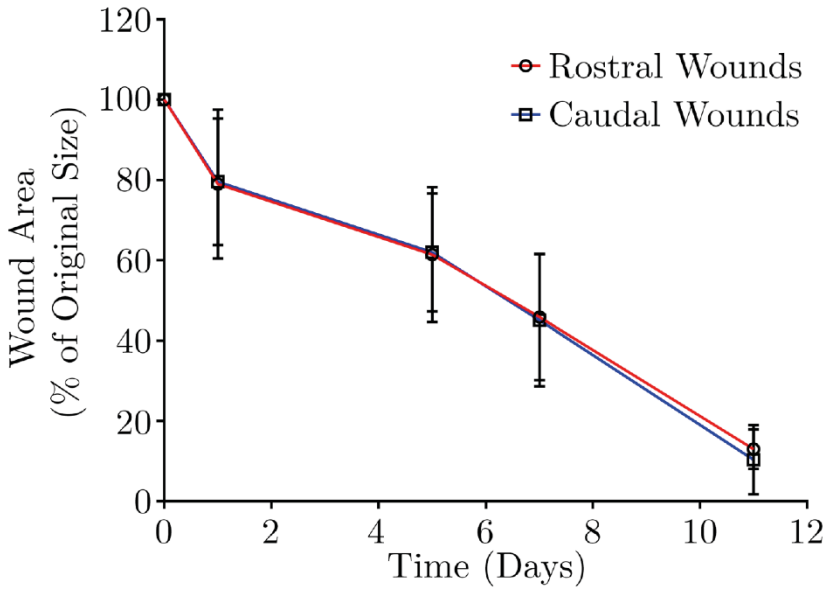

Figure 4.9. Differences between rostral and caudal wound locations on mouse dorsum. (A) Descriptive statistics of wound closure rates and (B) data plotted over time; no significant differences of wound closure between rostral and caudal wound locations were present. Two-way ANOVA analysis was performed using Tukey's multiple comparison post-hoc test.

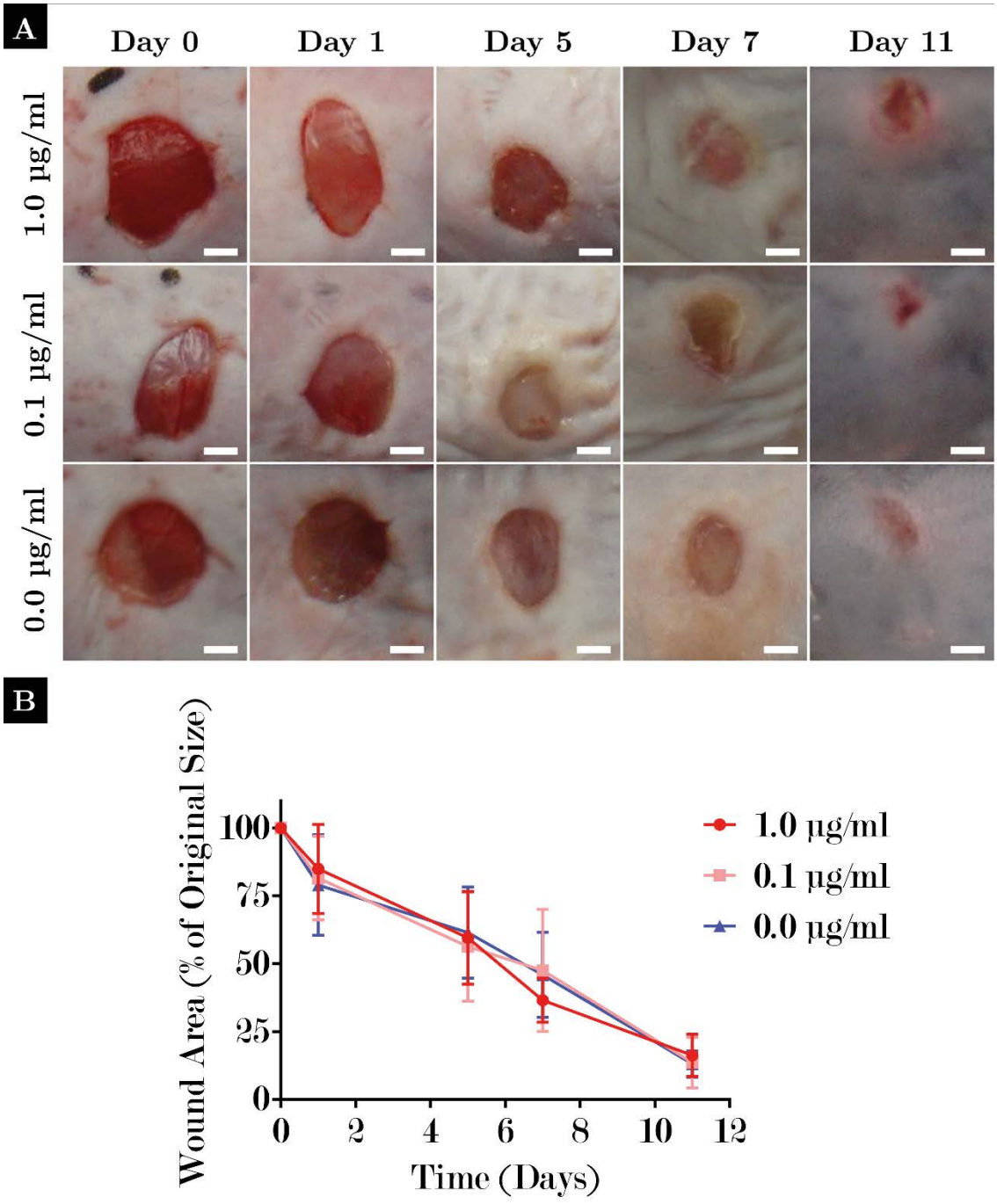

Figure 4.10. Wound closure of mouse wounds measured over 11 days treated with Laponite gels containing a low VEGF dose (0.1 µg/ml) and a high VEGF dose (1.0 µg/ml). (A) Macroscopic images of each treatment group shown over time and (B) the wound area difference (%) plotted over time measured from all wound photos; wounds close in a near-linear fashion over time with $> 80\%$ closure achieved by day 11 (all treatment groups). No significant differences of wound closure between wound treatment groups were measured. Two-way ANOVA analysis was performed using Tukey's multiple comparison post-hoc test. Scale = 2 mm.

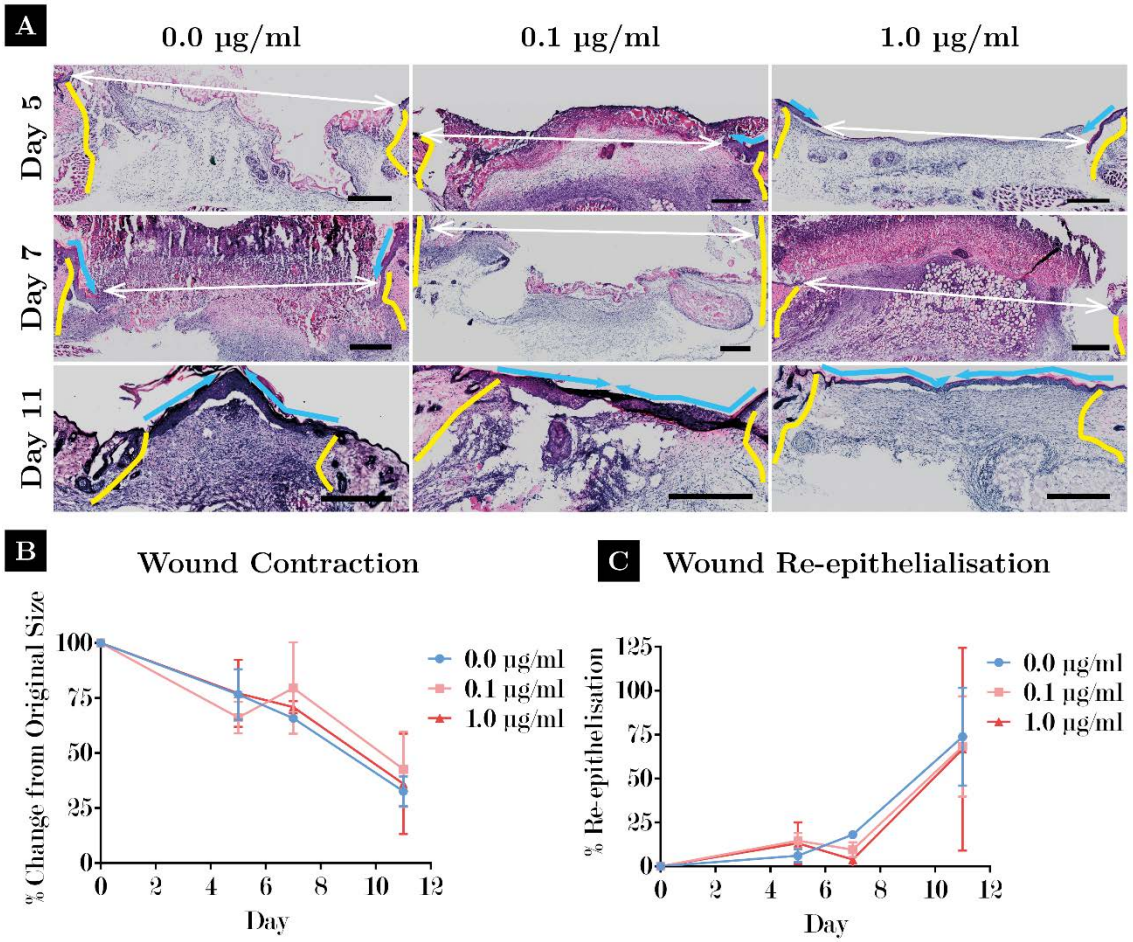

Figure 4.11. Negligible differences in wound closure by contraction or re-epithelialisation with Laponite gel treatments containing low VEGF doses (0.1 µg/ml) or high VEGF doses (1.0 µg/ml). (A) Haematoxylin and eosin stained tissue sections of tissue sampled at different time points. Yellow lines show margins between wound granulation and healthy tissue; measuring between these lines shows the size of the original defect at each time point. Comparing the original defect size between time points can be used to determine wound closure due to contraction. White arrows show the remaining defect; the differences between the two can approximately calculate the wound closure due to re-epithelialisation (depicted by blue arrows). (B) Wound closure rate calculated by the % change of the original defect size overtime and can be used to track wound contraction. There were no significant differences in wound contraction between treatment groups at any time point. (C) The rate of re-epithelialisation between treatment groups was negligible. Two-way ANOVA analysis performed with Tukey's post-hoc test applied for multiple comparisons. Scale = 500 µm.

More detailed information into wound closure rates was determined by serial sections of wound tissue (stained with H&E) harvested at day 5, 7 and day 11 (Figure 4.11 A). Wound closure rate calculated by the % change of the original defect size overtime and can be used to track wound contraction. There were no

significant differences in wound contraction between treatment groups at any time point (Figure 4.11 B).

Although wound contraction is an indicator of the progress of healing overtime, a more important change is the rate of re-epithelialisation. This was shown to be negligible between all treatment groups (Figure 4.11 C).

4.2.3.4 VEGF Premixed in Laponite (≤ 1.0 µg/ml) Does Not Stimulate Significant Blood Vessel Growth

A selective endothelial marker was used (anti-CD31) as a tool for determining blood vessels present within granulation tissue of wounds. Comparisons of anti-CD31 staining between treatment groups was then performed to determine if there were any changes in blood vessel coverage. Thus, an increase in anti-CD31 staining within VEGF treated groups would support the hypothesis that Laponite localises active VEGF.

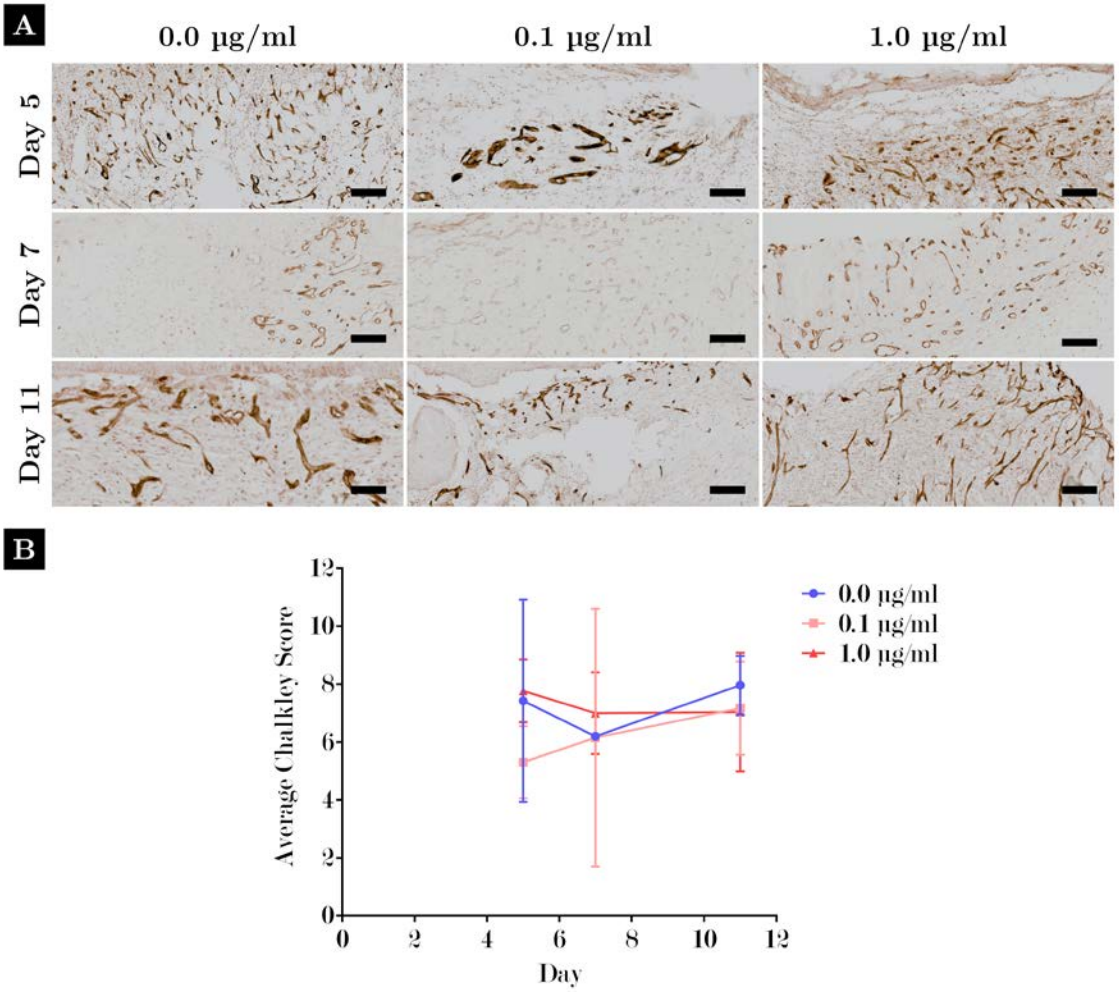

Figure 4.12. Localisation of ≤ 1.0 µg/ml $VEGF_{165}$ encapsulated by Laponite hydrogels does not stimulate in vivo angiogenesis. (A) Tissue samples stained with the blood vessel marker anti-CD31 showed extensive blood vessel growth throughout the wound healing period in all wound treatment groups. Scale = 100 µm. (B) Chalkley count analysis showed that there were negligible differences of blood vessel growth between all treatment groups. Error bars = SD.

Quantification of blood vessel from anti-CD31 stained images was done using a digital Chalkley grid. The digital grid was overlayed over anti-CD31 stained images and rotated until the maximum number of dots land on positively stained vessels (refer to methods Chapter 2.3.9 for more detail).

Tissue samples stained with the blood vessel marker anti-CD31 showed extensive blood vessel growth throughout the wound healing period in all wound treatment groups (Figure 4.12 A). However, Chalkley count analysis showed that there were

negligible differences of blood vessel growth between all treatment groups (Figure 4.12 B).

4.2.3.5 Encapsulated VEGF By Laponite Can Stimulate *In Vivo* Angiogenesis at High VEGF Concentrations (> 1 µg/ml)

Although a VEGF concentration of 1.0 µg/ml exerted a bioactive effect *in vitro* (refer to Chapter 3.2.4), it did not translate to positive effects when applied topically to healthy wounds (Chapter 4.2.3.4). To test whether higher concentrations may be required to stimulate a biological effect *in vivo*, an alternative study approach was undertaken (refer to methods Chapter 2.3.2 for details).

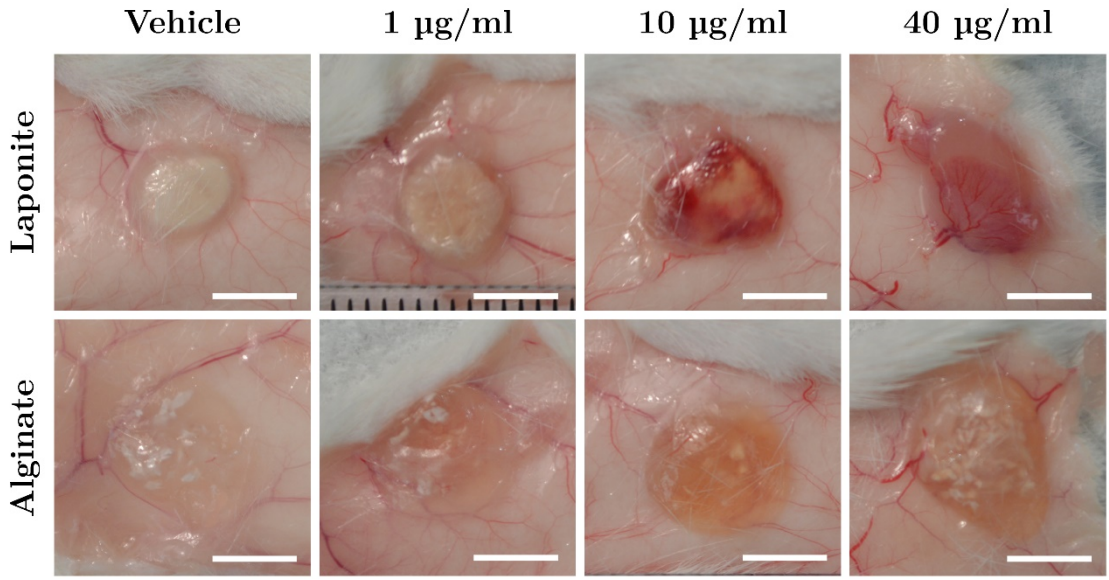

Figure 4.13. Macroscopic images of harvested Laponite/alginate subcutaneous gels after 21 days showed that $VEGF_{165}$ incorporated within Laponite gels stimulated in vivo angiogenesis. Scale bars = 5 mm.

Encapsulated VEGF in Laponite gels was injected subcutaneously on the dorsum of mice. A higher range of VEGF concentrations were tested (1 – 40 µg/ml) to

maximise the chance of determining biological activity *in vivo.* The lowest concentration of 1 µg/ml was chosen given that this was the threshold for significant biolocial activity *in vitro* (refer to chapter 3.2.4). The biomaterial hydrogel 1.1% alginate was also tested as a comparative control. This material had been previously used during rheological analysis in Appendix A.1, primarily because it is well-documented as a biomaterial used in drug delivery applications [277]. It was thought however, that given Laponite's superior adsorption properties alginate would not retain the same quantitiy of VEGF during the 21-day study. This in turn should result in less significant angiogenesis.

Tissue harvested after 21 days showed that Laponite hydrogels encapsulating VEGF exhibited excessive blood vessel growth from surrounding tissue into the Laponite biomaterial (Figure 4.13).

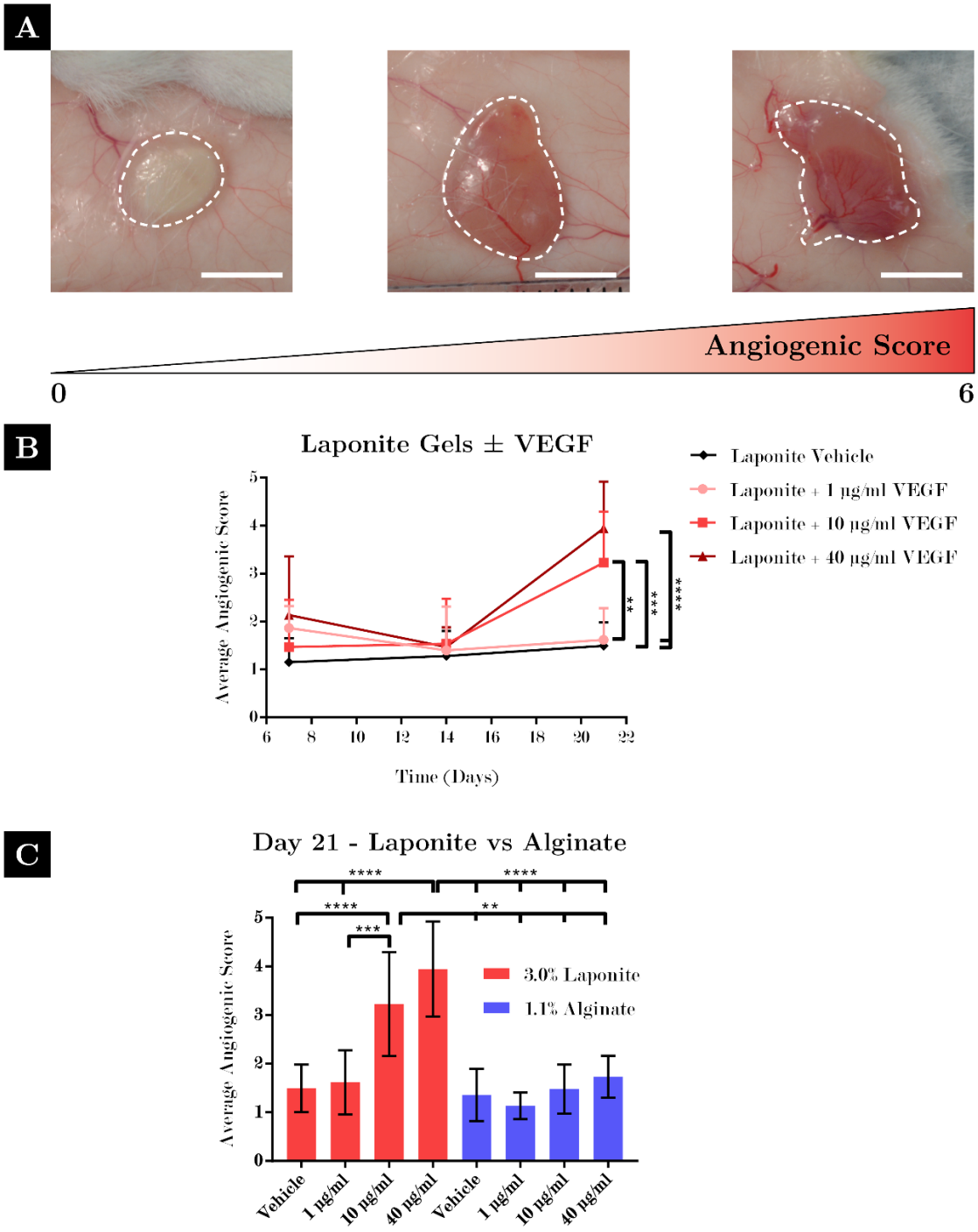

Figure 4.14. $VEGF_{165}$ encapsulated by Laponite hydrogels stimulates in vivo angiogenesis; macroscopic image analysis. (A) The degree of redness/vessel growth into biomaterial gels was scored blindly from 0-6 (only vessels within the biomaterial area was included as shown by the dotted line). (B) Scored data confirmed that there was a significant increase in angiogenesis in Laponite-VEGF treated groups at VEGF concentrations 10 and 40 µg/ml. Error bars = SD. (C) Between alginate groups, there was a slight rise in angiogenic scoring 10 and 40 µg/ml VEGF concentrations but this was not significantly different. Between Laponite and alginate groups, both 10 and 40 µg/ml VEGF concentrations within Laponite had a significantly greater angiogenic score than alginate. Two-way ANOVA analysis performed with Tukey's post-hoc test applied for multiple comparisons. *, **, *** and **** denotes that p = < 0.05, < 0.01, < 0.001 and < 0.0001 respectively. Scale = 5 mm.

This was only apparent with higher concentrations of VEGF (10 and 40 µg/ml), which is 10 and 40 times more concentrated that the stimulatory effect exerted previously *in vitro*. In contrast, VEGF encapsulated by alginate hydrogels exhibitied negligible blood vessel ingrowth.

Blood vessel ingrowth was quantified using visual blinded scoring by volunteers, from 0 (no evidence of angiogenesis) to 6 (excessive redness and vessel ingrowth) (Figure 4.14 B & C). For Laponite samples, image scoring included tissue harvested over the whole time frame (Figure 4.14 B) whereas alginate treatments were only harvested at day 21.

A signficiant increase in angiongenesis in Laponite-VEGF was present in day 21 samples compared to day 7 and 14 samples (10 – 40 µg/ml only). Clearly the period of time after day 14 was critical for blood vessel growth to occur and highlights the importance of sustained localisation of bioactive VEGF (Figure 4.14 B). Between Laponite-VEGF groups at day 21, only 10 and 40 µg/ml was shown to be significantly greater (4.5 ± 4.1 and 8.8 ± 1.4 respectively, $p = < 0.001$, error = SD). Between alginate groups, there was a slight rise in angiogenic scoring 10 and 40 µg/ml VEGF concentrations but this was not significantly different (Figure 4.14 C). Comparing Laponite and alginate groups, both 10 and 40 µg/ml VEGF concentrations had a significantly greater angiogenic score than alginate (10 µg/ml: 4.5 ± 4.1 (Lap) vs 0.2 ± 0.3 (Alg); 40 µg/ml: 8.8 ± 1.4 (Lap) vs 0.0 ± 0.0 (Alg), $p = < 0.001$, error = SD).

4.2.3.6 Histological Analysis

Biomaterial tissue samples were harvested, sectioned and stained with histological dyes. Haematoxylin and eosin (H&E) staining of day 21 Laponite and alginate

samples containing 40 µg/ml VEGF showed a marked difference in biomaterial recovery; Laponite samples appeared rich in cells with notable quanitities of biomaterial still present (Figure 4.15) whereas alginate samples contained large open spaces devoid of cells (Figure 4.16). The presence of Laponite biomaterial was confirmed by Auramine O staining (Figure 4.15 b, d, f). Higher magnification images of Figure 4.15 a and b showed in greater detail the integration of tissue and migration of cells within Laponite fragments. Please note that the staining colour of Laponite in Figure 4.15 is inconsistent with previous Auramine O images (Figure 4.3 to Figure 4.6, which shows Laponite stained as yellow not orange) due to the filter set unavailability; however, the stain's selectively of Laponite was not affected.

Analysis of these H&E images involved software-based removal of eosin stain and segmentation of haematoxylin hotspots, which is selective for cell nuclei and can determine gross cellular infiltration (Figure 4.17 A & B). Image analysis showed that there was greater cellularity within Laponite samples with increasing VEGF concentrations (Figure 4.17 B). However only 40 µg/ml VEGF concentrations were shown to be significantly greater (Figure 4.17 C, 18.4 ± 9.7% $p = < 0.05$, error = SD). In contrast, alginate samples showed negligible invasion of cells across all VEGF concentrations groups.

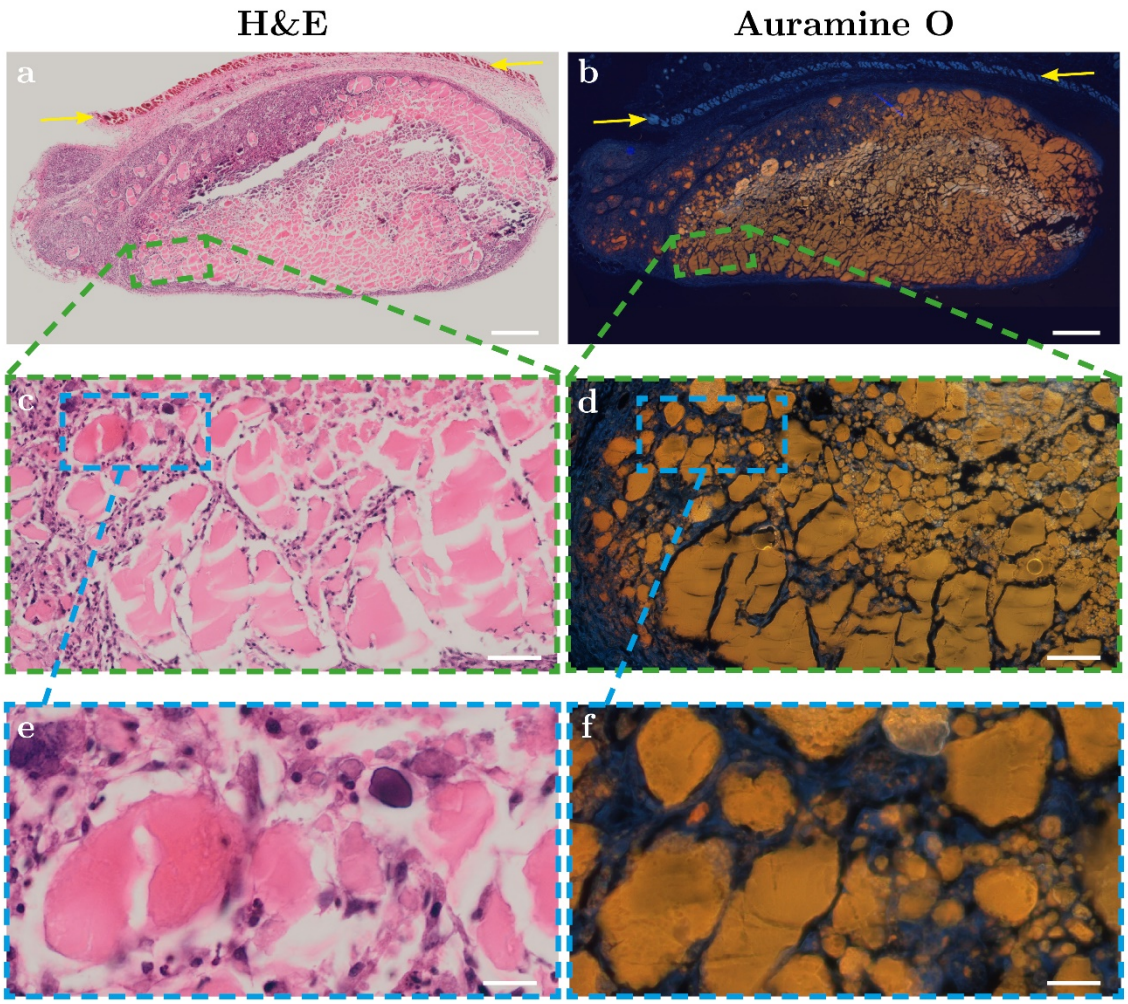

Figure 4.15. Evidence of substantial cell invasion and tissue integration within Laponite gels subcutaneously injected under dorsum of mice (harvested after 21 days). A substantial proportion of Laponite biomaterial was seen in histological section stained with haematoxylin & eosin (H&E); the presence of Laponite biomaterial was confirmed by Auramine O staining, which is a selective fluorescent marker for clays (b, d, f). Filter set 16 (FITC) used (please refer to Chapter 2.3.8.1, Table 2.2 for filter details). Higher magnification images of a and b showed in greater detail the integration of tissue and migration of cells within Laponite fragments (e-f). Yellow arrows depict the panniculus carnosus (a thin layer of striated muscle) indicating that Laponite biomaterial was present subcutaneously. Scale = 1 mm (a & b), 100 µm (c & d) and 25 µm (e & f).

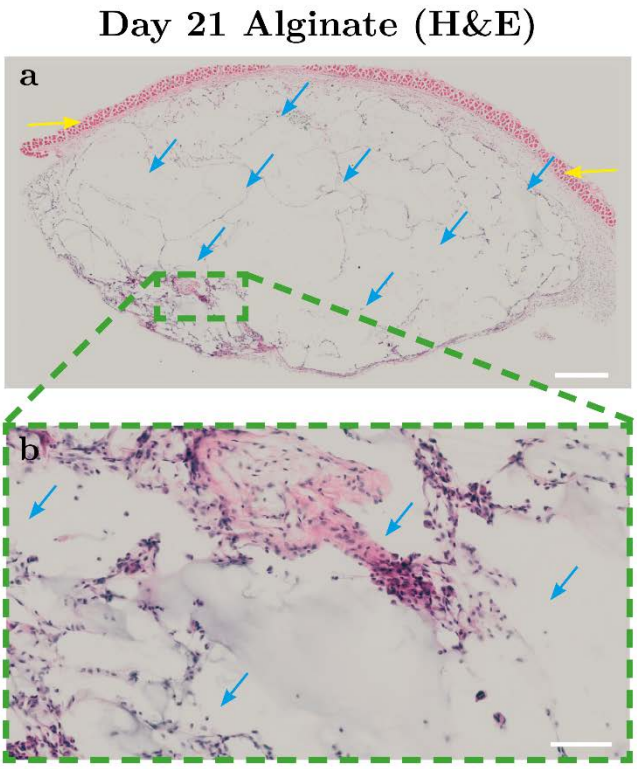

Figure 4.16. Minimal cell invasion and tissue integration within alginate gels subcutaneously injected under dorsum of mice (harvested after 21 days). H&E stained tissue specimen of day 21 alginate samples showed that large areas devoid of alginate biomaterial and cell/tissue content (blue arrows). Image panel b shows a region of higher magnification (x20) where there was evidence of cells and tissue within the treated area; the quantity of biological tissue integration was much less than Laponite-treated samples shown in the previous figure. Yellow arrows depict the panniculus carnosus (a thin layer of striated muscle) indicating that alginate biomaterial was present subcutaneously. Scale = 1 mm (a) and 100 µm (b).

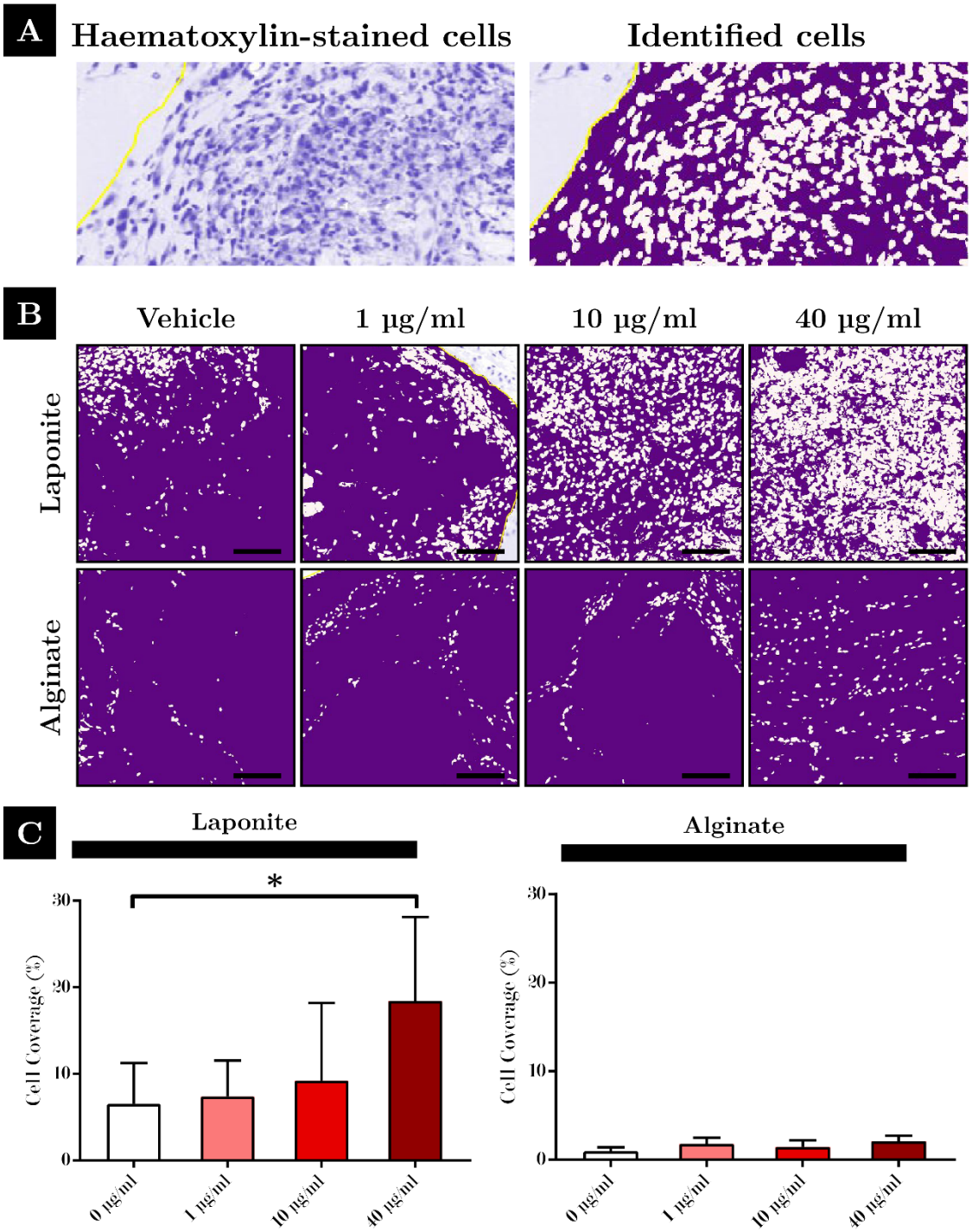

Figure 4.17. Comparison of cell invasion within Laponite and Alginate biomaterial at 21 days. (A) Example image of high powered magnification of cells stained with haematoxylin (left panel); using computer-based software, cell invasion into biomaterial was identified, segmented and density of cells measured by percentage cell coverage. Scale = 100 µm. (B) Segmented cell analysis showed greater cell invasion in Laponite-treated groups when incorporated with increasing VEGF concentrations; in contrast alginate treatments showed very minor changes. (C) Quantification of cell coverage as described in (B) confirms this trend; only 40 µg/ml VEGF mixed within Laponite exhibited a significant difference. Error bars = SD. One-way ANOVA analysis performed with Tukey's post-hoc test applied for multiple comparisons. * denotes that $p = < 0.05$.

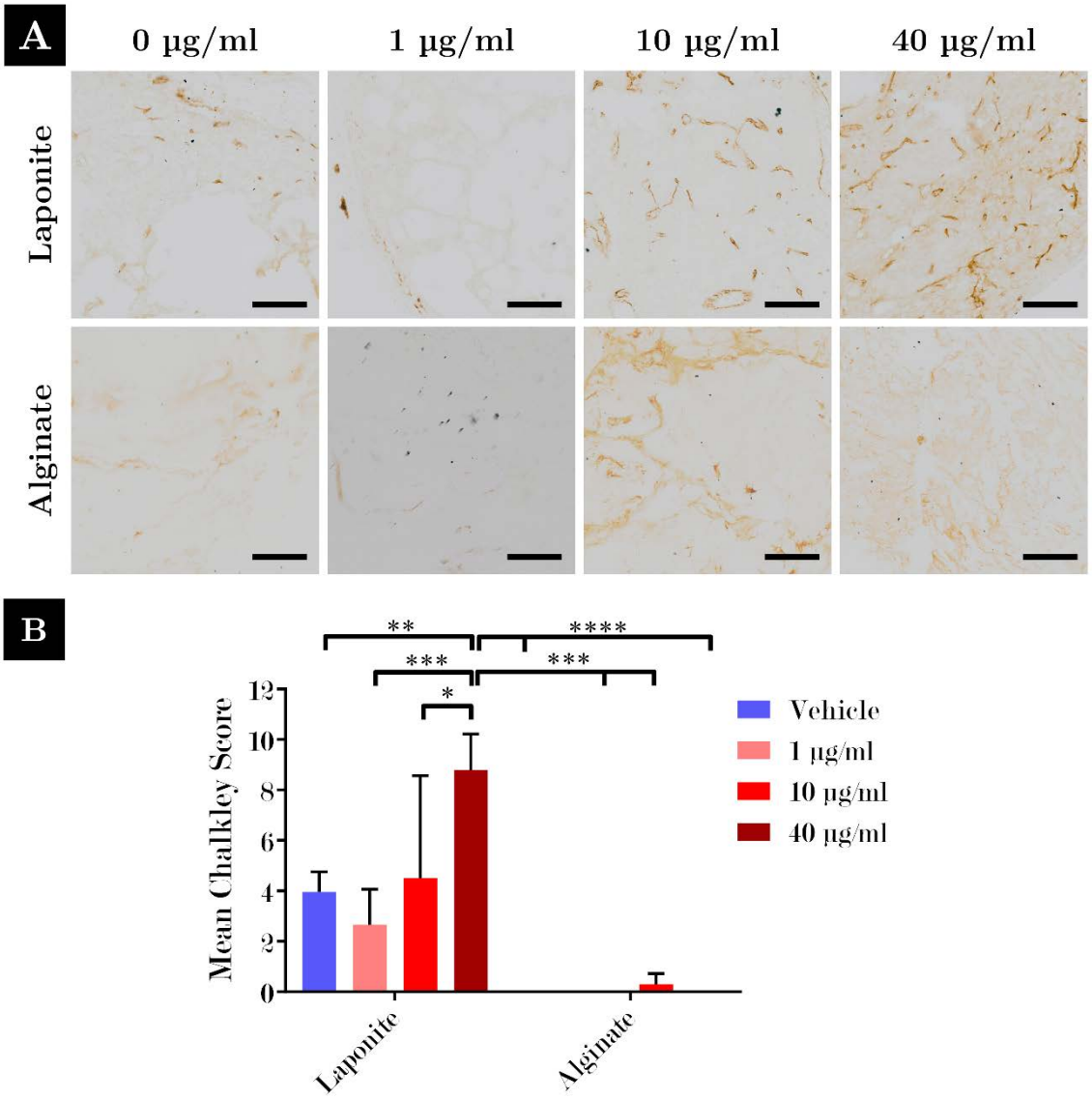

Figure 4.18. Localisation of $VEGF_{165}$ encapsulated by Laponite hydrogels stimulates in vivo angiogenesis; immunohistochemical analysis. (A) Tissue samples stained with the blood vessel marker anti-CD31 showed greater density of blood vessels at higher (10 & 40 µg/ml) VEGF concentrations when localised by Laponite biomaterial; there was a minor change with alginate biomaterial treatment. Scale = 100 µm. (B) Chalkley count analysis showed that 40 µg/ml VEGF mixed within Laponite caused significant growth of novel blood vessels when compared to lower VEGF concentrations and all VEGF concentrations present within alginate biomaterial. Error bars = SD. One-way ANOVA analysis performed with Tukey's post-hoc test applied for multiple comparisons. *, **, *** and **** denotes that staining of blood vessel marker, anti CD31 shows a significant increase ($p = < 0.05, < 0.01, < 0.001$ and < 0.0001 respectively).

Staining of tissue sections with anti-CD31 (an endothelial cell marker) showed a greater density of blood vessels at higher (10 & 40 µg/ml) VEGF concentrations when localised by Laponite biomaterial. There was a minor change with alginate

biomaterial treatment (Figure 4.18 A). Chalkley count analysis showed that the number of vessels increased with higher VEGF concentrations in Laponite samples. Only 40 µg/ml VEGF was shown to be significantly different when compared to other concentrations and Laponite vehicle (8.8 ± 1.4 angiogenic score (40 µg/ml) vs 4.0 ± 0.8 (0 µg/ml); $p = < 0.01$, error = SD). Conversely, there was negligble detection of blood vessels in alginate samples (Figure 4.18 C).

4.2.4 *In vitro* Release of VEGF from Laponite Hydrogels

Compared to aqueous VEGF concentrations *in vitro*, the concentration of VEGF required to induce a biological response through Laponite encapsulation was between 25-fold larger (*in vitro* tubule assay) and 250-fold larger (*in vivo*). This reduction in activity was hypothesised due to the retension of VEGF within the gels. Although, whether or not increasing the concentration past a particular threshold amount results in release of 'free' VEGF is unknown; release may not occur and sustained localisation may be responsible.

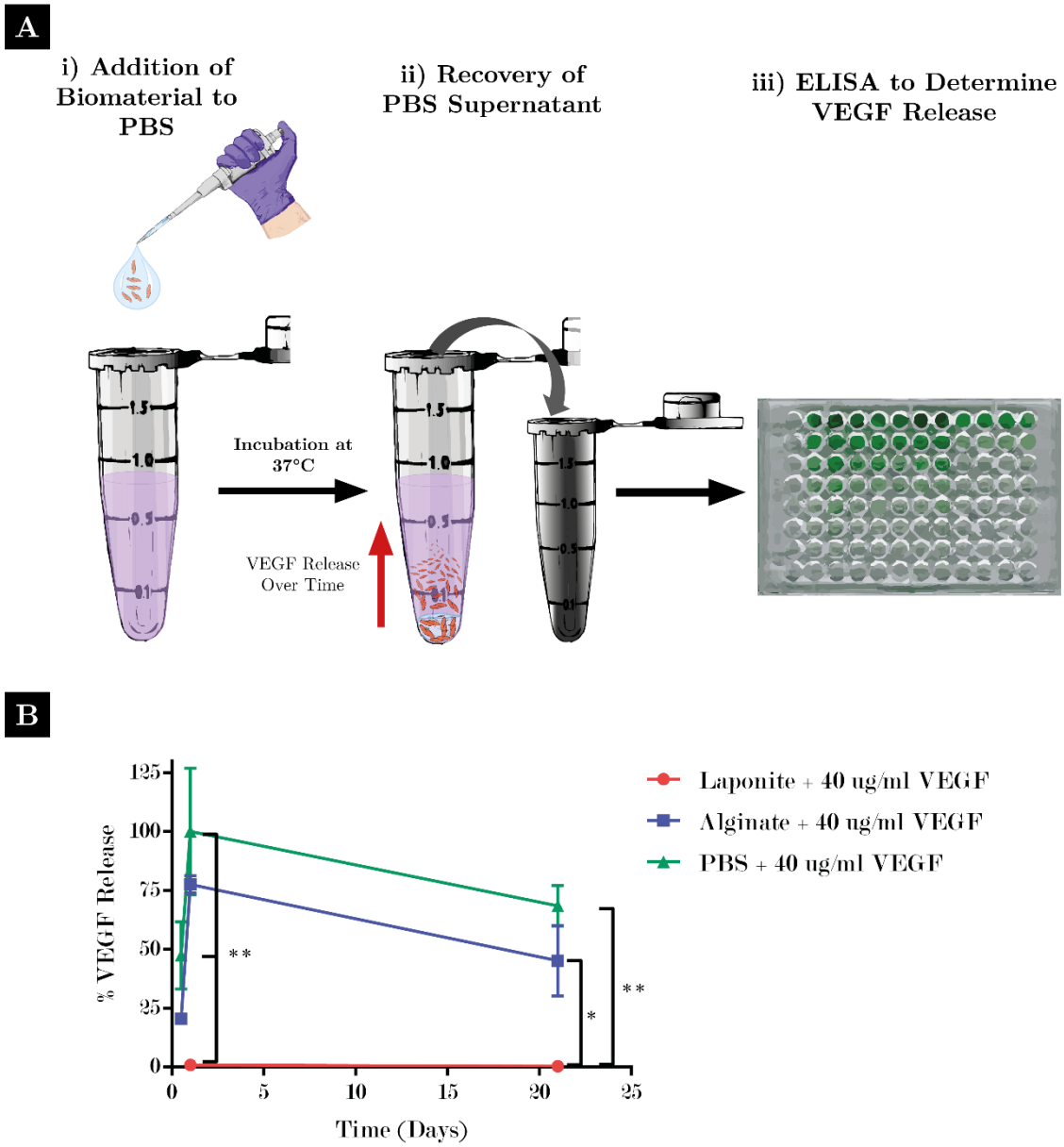

Figure 4.19. **Laponite hydrogels exhibits minimal release of proangiogenic VEGF$_{165}$ measured over 21 days. (A)** Diagram showing the study setup; i) Laponite/Alginate biomaterial was pre-mixed with VEGF (sterile water for vehicle control) prior to adding to sterile PBS (final VEGF concentration was 40 µg/ml). Biomaterial was then added dropwise into PBS as a 1:10 dilution and each tube incubated at 37°C. ii) At various time points between 30 minutes to 21 days, a sample of the PBS supernatant was recovered and frozen; iii) To determine VEGF concentration (and thus release from the biomaterial), an ELISA was performed. (B) There was negligible release of VEGF from Laponite gels whereas a burst release was exhibited from alginate gels. The amount of VEGF measured at 21 days was reduced in both alginate and PBS groups suggesting that the stability of VEGF had diminished overtime; the amount released at this time point was still significantly greater than the Laponite gel group. Two-way ANOVA analysis performed with Tukey's post-hoc test applied for multiple comparisons; * and ** denotes that p = < 0.05 and < 0.01 respectively. Error bars = Standard error of the mean (SEM).

To test this an *in vitro* release assay was performed where encapsulated VEGF in Laponite was added dropwise into PBS. Samples of PBS were recovered at various time points and VEGF content analysed using an ELISA (Figure 4.19 A). There was negligible release of VEGF from Laponite gels after 21 days (0.3 ± 0.4% release). In contrast, a burst release was exhibited from alginate gels with 77.5 ± 6.6% VEGF released after 1 hour. The amount of VEGF measured at 21 days was reduced in both alginate and PBS groups suggesting that the stability of VEGF had diminished overtime. The amount released at day 21 was still significantly greater than the Laponite gel group (Figure 4.19 B; mean difference between Laponite and alginate after 21 days: -44.8 ± 14.1%, $p = < 0.05$, error = SEM).

4.3 Discussion

The main aim was to develop a suitable wound healing model and test the hypothesis that Laponite can localise bioactive factors (specifically VEGF) and increase the rate and degree of wound healing. This was tested in healthy mice to optimise a model in addition to having a control sample for comparison. Initially the model was adapted from and tested with Laponite biomaterial alone; this was to ensure that Laponite could be located at a wound site and be retained for at least 1 week, investigate the general biocompatibility within a skin defect and determine any potential effects (positive or negative) on wound healing.

Reduced closure rates exhibited in Laponite gel treatments compared to the PBS control was likely due to inhibited wound contraction. Despite this, there was negligible difference in wound re-epithelialisation. It is well known that mouse wounds contract significantly whereas human wounds heal predominantly by re-epithelialisation [278]. Laponite wounds exhibited greater cellularity in the wound bed compared to the PBS; this was likely due to Laponite's sorptive abilities which can act as a scaffold and localise cellular cues as a chemoattractant [13, 279].

Our research has proven that Laponite was retained from a single application at day one for a minimum of 7 days, including removal and replacement of dressings. Multiple applications of growth factors are not desirable due to the negative repercussions they can exhibit. A study by Galiano *et al* [146] documented that multiple applications of 40 μg VEGF per wound was required to stimulate accelerated wound healing. The requirement to use such high doses was speculated to overcome the fragility of the protein *in vivo* (low biological half-life) [147].

However, it was reported that this led to an unwanted systemic response in the contralateral PBS wound. Other growth factors have also shown to exhibit negative side-effects when applications are in excess, including ectopic bone growth when using bone morphogenetic protein-2 (BMP-2) [280] and increased risk of malignancy with PDGF-BB [281]. Therefore, the retention of the biomaterial at the wound site is an encouraging finding, which supports the notion that it could act to sustain growth factor delivery in a controlled fashion over a prolonged length of time.

Alginate was used as a control due to its well-established use as a biomaterial for drug delivery [231, 234]. Systems that use alginate gels for drug delivery usually combine it with other biomaterials such as Poly (D, L)-lactide-co-glycolide (PLGA) to obtain slower release [231, 282]. Otherwise, alginate gels alone mixed with VEGF will result in complete release up to 7 days [283]; this is similar to the release documented in this chapter. Interestingly the study by Lee *et al* [283] showed a significant increase of blood vessels surrounding granulation following alginate hydrogel injection when ≥ 20 µg/ml VEGF was incorporated. This contrasted with our results where the highest VEGF concentration (40 µg/ml) did not show much vessel growth. One possible explanation could be the difference in mouse strain as Lee *et al* [283] used immunodeficient (SCID) mice.

Auramine O enabled simple, effective tracking of the Laponite by its fluorescence. It is a substituted diphenyl-methane cationic dye that can interact and adsorb to the negatively charged surface of clay particles [284]. Upon binding with clay particles the Auramine O molecules exhibit an internal conversion process via rotational diffusion of the phenyl rings; this excited state leads to fluorescence

[285]. The distribution of Auramine O staining suggests biocompatibility and possible cellular uptake of Laponite fragments (e.g. endocytosed Laponite) (see Figure 4.6). In contrast, this evidence may just show more extensive cell infiltration within Laponite biomaterial. However, further study would be required to track Laponite over a longer time frame to determine how Laponite would be removed from the body. A longer wound healing study to the point of complete wound recovery would be required and perhaps alternative methods of detecting removal of Laponite waste management (i.e. harvesting liver tissue).

Four wounds per mice were used to decrease the number of experimental animals used in the study. It has been shown by Park *et al* [286] the process of wound healing between rostral and caudal regions are similar. The use of multiple wounds per mouse has been proven to be comparable between one another. The wounds could be considered as independent biological replicates [287]. This is also advantageous to meet the 'reduction' aspect of the 3R's [288, 289]. Our results corroborated previous literature that wound closure between multiple wounds (rostral versus causal) had negligible differences.

Blood glucose and weight levels did not change over the course of the study and are in line with other documented research using healthy mice [290].

It has been well established by Dawson *et al* [235] that Laponite gels can easily be extruded through a 25G needle. In addition, its viscosity can be temporarily reduced after applying a shear force, further improving its ability to be applied via injection or topically. In this Chapter, it was confirmed that Laponite gels do exhibit good thixotropic behaviour at both 25°C (ambient storage) and 37°C (body temperature) (refer to Appendix C.1). Cross-linked alginate gels also

exhibited good thixotropy although the viscosity of these gels was much greater. While both Laponite and alginate gels could be administered through a 25G needle, Laponite gels exhibited potentially better effective delivery due to its lower viscosity.

The addition of VEGF to Laponite gels did not improve the rate of wound healing in this preliminary study. One explanation for this is that the concentration of VEGF used was insufficient. This was supported by the subsequent *in vivo* experiments showing that higher doses of VEGF injected subcutaneously markedly increased angiogenesis, and illustrates a disparity between the *in vitro* experiments (Chapter 3.2) and the *in vivo* experiments reported here.

Higher concentrations of VEGF also led to higher cellularity in wounds; VEGF is known to be a chemokine that stimulates cell invasion [291]. It would have been interesting to determine what types of cells were present in greater numbers, specifically those that are linked to inflammation and proliferations (neutrophils, macrophages and fibroblasts). Further staining using markers for these cell types could have provided further insight for this investigation.

The release study showed that negligible VEGF was released from Laponite gels containing high (40 µg/ml) VEGF. Previous *in vitro* studies [292] have reported greater VEGF retention within Laponite ($\leq$ 34 days). Whether Laponite's ability to retain proteins *in vivo* is comparable to *in vitro* is not easy to conclude as a variety of external parameters are at play in a biological system [293].

Testing the hypothesis that the release kinetics would be the same *in vivo* would also be challenging. A possible method could be to increase the number of

Laponite droplets added to PBS in the *in vitro* release study. This could increase the surface area of the Laponite to the release environment and induce a greater chance of diffusion. Another possibility could be to agitate a gel capsule to mimic any potential release from the Laponite. However, *in vivo* approaches would be advantageous and could include encapsulating fluorescently-tagged protein/ VEGF within Laponite gels, fluorescently tagging Laponite and measure its degradability over time [294] or using an *in vivo* imaging system to track protein release [293].

The key findings of these results were: that Laponite can be retained within a wound site a minimum of 7 days; encapsulated VEGF $\leq$ 1 µg/ml did not increase the rate of wound closure, re-epithelialisation and formation of blood vessels; and the subcutaneous study showed that higher concentrations ($\geq$ 10-fold increase) of encapsulated VEGF was required to initiate a proangiogenic response *in vivo* (most likely due to localisation of VEGF opposed to controlled release of VEGF).

These studies offered a good framework to test further whether Laponite hydrogels can deliver (via localisation) VEGF to increase the rate and degree of wound healing in a delayed (*db/db)* wound model.

Chapter 5:

Laponite Gels for Localising Bioactive VEGF in a Diabetic Model of Wound Healing

5.1 Introduction

So far, data in this thesis has shown that Laponite can effectively retain bioactive factors at wound sites, promoting aspects of wound healing both *in vitro* and *in vivo*. The most promising finding was that localisation of 3% Laponite gels containing ≥ 10 µg/ml VEGF successfully stimulated blood vessel growth under the dorsal skin of healthy mice (refer to Chapter 4.2.3.5). However, to fulfil the overarching aim for Laponite to deliver bioactive factors (in this specific case, VEGF) to improve the recovery of chronic non-healing wounds, a more suitable testing model is required.

There are several animal chronic wound models that represent diabetes, including those with a genetic predisposition or those that have been chemically induced [295]. A chemically-induced method involves injection of streptozotocin, which destroys pancreatic beta cells (leading to cessation of insulin production) and mimics symptoms of type 1 diabetes. Another model of type 1 diabetes are Akita mice. Representative models of type two diabetes include *db/db* mice and NONcNZO10 mice [295].

Mice representing a model of type 2 diabetes were selected because it is the most dominant form of diabetes worldwide, accounting for about 90% of all cases (refer to Chapter 1.2.1). *db/db* mice were chosen since they are well-established as a model of delayed wound recovery that have been used in many wound healing studies [146, 296, 297]. Furthermore, previous studies have used these mice to investigate the biological effect that VEGF can exert on diabetic wound healing [146]. The development of diabetes in *db/db* mice is due to a deficiency in leptin

receptor activity. Activity is diminished because *db/db* mice are homozygous for a point mutation within the leptin receptor gene [298]. As leptin is a hormone that has a major influence on energy balance and the feeling of satiety [299], food intake increases dramatically. By 6-weeks old the impact of leptin deficiency is very significant, where they have developed symptoms of severe obesity, dyslipidaemia and type 2 diabetes [300].

The delayed healing response manifested in *db/db* mice is understood to be a result of reduced growth factor production, especially VEGF [146]. In addition, wound contraction is severely reduced compared to healthy mice; this reduction in contraction is advantageous as human skin does not contract as prominently and heals via re-epithelisation. Therefore, reduced contraction exhibited by *db/db* mice skin will allow for better opportunities to detect re-epithelisation in wound healing.

This chapter will focus on testing the hypothesis that Laponite gels can localise VEGF to wounds and increase the rate and quality of wound healing in a model of diabetic healing. To achieve this, the aim of this chapter was:

- To determine the effect of vehicle Laponite gels on wound healing in *db/db* mice by compared to saline control.
- To investigate localisation and bioactive effect of VEGF- containing Laponite by:
    - Treating *db/db* wounds with Laponite and alginate gels containing 40 µg/ml VEGF

- Comparing against a control biomaterial (alginate), which does gel with and without ± VEGF
- Using a marker of Laponite (Auramine O) to track the integration and persistence of Laponite within the wound environment over an 18-day time frame.

5.2 Results

5.2.1 Weight and Blood Glucose Measurements

The mean weight and blood glucose levels of *db/db* mice were measured to clarify that symptoms that are associated with type 2 diabetes (e.g. significantly greater mass and chronic hyperglycaemia (≥ 11.1 mmol/l or ≥ 200 mg/dl) compared to healthy mice) were present throughout the study. This was aided by comparing the mean weight and blood glucose levels with measurements taken from non-diabetic (healthy) mice documented in Chapter 4.2.3.

5.2.1.1 Comparison of Average Weight Between Healthy and Diabetic Mice

The mean weight of *db/db* mice decreased slightly 1-day post-surgery, but then there was a gradual rise in mean weight up until day 11 (the mean day 11 weight was equivalent to the mean pre-surgery weight) (Figure 5.1). The mean weights of healthy mice taken from previous studies (refer to Chapter 4.2.3.2) has been included on this graph for comparison; it was clear that *db/db* mice had a significantly greater mass (~40%) than healthy C57BL/6 mice (Day 14 difference, 14.5 ± 1.3 g, $p = < 0.0001$, error = SE)

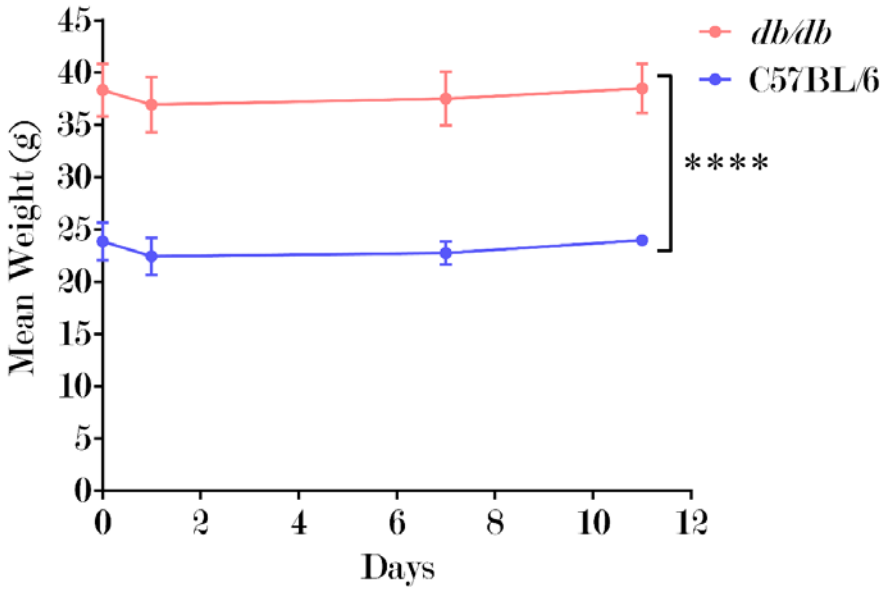

Figure 5.1. Differences in the mean weight of *db/db* and C57BL/6 mice over 11 days. *db/db* mice weighed significantly more than healthy C57BL/6 mice due to severe obesity from excess eating. Both strains of mice exhibited an initial drop in weight post-surgery which was attributed to lack of eating after recovering from anaesthesia. Two-way ANOVA analysis was performed using Tukey's multiple comparison post-hoc test, p = < 0.001 (denoted by ****).

5.2.1.2 Comparison of Average Blood Glucose Between Healthy and Diabetic Mice

The mean blood glucose of fasted mice was 21.6 ± 8.4 mmol/l compared with 23.8 ± 4.6 mmol/l measured in the non-fasted group and the difference was not statistically significant (error= SD, $p = 0.09$).

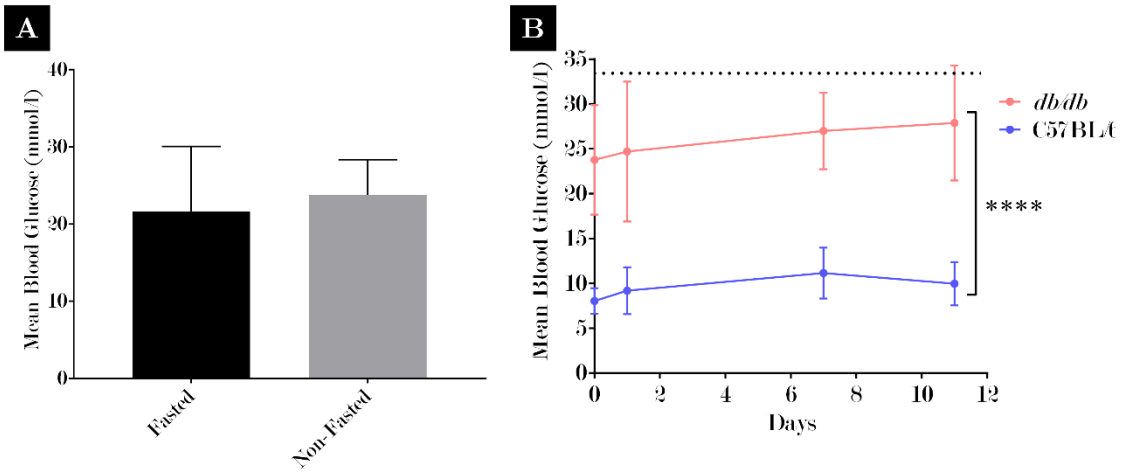

Figure 5.2. Differences in mean blood glucose levels of db/db and C57BL/6 mice over 11 days. (A) Comparison between 6-hour fasted and non-fasted blood glucose levels of db/db mice prior to surgery; there were negligible differences between fasted and non-fasted and it was determined that non-fasted blood glucose testing could be used for the duration of the study (21.6 ± 8.4 mmol/l vs 23.8 ± 4.6 mmol/l, p = 0.09). (B) db/db mice exhibited severe hyperglycaemia over 11 days during the wound healing study period; compared to healthy C57BL/6 mice used in previous studies (refer to Chapter 4.2.3.1), the average blood glucose levels were significantly higher. p = < 0.001 (denoted by ****). Two-way ANOVA analysis was performed using Tukey's multiple comparison post-hoc test.

The mean blood glucose of *db/db* mice increased slightly over the 11-day measuring period, although this was not significant Figure 5.2 B.

The mean blood glucose of healthy mice taken from previous studies (refer to Chapter 4.2.3.1) has been included on this graph for comparison. *db/db* mice exhibited significantly higher blood glucose levels (25.8 ± 1.9 mmol/l) than healthy mice (9.6 ± 1.3 mmol/l), which confirms that *db/db* mice were severely hyperglycaemic (error = SD, $p = < 0.0001$).

5.2.2 Diabetic (*db/db*) Mice Exhibited Delayed Wound Closure Compared to Healthy Mice

To confirm that *db/db* mice exhibited delayed wound healing as per reports documented in the literature [146, 296, 297], wound closure rates between *db/db*

and non-diabetic (healthy) mice were compared. Healthy wound closure data was previously reported in Chapter 4 and has been adapted for the purposes of comparison with *db/db* mouse data (please note that there were minor experimental differences between these studies; refer to methods Chapter 2.3.3 for details).

Wound healing was first compared between healthy and *db/db* mice with addition of PBS control. This was achieved by comparing wound photographs taken over time to assess the change in wound size and determine the average closure rates (Figure 5.3 A). It showed that *db/db* mice exhibited a minor reduction in the rate of wound closure between day 0 and day 7 compared to MF1 (healthy) mouse wounds (Figure 5.3 B). Due to the lack of testing data available from the previous healthy mice study, no further comparisons after 7 days could be made.

A more robust comparison between wounds that had been treated with vehicle Laponite gels $\leq$ 11 days in C57BL/6 mice was then performed (Figure 5.4). Macroscopic wound images show that *db/db* wounds closed more slowly than C57BL/6 (Figure 5.4 A). Interestingly, the wound surface area of *db/db* day 0 wounds appeared larger than C57BL/6 (original diameter of both circular wounds was 6 mm). Analysis of wounds images confirmed that *db/db* wounds showed a significant reduction in wound closure compared to C57BL/6 mice (Figure 5.4 B, $p = < 0.001$). These results prove that *db/db* mice of a similar age (8-10 weeks) used in subsequent studies exhibited delayed wound closured compared to healthy mice.

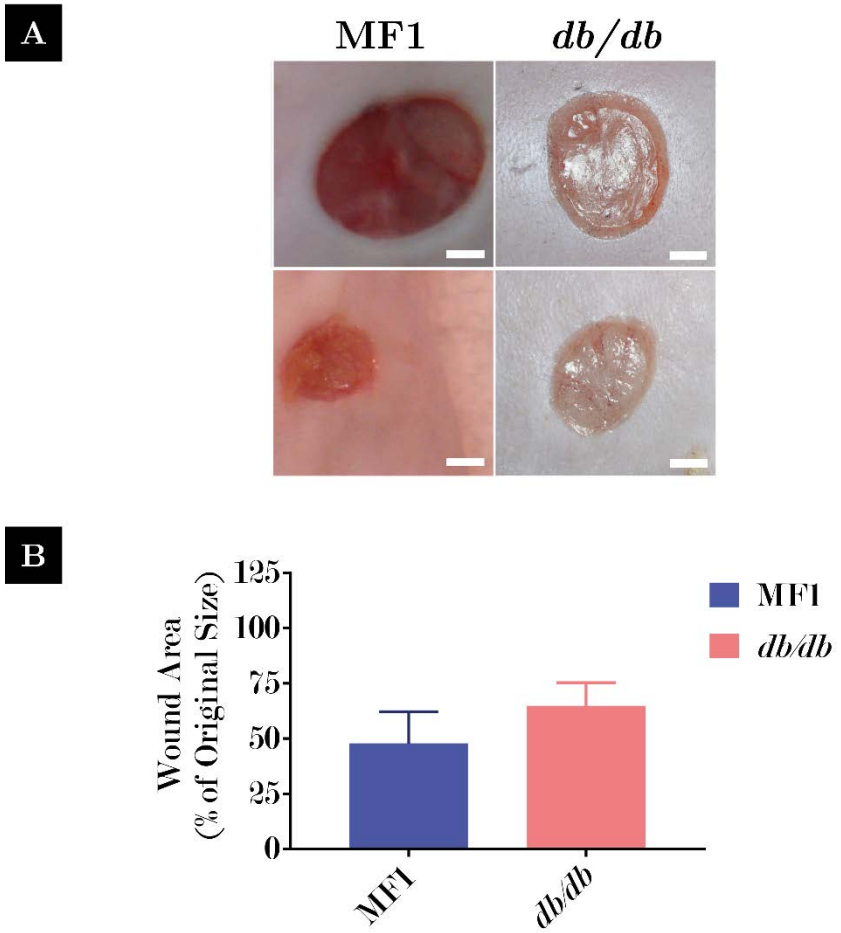

Figure 5.3. Differences in wound closure rates (PBS treatment) in MF1 (healthy) and *db/db* (diabetic) mice up to 7 days. (A) Macroscopic images of healthy vs diabetic wounds treated with Laponite and PBS. Scale bars = 2 mm. (B) Wound closure rates from day 0 to day 7 measured from macroscopic images in A. Healthy mice exhibited a slight increase in wound closure compared to diabetic mice in both treatment groups. PBS treatment also exhibited a greater increase in wound closure than Laponite gels in both mice. However, none of these differences were significant. Error bars = SD.

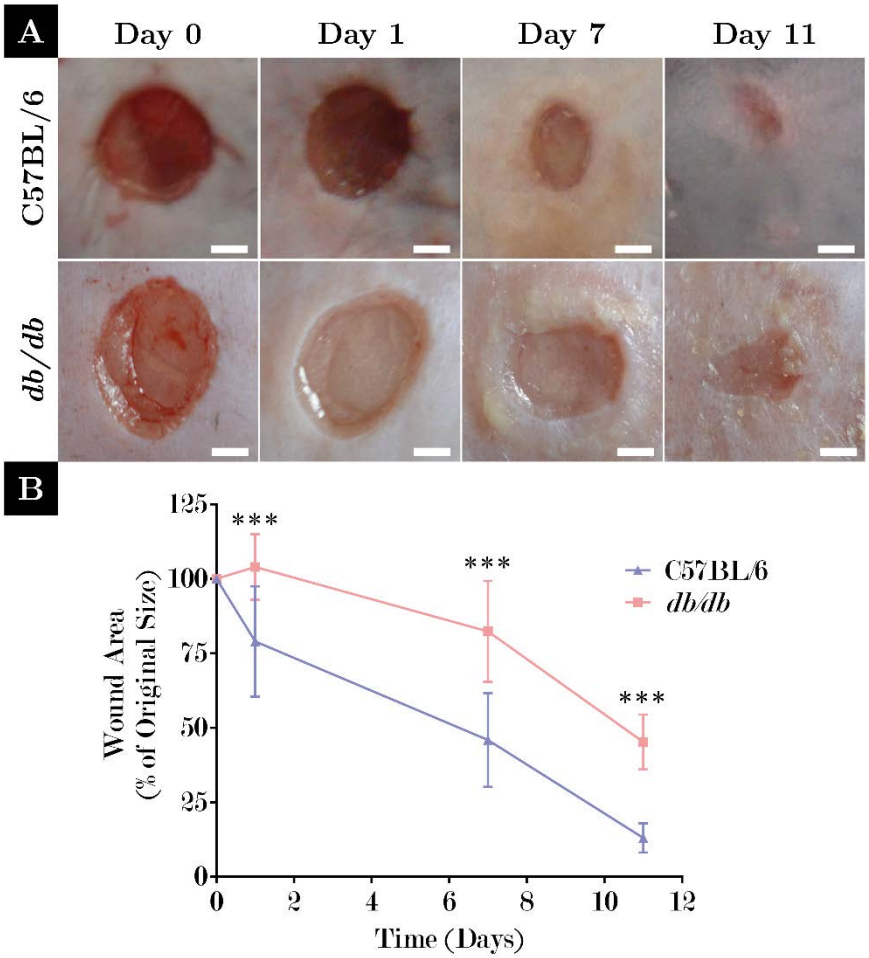

Figure 5.4. Differences in wound closure rates between C57BL/6 (healthy) and *db/db* (diabetic) mice treated with vehicle Laponite gels up to 11 days. (A) Macroscopic images of healthy vs diabetic wounds treated with Laponite; healthy wounds closed more quickly than diabetic. Scale bars = 2 mm. (B) Wound closure rates measured from macroscopic images in A. Healthy mice treated with Laponite gels closed at a significantly quicker rate than diabetic mice at all time points up to 11 days. *** denotes that $p = < 0.01$. Error bars = SD. Two-way ANOVA analysis was performed using Tukey's multiple comparison post-hoc test.

5.2.3 The Effect of Laponite Hydrogels on Wound Appearance, Closure & Re-epithelialisation in *db/db* mice

5.2.3.1 Changes in Macroscopic Appearance

The changes in the macroscopic appearance of wounds can be a useful guide of determining the progress of wound healing. Therefore, wound photographs taken over time were arranged to compare differences in wound size and colour at different anatomical sites treated with Laponite or PBS (Figure 5.5). Wounds from different dorsal locations (rostral or caudal) were initially separated to clarify any potential effects that wound location may exert in *db/db* mice.

The first observation was that there was a similar wound size reduction in all treatment groups at both locations (Figure 5.5 A and B). Residual wound exudate was present in and around Laponite treated wounds; this can be seen most clearly within the rostral and caudal day 7 wounds. History of this exudate was evident by a red impression (day 7 and 11 rostral Laponite images) and/or the presence of dehydrated tissue debris (day 11 rostral and caudal Laponite images). At day 14, healthy tissue adjacent to the Laponite rostral wound was now grey as opposed to red. Within 4 days the grey region had become significantly darker and resembled the pigmentation associated with hair follicle anagen. This was also present within the caudal Laponite-treated wound at day 18, albeit to a lesser degree. In contrast, there was no evidence of wound exudate or the formation of dark pigmentation within any of the PBS-treated wounds.

Other changes in wound appearance from day 11 until day 18 suggested that Laponite wounds exhibited an improvement in wound "quality" compared to PBS. These changes can be seen in more detail in Figure 5.6. It shows that the caudal Laponite wound (Figure 5.6, c) had a less red and dehydrated appearance compared to other day 11 wounds and exhibited wrinkling around the wound margins.

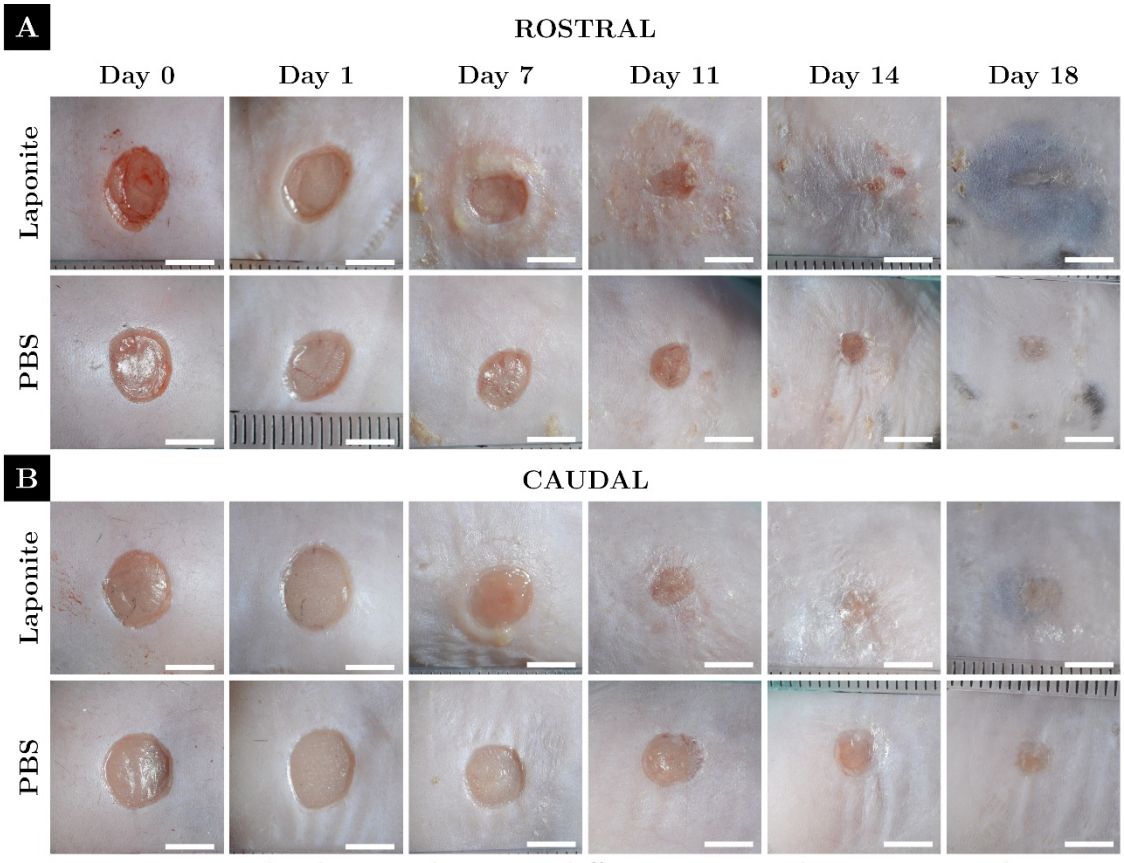

Figure 5.5. Differences in closure rates between rostral and caudal wounds. (A) Wound photographs were taken over time to assess the change in wound size and determine the average closure rate in wounds located towards the rostral end of the mouse dorsum. (B) The same study as (A) but for wounds located towards the rostral end of the dorsum. Scale bars = 5 mm.

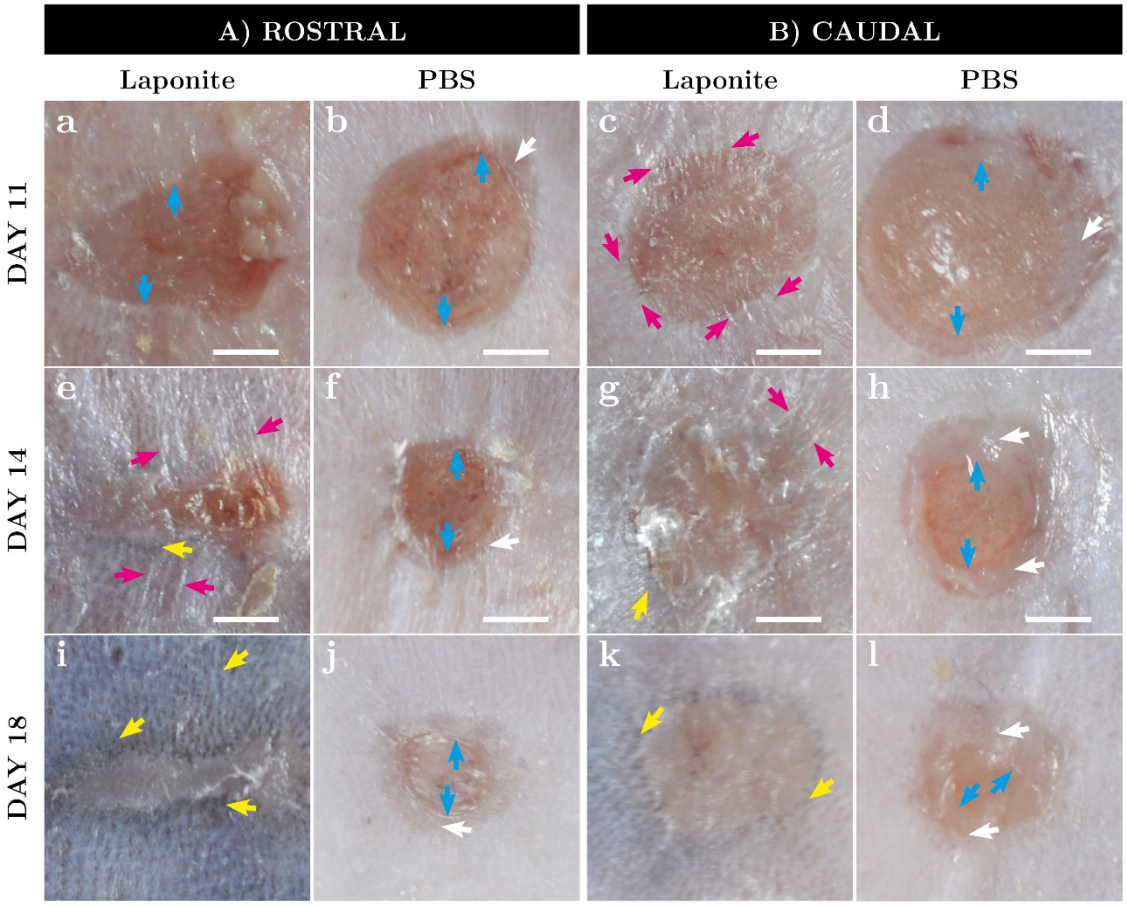

Figure 5.6. Macroscopic evidence showing that Laponite-treated wounds exhibited a more mature, fibrous appearance between day 11 and 18 in both rostral and caudal locations. DAY 11: Wounds all exhibited a red, well perfused appearance. (a-d). Caudal Laponite wound (c) had a less red and dehydrated appearance compared to other day 11 wounds with wrinkling around the wound margins (pink arrows). DAY 14: Laponite-treated wounds (e and g) less red appearance compared to PBS treatments (f and h). These wounds also had a "flaky", dehydrated texture with wrinkling around the wound edge. Additionally, grey areas had formed around the edge of the original defect margin (hair follicle anagen - yellow arrows). Both PBS wounds (f and h) had a red depressed centre region. Beyond the circular depression region, there was evidence of soft tissue formation (indicative of epithelial migration, depicted by white arrows). DAY 14: Laponite wounds exhibited negligible redness (i and k) with a light pink/grey colour. Increased grey areas (hair follicles) around the wound and healthy tissue (yellow arrows). These wounds looked less dehydrated, with reduced wrinkling and less tissue debris. Both PBS wounds exhibited a reduced red/perfused appearance than day 11 (j and l); red appearance was more apparent than day 18 Laponite-treated wounds (i and k). The rostral PBS wound (j) also had a depressed inner circle region, albeit, smaller than day 14 and was covered with a thin tissue layer. Scale bars = 2 mm.

By day 14, Laponite-treated wounds (Figure 5.6, e and g) showed a marked reduction in red appearance compared to PBS treatments (Figure 5.6, f and h). These wounds also exhibited a "flaky", dehydrated texture with wrinkling around the wound edge. Additionally, evidence of hair follicle pigmentation as previously

mentioned can be clearly seen. Both PBS day 14 wounds (Figure 5.6, f and h) had a depressed centre region which appeared more red and raw than adjacent tissue. This centre region most likely comprised of wound granulation with the partial exposure of subcutaneous tissue.

Beyond the circular depression region of f and h wounds and towards the margin of the original defect, there was evidence of soft tissue formation, which is indicative of epithelial migration. By day 18, all Laponite wounds exhibited negligible redness (Figure 5.6, i and k) showing more of a light pink/grey colour; this may have been the result of reduced blood perfusion, greater collagen deposition and increased re-epithelialisation. The grey areas around the wound margin and healthy tissue were much darker in appearance at day 18. These wounds looked less dehydrated, with reduced wrinkling and the presence of fewer fragments of tissue debris in or around the wound. Both PBS wounds exhibited a reduced red and raw appearance than day 11 (Figure 5.6, j and l). However, their red appearance was more apparent than day 18 Laponite-treated wounds (Figure 5.6, i and k). The rostral PBS wound (Figure 5.6, j) also had a depressed inner circle region (like f and h) which appeared smaller than day 14 and covered with a thin tissue layer. These factors combined strongly suggests that Laponite-treated wounds exhibited a more mature, fibrous appearance than PBS wounds. Furthermore, it could be speculated that PBS wounds were in an earlier phase of wound healing.

5.2.3.2 Laponite-treated Wounds Exhibited Minimal Differences in Wound Closure Compared to PBS

Wound margins were traced and the area calculated (as in methods Chapter 2.3.5) to calculate closure rates. To ensure that the closure rates of wounds located at different regions on the mouse dorsum did not differ in *db/db* mice, wound areas of rostral and caudal control wounds were initially compared independently (Figure 5.7 A). This showed that there were no differences in the rate of wound closure between rostral and caudal regions treated with Laponite gels. In contrast, PBS-treated wounds exhibited a significant reduction in the rate of wound closure from 11 days onwards.

The differences between treatment type (Laponite vs PBS) was then compared within each independent wound region. This showed that rostral PBS-treated wounds exhibited slightly accelerated wound closure rates after the first day compared to Laponite-treated wounds. However, these differences were not significant. Among caudal wounds, PBS wounds initially closed slightly more rapidly $\leq$ 7 days shortly being overtaken by Laponite treatments.

Combining the replicates of rostral and caudal regions to form a mean was then performed. This showed PBS-treated wounds having a slight, but not significant acceleration of wound closure for the first 7 days. After 7 days, there were no apparent differences between the two treatments.

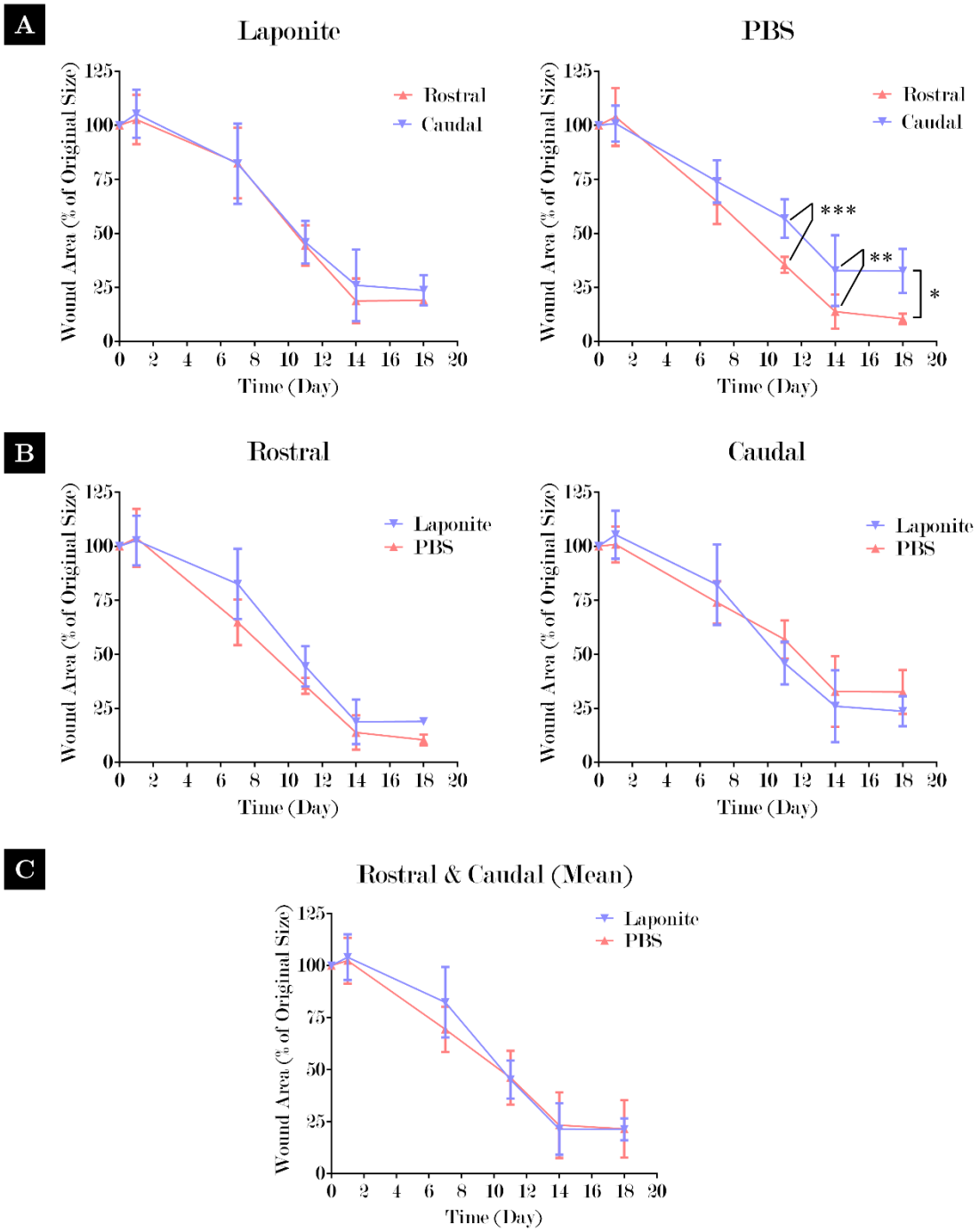

Figure 5.7. Laponite vs PBS-treated wound closure rates at separate locations (A) Rostral/caudal wound closure rates when treated with the same intervention (Laponite or PBS): Minimal differences between rostral/caudal regions when treated with Laponite gels. In contrast, caudal wound closure rates were significantly less than rostral wounds ≥ 11 days. (B) Laponite vs PBS comparing wound regions independently: Rostral PBS wounds exhibited accelerated closure rates after day 1 compared to Laponite (not significant). This was less obvious caudally as ≤ day 7, PBS closed more quickly. After day 7 Laponite exhibited greater overall closure by day 18 (not significant). (C) Laponite vs PBS irrespective of wound location (combined mean): PBS wounds accelerated closure for ≤ 7 days, after which there were negligible differences (not significant). Two-way ANOVA analysis was performed using Tukey's multiple comparison post-hoc test. *, ** and *** denotes that p = < 0.05, < 0.01 and < 0.001 respectively. Error bars = SD.

5.2.3.3 Rate of Re-epithelialisation

To determine the rate of epithelialisation, wound tissue was harvested at day 7, 11 and 18 post-surgery, serially sectioned and stained with haematoxylin and eosin (H&E) (Figure 5.8 A and B). Caudal wounds exhibited slightly faster re-epithelialisation compared to rostral wounds up to day 14 (both PBS and Laponite). This was not deemed significantly different, however, the rostral and caudal wound data for each treatment group was combined/averaged.

It was determined that by day 18 all Laponite-treated wounds had fully re-epithelialised whereas PBS-treated wounds had not (Figure 5.8 D $p = < 0.01$). Between Laponite and Laponite-VEGF groups there were negligible differences in re-epithelialisation rates.

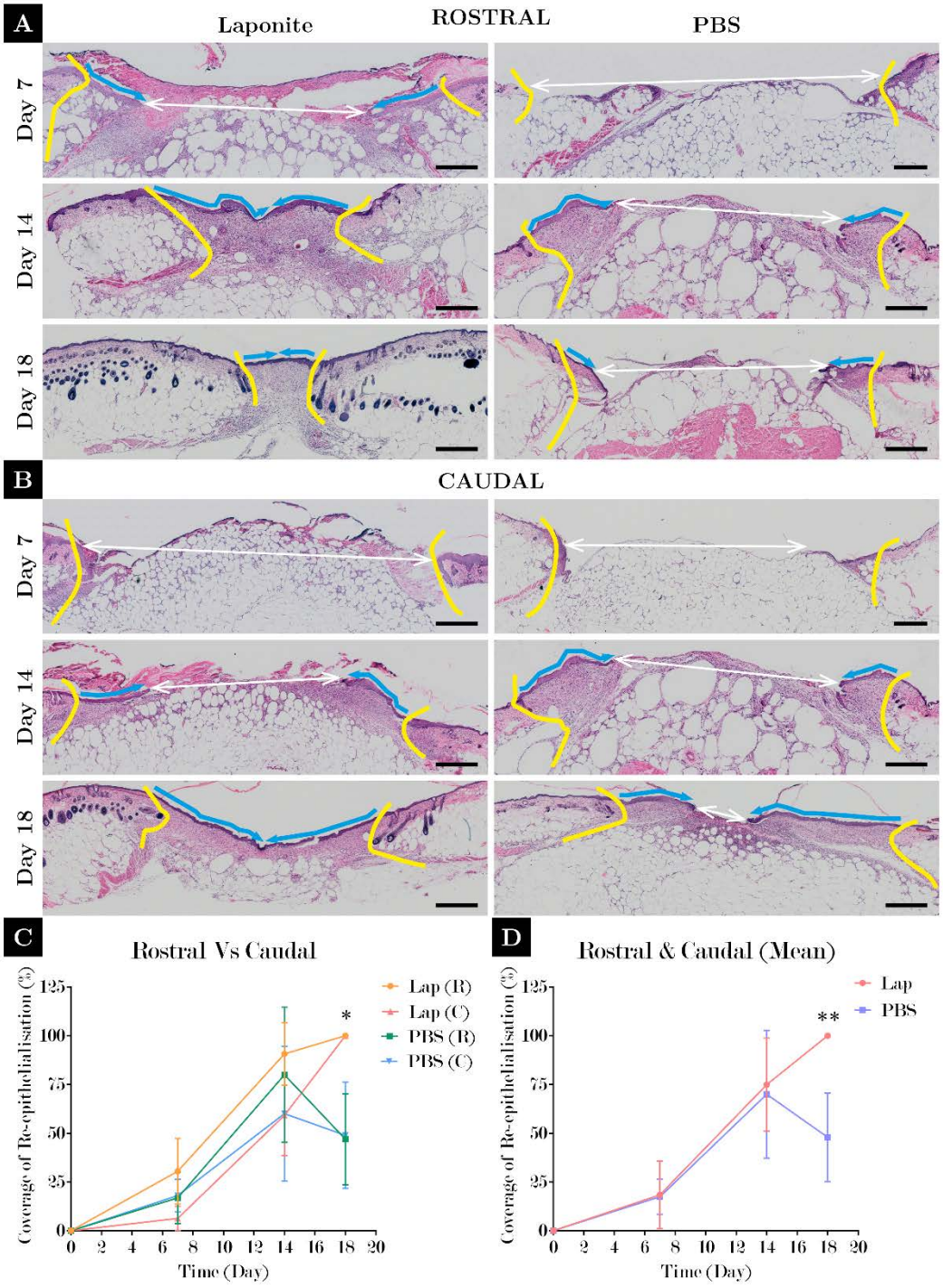

Figure 5.8. Laponite-treated wounds stimulates greater re-epithelialisation over 18 days. (A) H&E-stained tissue sections of rostral wounds and (B) caudal wounds showing re-epithelialisation between day 7 and day 18; yellow lines = wound margins from original defect; white arrows = open wound and blue arrows = re-epithelialisation coverage. (C) Difference of rate of re-epithelialisation between rostral and caudal wounds shows a general trend of greater re-epithelialisation within rostral wounds up to day 14 (both PBS and Laponite). This however was not deemed significantly different and so the rostral and caudal wound data for each treatment group was combined/averaged. This data is shown in (D); this shows that by day 18 all Laponite-treated wounds had fully re-epithelialised whereas PBS-treated wounds had not ($p = < 0.01$, denoted by **). Two-way ANOVA analysis was performed using Tukey's multiple comparison post-hoc test. Scale bars = 500 µm

5.2.3.4 Differences in Epithelial Thickness

Next, the thickness of the epidermal layer was measured in Laponite-treated compared to PBS treated wounds. As shown in Figure 5.9, and in methods Chapter 2.3.11, epithelial thickness was measured perpendicular to the surface of the epidermis at 3-6 points across the thickness of the wound, marked by white lines in Figure 5.9 B.

Epidermal thickness was significantly greater in Laponite treated wounds compared to PBS treated wounds at day 14 only (Figure 5.9 B, ii; d14 mean diff. $= 32.0 \pm 11.3\%$; error = standard error (SE); $p = 0.02$). The epidermis comprised a multilayer of cells with (~ 10 cells thick in Laponite-treated and ~5 cell think in PBS-treated, Figure 5.9 B, i). There was evidence of changes in the morphology of the cells as a function of the distance from the basal cell layer. At the basal layer, cells were larger in size and had had darkly stained nuclei. At more distal cell layers, nuclei were less evident and cells appeared more stratified.

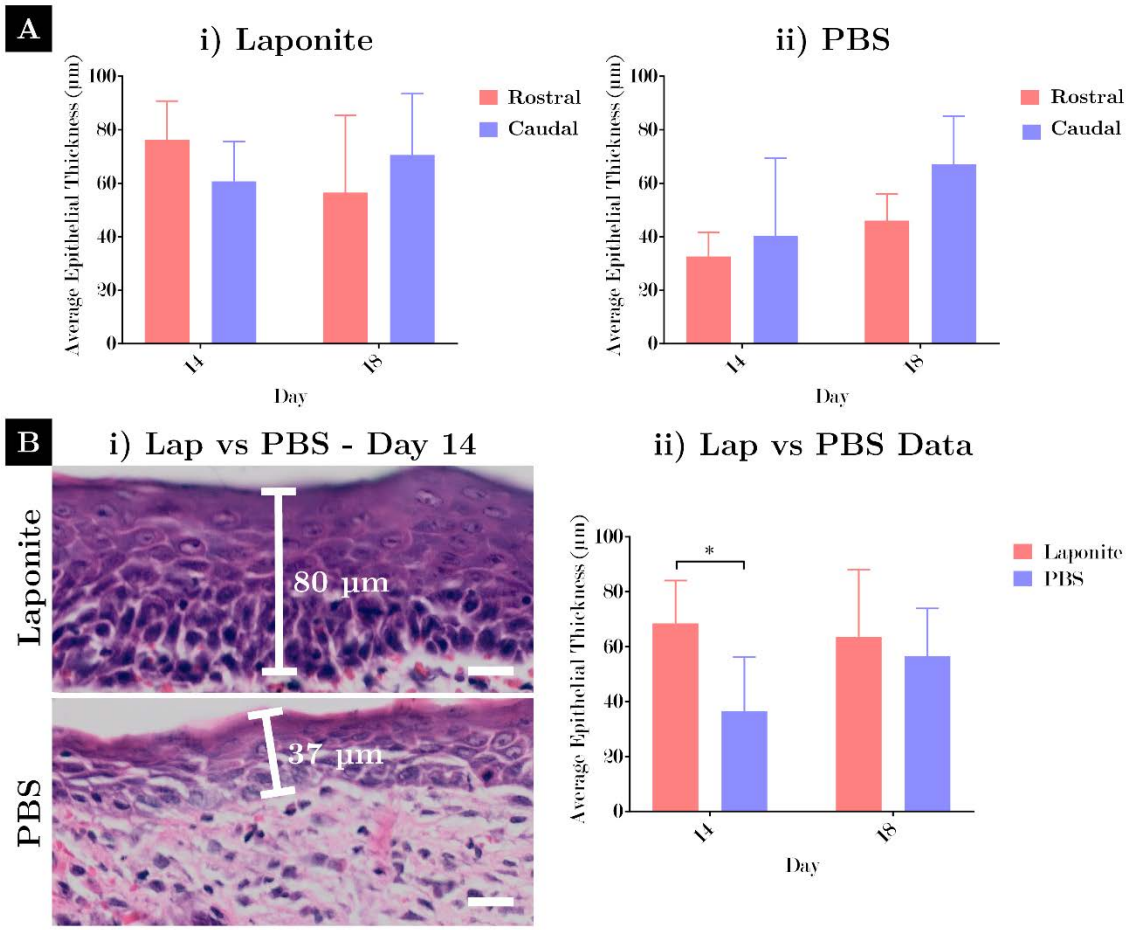

Figure 5.9. Laponite-treated wounds exhibited greater thickness of newly-formed epithelium. (A) Comparison between rostral and caudal wound regions treated with Laponite; newly formed epithelium was slightly thicker within rostral wounds at day 14 whereas at day 18 the average epithelial thickness was thicker within caudal wounds. These differences were not significant. (B) Comparison of between rostral and caudal wound regions treated with PBS; newly formed epithelium was slightly thicker within rostral wounds at day 14 and 18. These differences were not significant. (C) Comparison between Laponite and PBS treated wounds; Laponite wounds exhibited growth of new epithelial tissue that was significantly thicker than PBS-treated wounds at day 14. The average thickness of Laponite-treated wounds did not change between day 14 and 18 whereas there was a slight increase in PBS-treated wound epithelial thickness; newly formed epithelium was still thicker in Laponite-treated compared to PBS at day 18, however this difference was no longer significant. ($p = < 0.05$, denoted by *). Two-way ANOVA analysis was performed using Tukey's multiple comparison post-hoc test.

5.2.3.5 Differences in Cell Proliferation

Newly-formed epithelium within Laponite-treated wound shows evidence of highly proliferative cells towards to basal layer, which is characteristic of mature, healthy epithelial tissue (Figure 5.10 A and C). PBS wounds did not exhibit newly formed epithelium like Laponite-treated tissue (Figure 5.10 B and D) at the same time

during the study. There was evidence of highly-proliferative cells present towards the basement membrane of the epithelial tongue at the wound margins (Figure 5.10 E), akin to a wound at an early stage of wound repair.

5.2.3.6 PBS Wounds Exhibits an Inflammatory State

Wound tissue was stained by anti-myeloperoxidase (anti-MPO), which is a marker for inflammatory neutrophils. It was shown that there were no neutrophils present within Laponite-treated tissue after 18-days post-surgery (Figure 5.11 A and C). In contrast, PBS-treated wounds exhibited neutrophil activity within the wound bed indicative of a wound still within an inflammatory stage of wound repair (Figure 5.11 B - E)

5.2.4 Laponite Gels Stimulates Hair Follicle Anagen

As previously described in Chapter 5.2.3.1, hair follicle pigmentation was evident within both examples of rostral and caudal Laponite-treated wounds. A more detailed image of the rostral Laponite wound originally described in Chapter 5.2.3.1 is shown in Figure 5.12. It can be clearly seen that a dark pigmented shadow is present within the healthy skin tissue that is adjacent to the wound.

The formation of dark pigmentation was also prominent in other Laponite-treated wounds. Figure 5.13 shows an example of four different Laponite wounds from day 7 to 18 (i-iv). The first visible signs of pigmentation were noticeable by day-14 post surgery; this was most striking after 18 days post-surgery (Figure 5.13, panels i-iv, Day 18). In contrast, this phenomenon did not occur in any of the PBS-treated wounds (Figure 5.13, panel v, Day 18).

A correlation was noted between the formation of hair follicle pigmentation and the presence of wound exudate (exudate was most prominent during earlier wound times points). To demonstrate this finding, the approximate region of hair follicle formation at day 18 was traced. The trace was used to overlay the same wound at earlier time points during the study (some alterations in scale were applied to factor in contraction).

Speculatively, localised wound exudate (facilitated by Laponite gels) may have initiated an anagen-inducing effect and stimulated hair follicle growth (Figure 5.13). Whilst this is difficult to comprehensively prove in the scope of these experiments, further evidence was documented to help expand this theory, as shown in Figure 5.14. This figure further emphasises that the presence of a large quantity of exudate within a specific region of healthy tissue adjacent to the wound results in more substantial hair follicle growth (day 7 vs day 18 harvest image; Figure 5.14 i & ii). A cross-section of this tissue sample stained with H&E (taken approximately at the location depicted by the dotted line in Figure 5.14 ii), shows that there was a greater number of hair follicles present in the left side than the right side. A high proportion of the hair follicles existed within the subcutaneous layer (Figure 5.14 iv, blue arrows) which is indicative of hair follicles undergoing anagen. There were only a couple of deep residing hair follicles within the right side of the tissue (Figure 5.14 v, blue arrows) where there was an absence of exudate earlier during the study (Figure 5.14 i).

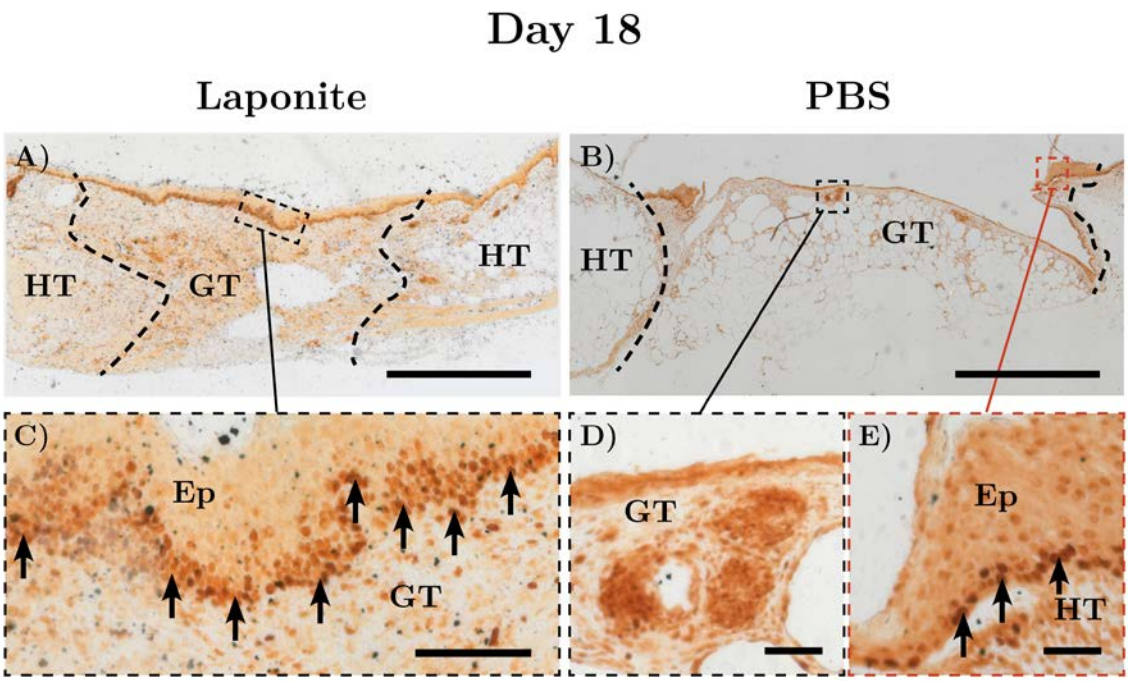

Figure 5.10. Comparison of day-18 Laponite-treated and PBS-treated wounds stained with a marker for cell proliferation (anti-Ki67). Newly-formed epithelium within Laponite-treated wound shows evidence of highly proliferative cells towards to basement membrane, which is characteristic of mature, healthy epithelial tissue (A and C). PBS wounds did not exhibit newly formed epithelium like Laponite-treated tissue (B and D) at the same time point. There was evidence of highly-proliferative cells present towards the basement membrane of the epithelial tongue at the wound margins (E), akin to a wound at an early stage of wound repair (B and E). A and B scale = 1 mm, C scale = 200 µm, D and E scale = 100 µm. Dotted line = wound margin; Black arrows = positively stained cell undergoing proliferation. Ep = Epithelium, GT = Granulation tissue, HT = Healthy tissue. Please note: negative control (omission of primary antibody) was performed however scanned dotSlide image was not available upon thesis submission.

A histological cross-section of a wound that had exhibited asymmetrical localised exudate at day 7 (Figure 5.14 i, left side) which resulted in hair follicle growth with similar asymmetry (Figure 5.14, ii), was stained with H&E (Figure 5.14, iii). There were a greater number of hair follicles present in the left side of healthy tissue that was adjacent to the wound than the right side. Furthermore, there were many hair follicles that exist deep within the subcutaneous layer of the skin.

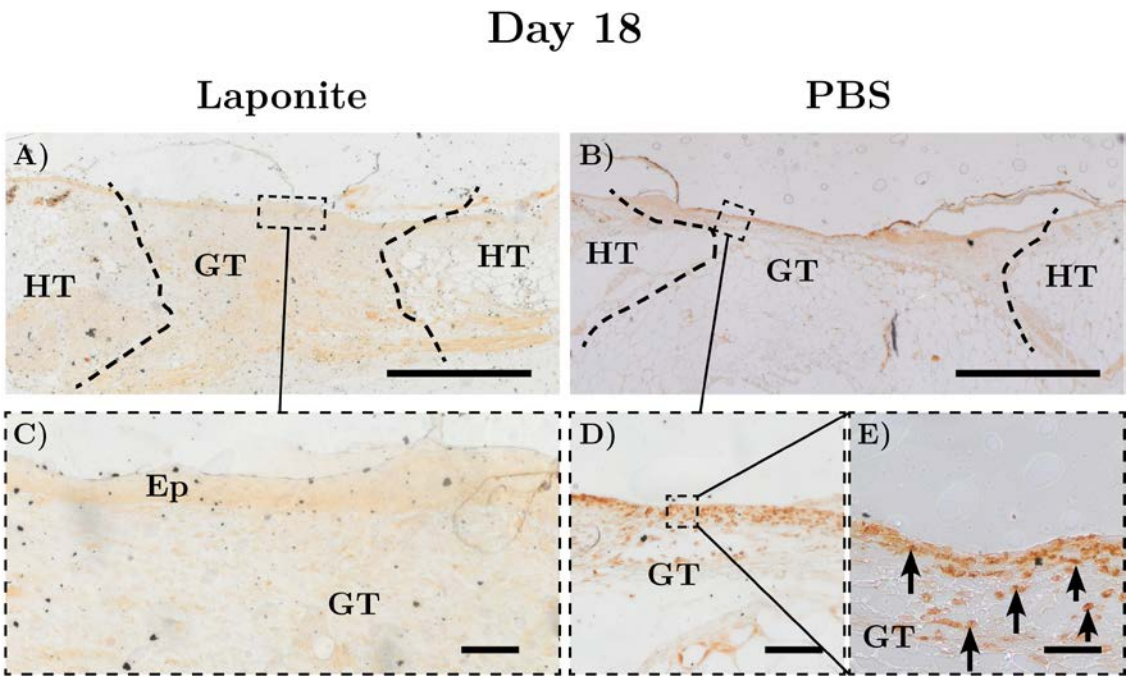

Figure 5.11. Comparison of day-18 Laponite-treated and PBS-treated wounds stained with a marker for inflammatory neutrophils (anti-myeloperoxidase or anti-MPO). There was no evidence of inflammatory neutrophils present within Laponite-treated tissue after 18-days post-surgery (A and C). In contrast, PBS-treated wounds exhibited neutrophil activity within the wound bed indicative of a wound still within an inflammatory stage of wound repair (B - E). A and B scale = 1 mm, C scale = 200 µm, D and E scale = 100 µm. Dotted line = wound margin; Black arrows = positively stained neutrophil, Ep = Epithelium, GT = Granulation tissue, HT = Healthy tissue. Please note: negative control (omission of primary antibody) was performed however scanned dotSlide image was not available upon thesis submission.

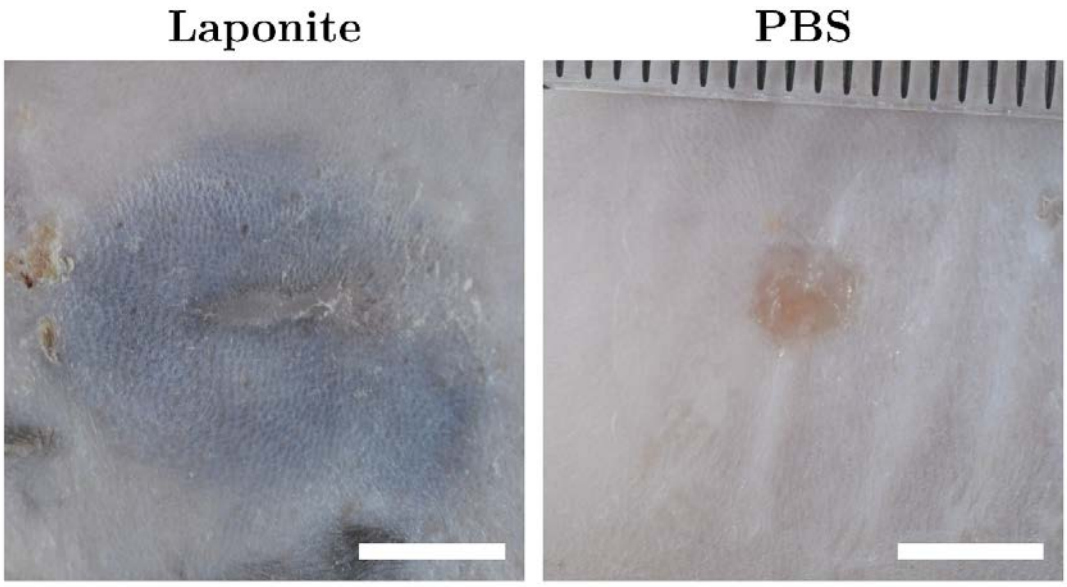

Figure 5.12. Significant hair follicle formation around wound margin and adjacent healthy tissue of Laponite-treated wounds at day-18 post-surgery. A dark 'ring' (suggestive of hair follicle anagen, refer to text for more details) was prominent around a high proportion of Laponite-treated wounds (± VEGF) (left panel), whereas this was not evident in any of the PBS-treated wounds (right panel). Scale bars = 5 mm.

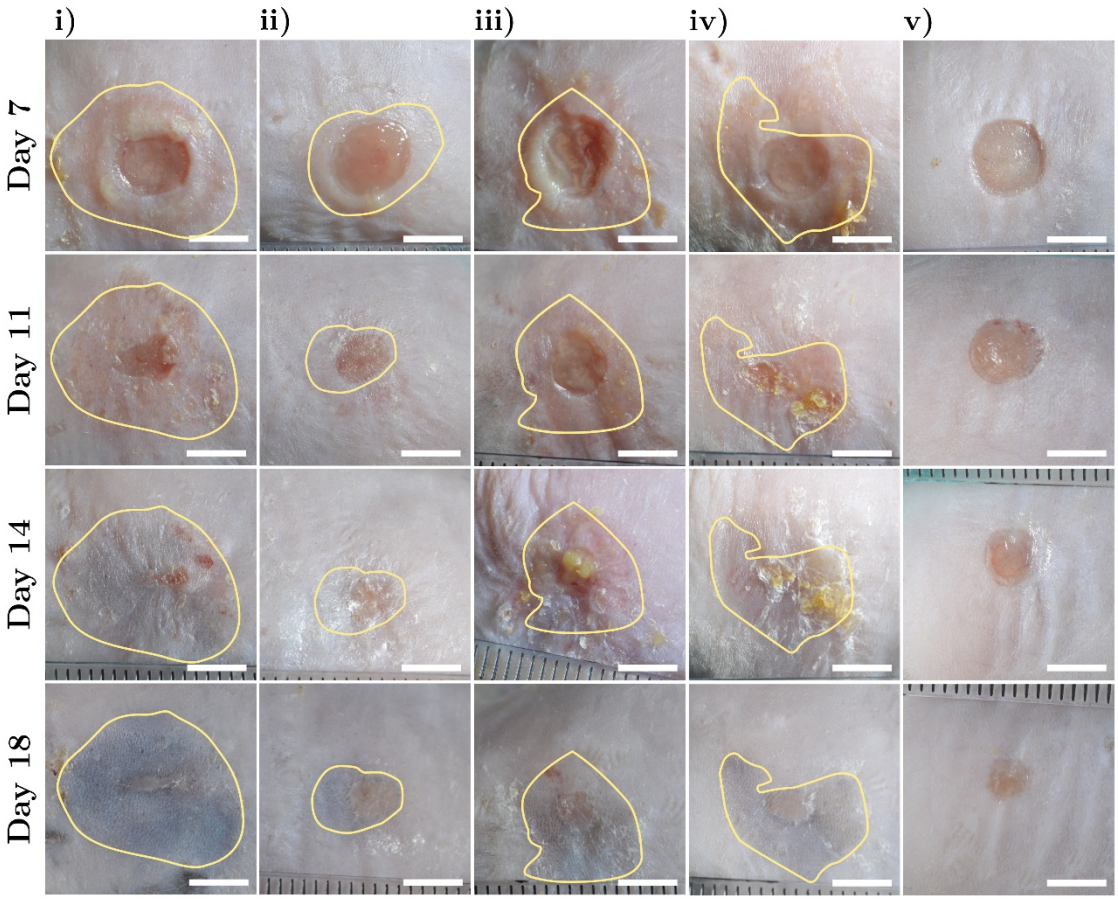

Figure 5.13. Wound exudate localised by Laponite gels stimulates hair follicle anagen. i-iv) Four different wounds treated with Laponite over the 18-day study period tracking wound exudate that had been left around the wound margin. In all these examples, there is a distinct ring (some more prominent than others) of hair follicle growth around the wound margin; a trace of the approximate hair follicle coverage (yellow line) at day 18 overlaid over images of the same wound taken at day 7 to day 14 suggests that hair follicle stimulation could have occurred by wound exudate. v) PBS-treated wounds did not exhibit the production of exudate as seen in Laponite-treated wounds. Scale bars = 5 mm.

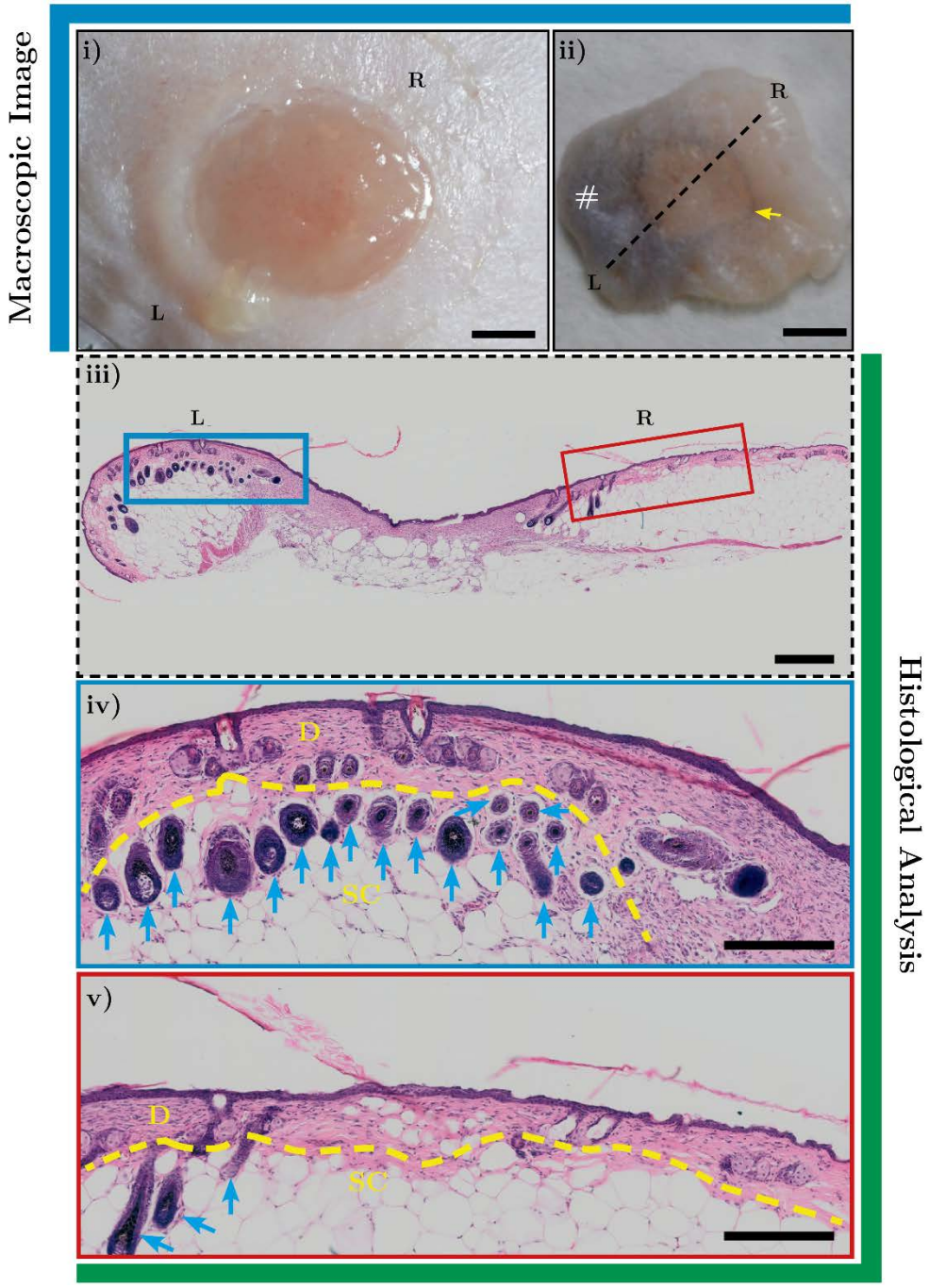

Figure 5.14. Evidence of hair follicle anagen induction in Laponite-treated wounds. i) Day 7 wound (Laponite-treated) with localised exudate towards the left side of wound periphery and surrounding healthy skin (Scale = 2 mm). ii) Same wound at tissue harvest (day 18); evidence of marked hair follicle growth around the defect margin (dark ring, pointed out by yellow arrow). Hair follicle growth extends further towards the left and top-left side of the healthy wound tissue, in the similar region where exudate was present at day 7 (#) (Scale = 2 mm). iii) Tissue cross-section taken approximately at the location depicted by the dotted line in ii, with the orientation of the tissue shown by left (L) and right (R) (Scale = 500 µm) iv) Higher magnification image of the right region (red box in iii), and v) the left region (blue box in iii) (Scale = 200 µm); there was a greater number of hair follicles present in the left side than the right side. A high proportion of the hair follicles existed within the subcutis (blue arrows) which is indicative of hair follicles undergoing anagen. Yellow dotted line = dermis/subcutis boundary; D = Dermis, SC = Subcutis.

5.2.5 The Effect of Localised VEGF by Laponite Gels on Wound Healing in *db/db* Mice

5.2.5.1 Differences in Wound Appearance

After the positive effects from the Laponite gels on *db/db* wounds the next stage was to investigate the potential of adding VEGF to Laponite. It was hypothesised that localisation of VEGF would offer further improvements to wound healing quality and closure rates.

Figure 5.15 shows photos of wounds taken from day 1 to day 18 after being treated with Laponite/alginate gels (± VEGF) 1-day post-surgery. At earlier time points (day 0 to day 8), all wounds were a comparable size but differences in appearance were present. There was a white precipitate within the wound bed of alginate-treated wounds at day 8 and 11; after day 11 this white precipitate was no longer visible. Both alginate treated wounds exhibited a more red and raw appearance than Laponite wounds by day 11. The day 8 Laponite VEGF wound appeared opaque with negligible red colouring due to a covering of Laponite biomaterial.

Figure 5.16 shows wound images from day 11 to day 18 in more detail. By day 11 both Laponite-treated wounds (a and b) exhibited a dehydrated appearance with the presence of wound debris and/or Laponite biomaterial within the wound bed. In contrast, both alginate-treated wounds (c and d) were moist and shiny in appearance. Alginate-VEGF (C) contained a white precipitate as mentioned previously (presumably a precipitate of alginate biomaterial).

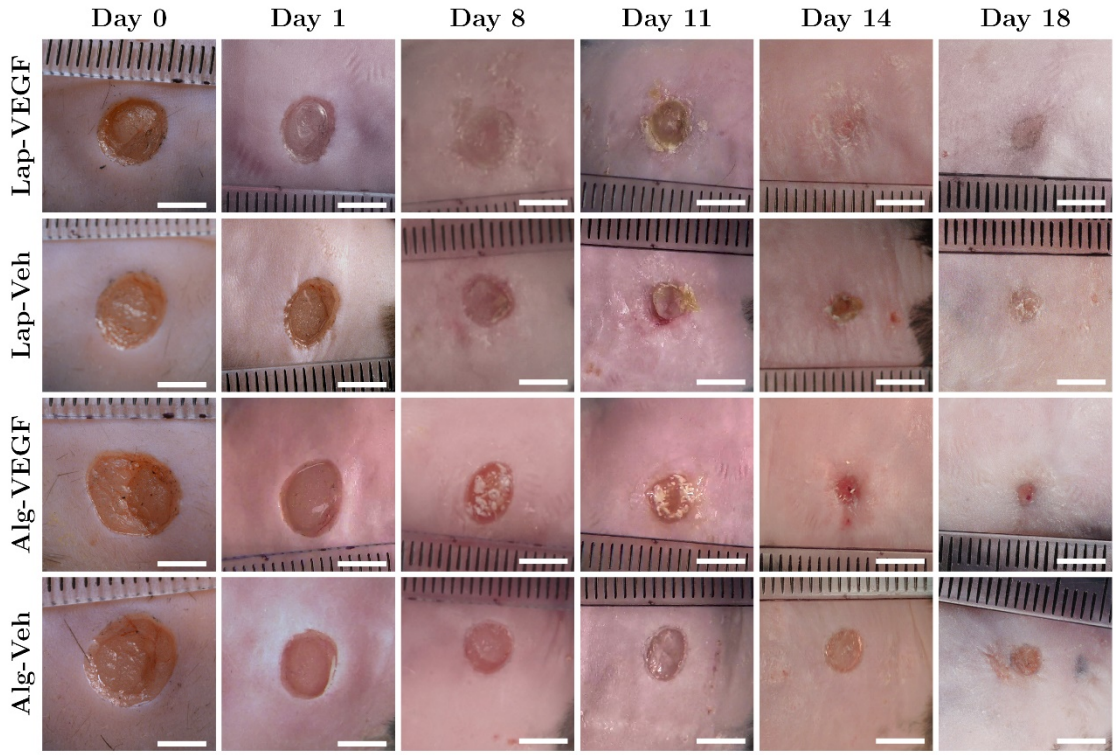

Figure 5.15. VEGF incorporated within Laponite gels does not stimulate increased wound closure/contraction in db/db mice over an 18-day period. Macroscopic images of wounds treated with 40 µg/ml VEGF encapsulated within Laponite gels and alginate gels (control); vehicle controls were used to treat contralateral wounds for both biomaterials. Scale bars = 5 mm.

By day 14, the Laponite-VEGF (Figure 5.16, e) wound was barely visible due to a covering of laponite debris/eschar over the wound. Also, the wound colour was less red and raw, exhibiting a grey/pink colour. The alginate-VEGF wound exhibited a substantial reduction in wound closure compared to the alginate vehicle. Its colouration was intense red with a moist appearance. In contrast, the alginate vehicle wound exhibited only minor changes in size and appearance compared to day 11. By the final time point both Laponite wounds (i and j) were light pink/grey in colour. The Laponite-VEGF wound (i) also had a black pigmented ring around the wound margin, which is a similar observation made in other Laponite treated wounds (see Figure 5.5). Alginate-VEGF (k) exhibited the greatest reduction in wound size but still exhibited redness. Wounds i-k all looked

like there was near to full closure whereas the alginate vehicle wound still exhibited a granulated appearance.

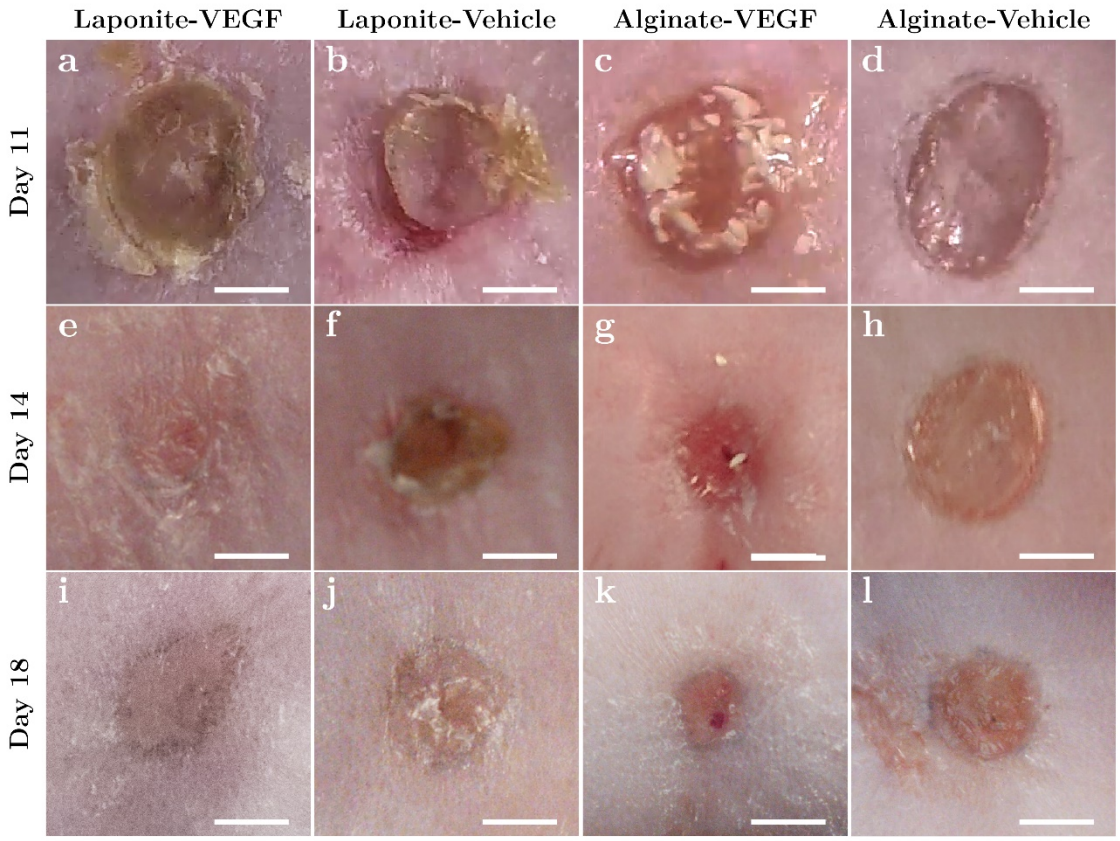

Figure 5.16. Macroscopic evidence showing that wounds treated by Laponite containing VEGF negligible differences in wound appearance. By day 11 both Laponite-treated wounds (a and b) exhibited a dehydrated appearance with the presence of wound debris and/or Laponite biomaterial within the wound bed. In contrast, both alginate-treated wounds (c and d) were moist and shiny in appearance. Alginate-VEGF (C) contained a white precipitate as mentioned previously (presumably a precipitate of alginate biomaterial). By day 14 the Laponite-VEGF (e) wound was barely visible due to a covering of laponite debris/eschar over the wound. Also, the wound colour was less red and raw, exhibiting a grey/pink colour. The alginate-VEGF wound exhibited a substantial reduction in wound closure compared to the alginate vehicle. Its colouration was intense red with a moist appearance. In contrast, the alginate vehicle wound exhibited only minor changes in size and appearance compared to day 11. By the final time point both Laponite wounds (i and j) were light pink/grey in colour. The Laponite-VEGF wound (i) had a black pigmented ring around the wound margin, which is a similar observation made in other Laponite treated wounds. Alginate-VEGF (k) exhibited the greatest reduction in wound size but still exhibited redness. Wounds i-k all looked like there was near to full closure whereas the alginate vehicle wound still exhibited granulated appearance. Scale bars = 2 mm.

5.2.5.2 VEGF Addition Induced Negligible Differences in Laponite Wound Closure Rates

Wound closure rates were then analysed and compared. As described previously, wound closure rates between rostral and caudal regions were compared to clarify any differences with location. Initially this was performed by comparing between wounds treated with the same intervention. It was showed that there were minimal differences between rostral and caudal regions when wounds were treated with Laponite containing VEGF or Laponite vehicle (Figure 5.17 A). Wounds that were treated with alginate-VEGF exhibited negligible differences in wound closure rates between wound locations (Figure 5.17 B, first graph). However, caudal alginate-vehicle wounds closed at a reduced rate compared to rostral wounds, however this was statistically significant.

Figure 5.17 C shows the comparison of wound closure between treatments at rostral and caudal locations. Caudal wounds exhibited significantly accelerated wound closure when treated with alginate-VEGF at day 1, 11 and 14 (day 11; mean diff. = 31.1 ± 9.2%; $p = 0.007$; error = SE). This increase was the largest compared with alginate vehicle whereas the difference was minor compared to both Laponite treatments (day 1 to 18). Both Laponite treatments compared with each other exhibited only minor differences in caudal wound closure.

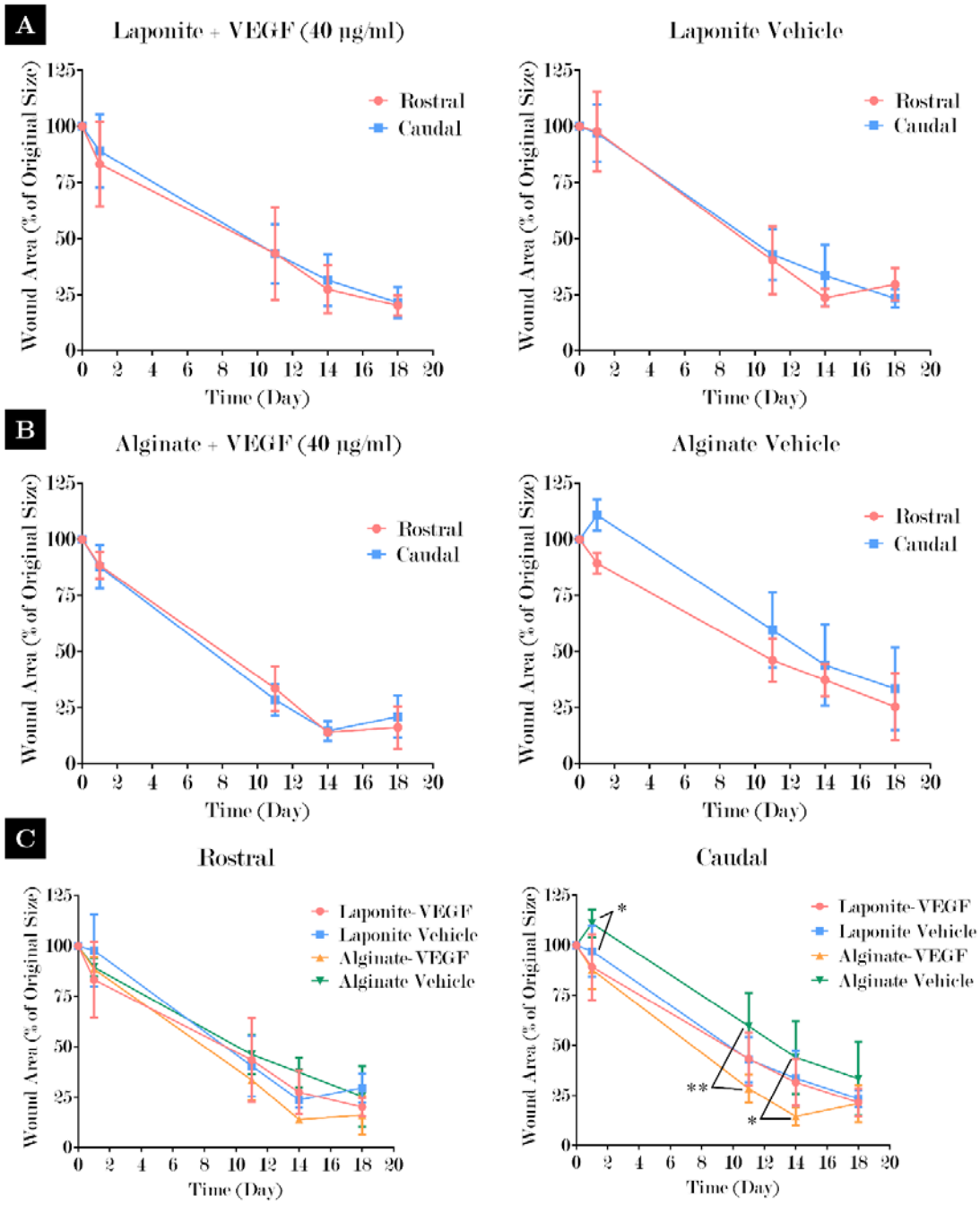

Figure 5.17. Laponite vs alginate-treated wounds ± 40 µg/ml at separate wound locations. (A) Rostral/caudal closure rates treated with the same Laponite intervention (± VEGF): There were minimal differences between rostral/caudal regions. (B) Rostral/caudal closure rates treated with the same alginate intervention (± VEGF): Minimal differences between rostral regions with VEGF. Rostral wounds treated with vehicle exhibited faster wound closure (day 0-18). (C) Laponite vs alginate ± VEGF treating regions independently: Alginate -VEGF exhibited accelerated closure rostrally whereas the differences were minor compared to both Laponite treatments (day 1-18). Laponite treatments; minor differences rostrally and caudal regions were similar. However, differences between alginate ± VEGF were significantly greater. Alginate-VEGF exhibited an increase from day 0-18; this became significant at day 11/14 between alginate vehicle. By day 18, alginate-VEGF closure remained greater. Two-way ANOVA analysis using Tukey's multiple comparison post-hoc test. * and ** denotes that $p = < 0.05$, and < 0.01 respectively. Error bars = SD.

Rostral and caudal replicates were combined to increase the power of the study and to compare how the addition of VEGF to each biomaterial affected wound closure (Figure 5.18 A). This showed that the addition of VEGF to Laponite gels had a negligible effect on wound closure rates (Figure 5.18 A, first graph). In contrast, alginate-VEGF gels exhibited a significant increase in wound closure between 11 and 14; wound closure was still greater than vehicle alginate after 18 days but was no longer significant.

A comparison between different biomaterials were then shown in Figure 5.18 B. It was shown that VEGF mixed in alginate exhibited increased wound closure after day 1 when compared to Laponite-VEGF treatment. This increase was most apparent at day 11 and 14. There were only minor differences between both vehicle biomaterial treatments.

Figure 5.18 C shows a combined graph that compares all treatment groups with the inclusion of PBS closure rate data. It showed that PBS wounds exhibited an increase in wound closure compared to all treatment groups except alginate containing VEGF. The increase in alginate-VEGF closure compared to PBS was significant at day 14.

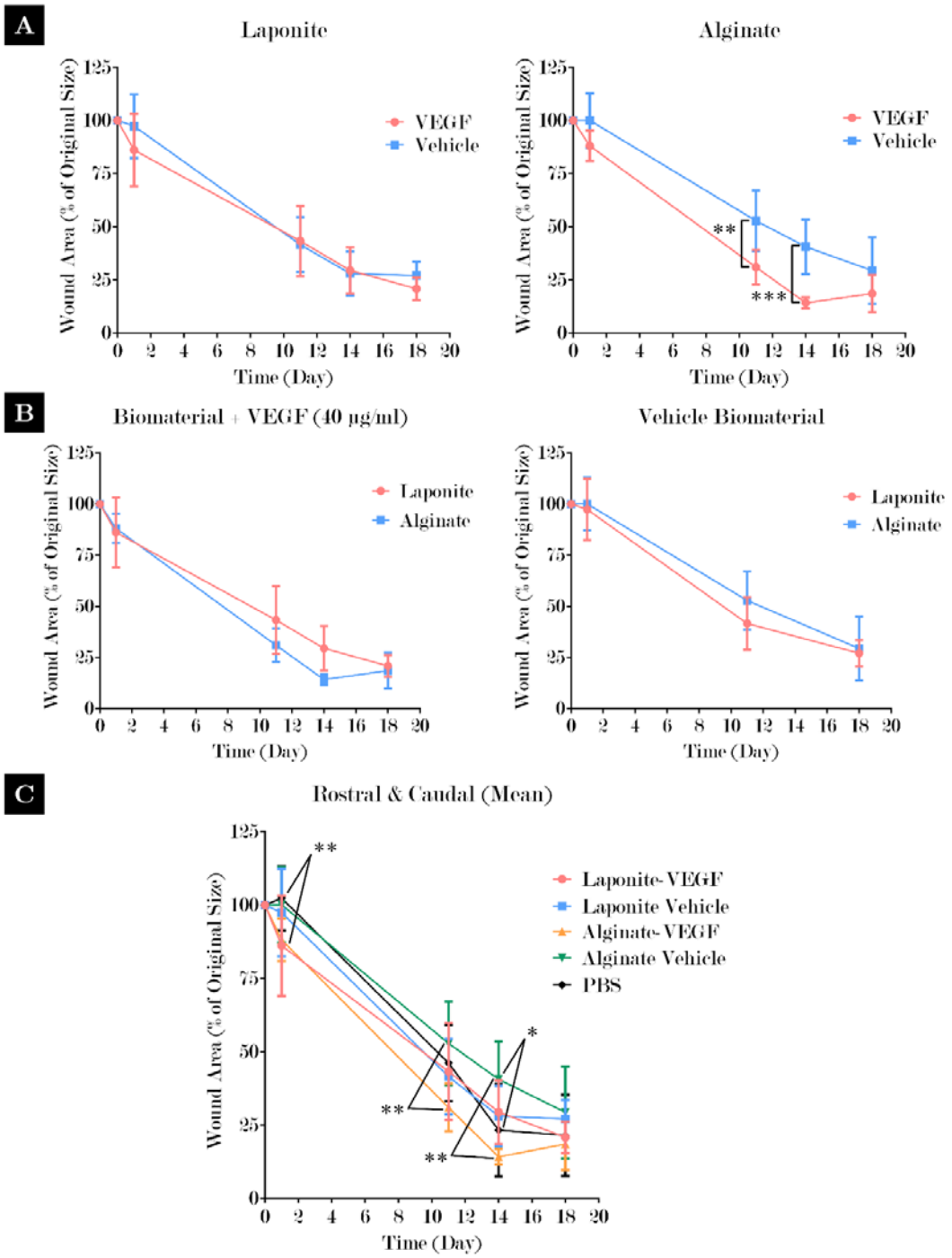

Figure 5.18. Differences in wound closure rates between Laponite and alginate-treated wounds (± VEGF 40 µg/ml) using the combined rostral/caudal means. (A) Comparing alginate/Laponite independently: There were minimal differences between wound treated with Laponite ± VEGF. In contrast, the incorporation of VEGF to alginate gels stimulated an acceleration in wound closure (significance at day 11 and 14). (B) Comparing the addition of VEGF independently: alginate-VEGF exhibited increased closure after day 1 than Laponite-VEGF. This increase was most apparent at day 11/14 (not significant). (C) A combined graph comparing all treatment groups (including PBS). The same conclusions as described in (B), but with the addition of PBS. PBS wounds exhibited an increase in wound closure than all treatment groups except alginate-VEGF. The increase in alginate-VEGF closure compared to PBS was significant at day 14. Two-way ANOVA analysis was performed using Tukey's multiple comparison post-hoc test. *, ** and ** denotes that p = < 0.05, < 0.01 and < 0.001 respectively. Error bars = SD.

5.2.5.3 Differences in Rate of Re-epithelisation Between Laponite and Alginate

H&E-stained tissue sections of wounds treated with Laponite-VEGF and vehicle Laponite showed minor differences of re-epithelialisation rates over 18 days; at day 14 there was a slight increase in re-epithelialisation coverage in Laponite-VEGF wounds (Figure 5.19 A)

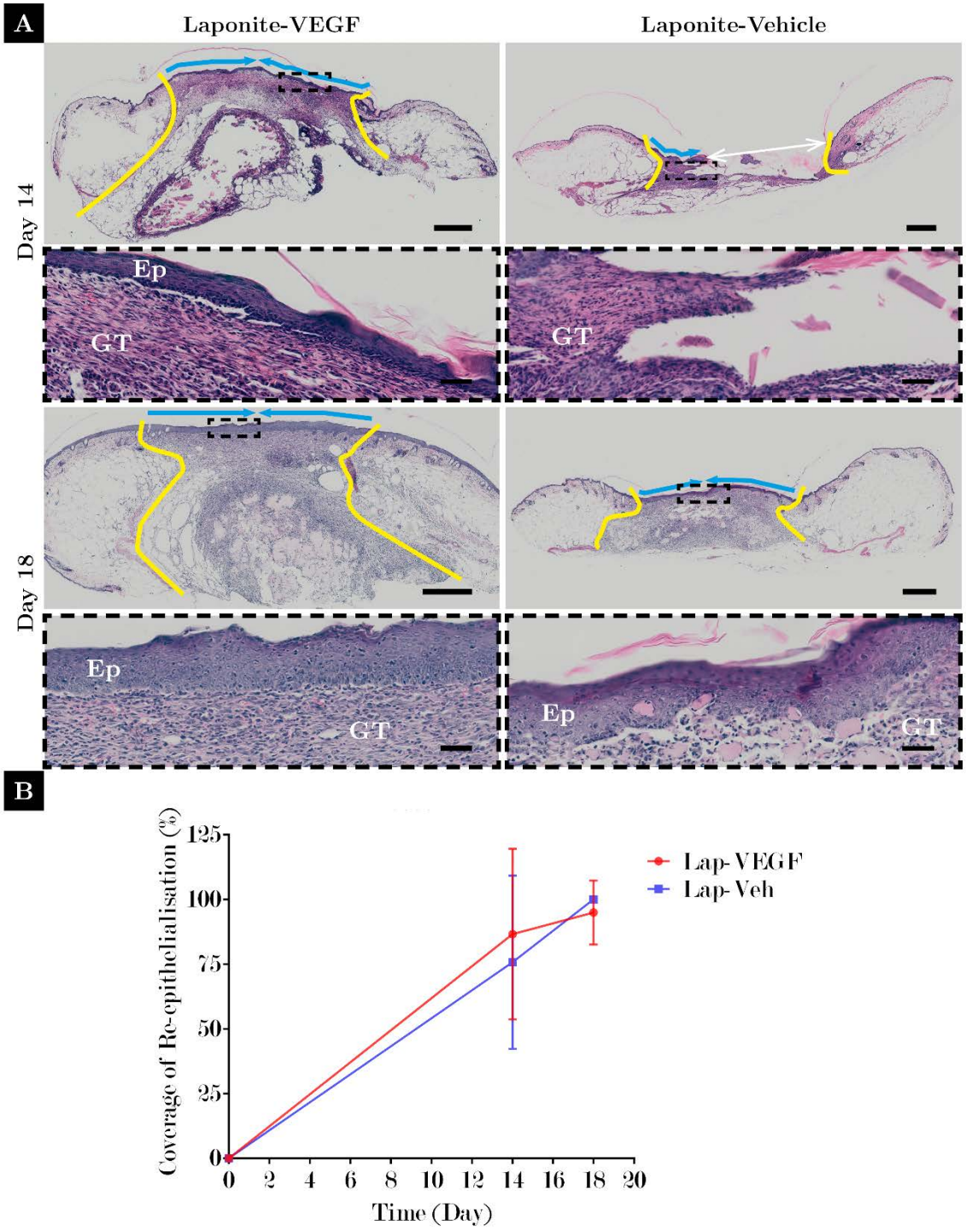

Figure 5.19. VEGF encapsulated within Laponite gels does not stimulate greater re-epithelialisation compared to vehicle control over 18 days in db/db mice. (A) H&E-stained tissue sections of wounds treated with 40 µg/ml VEGF encapsulated within Laponite gels and vehicle Laponite at day 14 and day 18; yellow lines = wound margins from original defect; white arrows = open wound and blue arrows = re-epithelialisation coverage; Ep = epithelium, GT = granulation tissue. (B) The rate of re-epithelialisation between Laponite-VEGF and vehicle Laponite showed minor differences over 18 days. Error bars = SD.

The rate of re-epithelialisation between Laponite ± VEGF and alginate vehicle was significantly greater (Figure 5.20 B). Interestingly, the encapsulation of VEGF within alginate significantly increased the rate of re-epithelialisation than without VEGF (Figure 5.20 B).

5.2.5.4 Differences in the Epithelial Thickness Between Laponite and Alginate-Treated Wounds

Laponite vehicle wounds exhibited a thicker newly-formed epithelium after 14 days post-surgery compared to Laponite that contained VEGF (Figure 5.21 A). However, this difference was the opposite by day 18 as Laponite-VEGF wounds exhibited slightly thicker epithelial tissue (Figure 5.21 A). There were minor differences in epithelial thickness between Laponite and alginate-treated wounds at day 18 (Figure 5.21 B).

5.2.5.5 Differences in Cellularity Within Laponite-VEGF Wounds

To assess if there were any subtle differences in wound healing when VEGF is encapsulated by Laponite, the degree of cellularity was compared with vehicle Laponite wounds (Figure 5.22 A). Analysis of segmented cell coverage showed greater cell invasion within Laponite-VEGF treated wounds than vehicle treatment at day 14. Day 18 Laponite-VEGF wounds exhibited reduced cellularity than vehicle-treated wounds; this reduction in granulation tissue cellularity was significantly less than day 14 wounds (Figure 5.22 B).

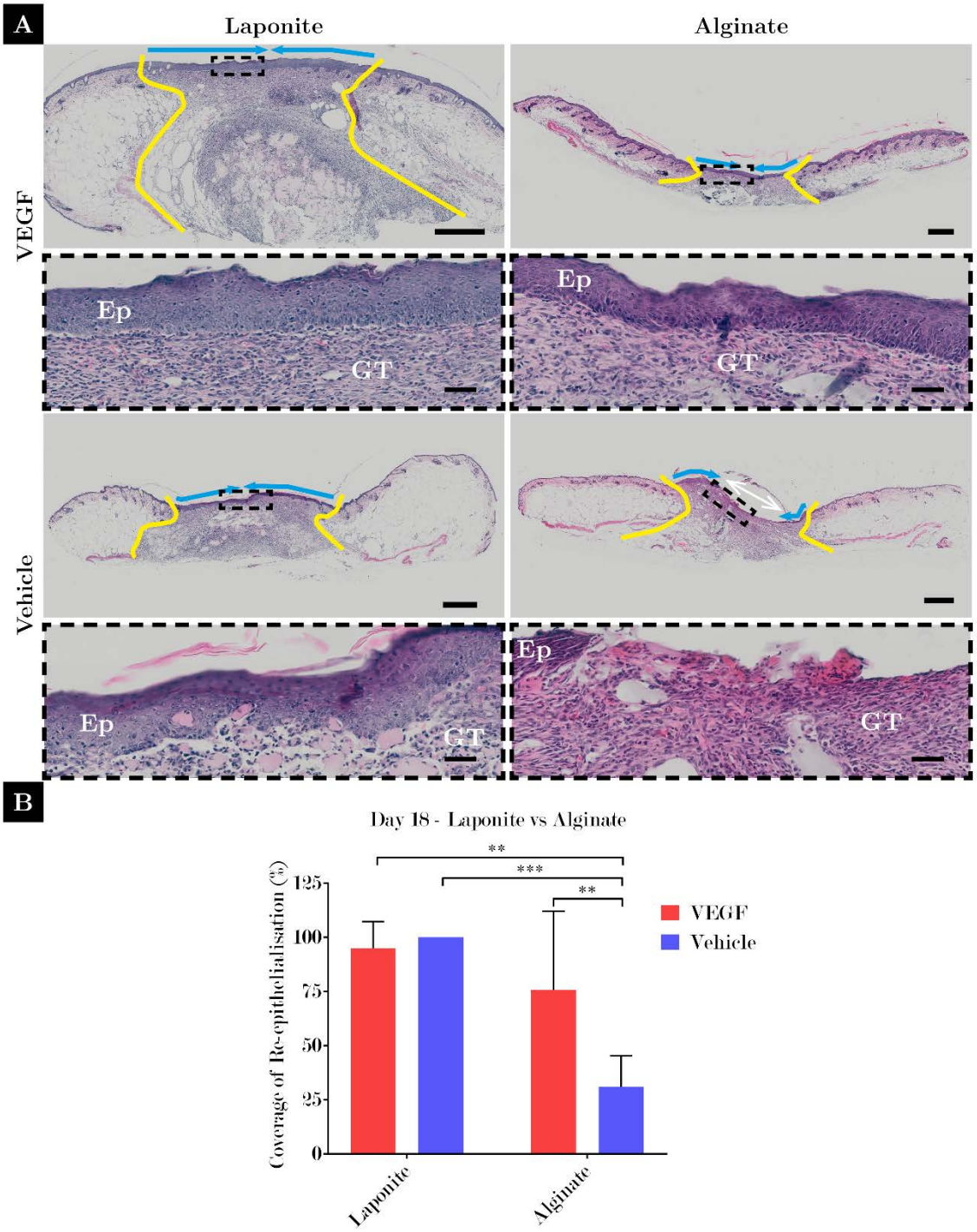

Figure 5.20. Day 18 wounds treated with Laponite gels ± VEGF stimulated greater re-epithelialisation compared vehicle alginate gels in *db/db* mice. (A) H&E-stained tissue sections of day 18 wounds that had been treated with 40 µg/ml VEGF encapsulated within Laponite gels and alginate gels; yellow lines = wound margins from original defect; white arrows = open wound and blue arrows = re-epithelialisation coverage; Ep = epithelium, GT = granulation tissue. (B) The rate of re-epithelialisation between Laponite ± VEGF and alginate vehicle was significantly greater. Laponite ± VEGF gels were also greater than alginate encapsulating 40 µg/ml VEGF Interestingly, the addition of VEGF within alginate significantly increased the rate of re-epithelialisation than without VEGF. ** and *** denotes that p = < 0.01 and < 0.001 respectively. Two-way ANOVA analysis was performed using Tukey's multiple comparison post-hoc test. Error bars = SD.

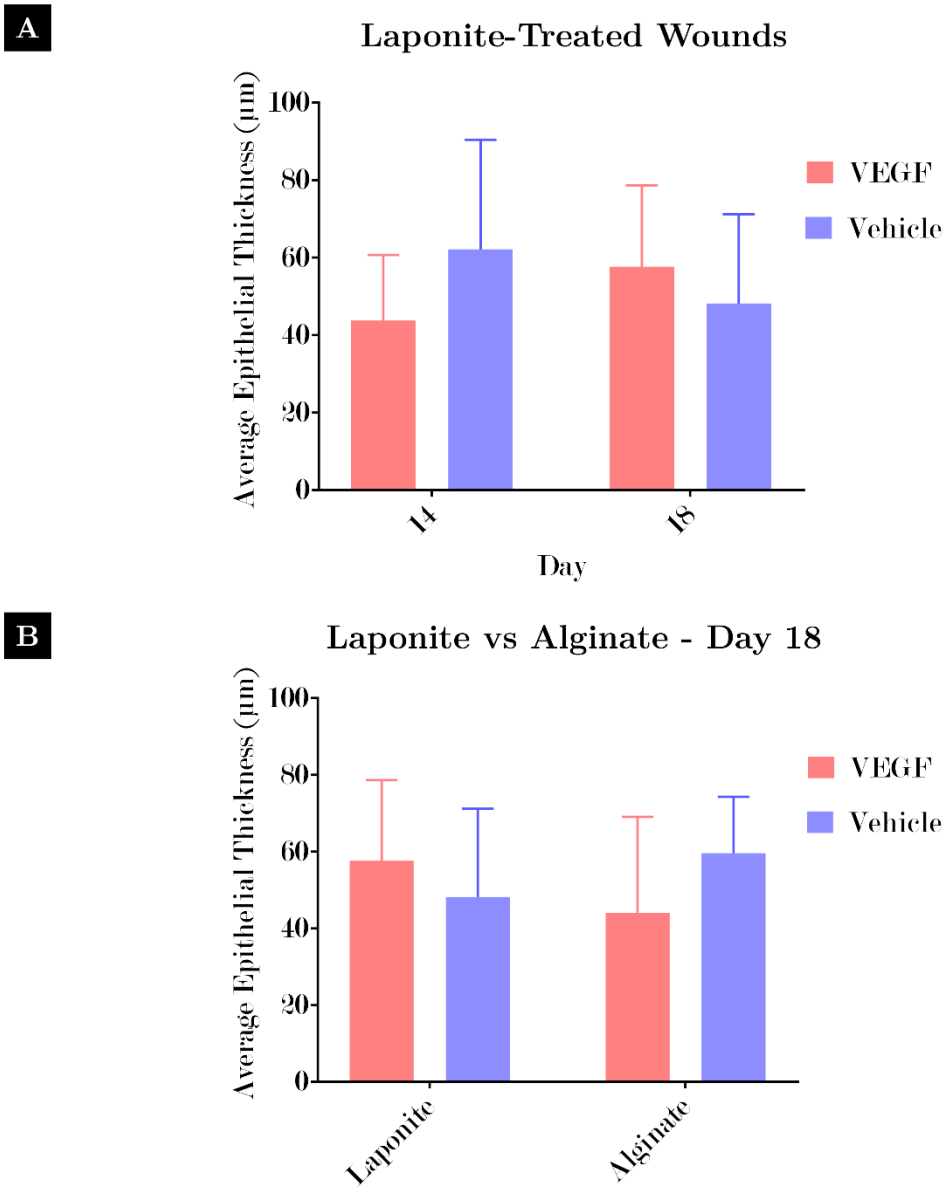

Figure 5.21. Wounds treated with Laponite encapsulating VEGF did not increase thickness of new-formed epithelium. (A) Laponite vehicle wounds exhibited slightly thicker new-formed epithelium after 14 days post-surgery compared to Laponite containing VEGF. However, this difference was the opposite by day 18; none of these differences were significant. (B) There minor differences in epithelial thickness between Laponite and alginate-treated wounds at day 18. Two-way ANOVA analysis was performed using Tukey's multiple comparison post-hoc test.

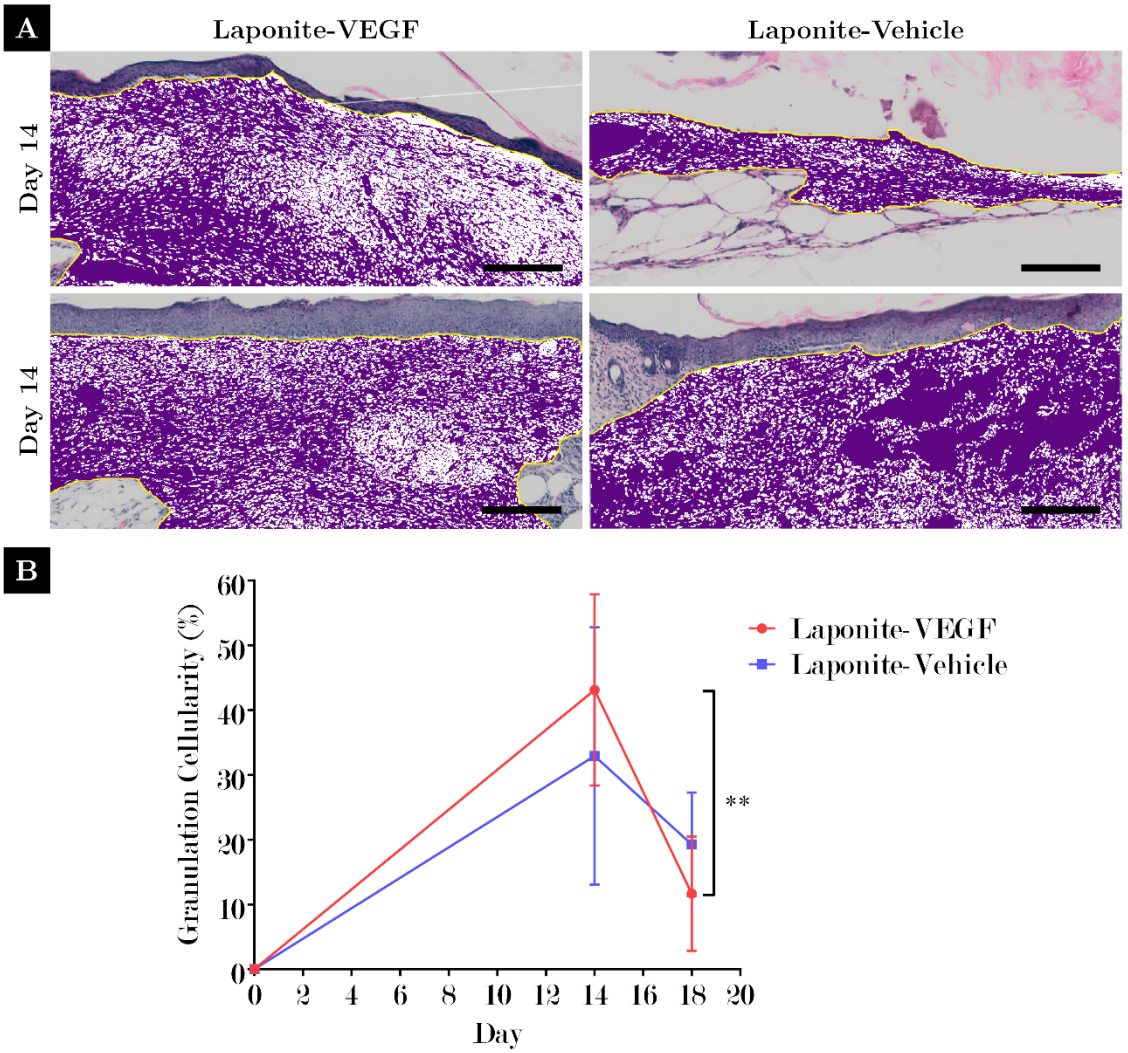

Figure 5.22. Greater cellularity within the granulation tissue of Laponite-VEGF treated wounds at day 14 in *db/db*. (A) Segmentation of haematoxylin-stained granulation tissue (i.e. cells within wound granulation) and (B) analysis of segmented cell coverage showed greater cell invasion within Laponite-VEGF treated wounds than vehicle treatment at day 14). Day 18 Laponite-VEGF wounds exhibited reduced cellularity than vehicle-treated wounds; this reduction in granulation tissue cellularity was significantly less than day 14 wounds ($p = < 0.01$, denoted by **). Error bars = SD. One-way ANOVA analysis performed with Tukey's post-hoc test applied for multiple comparisons. Scale bars = 1 mm.

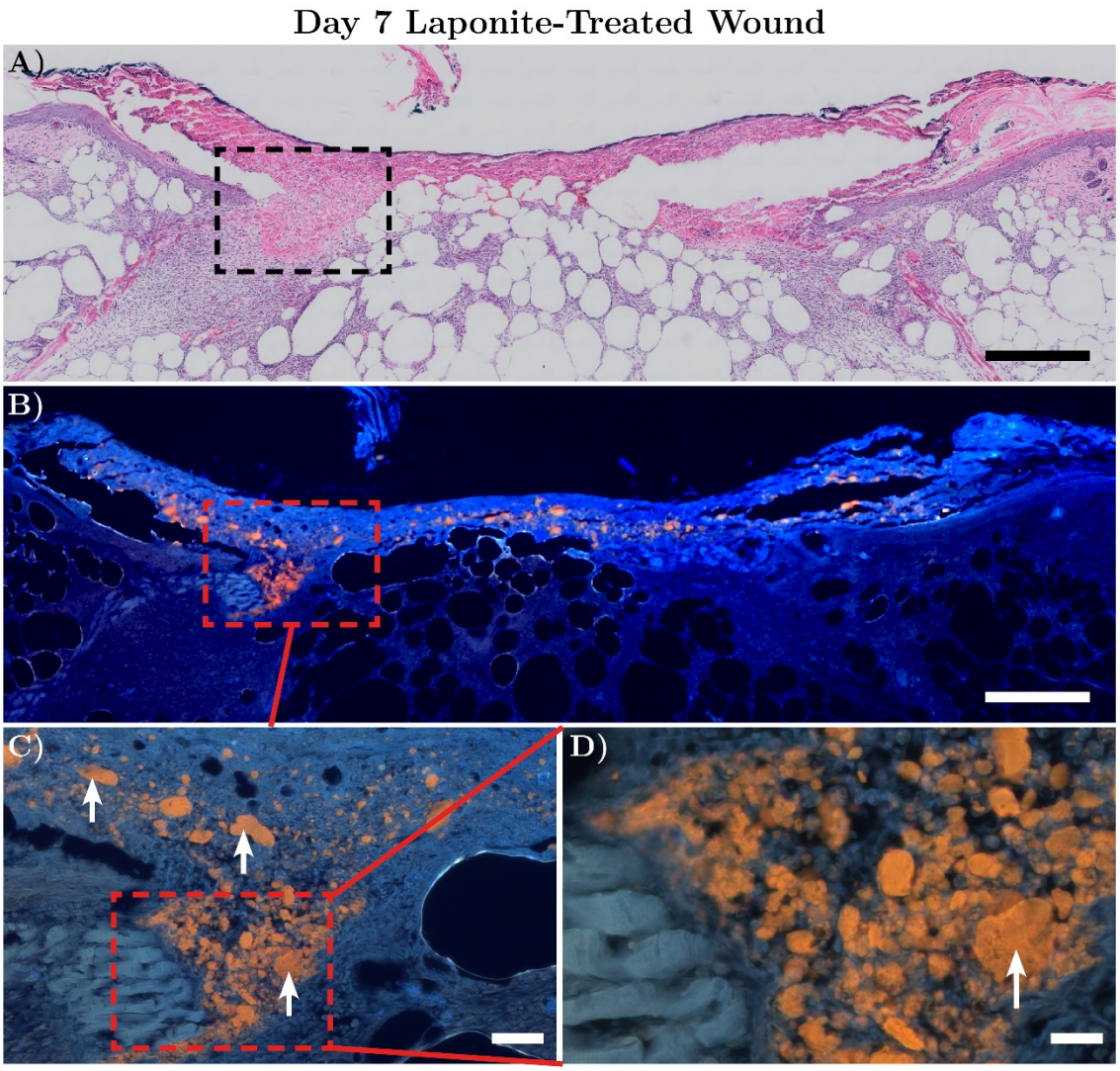

Figure 5.23. Day 7 Laponite-treated wound stained with Auramine O showing that Laponite biomaterial was well-incorporated with tissue within the wound bed. A and B scale = 500 µm, C scale = 200 µm, D scale = 100 µm. White arrows = positively stained Laponite biomaterial. Image B-D filter set 16 (FITC) used (please refer to Chapter 2.3.8.1, Table 2.2 for filter details).

5.2.6 Observations of Laponite Integration/Exclusion within Laponite-Treated Wounds

5.2.6.1 Laponite Early Integration

It was clear that the integration of Laponite within the wound bed was prominent during initial stages of the study (day 7, Figure 5.23). Please note that the staining colour of Laponite in Figure 5.23 and upcoming Figure 5.25 is inconsistent with several other Auramine O figure images (Figure 4.3 to Figure 4.6, Figure 5.24, Figure 5.26 to Figure 5.28, which shows Laponite stained as yellow not orange and tissue as green not blue) due to the filter set unavailability; however, the stain's selectively of Laponite was not affected (please refer to Chapter 2.3.8.1 for filter details).

5.2.6.2 Laponite Exclusion

By day 14 there was evidence that exclusion of Laponite from wounds occurred; Figure 5.24 clearly shows a large mass of Laponite (stained with the fluorescent marker Auramine O) containing wound debris had become separated from a wound that had fully re-epithelised. Further evidence that wounds exclude Laponite can be seen in Figure 5.25 as this fully re-epithelised day-18 wound had no residual Laponite present in or around the wound bed.

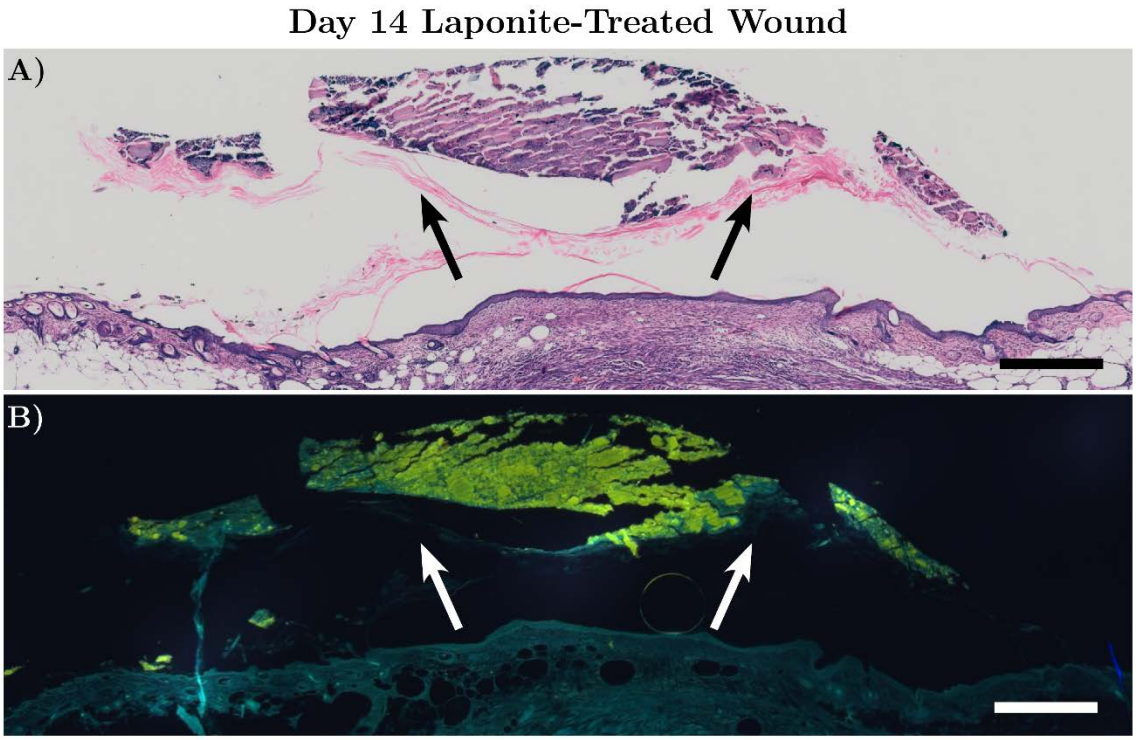

Figure 5.24. Laponite-treated wound stained with Auramine O at day 14 showing evidence of Laponite biomaterial exclusion from the wound. White/black arrows = positively stained Laponite biomaterial that had become separated from the wound bed, suggesting that a sizeable proportion of localised Laponite is excluded from the wound. A and B scale = 500 µm. Image B filter set 2 (DAPI) used (please refer to Chapter 2.3.8.1, Table 2.2 for filter details).

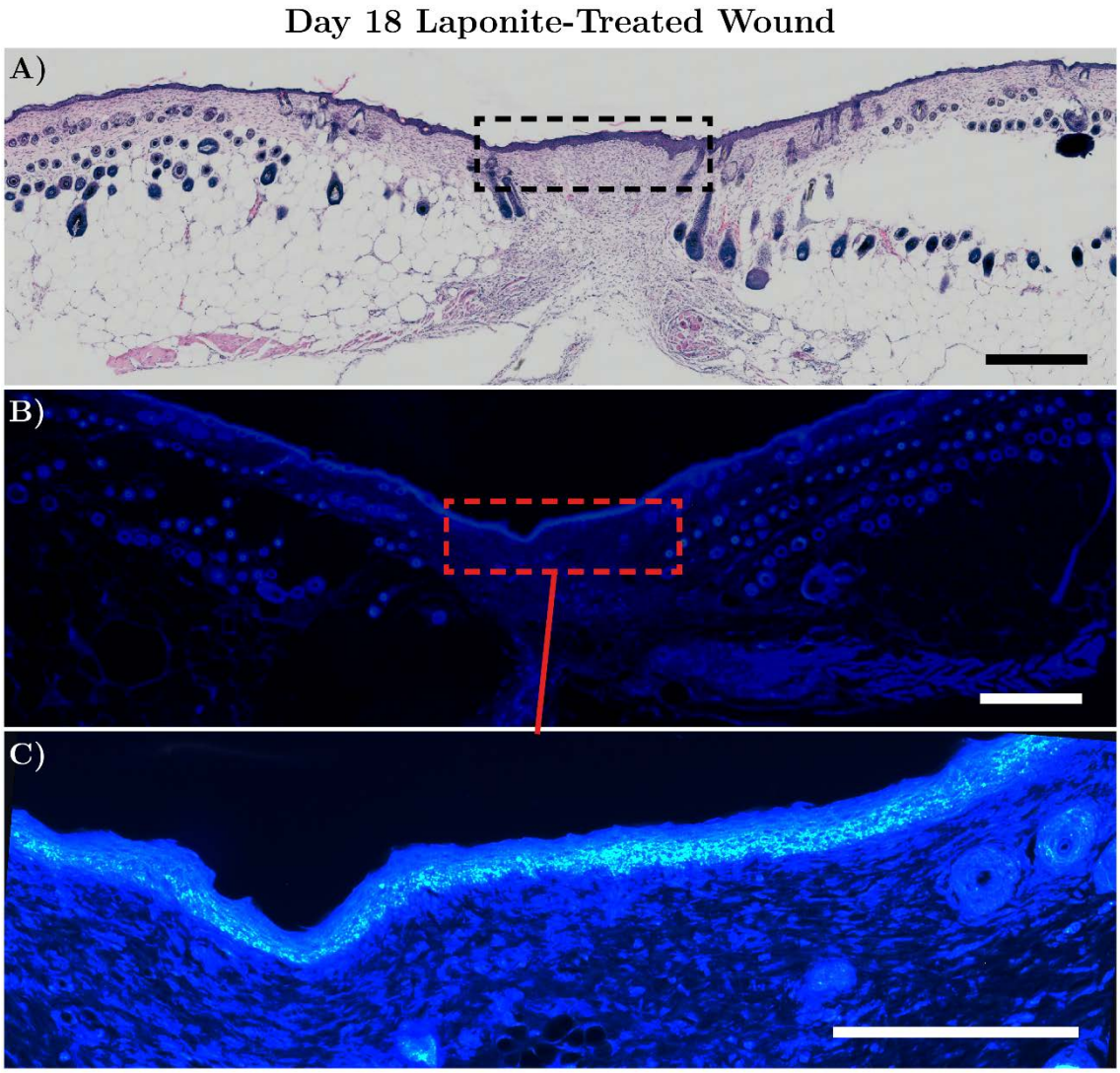

Figure 5.25. Laponite-treated wound at day 18 stained with Auramine O showing no evidence of incorporated Laponite biomaterial within the fully-recovered wound bed. A and B scale = 500 µm, C scale = 200 µm. Image B and C filter set 16 (FITC) used (please refer to Chapter 2.3.8.1, Table 2.2 for filter details).

5.2.6.3 Examples of Laponite Persistence

In contrast to exclusion of Laponite, there were examples that Laponite did persist within the wound environment for up to 18 days post-surgery. Both Figure 5.26 and Figure 5.27 shows that a large quantity of residual Laponite (white arrows) was present within the adipose tissue of the subcutaneous layer of the skin (red arrows); this remaining Laponite was present after the both wounds had fully re-epithelised.

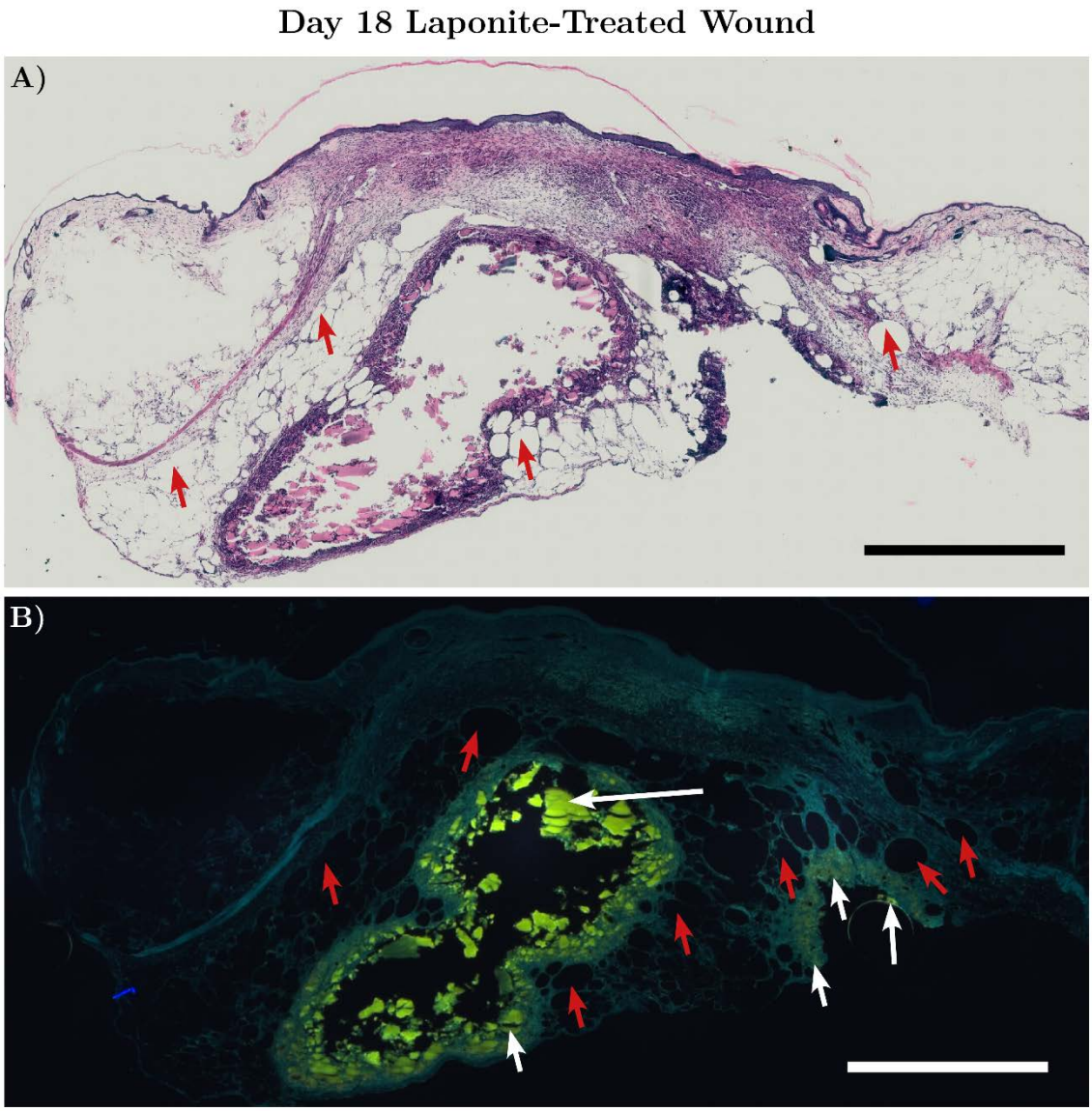

Figure 5.26. Fully re-epithelialised Laponite-treated wound (day 18) stained with Auramine O showing incorporated Laponite biomaterial within the hypodermis of the skin (Example 1). Evidence of a large quantity of residual Laponite biomaterial present within the adipose tissue of the skin; this is directly below the site of the original defect which has fully re-epithelialised. A and B scale = 1 mm. White arrows = Laponite biomaterial positively stained with Auramine O, red arrows = adipose tissue. Image B filter set 2 (DAPI) used (please refer to Chapter 2.3.8.1, Table 2.2 for filter details).

A final example shows the persistence of Laponite can sometimes occur within the wound granulation after a wound had fully re-epithelialised (Figure 5.28). Interestingly, there was evidence that fragments of Laponite had become encapsulated within the newly formed epithelium (red arrows).

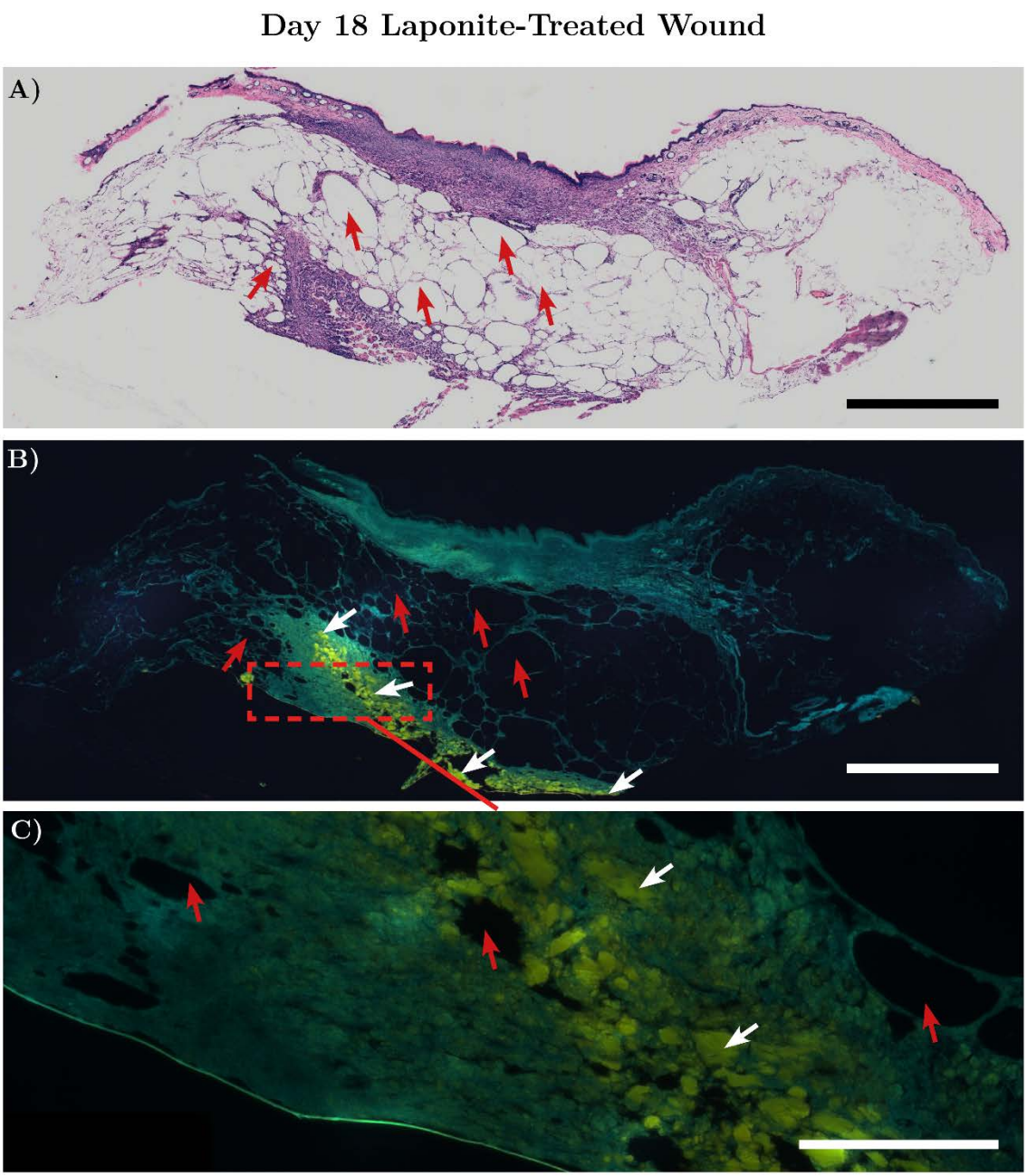

Figure 5.27. Fully re-epithelialised Laponite-treated wound (day 18) stained with Auramine O showing incorporated Laponite biomaterial within the hypodermis of the skin (Example 2). Evidence of a large quantity of residual Laponite biomaterial present within the adipose tissue of the skin; this is directly below the site of the original defect which has fully re-epithelialised. A and B scale = 1 mm, C scale = 200 µm. White arrows = Laponite biomaterial positively stained with Auramine O, red arrows = adipose tissue. Image B and C filter set 2 (DAPI) used (please refer to Chapter 2.3.8.1, Table 2.2 for filter details).

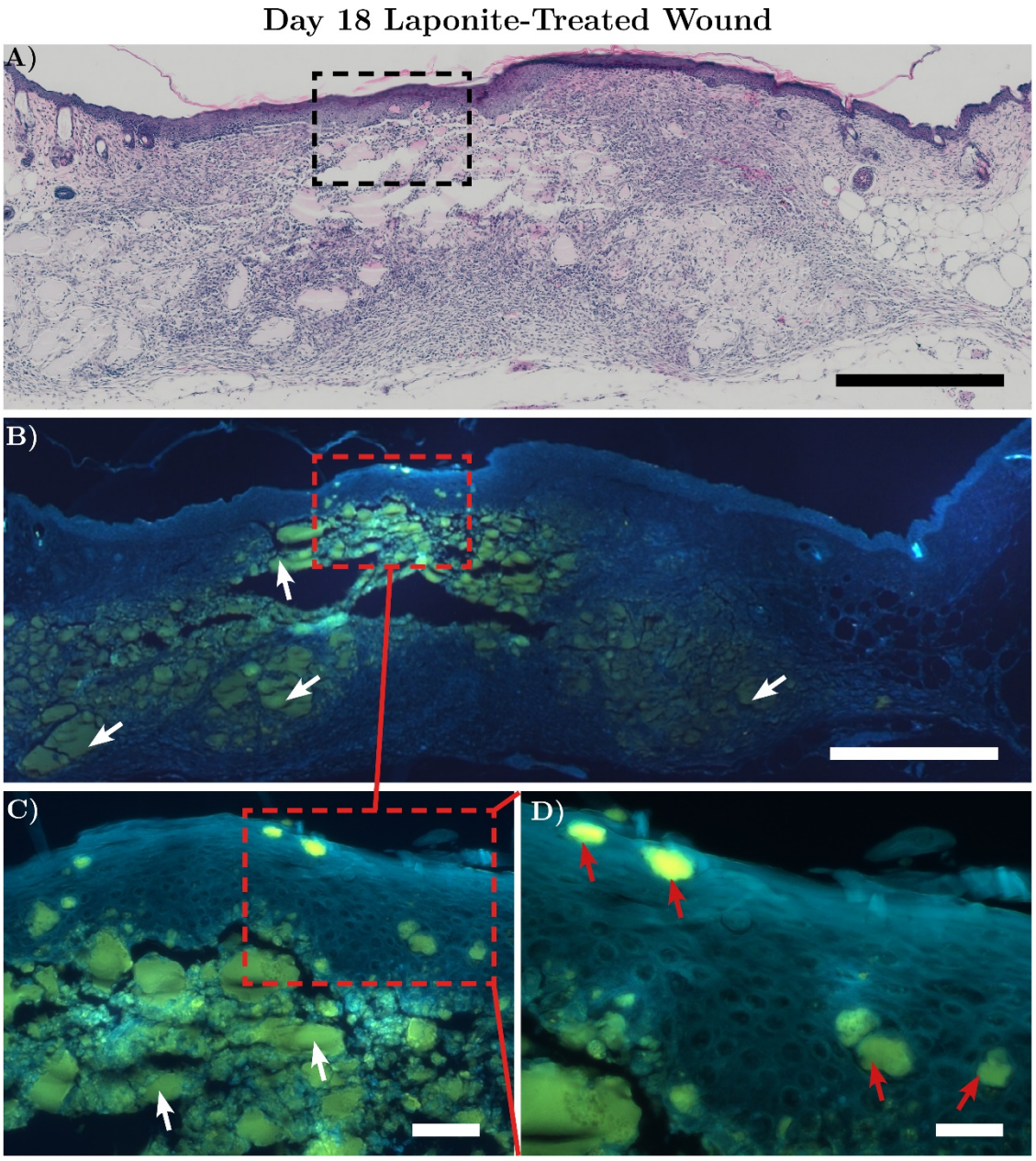

Figure 5.28. Fully re-epithelialised Laponite-treated wound (day 18) stained with Auramine O showing an example of incorporated Laponite biomaterial throughout the wound bed and within newly-formed epithelium. Evidence of a large quantity of residual Laponite biomaterial still present within the wound bed. Interestingly, there was fragments of Laponite biomaterial that had been incorporated within the newly formed epithelial tissue (red arrows). adipose tissue of the skin; this is directly below the site of the original defect which has fully re-epithelialised. A and B scale = 500 µm, C scale = 200 µm, C scale = 100 µm. White arrows = Laponite biomaterial positively stained with Auramine O, red arrows = Laponite embedded within epithelial tissue. Image B-D filter set 2 (DAPI) used (please refer to Chapter 2.3.8.1, Table 2.2 for filter details).

5.3 Discussion

The focus of this chapter was to test the hypothesis that VEGF encapsulated within Laponite would increase the rate and quality of wound healing when applied to a model of delayed wound healing. The mice used in these studies were shown to exhibit severe hyperglycaemia at the time of surgery and throughout the study; this is akin to other reports that have adopted *db/db* mice as model for type 2 diabetes [297].

As a minor note, it is preferable to use littermates related *db/db* mice that are not leptin receptor deficient (i.e. heterozygous BKS. CG-+$Lepr^{db}$/-$Lepr^{db}$ mice) as non-diabetic controls. However due to financial constraints C57BL/6J were used instead. The *db/db* mice used were provided on a C57BLKS/J background which is a substrain of the 6J mice. However, it has been shown that only 71% of 6J genome is retained by the C57BLKS/J mice due to breeding contamination of 6J stock in the 1940s [301]. Whilst the two strains may not be directly comparable, the overall aim was to compare to non-diabetic mice to ensure that the *db/db* mice used in these studies were indeed diabetic. In addition, when interventions were applied, vehicle controls were always used as a baseline within the same animal; therefore, any measurable changes would be attributable to the invention being tested.

5.3.1 Testing and Determination of Plasma Blood Glucose Levels

Blood glucose concentration was measured in fasting and fed states. Fasting glucose concentration is known to be more consistent [302], and for this reason it is preferable to use fasted mice. However, fasting mice on multiple occasions during the study would be unethical due to stress inflicted by surgery as well as potentially affecting their natural baseline of recovery. In addition, in this study no significant changes were found in glucose concentration. Therefore, fasted mice were not used in these studies.

5.3.2 Effects of Laponite Hydrogels Alone on Wound Recovery

5.3.2.1 Closure Rates Conclusion

As it was previously reported that Laponite-treated wounds exhibited greater cellularity during wound healing in non-diabetic mice (Chapter 4.2.3.6), it was hypothesised that a greater positive effect was may occur within mice that exhibit a delayed wound healing response.

Unlike non-diabetic mice, the rate of wound contraction in Laponite gel treatments compared to PBS were similar; this could be attributed to the fact that *db/db* mouse wounds contract less than non-diabetic mice [303].

Significant differences in wound closure were measured between rostral and caudal wounds treated with saline control. As reported previously in results Chapter

4.2.3.3 and by other researchers [286], site-specific differences in non-healthy mice were found to be negligible. This was not true of *db/db* wounds. Knowledge of site specific differences in wound recovery repair in *db/db* mice is limited. A study by Sullivan *et al* [297] validated the use of multiple (~4) wounds in *db/db* mice but did not directly compare the closure rates of rostral and caudal wounds. They did suggest that comparisons of multiple wounds should be limited to wounds that are in a similar rostral-caudal position, however this statement was based on previous work by Märtson *et al* [304]. This work showed that reductions in the number of fibroblasts in early wound healing ($\leq$ 4 days) in caudal compared to rostral wounds. A reduction in fibroblast number early in the wound healing cycle could result in reduced contraction by myofibroblasts (which result from the differentiation of fibroblasts and are critical for wound contraction) [305, 306]. However, these studies used rats rather than mice and so may not be directly comparable, although other studies have suggested that site-specific differences in healthy mouse wounds are insignificant [286]. These findings make it a challenge to draw firm conclusions. As rates of re-epithelialisation and epithelial thickness in rostral and caudal PBS wounds were similar it suggests wound repair between the two regions are comparable.

5.3.2.2 Rates of Re-epithelisation

Arguably the most interesting observation regarding Laponite vs PBS-treated study was that the rates of re-epithelisation for PBS wounds was significantly less than that of Laponite-treated. The importance of this result is underscored taking into consideration that other reports have shown that full wound closure can take an average of $\geq$ 28 days [146, 297, 307]. The data that are most comparable would be the rates of closure documented by Sullivan *et al* [297] as they also

covered wounds with a semi-occlusive Tegaderm dressing (many other researches adopt the use of a splint to reduce contraction [296]). Although they did not directly measure the rates of re-epithelisation using histology, they did report that 38% of the *db/db* wounds assumed to closed by gross examination were not when checked using histology.

Other measurements indicated that Laponite-treated wounds healed better than control wounds. Epidermal thickness was increased and there was evidence of extensive cell proliferation (marked by positively-stained Ki67 cells) in the basal layer of the newly-formed epithelium. Apart from less overall re-epithelisation, the presence of neutrophils within day-18 PBS-treated wounds tentatively suggests that some of these wounds were still in a state of early inflammation [308]. The process of inflammation initially begins with the invasion by neutrophils which are then replaced by monocyctes/macrophages (refer to Chapter 1.4.2). To investigate this further, a comparison between the proportion of neutrophils and macrophages could be compared. The presence of neutrophils at such a late timepoint is characteristic of a wound that is delayed and is a common occurrence within DFUs and other chronic wounds [308-310]. Speculatively, Laponite may act upon the wound to reduce inflammatory cytokines through absorption. This in combination to Laponite's eventual exclusion from the wound which was documented in a few examples, may serve as an indirect anti-inflammatory mechanism. One way to test this hypothesis would be to recover excluded Laponite and measure cytokine content of the biomaterial (e.g. cytokine measurements, cell-specific staining) [311].

5.3.3 Hair Follicle Stimulation

Evidence of hair follicle growth was another interesting finding. In the literature, it states that natural hair follicle growth occurs as a wave, moving across the dorsum. However, this usually occurs at specific times within the first 14 weeks after birth (documented in healthy mice) [312]. This phenomenon occurs due to a set of events known as the hair follicle cycle and are characterised as anagen (growth phase), catagen (regression phase) and telogen (resting or quiescent phase) [313]. At approximately 7 weeks old, the hair cycle enters a prolonged state of telogen, lasting until 12 weeks when the anagen phase begins [312]. The age of mice chosen for these studies was between 8-10 weeks to ensure consistency and to minimise the possibility of hair growth reducing adhesion of the Tegaderm dressing. Therefore, it was striking that hair follicle stimulation occurred during a natural period of telogen.

H&E staining confirmed that hair follicles in these regions where hair follicle growth was suspected were dense, with a high proportion existing with the subcutaneous tissue; the increase in the number of follicles within the deep layer of skin is indicative of the anagen phase compared to telogen phase, in which hair follicle exist exclusively within the dermis [314].

Excitingly, the evidence suggests that Laponite gels may have facilitated this stimulatory effect by localising exudate produced in and around the wounds. Speculatively, the sorptive properties of Laponite could have retained cell signalling/bioactive molecules and concentrated them within the region where the hair follicles were most prevalent. A growth factor that is endogenously produced

during wound healing and also a known stimulator of hair follicle growth is insulin growth factor-I (IGF-I) [315-319].

A simple way to determine whether this growth factor is responsible would be to collect and analyse the protein content within the wound fluid; this could be achieved by multiple testing systems including high-performance liquid chromatography (HPLC), enzyme-linked immunosorbent assay (ELISA), Meso Scale Discovery (MSD) and electrochemiluminescence and bead based multiplex immunoassays (MIA) [320].

Another approach could involve incorporating a hypothesised growth factor with Laponite gels and topically apply it to mouse skin during telogen. Hypothetical growth factors could include the IGF-I or a cytokine determined by analysing the protein content of wound exudate.

Regardless of the bioactive molecule(s) responsible for this stimulation of hair follicles, the most important aspect would be to determine that Laponite was accountable for localising said bioactive factors. To test this hypothesis, samples of wound exudate stimulated by Laponite-treated wounds could be collected an applied to an unwounded area of skin and covered with a dressing; evidence of hair follicle growth can then be assessed and compared to a control region.

5.3.4 Observations of Prolonged Laponite Persistence

As mentioned previously (Chapter 4), the selective fluorescent marker, Auramine O was an essential histological for effective detection and tracking of the Laponite

within Laponite-treated wounds. The detection of Laponite using Auramine O showed further evidence of biocompatibility (e.g. incorporation within newly-formed epithelium) and possible cellular uptake of Laponite fragments (e.g. endocytosed Laponite) or just more extreme cell infiltration. It additionally showed that it was difficult to predict how the length of time Laponite would persist in the wound environment; there was evidence that suggested wounds excluded Laponite around 7 days post-surgery. Yet in some cases there was significant content of Laponite present after 18 days. Speculatively, the method of administration will likely play a role in its persistence. By injecting under the Tegaderm dressing, in some cases Laponite may have been incorporated deeper within the subcutaneous tissue of the wound.

It has been previously stated that further studies would be useful to track the length of time Laponite may persist within the skin. This would be essential to document because prolonged persistence of Laponite could become a potential hazard if used to deliver bioactive molecules. For instance, continued localisation of VEGF could lead to uncontrolled angiogenesis [321, 322]. It is also well established that overexposure to certain growth factors such as PDGF-BB may increase the risk of cancers to develop [323, 324]. Therefore, future work must consider the potential health implications they may be associated with Laponite and bioactive molecule delivery.

5.3.5 Effects of Localised VEGF Encapsulated by Laponite Gels

The decision to incorporate 40 µg/ml VEGF within Laponite gels was based on conclusions documented from studies in the previous chapter (refer to Chapter

4.2.3.5). Although a lower concentration (10 µg/ml) of VEGF was a positive stimulator of angiogenesis *in vivo*, it was thought that using the higher concentration would maximise the potential to induce a positive biological effect on wound recovery in *db/db* mice.

The addition of alginate was also investigated as it was thought that Laponite would result in localisation of VEGF whereas alginate would represent a biomaterial that exhibits rapid release of the protein [235]. Therefore, alginate gels were used to help prove the hypothesis that Laponite gels offers a superior was to deliver growth factors.

There were no measurable differences in the rate of wound closure, re-epithelisation or epithelial thickness with the addition of VEGF to Laponite gels. However disappointing, the probable reason could have been due to experimental limitations. For example, the benefits that Laponite alone exerts on the wound environment may mean that any further improvements were either not present or went undetected. Unfortunately, due to time constraints the identification and analysis of blood vessel formation (using the endothelial cell marker anti-CD31) as used in Chapter 4.2.3.6 was not performed. The use of this marker may have elucidated in more detail the cellular changes that is difficult to detect from gross macroscopic and basic histological analysis.

There was an indication that there was greater cell invasion within Laponite-VEGF treated wounds at day 14, which then resulted in a significant reduction by day 18. This trend was present in the vehicle Laponite group but interestingly the reduction was greater with the addition of VEGF. It is likely that the time

between day 14 and 18 marked the transition from proliferation to remodelling due to the reduction of cell number (refer to Chapter 1.4). That a more significant reduction occurred in wounds treated with Laponite containing VEGF may suggest that localised VEGF may have played a part in ensuring remodelling occurred more quickly [88]. To measure the proliferation/remodelling transition more accurately, staining for collagens would be a useful indicator, especially the ratio of type I and type III collagen [67, 325-327]

A surprising finding was that addition of VEGF to alginate gels resulted in a significant improvement in wound closure and re-epithelisation rates. This was akin to the improvements seen with Laponite vs PBS. As previously documented in Chapter 4 (Figure 4.16) the release of VEGF from alginate gels was shown to be ~75% within 24 hours. Dawson *et al* [234] also documented similar release profiles from alginate using model proteins lysozyme and albumin. Thus, the process of rapid VEGF release was more advantageous than Laponite's ability of retention in these wound studies. Rapid release of biomolecules is contrary to conventional wisdom within tissue engineering, where the attention is focused on slow and sustained release [135, 328]. However, the rapid release of VEGF into a wound environment maybe beneficial in context of the wound healing studies reported in this chapter. It is known that VEGF mRNA and protein levels increase at initial time points (~3 days) following injury in healthy skin [329, 330]. This helps stimulate angiogenesis early during wound healing and ensure that a rich blood supply is present for the formation of healthy granulation tissue (as described in Chapter 1.6). In *db/db* mice, it is known that VEGF mRNA expression initially increases following injury, but then decreased to negligible levels by day 5 [101]. Therefore, a burst release of VEGF within the first 24-48

hours may help stimulate early angiogenesis and initiate more rapid formation of granulation tissue.

If the above hypothesis was correct, then it could be suggested that a more rapid release profile would be more advantageous for VEGF delivery. However, translation of this effect in human chronic wounds may not be as successful. Chronic wounds in humans such as DFUs, exhibit a complex environment that is commonly in a prolonged state of inflammation (refer Chapter 1.3). Individuals that suffer with DFUs can have symptoms that last for extensive periods of time (months to years) [237]. Therefore, rapid release of VEGF under these circumstances would be futile. In contrast, sustained release may initiate a bioactive effect, although its delivery to target cells could still be hampered by degradative proteases. An alternative approach could be sustained localisation by Laponite gels with the hypothesis being that Laponite would protect VEGF from degradation. This means that whilst the studies in this chapter have not proven the main hypothesis of this thesis to be true, its potential to be proven correct may still stand.

A potential criticism of the alginate gel studies was that the number of mice used was low compared to Laponite treatment groups (3 vs 6). Whilst it could be argued that it is statistically underpowered, the use of 4 wounds per mouse aimed to increase the number of treatment replicates from 3 to 6. Some minor differences between rostral and caudal wounds were acknowledged and discussed. However, it was concluded that using multiple wounds as replicates was acceptable and in line with previously documented literature [286, 297].

5.3.6 Conclusion

The key findings that were reported and discussed in this chapter were: (1) vehicle Laponite gels were shown to improve the rate and quality of wound healing compared to saline in *db/db* mice, (2) localisation of wound exudate facilitate by Laponite gels stimulated hair follicle anagen in *db/db* mice at the wound margins and within adjacent healthy skin tissue, (3) localisation of a high concentration of VEGF (40 µg/ml) via premixing within Laponite gels did not offer any detectable improvements in the rate and quality of wound healing in in *db/db* mice, (4) delivery of 40 µg/ml VEGF by the control biomaterial hydrogel (alginate) significantly improved the rate/quality of wound healing in *db/db* mice suggesting that a rapid release of VEGF within ~48 hours was advantageous, and (5) Laponite gels exhibited signs of exclusion from the wound environment but in many cases residual Laponite did persist at the wound site for ~18 days.

In conclusion, 3% Laponite gels may offer unique benefits to wound healing, albeit without the addition of VEGF. Although rapid release of VEGF from alginate gels was shown to offer significant improvements to wound healing, its translation to human chronic wounds may not be as successful; it was postulated that the benefits of sustained VEGF localisation by a Laponite gels may be more beneficial in an environment that is chronically delayed (weeks/months). This would require further investigation with a modification to the wound model proposed in this chapter. Promisingly, it still suggests that Laponite gels have the potential to localise bioactive factors that may increase the rate and degree of wound healing in chronic diabetic wounds.

Chapter 6:

Discussion

6.1 Summary of Thesis Outcomes

The main aim of this thesis was to investigate the potential of a synthetic smectite clay, Laponite, to sequester therapeutic small molecules and proteins and to deliver them in vivo to improve wound repair. Ensuring that therapeutic molecules exert a biological effect at a target site requires an important prerequisite; delivery in a sustained, economical and safe manner. The thesis achieved this aim by showing:

- Laponite clay gels sequester molecules important in wound healing and angiogenesis, and retain their bioactivity in *in vitro* models
- *In vivo* murine models can be used to test the activity of injectable clay biomaterials, both in subcutaneous and cutaneous wound-healing assays.
- VEGF-Laponite induces a potent angiogenic response *in vivo*, but this effect occurs via cell invasion rather than by passive release
- Laponite alone accelerates wound healing and improves wound healing quality and may act to promote anagen at wound sites

Initial experiments (Chapter 3) included analysing the *in vitro* retention and release of a small molecule Wnt signalling agonist (BIO) and a larger, protein (VEGF). The main findings were:

- VEGF, when incorporated, in Laponite stimulated HUVEC tubule formation.
- Higher concentrations of VEGF were required for activity in gels where VEGF was incorporated in the bulk as compared to adsorbed on the surface. This is likely due to VEGF being sequestered away from the cells.

- Following encapsulation BIO was retained in Laponite gels for up to a 7-day period.
- Preliminary adsorption data showed that BIO does not interact as well as VEGF.

In subsequent chapters, this extended into more detailed analysis of the bioactive response that clay-VEGF gels exert when applied *in vivo*. This initially started with measuring the effects of clay-VEGF gels within a healthy acute wound healing model and then extended into detailed account of VEGF dosage required within Laponite gels via subcutaneous injection study (Chapter 4). The main findings were:

- Laponite-VEGF gels are proangiogenic *in vivo* in a VEGF dose dependent manner.
- A minimum 10-fold increase of VEGF concentration ($\geq$ 10 µg/ml) incorporated within Laponite gels was required for a biological effect compared to *in vitro*-based models.
- *In vitro* release kinetics showed negligible release of VEGF from Laponite gels compared to the burst release measured for alginate gels.

Finally, optimised Laponite-VEGF gels (i.e. using a VEGF dosage capable of a biological effect) were assessed in a diabetic wound model, which represents delayed wound recovery (Chapter 5). The main findings were:

- Laponite gels alone induced a therapeutic effect on wound healing with evidence of increased re-epithelisation and cell proliferation compared to PBS-treated control wounds.

- Laponite gels may have initiated hair follicle anagen in healthy skin immediately adjacent to wounds as a high proportion of Laponite-treated wounds (regardless of the incorporation of VEGF) had many follicles within the deep layer of skin (this is indicative of the anagen phase); it was proposed that localisation of wound exudate may have stimulated this phenomenon as the shape and size of the increased follicle growth were similar to area of deposited wound exudate during early time points (~ 7 days post-surgery). This is however, a highly suggestive claim that would require further investigation to robustly prove.
- Localisation of VEGF by Laponite hydrogels did not stimulate any measurable increase in wound recovery
- The addition of VEGF to alginate gels surprisingly initiated a significant increase in wound closure rates and wound "quality".

6.2 Discussion of Results

Delivery of drugs and bioactive molecules using natural clay minerals and synthetic-based clays has been of significant interest in recent times [14]. The mechanism of clay interaction with biological tissue and charged species exerted by bioactive molecules/drug are complex [331]. Furthermore, the potential benefits of cationic clays such as Laponite specifically on wound healing is not well understood scientifically. However, it is understood that the adsorption properties of clays can remove toxins, oils and other contaminants from skin and have excellent rheological properties [249].

The combination of the properties listed above led to the hypothesis that Laponite gels could deliver bioactive molecules to increase the rate and degree of wound healing. Over the next few subchapters, the results documented in this thesis will be addressed as to whether this hypothesis was proven correct with regards to the wider context of pre-existing literature.

6.2.1 Localised Delivery of VEGF by Laponite Gels

Novel treatment options for chronic wounds are predominantly administered as topical creams or gels [332], in addition to the formulation of advanced wound dressings that contain therapeutic molecules [333]. Thus, incorporation of therapeutic molecules within a biomaterial vehicle consisting of hydrogels, polymers and/or clay is advantageous.

Previous work using Laponite clays had only elucidated that protein biomolecules were capable of significant retention by highly charged nanoclay particles [235]. Bioactive effects were only measured following adsorption of VEGF to the surface

of Laponite gels, rather than following incorporation within the gels. In addition, these studies showed that Laponite sequestered, but did not release a model protein. Based on this work, it was hypothesised that the bioactivity of incorporated biological molecules is retained when mixed in the bulk of the gel, but that the effective concentrations may differ.

In Chapter 3 and 4 it was found that a significant biological effect was induced when VEGF was incorporated into Laponite gels at a concentration ≥ 1 µg/ml *in vitro* - greater than required *in vitro* (Chapter 3.2.4) and ≥ 10 µg/ml *in vivo* (Chapter 4.2.3.5). The disparity between bioactive concentrations required *in vitro* and *in vivo* was an important finding that can have negative implications if not considered carefully. Lack of *in vitro* to *in vivo* translatability is a common issue that applies to other tissue engineering and biological research strategies [334].

Laponite and alginate (a control hydrogel) were both found to be retained at injection sites for a period of 21 days, however there was less prevalent cell or tissue integration in alginate than in Laponite. This contrasted to previous research by Lee *et al* [283] where concentrations of ≥ 20 µg/ml VEGF induced significant cell invasion, proliferation and blood vessel growth. VEGF concentrations ~ 40 µg/ml did not result in any significant changes in blood vessel density in our studies (Chapter 4.2.3.5); this was likely due to experimental differences as mentioned within the chapter. A key finding was that alginate gels exhibited more rapid VEGF release than Laponite gels. This may be due to differences in immunological response to Laponite vs. alginate, to mechanical differences in the material, or perhaps more likely due to the differing release profiles between the two carriers.

For instance, VEGF premixed within Laponite gels exhibited a biological effect without any evidence of 'release' as *in vitro* release was negligible for up to 11 days. This was comparable to a previous report where it was shown that minimal release of a growth factor over a period of 35 days [292]. The lack of measurable release is not necessarily a drawback of the proposed technique as shown in Chapter 4.2.3.5. This approach enabled the growth factor to be localised at a target site for a prolonged period for a sustained biological effect. Contrastingly, the lack of any measurable bioactive effect by alginate-VEGF (see Figure 4.13), for which release occurs rapidly, illustrates this. A possible mechanism proposed in both Chapter 3 and 4 explained that biological availability without release was because Laponite 'localises' VEGF in an active form. An example of the mechanism of action is depicted in Figure 6.1. This figure proposes that biological tissue exposed to clay-VEGF for a sustained period stimulates a biological response. Due to the hydrogel-like properties of these Laponite gels, cells invade within pores that exist between clay particles and directly interact with clay-bound VEGF. Supporting this, Laponite surface-adsorbed VEGF exerts a strong angiogenic effect in *in vitro* experiments, when no (soluble) VEGF is present in the growth medium.

As discussed in Chapter 1.7, clays are often used as modifiers for many other types of hydrogels to improve mechanical strength; this is essential for biomaterial treatments as scaffolds for tissue engineering [14] and is the reason why Laponite gels are strongly viscoelastic [335].

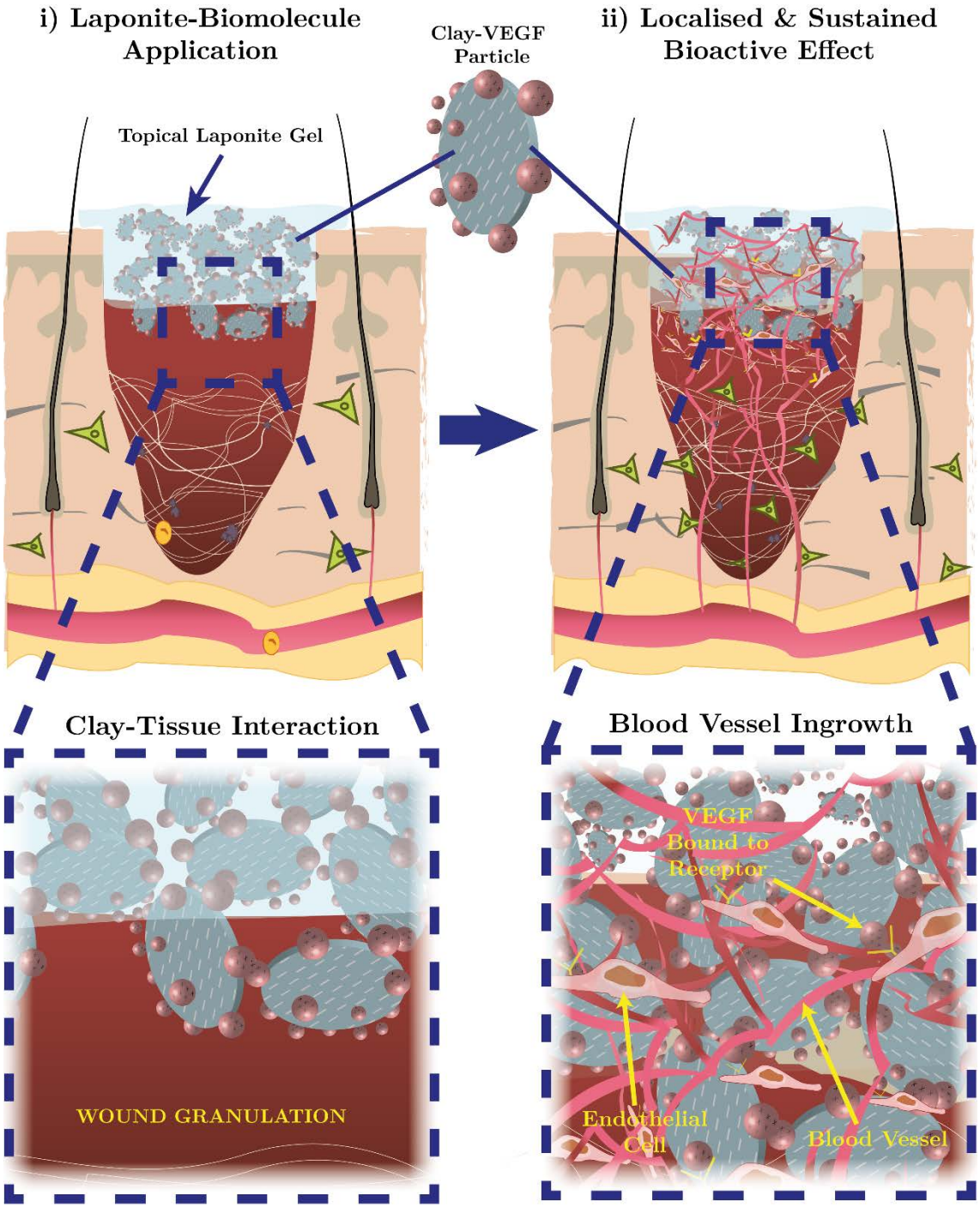

Figure 6.1. Illustration depicting a proposed method of bioactive molecule (VEGF) delivery via localisation by Laponite hydrogels. **i)** Topical application of Laponite gel premixed with VEGF at the site of a skin defect. Clay-VEGF particles can interact directly with wound granulation tissue. **ii)** Sustained and localised delivery of VEGF leads integration and interaction with endothelial cells; this stimulates ingrowth of blood vessels into the Laponite gel, inducing wound repair.

This may aid Laponite's ability to localise bioactive molecules as these gels can withstand high mechanical shear without losing viability. This was demonstrated through the persistence of Laponite gels, both when administered subcutaneously

and at a wound site (Chapter 4 and 5). Furthermore, the strong viscoelasticity properties may allow Laponite to act as a scaffold when in gel form, allowing cells to interact and proliferate. This could be further modulated by the adsorption of endogenous proteins and other biological molecules produced by the host tissue, further supporting a proliferative environment.

The adsorption of endogenous tissue components may provide an alternative explanation of biomolecule delivery by Laponite gels. The basis of this method was initially proposed by Aguzzi *et al* [336] and is summarised in Figure 6.2.

The main concept behind this delivery mechanism is that clay particles are loaded with a drug/bioactive molecule via cationic exchange. This occurs between positively charged species of target biomolecules (e.g. ions, functional side groups) and interlayer cations between clay particles (Figure 6.2. i). After clay application, loaded clay-biomolecule particles interact with biological counter ions which then undergo cation exchange (Figure 6.2. ii). This 'releases' free bioactive molecules that are subsequently absorbed by host tissue where they interact with target cells (Figure 6.2. iii-iv). Spent, unloaded clay particles are ideally eliminated via exclusion from the wound or excreted by the body (via the bloodstream) (Figure 6.2. v).

Although simple drugs are more likely to be delivered via this alternative approach, larger, protein-based molecules may be released in a comparable way via interaction with positively charged side groups.

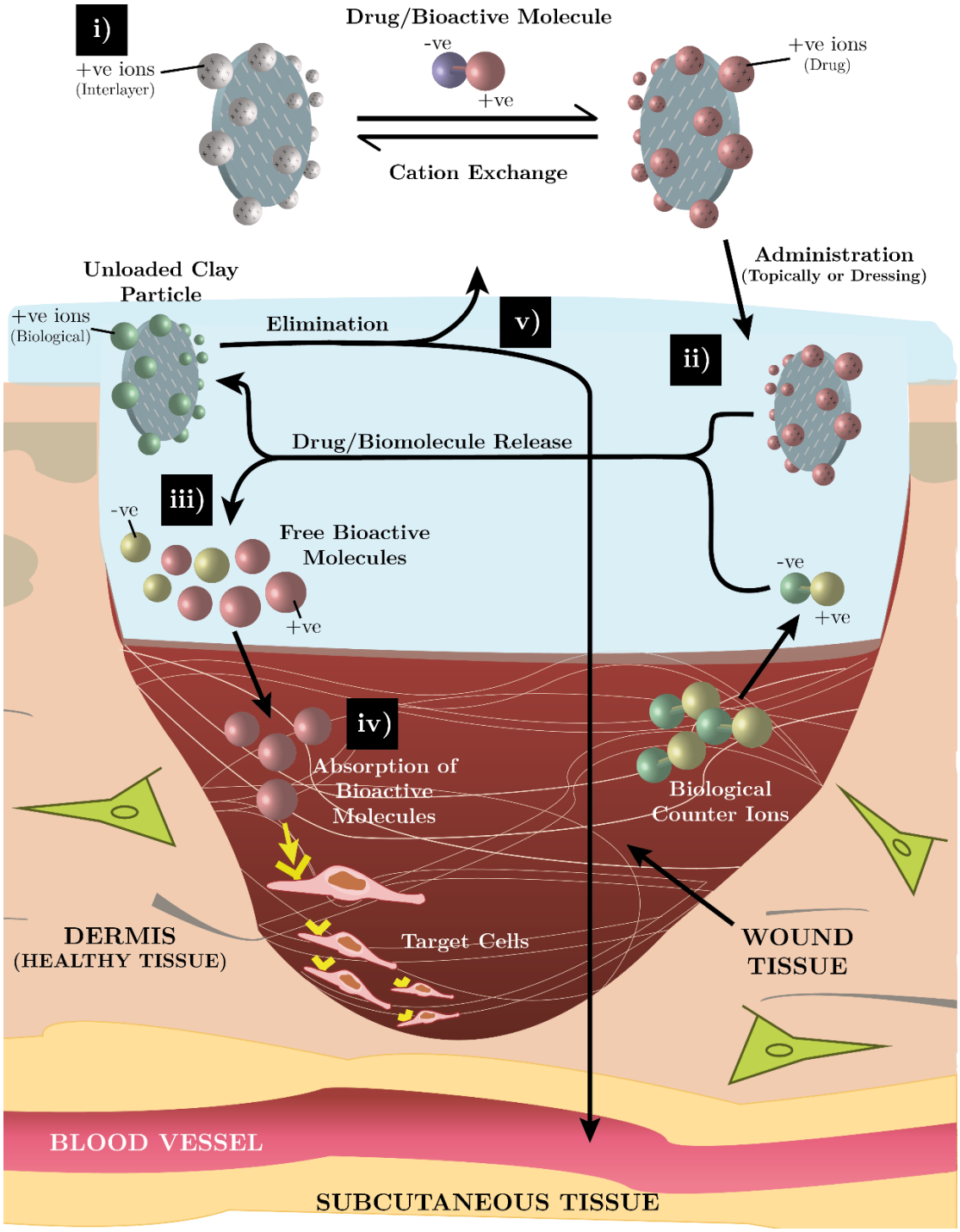

Figure 6.2. Idealised theoretical delivery mechanism of bioactive molecules/drugs by clay particles (figure adapted from [336] and [331]). Delivery of drugs or bioactive molecules by clays (such as Laponite) may involve a complex set of events when exposed to a biological environment. These include: i) Clay particles loaded with drug/biomolecules through ionic interaction with -ve charged clay particles; this is achieved via cation exchange of +ve charge interlayer cations with +ve charge ions/side groups of bioactive molecules. ii) Clay-drug particles administered to a defect site where they can interact with biological counter ions present within wound tissue. iii) Cation exchange between +ve ions/groups of bioactive molecules and biological counter ions leads to the 'release' of free bioactive molecules. iv) Free bioactive molecules absorbed into the wound environment where they can then interact with cell targets and stimulate a biological effect. v) Unloaded clay particles eliminated via exclusion from the wound environment and/or removed from the wound into the blood stream/lymphatic system and excreted.

Then endogenous proteins may undergo cation exchange with clay-bound protein and essentially result in target protein displacement/release into the defect milieu. This method also suggests that biomolecule/drug release from clay-based treatments are likely to be different in an *in vivo* environment.

It remains probable that bioactive VEGF was 'delivered' via localisation rather than release as indicated by other authors [235]. Speculatively. sustained localisation may allow cells within a biological system to become stimulated via presentation of bioactive molecules when tethered to Laponite gels. This however, makes determining the release kinetics of these therapies difficult to measure *in vivo* and is an area that warrants further investigation.

Surprisingly, the proangiogenic effect of Laponite-VEGF in the subcutaneous injection study (Chapter 4) did not translate to an improve wound healing response in *db/db* mice (Chapter 5). There was, however, an improvement in wound recovery with Laponite clays alone. Perhaps due to the baseline effects exerted by Laponite clays any further benefits from inclusion of VEGF localisation may be undetectable. It could be hypothesised that the sorptive properties of Laponite allows retention of endogenous bioactive signalling molecules, thereby localising them and increasing their bioavailability. However, if this was the case, it could be expected that negative mediators of chronic wounds (e.g. pro-inflammatory) may also become localised.

This conclusion may be premature, however as stated in Chapter 5 due to time restrictions crucial analytical techniques were not performed (e.g. anti-CD31 and anti-Ki67 staining). There are additional techniques that could offer a more robust

analysis that may uncover further details that suggested localised VEGF by Laponite exerted a positive effect. These may be investigated in future studies.

6.2.2 Laponite Hydrogels Exhibited an Intrinsic Bioactive Effect in Wound Healing

An exciting finding (secondary to Laponite's capability to localise VEGF) was that Laponite exerted an intrinsic stimulatory wound healing effect. As discussed in 6.2.1, this effect may have masked any pro-healing effect of clay-incorporated VEGF in *db/db* wounds.

Clay may alter the phases of wound healing at a cellular and biochemical level within a wound environment. In chronic wounds, healing is usually stuck in a cycle of inflammation. A clay (like Laponite) may localise endogenous cell mediators present within the wound bed, mitigating inflammation. Evidence of cationic clays localising endogenous factors has been recently suggested in advanced haemostatic dressings, like QuikClot® and WoundStat®. WoundStat® is made from a Food and Drug Administration (FDA) approved granular smectite clay and QuikClot® is a wound dressing gauze created with synthetic zeolite [337]; these have been reported to increase local concentrations of clotting factors, platelets and red blood cells and improve the clotting cascade [338].

A recent study by Dario *et al* [242] reported that Ocara clay (a natural clay originating from the Northeast region of Brazil) exerted positive effects on wound recovery in a rat model. Specifically, histological analysis suggested that overall wound quality was improved (e.g. increased re-epithelialisation rates, more dense collagen fibres) when treated with an emulsion/Ocara clay therapy. An important

side note however, was that these findings were only based on qualitative visual analysis. A comparison between Laponite gels and Ocara clays are not directly possible, but they did suggest that wound closure was not significantly improved. Based from this it could be suggested that the overall therapeutic benefits were not as significant as those documented by Laponite gels in this thesis. Speculatively, this may be because Laponite is a refined clay that contains low levels of impurities that may exert negative effects on wound healing.

Laponite and other clay-based wound therapies could potentially aid wound healing by adsorbing to wound exudate. This may lead to an increased concentration of local growth factors and reduce excessive protease activity. Certain advanced dressings are already capable of elevating local growth factor levels; an alginate-based dressing called Kaltostat® is known to promote pro-inflammatory cytokine levels such as IL-6 and TNF-α to support stimulation of local monocytes [339]. Laponite has been documented to exhibit greater absorbency than alginate *in vitro* and also retain encapsulated proteins more effectively [235]. Other types of advanced dressings, including hydrogels and hydroactive dressings (hydrogel/foam dressing mix) have shown promising benefits to selectively absorb/adsorb wound exudate, leaving secreted proteins present [340]. While there is some evidence of improved DFU recovery, many of these dressings are not effective as illustrated in a summary of clinical trials by Dunville *et al* [341].

6.3 Study Limitations

The studies undertaken throughout this thesis have been designed to try and mitigate error and uncertainty that may impact on the outcome of reported

results(s). However, experimental studies (*in vitro* and *in vivo*) only serve as a model of what may occur when a therapy or concept is used within the clinic. Following on from this, there will always be limitations and/or experimental error that will not allow complete certainty.

In this thesis, the *in vivo* murine models best represented what effect outcome would occur if Laponite gel treatments were used clinically. However, whilst mouse models share many physiological similarities to humans, there are key differences that reduced potential translatability. Specifically, mouse skin is physiologically different to human skin [342]. Apart from the obvious different in size and surface area, mouse skin is not directly anchored to subcutaneous tissue which is why they are "loose-skinned". In addition, mouse skin has a thin subcutaneous muscle layer called the *panniculus carnosus* [343, 344]. This muscle layer has been shown to be partly responsible for increased contraction that is seen during wound recovery in rodents. This is contrary to human wound healing which primarily heals by re-epithelisation [344-346]

db/db mice were used as a model of delayed wound healing, which many other reports agree is true. However, this model does not best represent the state of a chronic DFU in humans as, although wound recovery is delayed, their wound recovery is still akin to acute wound healing. DFUs are complex wounds which are incredibly difficult to mimic in a controlled way, especially as there are so many parameters and attributes that form a chronic wound. For example; the recovery of many DFUs is further inhibited due to infection [39], something that is difficult to test for during a full thickness-wound study. There have been reports where rodent wounds have been infected with appropriate bacteria to try and

factor in infection, although this can be ethically challenging as well as experimentally [347, 348].

The use of a swine model is considered the most ideal choice of animal for wound healing studies. This is because pig skin best represents human skin in terms of structure, recovery and area size [349, 350]. However, large animal models are costlier and require specific facilities to house them. In addition, specialised knowledge regarding handling is required [350]

6.4 Future Work

The findings from this thesis indicate that Laponite gels can interact with bioactive molecules and can be used to deliver them into biological systems to initiate a bioactive effect. Laponite gels successfully localised bioactive VEGF and initiated a proangiogenic response which could be advantageous in a chronic wound environment. Separate to this, Laponite gels alone were shown to exhibit a positive effect on the quality of wound healing with evidence of hair follicle stimulation. The combination of these results gives great promise for Laponite gels being used for a wound healing therapy, although further work would be required.

As Laponite appears to have an intrinsic ability to improve wound healing, it may be hypothesised that this occurs through adsorption and retention of endogenous proteins (as discussed in Chapter 3:). Analysis of proteins present within the wound environment would be useful to determine. Dysregulation of cell mediators and proteases contribute to DFU pathogenesis and the physiological repercussions this has on the wound milieu includes: a chronic inflammatory state, impaired angiogenesis, poor cellular infiltration, poor

macrophage activation and reduced formation of granulation tissue that can inhibit re-epithelisation [351]. Thus, measuring and comparing the levels of proteins within tissue samples would be beneficial at assessing the stage and progression of wound healing (i.e. chronic vs acute state). This would be specifically interesting when comparing Laponite-based treatment against no treatment. Methods to achieve this could include:

a. Simultaneously measuring the cytokine levels within wound tissue via Western Blotting [352] or through the use of multiplex assays [199]. Multiplex assays include the Luminex® Assay. The general principle of this assay involves using a polystyrene bead set that is pre-coated with specific antibodies that can target a cytokine of interest (the set can involve multiple analytes). Following antibody binding with a target analyte, a secondary biotinylated antibody is added, conjugated with R-phycoerythrin (R-PE) to form a 'sandwich' of antibody-analyte-antibody. Beads are then analysed with a dual-laser flow based detection system to determine the spectral difference of each bead and RPE secondary antibody; this can allow for accurate detection of different analytes and their relative concentration [200].

b. The measurement of key mediators of inflammation. This is because pro-inflammatory cytokines are known to be increased within a chronic wound environment. Specific pro-inflammatory cytokines of interest include: IL-1, IL-6, and TNF-α [201]. In contrast the anti-inflammatory cytokine, IL-10 has been shown to be reduced in chronic leg ulcers [70]. The multifunctional cytokine TGF-β is also known to be downregulated within chronic wounds, which can have a profound effect on

inflammation and granulation tissue formation [202]. These mediators would be ideal targets to monitor in sample wound tissue that had been treated Laponite-VEGF hydrogels.

c. Measuring the tissue inhibitors of metalloproteinase (TIMP) to MMP ratio within harvested tissue could be beneficial for defining the wound state. This is based on the knowledge that poor granulation tissue formation within DFUs is often the result of increased MMP activity and reduced TIMP activity. MMPs that have been shown to be increased within wound fluid of chronic ulcers include: MMP-1, -2, -8 and -9. The regulators of these MMPS, TIMP-1 and TIMP-2 exhibit an abnormal reduction in protease level [203].

Although only a cursory investigation of the Wnt agonist, BIO, was performed during the course of this thesis due to success (and focus on) VEGF, there is still further development of the biological interactions and potential localisation of small molecule Wnt agonists (BIO). This may include:

a. Increasing the time frame of the BIO release study to a minimum of 7 days. This would determine how effective Laponite would be at retaining much smaller molecules.

b. The BIO availability of premixed BIO within Laponite hydrogels could be investigated using a modified *in vitro* assay. In brief, this could involve the use of a Laponite hydrogel film (a thin coat of Laponite on the surface of a well plate) premixed with a high concentration of BIO and containing a matrix

adhesion protein like fibronectin. 3T3 mouse fibroblast cells containing a luciferase reporter gene (as previously used in earlier *in vitro* assays, see Chapter 3.3) would be seeded onto the Laponite films and luciferase activity measured over a period. This would determine the bioavailability and activity of BIO when premixed within Laponite hydrogels.

c. Further to the release assay described in b, a similar assay investigating the bioavailability of adsorbed BIO by Laponite films would also be beneficial to investigate.

6.5 Conclusion

In summary, these studies demonstrate a comprehensive approach to clay-bioactive molecule interactions and drug delivery with regards to a wound healing application. The importance of novel bioactive molecule treatment options for chronic wounds and DFUs is well documented (refer to Chapter 1.6). However, progress has been restricted due to inherent problems associated with economical biomolecule delivery, fragility of bioactive molecules and hostile wound environments [39, 333]. Laponite gels are a positive step towards eliminating some of those restrictions, with evidence documented in this thesis of natural therapeutic benefits and localisation of bioactive VEGF. Further work is required to answer questions raised during this project in addition to areas that were only briefly explored. In conclusion, these studies may enable biomolecules (VEGF, BIO) localised by Laponite, to improve chronic wound healing and potentially lead to development of a novel DFU therapy.

Appendix A:

Supplementary Information for Methods (Chapter 2)

A.1.1 Subcutaneous Injection Study Questionnaire

Angiogenesis Scoring of Laponite Biomaterial +/- VEGF

Examine all the images below. After examining all the images, go back to the beginning and then score each image category below based on the degree of vascularisation from 0-6 (see below for more detail):

Categories:

BMS = Biomaterial score --> The degree of vascularisation (e.g. redness, blood vessels) **within and/or around the edge of the biomaterial.**

0* = no blood vessel perfusion within biomaterial
2* = slightly red within biomaterial OR at the periphery
4* = biomaterial appears very red in colour with evidence of some blood vessel sprouting
6* = Significant blood vessel perfusion; biomaterial is totally red or dark red, lots of mature vessels growing within.

GIS = Gross Image score --> The degree of vascularisation (e.g. redness, blood vessels) **within the whole image frame (biomaterial and surrounding tissue).**

0* = No blood vessels in whole image frame (biomaterial or surrounding tissue)
2* = Some mature blood vessels/redness present in whole frame (biomaterial or surrounding tissue)
4* = Evidence of lots of blood vessels/redness within biomaterial and/or surrounding tissue
6* = Massive blood vessel perfusion within the biomaterial and lots of vessels around the outside.
***Use 1, 3 or 5 scoring for images that do not quite match these scoring groups (in-between values)**

Useful Information

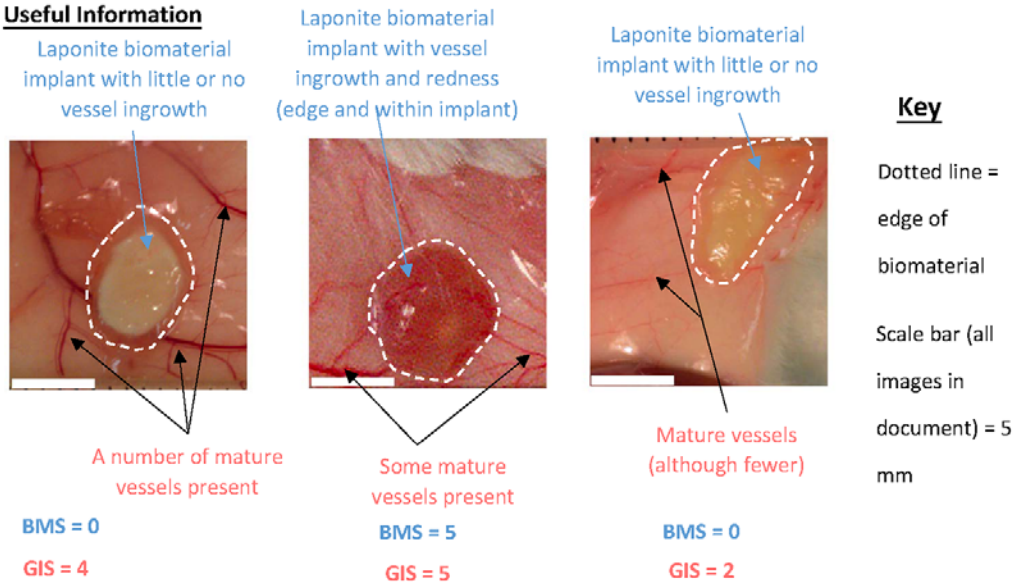

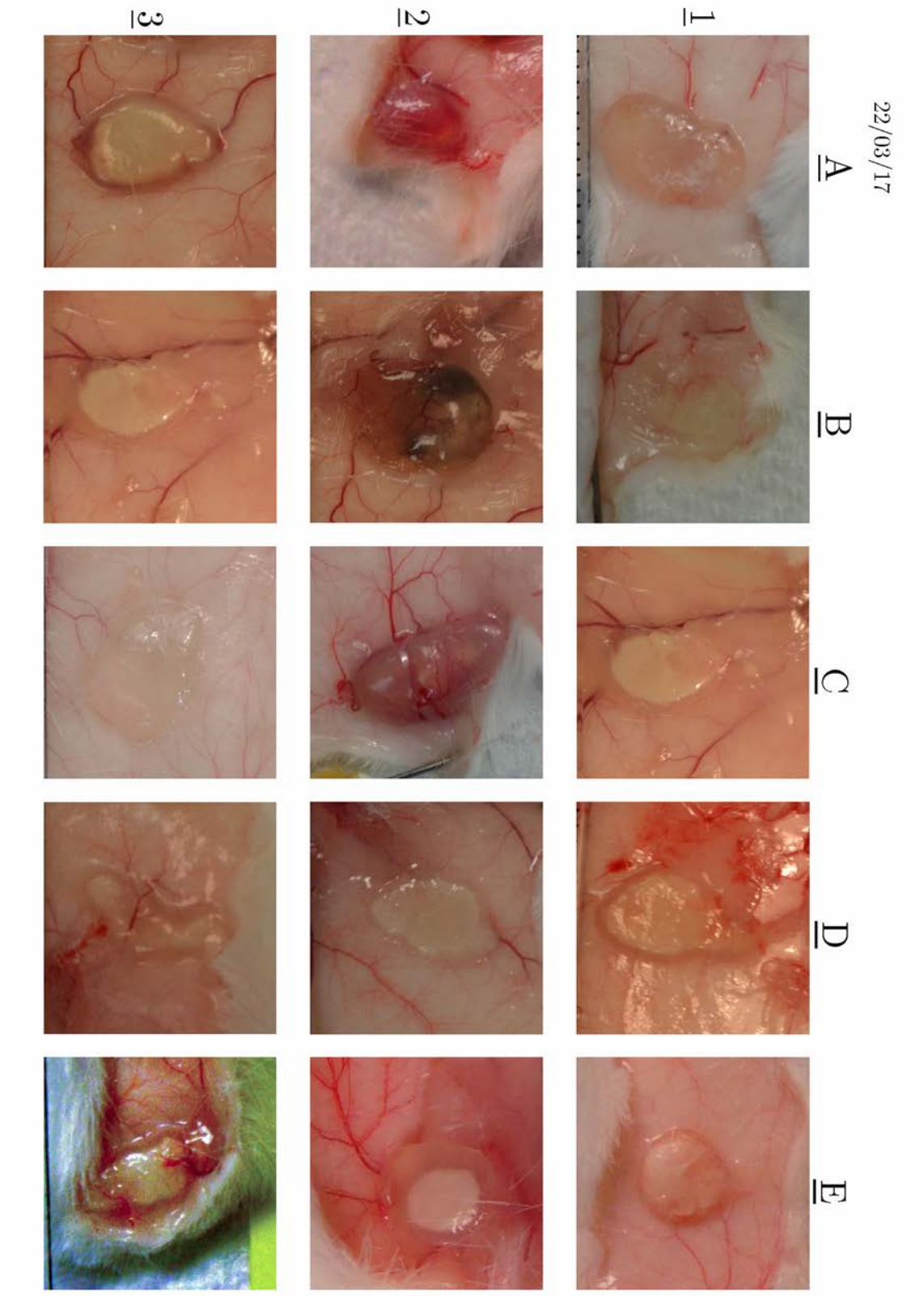
22/03/17
1
2
3
A
B
C
D
E

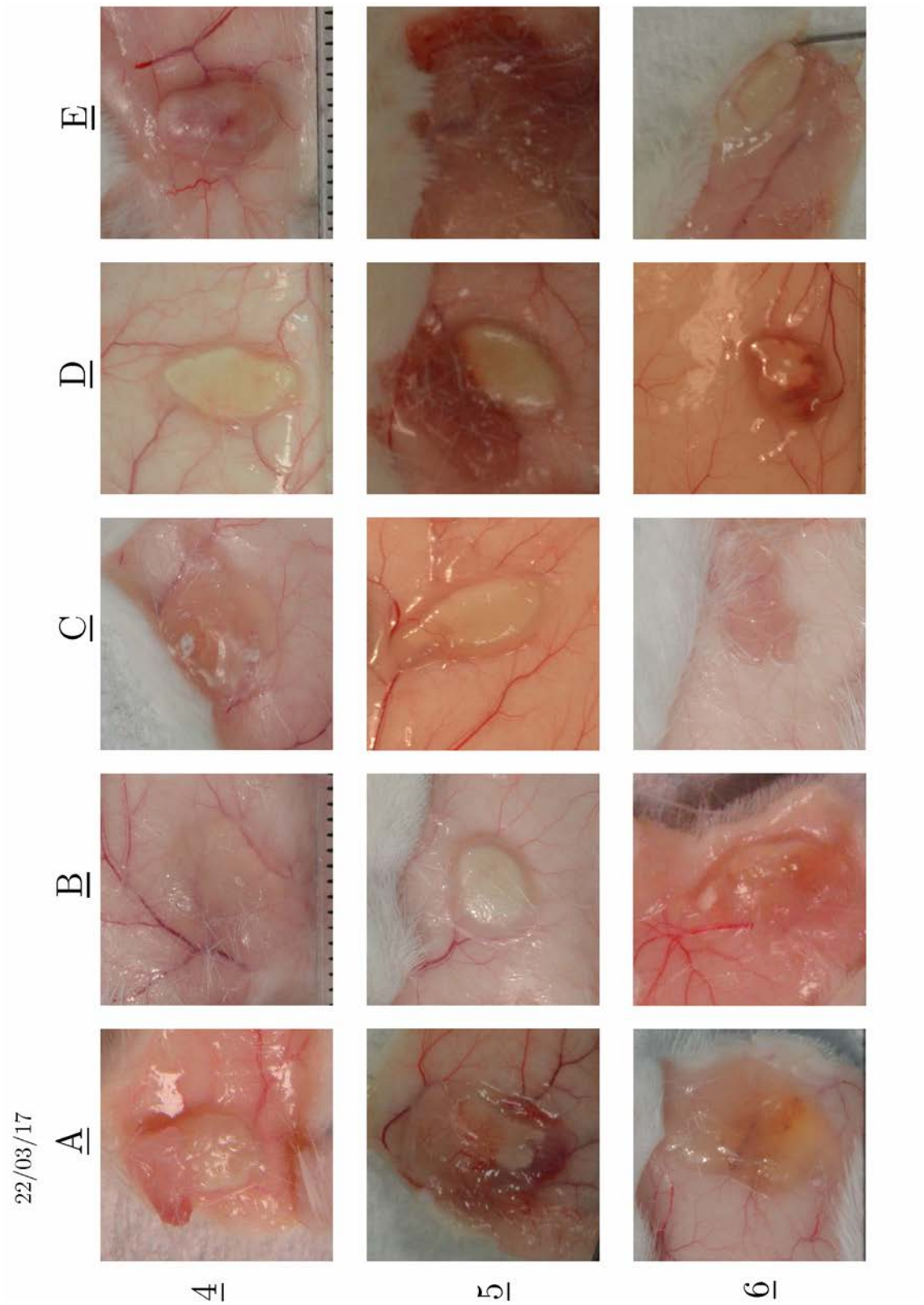
22/03/17
A
B
C
D
E
4
5
6

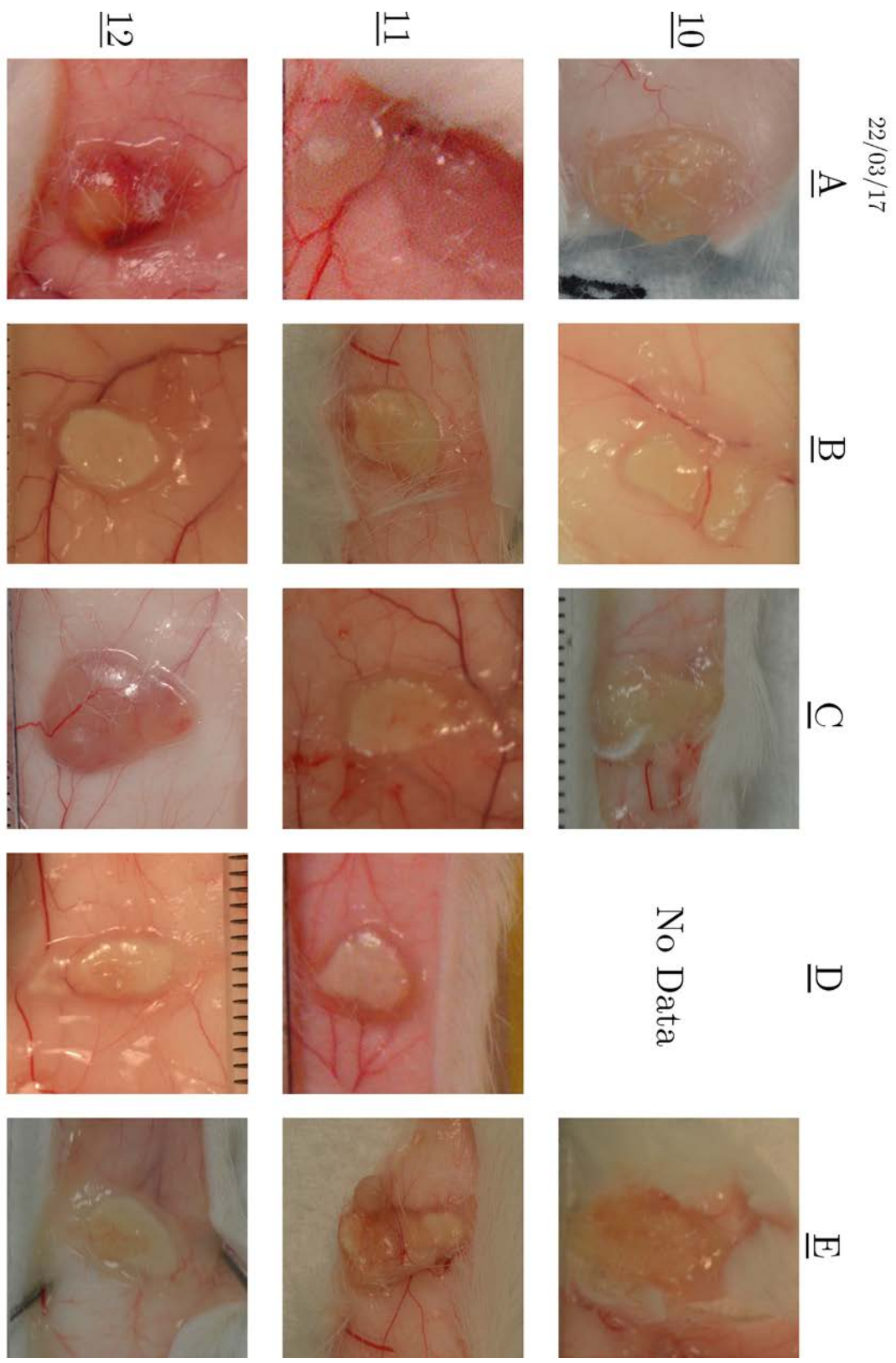
22/03/17
10
11
12
A
B
C
D
E
No Data

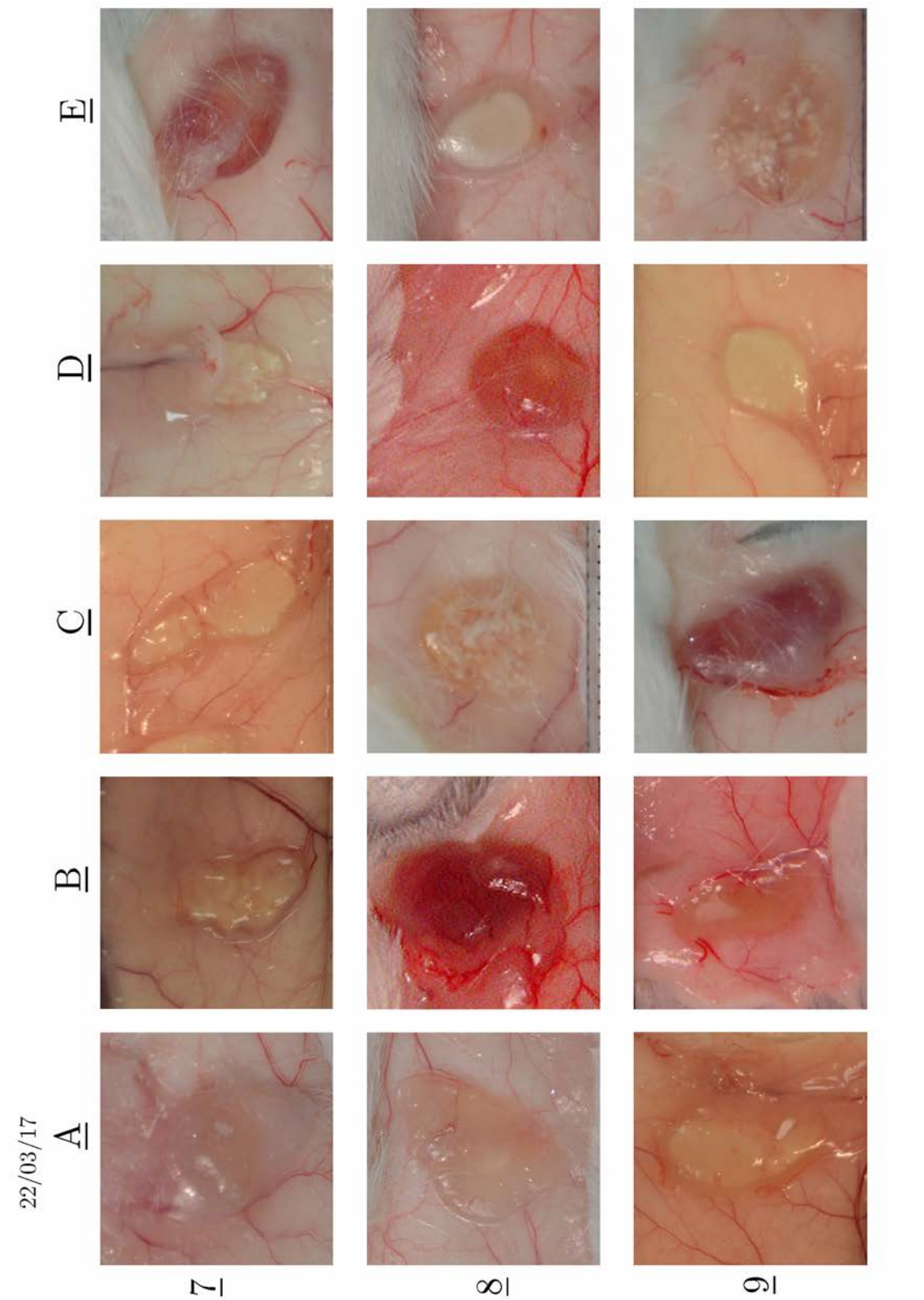
22/03/17
A
B
C
D
E
7
8
9

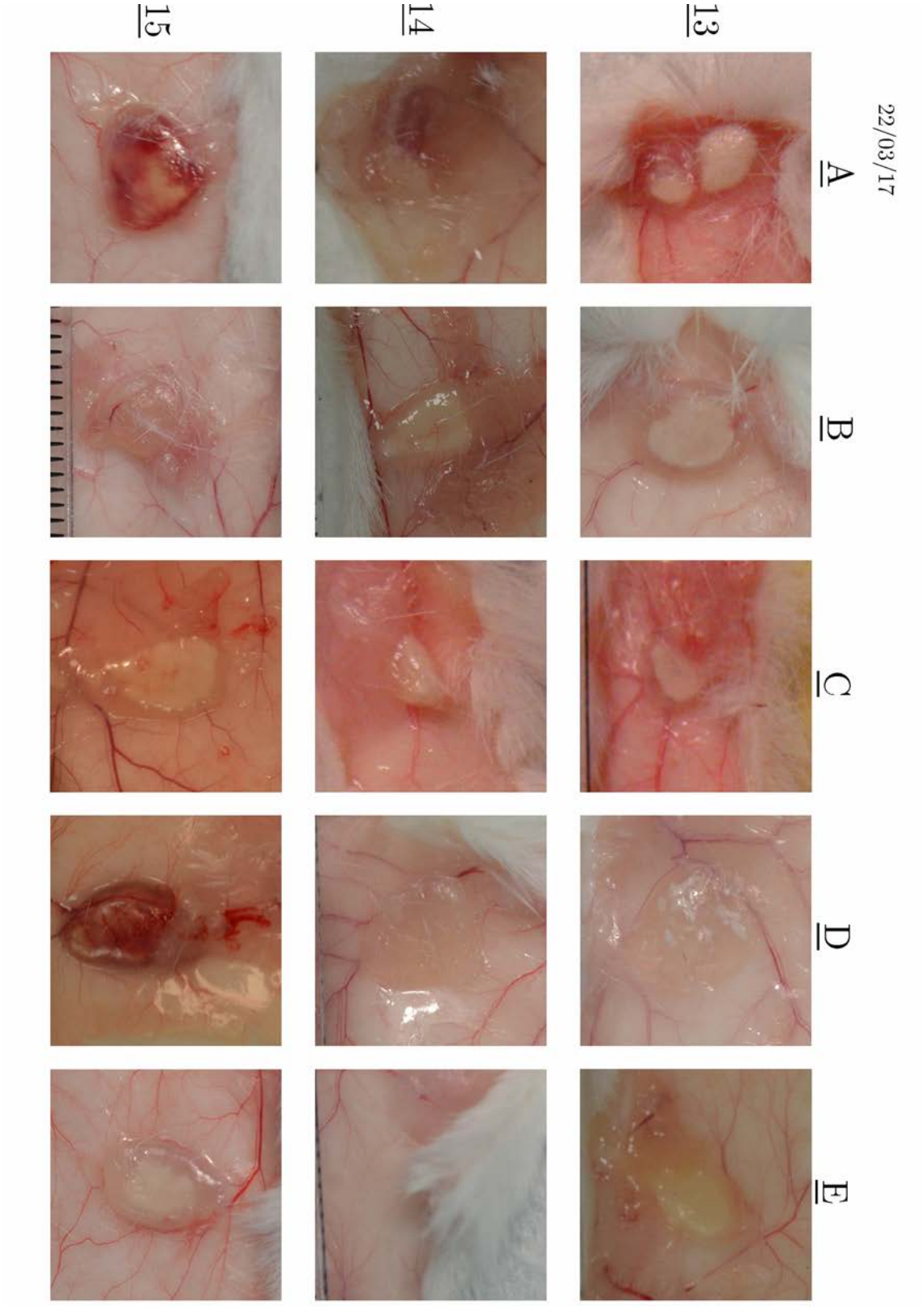
22/03/17
13
14
15
A
B
C
D
E

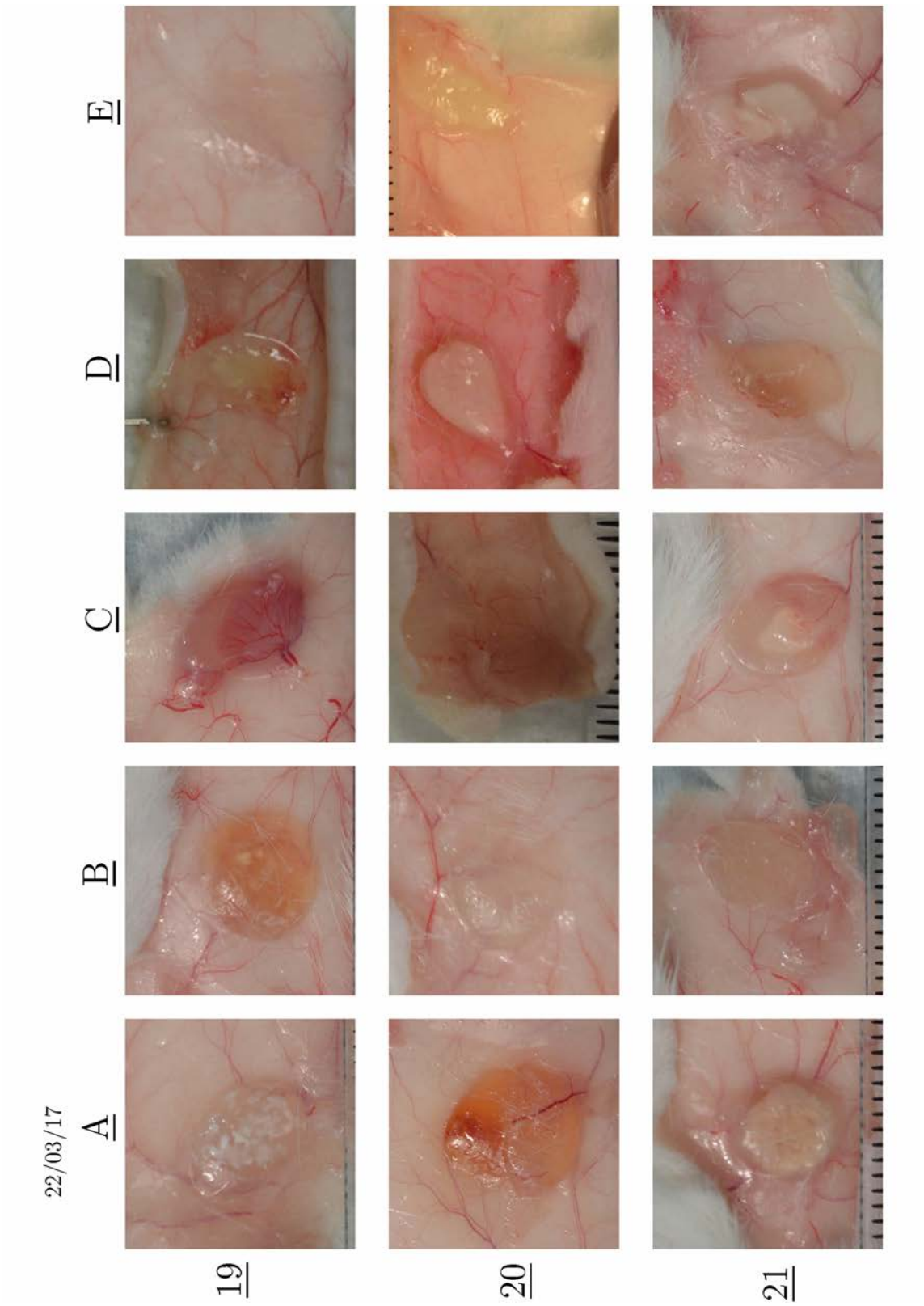
22/03/17
A
B
C
D
E
19
20
21

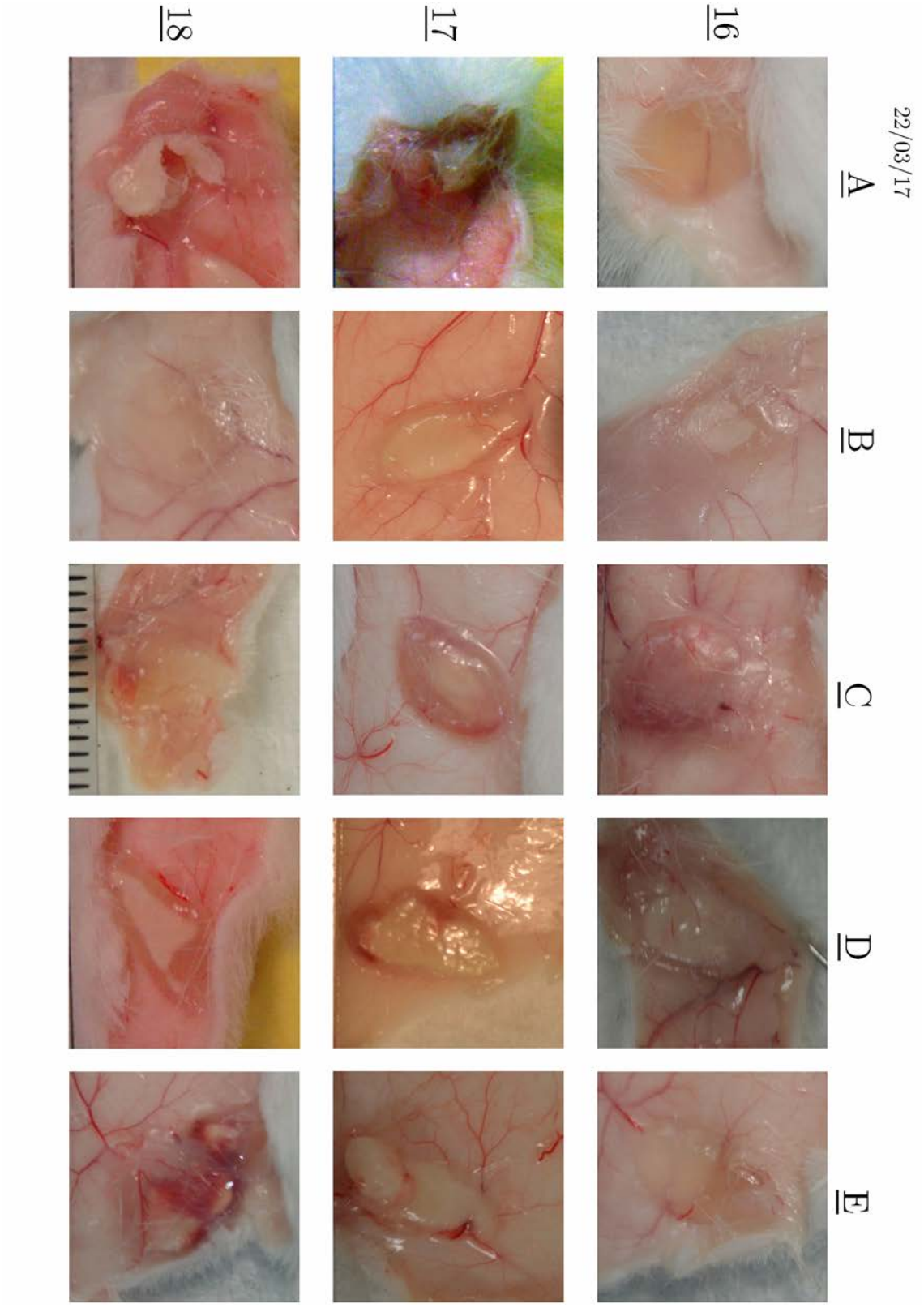
22/03/17
16
17
18
A
B
C
D
E

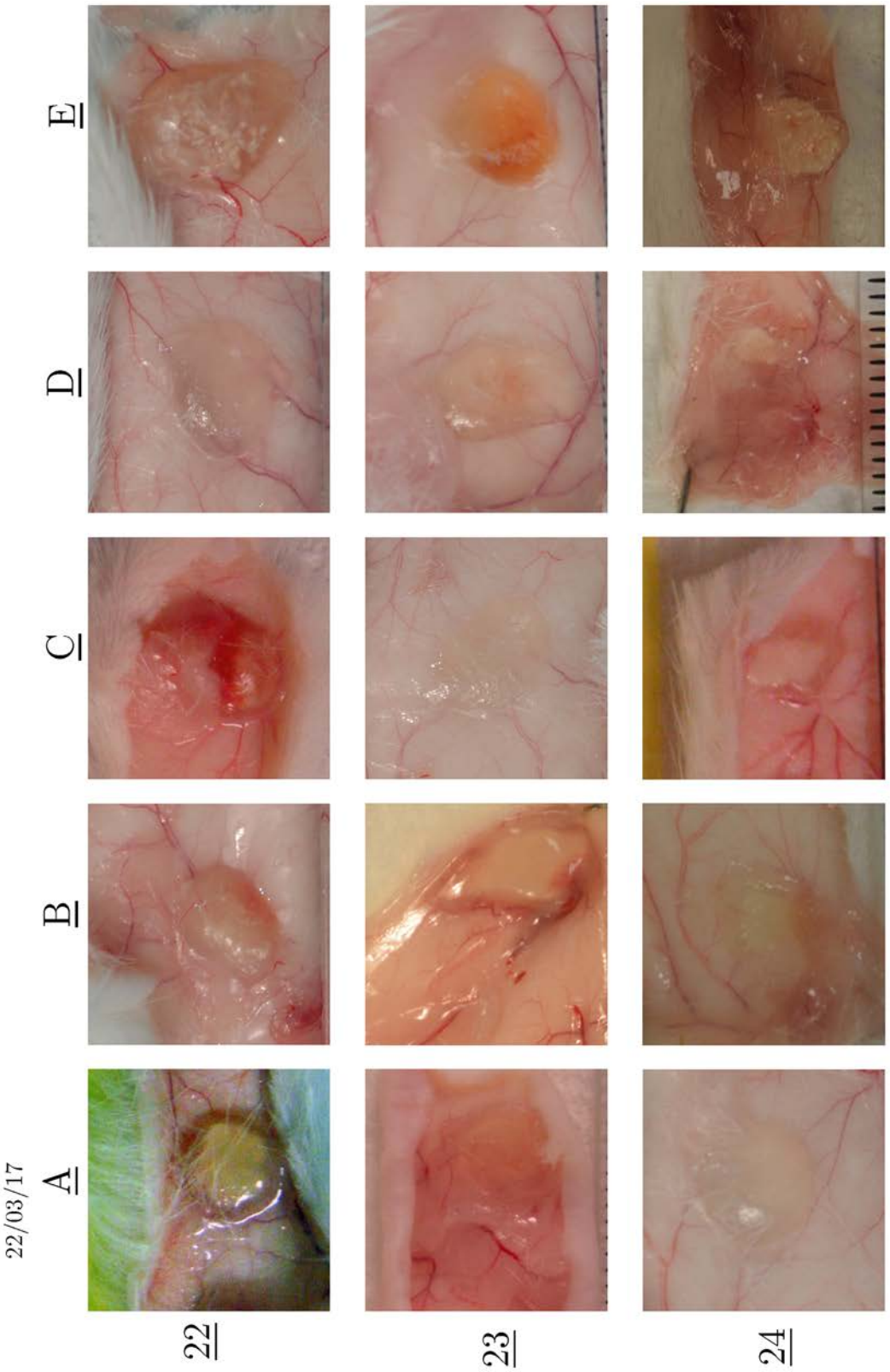
22/03/17
A
B
C
D
E
22
23
24

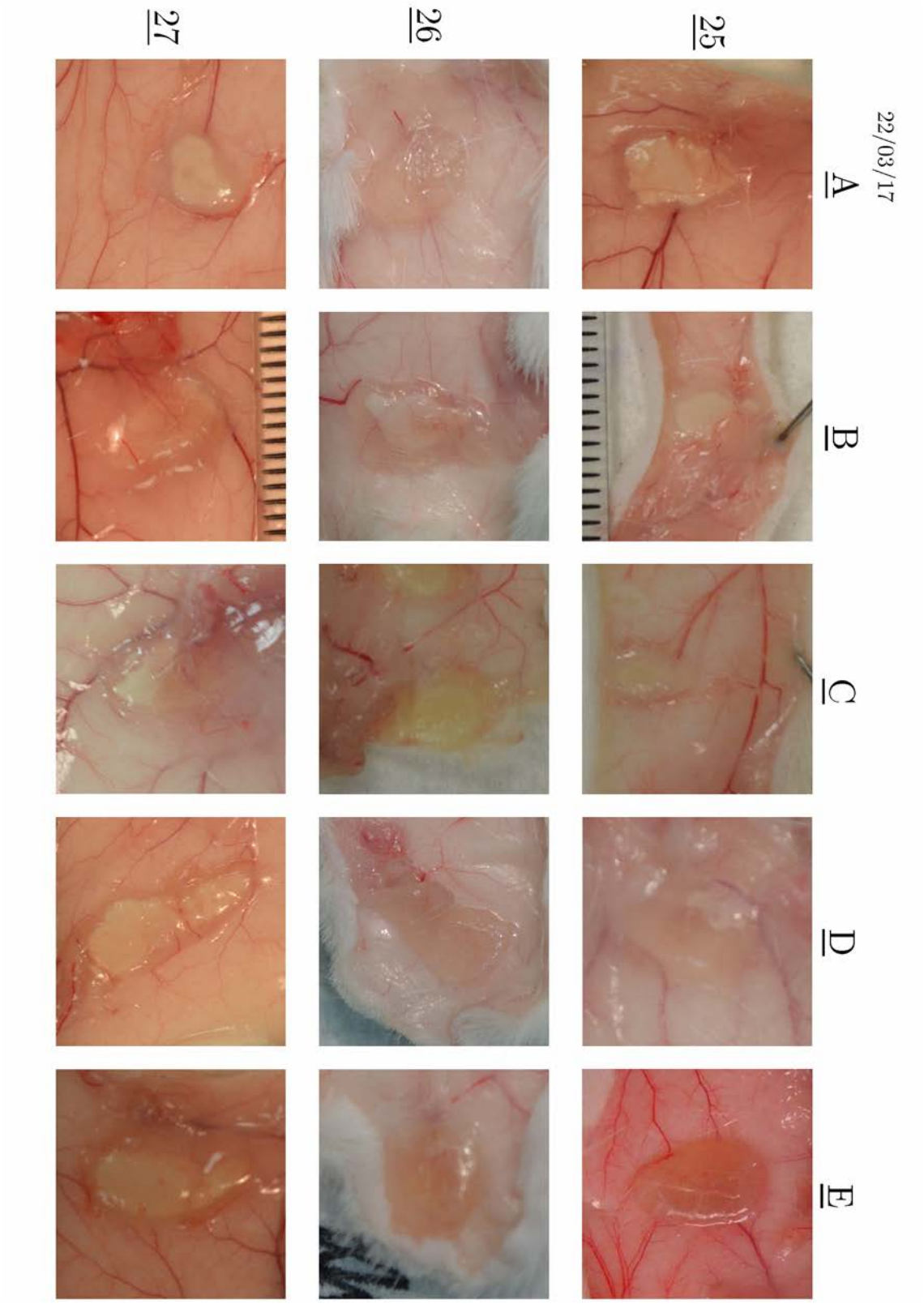
22/03/17
25
26
27
A
B
C
D
E

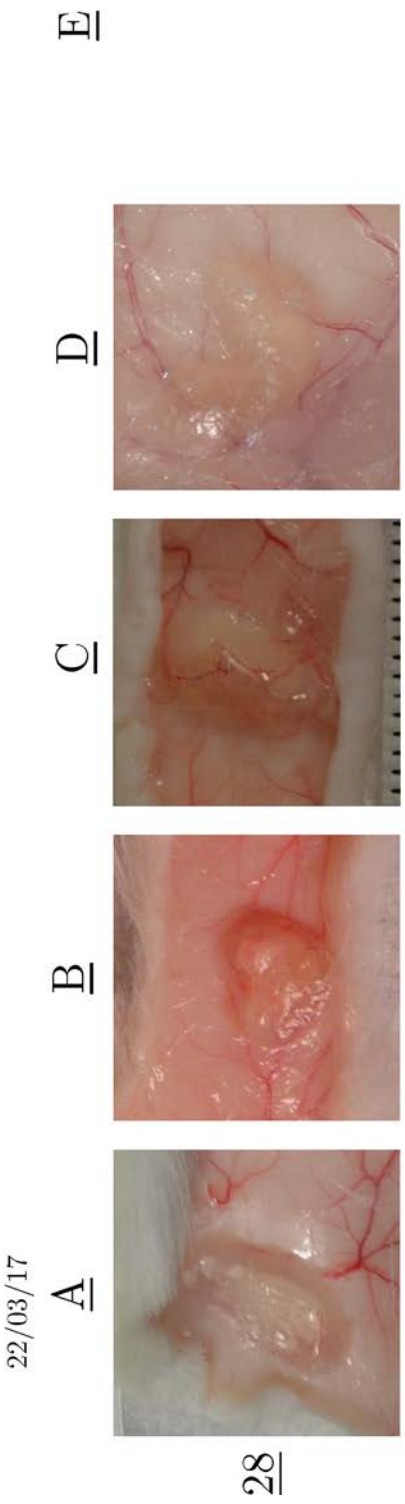
E
D
C
B
A
22/03/17
28

A.2 3-Interval Thixotropy Test Background

The 3-interval thixotropy test (3-ITT) consists of three interval states which provide information about the degree of recovery after shear stress is applied and deformation occurs. Understanding the thixotropic properties of biomaterial hydrogels can be useful to determine the ease-of-handling and potential for a specific application. For instance, a gel with good thixotropy can be defined as one that recovers ≥70% of its pre-shear viscosity [274], although 100% recovery is advantageous. In addition, the time required for recovery to occur is important. Recovery that is too swift may inhibit a gel's ability to be applied efficiently (e.g. the time between shear and injection via pipette or a hypodermic needle). Yet recovery that requires a long timeframe may exhibit reduced gel strength which could have a negative effect upon application to defect (e.g. gels applied may be easily removed through mechanical strain upon treatment due to lack of gel strength) [353, 354].

The three intervals that define the 3-ITT test are explained as follows:

First interval:

The first interval is a state at which gels were exposed to a constant low shear rate (resting or reference interval). The shear force applied to achieve this was automatically calculated by the rheometer during the test.

Second interval:

During this interval the gel material was deformed by a high shear stress to the point of complete deformation (shear force applied automatically calculated by the rheometer for the material being analysed).

Third interval:

The analytical conditions during the third interval are identical to those applied during first interval (i.e. measurements are recorded when low shear stress is applied). Therefore, during this interval the quantity and the time of the recovery can be determined. Using data collected during this test, the degree of deformation and the rate of viscosity recovery can be calculated [355].

Calculating the % of deformation:

The values of the G_i (the initial viscosity state of the gel) and the *G0* (*G'* viscosity value after deformation applied) are specified and used in following equation [355]:

$$\% \text{ of deformation} = \frac{G_i - G0}{G_i} \times 100$$

Calculating the % recovery:

The % recovery of gel samples at a specific time point post-shear can also be calculated using the following equation:

$$\% \text{ Recovery} = \frac{G_{txx}}{G_i} \times 100$$

Where G_i represents initial *G'* value of the sample and G_{txx} represents the G' viscosity values of the samples at a specific time in seconds ($_{txx}$).

A.3 Orbit Image Analysis Software Settings for Cellularity Dataset

A.3.1 General Configuration Settings

Feature configuration Settings:

Within the *Feature Configuration* window (click on option or by pressing F3 button on keyboard), the following settings within the *Classification* tab were applied:

Structure size: 4*; Median filter radius:* 0*; RGB channels used:* all checked*; Color Deconvolution Setup:* H&E*; Color Deconvolution Staining:* Stain 1 checked*; Classes for retrieving features/histograms:* leave blank*; Active fluorescence channels:* leave blank.

Within the *Segmentation* tab the following settings were applied:

Set Features for Secondary Segmentation: leave blank; *Cytoplasma Segmentation:* leave blank; *Minimum segmentation size:* 10; *Maximum segmentation length:* 500; *Minimum open distance:* 3; *Segmentation scale factor:* 1.0; *Disable object splitting:* unchecked; *Combine cross tile objects:* unchecked; *Discard tile border objects:* unchecked; *Mumford-Shah segmentation (cell clusters): Obj size* – 18 pixels, *Intens split* – 5; *Dilate:* 1; *Erode:* 0; *Dilate before erode:* checked; *Despeckle:* 0; *Smooth objects (GraphCut):* 0.0; *Nerve Detection Mode:* unchecked.

Within the *ROI* tab the following settings were applied:

Use annotations as ROI: All Groups; *Fixed circular ROI:* 0 pixels; *ROI offset X:* 0; *ROI offset Y:* 0.

Within the *Image Adjustments* tab the following setting was applied:

Use image adjustments: unchecked.

Configure Classes Settings:

Within the *Class Configuration* window (click button or press F4 on keyboard), two classes were defined: (1) *Background* in purple and (2) *Celltype 1* in white. Both classes had the *Only if used in Exclusion Model* option left as undefined.

A.3.2 Classification Model Training

The *Classification* module tab was selected and trained using a selection of ≥8 different images. As a rule, 1-2 images per sample group were chosen for each study (i.e. for subcutaneous injection study refer to subchapter 2.3.2), there were 8 different treatments groups (4 x Laponite, 4 x alginate) so a minimum of 8 images were used to train the model.

After loading selected images, the *Background* class was selected (within F4 menu). Within the *Classification* module tab, the *Polygon* draw tool was selected and used to trace around select regions which best represented the background. This included areas that had no staining and regions where cells were not stained (e.g. wound granulation, healthy skin tissue matrix). After 6 regions had been traced, the second class (*Celltype 1*) was selected within the *Background* class menu. Again, the *Polygon* tool was selected and traced around regions where there were cells present. In total, 6 cells or region of cells were traced. After that had been completed, the same set of steps were repeated with all other selected images.

After image tracing, the *Train* option (F7 on keyboard) within the *Machine Learning* module was selected; this would 'teach' the software to store pixel information regarding background and stained cells based on the region of interest (ROIs). Once the module had completed its algorithm then the model at the bottom of the program will state *Trained: yes*. Any models that were trained were then saved for future batch use.

A.3.3 Region of Interest (ROI) Selection

To analyse an image using a trained model, an ROI was selected using the *Annotations* module tab (right-hand side of the main program window). To do this, the *add polygon* tool was selected to trace around an ROI (e.g. the wound granulation tissue). After the ROI(s) had been drawn, they were selected in the *Annotations* module and the *edit annotation* option selected; within this window the *Type* field was changed to *ROI*. Once and ROI had been defined this information is automatically stored within the *OrbitOmero.properties.template* file located within the user profile of the program (please refer to manufactures instructions for more details). Therefore, images can be closed and re-opened for future analysis.

A.3.4 Image Analysis (Single)

After loading an image and training a model, images can be analysed for classified areas. To use a pre-existing model, it was loaded via the *Model* tab module. Then within the *Classification* module tab, the *Classify option* was selected (F8 on keyboard). The resulting output contained the ratio of both the *Background* class and *Celltype 1* class. Values generated from the *Celltype 1* class were multiplied by 100 to determine the % coverage of pixels that were identified as cells.

A.3.5 Image Analysis (Batch)

Most of the cellularity data was generated by analysing a batch of images following model training. First, a pre-existing trained model was loaded and then the *Batch* module tab selected. Using the *Local Execution* option, multiple files

could be selected for analysis using the class attributes within pre-loaded model. The output window contained the ratio of both the *Background* class and *Celltype 1* class. Values generated from the *Celltype 1* class were multiplied by 100 to determine the % coverage of pixels that were identified as cells.

Appendix B:

Data Tables & Statistics for

Chapter 3

B.1 2D HUVEC Tubule Assay Data

Rep No.	Total Tubule Branching Length (Pixels)			
	VEGF Within Growth Medium			
	No VEGF	0.01 µg	0.02 µg	0.04 µg
1	1215	12555	12840	18200
2	3645	9376	9606	16107
3	4091	No Data*	No Data*	13290
4	No Data*	No Data*	No Data*	No Data*

Table 6.1. Quantitative analysis of HUVEC network identified by 'Angiogenesis analyser' ImageJ plugin of VEGF in growth medium at different concentrations. All values were the total branching length ('master segments' and 'branches') in pixels. Each Rep was taken from a separate well (n=4). * no data was measured from these samples due to the Laponite surfaces being damaged upon reading (HUVEC network was disrupted).

Rep No.	Total Tubule Branching Length (Pixels)						
	VEGF Premixed in Laponite						
	No VEGF	0.04 µg	0.10 µg	0.50 µg	1.00 µg	2.00 µg	5.00 µg
1	1215	1554	4045	8711	9964	12614	16552
2	3645	948	5359	5453	9589	9268	18039
3	4091	870	646	4330	14392	16982	15774
4	No Data*	3444	1387	No Data*	No Data*	11322	No Data*

Table 6.2. Quantitative analysis of HUVEC network identified by 'Angiogenesis analyser' ImageJ plugin of VEGF premixed with 3% Laponite at different concentrations. All values were the total branching length ('master segments' and 'branches') in pixels. Each Rep was taken from a separate well (n=4). * no data was measured from these samples due to the Laponite surfaces being damaged upon reading (HUVEC network was disrupted).

Rep No.	Total Tubule Branching Length (Pixels)		
	VEGF "Bound" Study		
	No VEGF	0.04 µg VEGF in Media	"Bound" VEGF
1	6977	13946	16573
2	4566	20709	17548
3	5275	24234	18421
4	7035	16867	18995
5	7660	16524	13754
6	6390	16308	12334

Table 6.3. Quantitative analysis of HUVEC network identified by 'Angiogenesis analyser' ImageJ plugin of VEGF "bound" to 3% Laponite. All values were the total branching length ('master segments' and 'branches') in pixels. Each Rep was taken from a separate well (n=6).

B.2 Dose-response Control Raw Data

This is a summary of three separate studies; study 1 n = 2; study 2 & 3 n = 3.

All values as fold change from the background at 0 µM (response ratio).

Original Data								
BIO Concentration (µM)	Study Repeat 1		Study Repeat 2			Study Repeat 3		
	Luciferase Activity Ratio		Luciferase Activity Ratio			Luciferase Activity Ratio		
	Rep 1	Rep 2	Rep 1	Rep 2	Rep 3	Rep 1	Rep 2	Rep 3
0.0	1.0	1.0	0.8	0.9	1.3	1.0	1.0	1.0
0.5	1.6	1.6	1.1	1.1	1.5	1.0	1.1	1.0
1.0	3.1	3.5	2.8	2.5	3.0	1.2	1.2	1.2
1.5	5.7	8.2	8.8	6.7	10.9	1.4	1.4	1.4
2.0	10.2	9.3	17.7	24.4	15.8	2.2	2.1	2.0
3.0	45.8	35.7	42.3	40.1	41.1	6.4	6.9	5.9
5.0	60.3	60.5	41.8	46.2	42.7	40.6	42.0	43.4

Table 6.4. Raw data values luciferase activity measured from Wnt reporter cell line (3T3 fibroblasts) when exposed to different concentrations of BIO (dose-response control curve).

Normalised Data								
BIO Concentration (µM)	**Study Repeat 1**		**Study Repeat 2**			**Study Repeat 3**		
	Luciferase Activity (%)		**Luciferase Activity (%)**			**Luciferase Activity (%)**		
	Rep 1	**Rep 2**	**Rep 1**	**Rep 2**	**Rep 3**	**Rep 1**	**Rep 2**	**Rep 3**
0.0	1.7	1.6	1.6	2.0	2.9	2.3	2.3	2.3
0.5	2.7	2.6	2.4	2.4	3.3	2.3	2.5	2.4
1.0	5.0	5.8	6.0	5.4	6.6	2.8	2.8	2.7
1.5	9.5	13.6	19.0	14.5	23.5	3.3	3.3	3.2
2.0	16.8	15.3	38.4	52.8	34.2	5.0	4.9	4.5
3.0	75.6	59.0	91.7	86.9	89.1	14.8	16.0	13.5
5.0	99.7	100.0	90.6	100.0	92.5	93.6	96.8	100.0

Table 6.5. Normalised % of dose-response luciferase assay response ratio data shown in Table 6.4.

B.3 Validation of Adsorption of Assay Media Components by Laponite Hydrogels

B.3.1 60-Minute Study

Original Data						
Media Removal Time (Minutes)	**Study Repeat 1**			**Study Repeat 2**		
	Luciferase Activity Ratio			**Luciferase Activity Ratio**		
	Rep 1	**Rep 2**	**Rep 3**	**Rep 1**	**Rep 2**	**Rep 3**
0.5	30.2	34.8	27.4	15.6	16.1	14.5
2.0	27.9	16.6	24.5	17.3	17.8	16.5
5.0	27.2	22.0	27.6	14.3	16.9	15.6
10.0	34.9	13.4	27.0	18.6	14.4	17.4
30.0	Not Tested*			17.7	19.3	15.8
60.0	29.1	24.8	36.6	12.9	15.1	19.1

Table 6.6. Raw data values luciferase activity measured from Wnt reporter cell line (3T3 fibroblasts) when grown in media that had been spiked with 5 µM BIO following incubation with Laponite for 60 minutes. Raw values taken from two separate studies (n = 3) All values as fold change from the background at 0 µM (response ratio). * time point not tested in this study.

Normalised						
Media Removal Time (Minutes)	**Study Repeat 1**			**Study Repeat 2**		
	Luciferase Activity (%)			**Luciferase Activity (%)**		
	Rep 1	**Rep 2**	**Rep 3**	**Rep 1**	**Rep 2**	**Rep 3**
0.5	100.5	115.6	91.3	76.4	78.6	70.7
2.0	92.8	55.1	81.4	84.7	87.0	80.6
5.0	90.4	73.2	91.8	69.9	82.5	76.4
10.0	116.1	44.5	89.7	90.7	70.6	85.0
30.0	Not Tested*			86.5	94.3	77.0
60.0	96.9	82.5	121.6	63.0	73.6	93.5

Table 6.7. Normalised % of luciferase assay response ratio data shown in Table 6.6.* time point not tested in this study.

Averaged Normalised Data			
Media Removal	**Luciferase Activity**	**St. Dev (%)**	***n***
0.5	88.8	17.0	6
2.0	80.2	13.1	6
5.0	80.7	9.1	6
30.0	85.9	8.6	3
60.0	88.5	20.5	6
Control*	93.0	8.7	7

Table 6.8. Average Normalised from Table 6.7 data. * denotes average 5 μM dose-response control data from Table 6.5.

B.3.2 7-Day Study

Original Data					
Media Removal Time (Hours)	**Study Repeat 1**		**Study Repeat 2**		
	Luciferase Activity Ratio		**Luciferase Activity Ratio**		
	Rep 1	**Rep 2**	**Rep 1**	**Rep 2**	**Rep 3**
0.5	82.2	66.1	Not Tested*		
1.0	Not Tested*		55.9	54.8	58.8
24.0	72.9	46.2	42.8	55.4	46.5
168.0	84.8	47.5	39.4	57.2	39.8

Table 6.9. Raw data values luciferase activity measured from Wnt reporter cell line (3T3 fibroblasts) when grown in recovered media that had been spiked with 5 µM BIO after incubation with Laponite for 7 days. Raw values taken from two separate studies (n = 3). All values as fold change from the background at 0 µM (response ratio). * time point not tested in this study.

Normalised					
Media Removal Time (Hours)	**Study Repeat 1**		**Study Repeat 2**		
	Luciferase Activity (%)		**Luciferase Activity (%)**		
	Rep 1	**Rep 2**	**Rep 1**	**Rep 2**	**Rep 3**
0.5	135.8	109.2	Not Tested*		
1.0	Not Tested*		121.1	118.7	127.3
24.0	120.4	76.3	92.6	119.9	100.7
168.0	140.0	78.5	85.3	123.8	86.2

Table 6.10. Normalised % of luciferase assay response ratio data shown in Table 6.9. * not tested at this time point.

Averaged Normalised Data			
Media Removal Time (Hours)	**Luciferase Activity (%)**	**St. Dev (%)**	***n***
0.5	7.7	5.9	3
1.0	5.0	2.1	3
24.0	12.2	8.7	6
168.0	6.7	7.7	6
Control*	93.0	8.7	7

Table 6.11. Average Normalised Table A.3.5 data. * denotes average 5 µM dose-response control data from Table 6.5.

B.4 BIO Uptake from Media

Original Data			
Media Removal Time (Minutes)	**Study Repeat 1**		
	Luciferase Activity Ratio		
	Rep 1	**Rep 2**	**Rep 3**
0.0	14.4	18.5	20.8
0.5	8.0	10.7	12.9
2.0	11.5	10.3	13.4
5.0	14.2	12.7	11.3
10.0	13.3	12.4	15.8
30.0	7.8	13.6	15.2
60.0	12.9	17.7	17.9

Table 6.12. Luciferase assay response ratio data of media that contained 5 µM BIO; media samples were taken after incubation with Laponite for up to 60 minutes. n = 3. All values as fold change from the background at 0 µM (response ratio).

Normalised			
Media Removal Time (Minutes)	**Study Repeat 1**		
	Luciferase Activity (%)		
	Rep 1	**Rep 2**	**Rep 3**
0.0	70.5	90.4	101.7
0.5	39.2	52.3	63.0
2.0	55.9	50.4	65.3
5.0	69.5	61.9	55.4
10.0	65.1	60.5	77.0
30.0	38.0	66.5	74.2
60.0	62.9	86.4	87.2

Table 6.13. Normalised data generated from Table 6.12.

Averaged Normalised Data			
Media Removal Time	**Luciferase Activity (%)**	**St. Dev (%)**	***n***
0.0	87.5	15.8	3
0.5	51.5	11.9	3
2.0	57.2	7.6	3
5.0	62.3	7.1	3
10.0	67.5	8.5	3
30.0	59.5	19.1	3
60.0	78.8	13.8	3

Table 6.14. Averaged normalised Table 6.13 data.

B.5 BIO Released into Media

B.5.1 60-Minute Study

Original Data			
Media Removal Time (Minutes)	**Study Repeat 1**		
	Luciferase Activity Ratio		
	Rep 1	**Rep 2**	**Rep 3**
0.0	1.3	1.0	0.7
0.5	1.6	0.9	0.8
2.0	1.4	0.8	0.9
5.0	1.2	0.9	0.7
20.0	1.0	0.7	0.6
60.0	1.1	0.8	0.8

Table 6.15. Luciferase assay response ratio data of media that had been incubated with Laponite capsules that contained 50 µM BIO; media samples were recovered up to 60 minutes. n = 3. All values as fold change from the background at 0 µM (response ratio).

Normalised			
Media Removal Time (Minutes)	**Study Repeat 1**		
	Luciferase Activity (%)		
	Rep 1	**Rep 2**	**Rep 3**
0.0	4.4	3.2	2.4
0.5	5.3	3.0	2.5
2.0	4.5	2.7	2.8
5.0	3.8	2.9	2.3
20.0	3.3	2.4	2.1
60.0	3.7	2.5	2.6

Table 6.16. Normalised from Table **6.15 data**.

B.5.2 7-Day Study

Original Data						
Media Removal Time (Hours)	**Study Repeat 1**			**Study Repeat 2**		
	Luciferase Activity Ratio			**Luciferase Activity Ratio**		
	Rep 1	**Rep 2**	**Rep 3**	**Rep 1**	**Rep 2**	**Rep 3**
0.0	1.4	1.4	0.8	0.9	0.7	0.7
0.5	2.4	2.9	8.8	Not Tested*		
1.0	Not Tested*			3.4	1.7	1.8
24.0	12.7	1.2	2.6	9.2	3.2	8.6
168.0	1.2	2.0	13.5	2.2	1.3	2.4

Table 6.17. Luciferase assay response ratio data of media that had been incubated with Laponite capsules that contained 80 µM BIO; media samples were recovered up to 7 days. Summary of raw data values from two separate studies (n = 3). All values as fold change from the background at 0 µM (response ratio). * not tested at this time point.

Normalised						
Media Removal Time (Hours)	**Study Repeat 1**			**Study Repeat 2**		
	Luciferase Activity (%)			**Luciferase Activity (%)**		
	Rep 1	**Rep 2**	**Rep 3**	**Rep 1**	**Rep 2**	**Rep 3**
0.0	2.2	2.3	1.4	1.9	1.6	1.4
0.5	3.9	4.8	14.5	Not Tested*		
1.0	Not Tested*			7.4	3.7	3.8
24.0	21.0	1.9	4.3	20.0	6.9	18.7
168.0	2.0	3.3	22.3	4.8	2.7	5.3

Table 6.18. Normalised Table 6.17 data. * not tested at this time point.

B.5.3 Negative Control

Original Data						
Media Removal Time (Hours)	**Study Repeat 1**			**Study Repeat 2**		
	Luciferase Activity Ratio			**Luciferase Activity Ratio**		
	Rep 1	**Rep 2**	**Rep 3**	**Rep 1**	**Rep 2**	**Rep 3**
0.0	1.1	1.0	1.0	0.8	0.8	0.8
0.5	0.9	0.9	0.8	Not Tested*		
1.0	Not tested*			0.9	0.9	0.9
24.0	0.7	0.8	0.8	0.7	0.8	0.8
168.0	0.9	0.8	0.9	Not Tested*		

Table 6.19. Luciferase assay response ratio data of media that had been incubated with Laponite capsules absent of BIO; media samples were recovered up to 7 days. Summary of raw data values from two separate studies (n = 3). All values as fold change from the background at 0 µM (response ratio). * not tested at this time point.

Normalised						
Media Removal Time (Hours)	**Study Repeat 1**			**Study Repeat 2**		
	Luciferase Activity (%)			**Luciferase Activity (%)**		
	Rep 1	**Rep 2**	**Rep 3**	**Rep 1**	**Rep 2**	**Rep 3**
0.0	2.4	2.3	2.2	1.8	1.8	1.8
0.5	2.0	2.1	1.9	Not Tested*		
1.0	Not tested*			2.0	2.0	2.0
24.0	1.7	1.7	1.9	1.6	1.9	1.7
168.0	2.0	1.9	2.0	Not Tested*		

Table 6.20. Normalised from Table 6.19 data. * not tested at this time point.

B.6 BIO Concentration Calculations

B.6.1 Interpolation of the Standard Curve

To interpolate theoretical BIO concentration using the average luciferase activity data at 24 hours (12.15 ± 8.68%), GraphPad used this equation:

Equation 1: Y = Bottom + (Top - Bottom) / (1+ (10^logEC50 / X)^HillSlope)

The values calculated by GraphPad are shown in the table below:

Release Assay GraphPad Equation Values	
Best-fit values	
Bottom	4.80
Top	93.27
LogEC50	2.36
HillSlope	0.95
EC50	229.90
Span	88.47

Table 6.21. Standard curve values taken from the of the dose-response control curve. Values calculated by GraphPad.

B.6.2 Theoretical BIO Concentration Calculation (7-Day Study)

A total of 50 µl x 5 Laponite gel capsule (250 µl total) all containing 40 µM BIO was incubated with 500 µl media. Thus, if all BIO had been released from the Laponite capsule into the media:

500 / 250 = 2 dilution factor

80 / 2 = 40 µM BIO would be within media

When assay medium is added to 3T3 cell culture there is a 1.5 dilution factor.

Thus:

40/1.5 = 26.67

Approximately a maximum BIO concentration of 26.67 µM would have been available to 3T3 cells if there was 100% released from Laponite capsules.

Appendix C:

Data Tables & Statistics for

Chapter 4

C.1 Rheology Supplementary Data

C.1.1 Thixotropy of Laponite Gels

C.1.1.1 Results

To investigate the thixotropic properties of 3% Laponite gels, rheological analysis using a 3-interval-thiotropy test (3-ITT) was performed, whereby gels were subjected to three oscillatory intervals. A comparative control gel (crosslinked 1.1% alginate) was also tested as it is a well-documented biomaterial used in drug delivery [277]. These tests were performed at 25°C and 37°C to best represent ambient storage and biological conditions respectively.

Laponite gels exhibited good thixotropic recovery at both temperatures with ≥ 70% viscosity restored after 20 seconds during the test (Figure 6.3 and Figure 6.4); this equates to ~4 seconds following the removal of a shear force. After 15 seconds post-shear (31 seconds during the test), the recovery was 95% and 89.6% at 25°C and 37°C respectively (Figure 6.4). The dotted blue line in Figure 6.3 represents the hypothetical viscosity that would have been present if the second oscillatory interval had not occurred. It can be used to show to a point at which 100% recovery had occurred and shows that at 25°C this was successful after approximately 1 minute during the test.

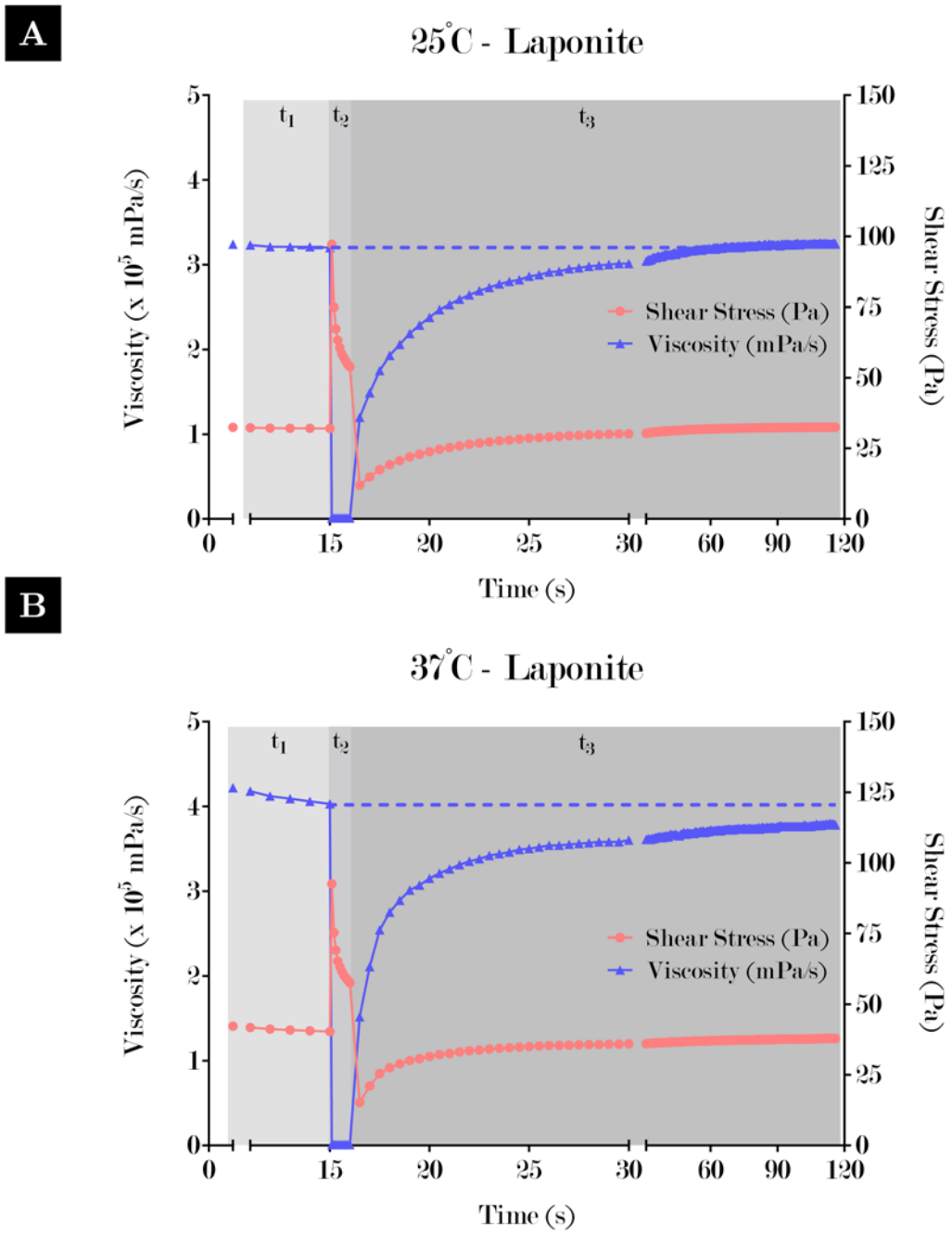

Figure 6.3. **3-interval thixotropy test (3-ITT) of 3.0% Laponite gels (vehicle) showed that it exhibited good thixotropic recovery at 25°C (A) and 37°C (B).** t_1, t_2 and t_3 denotes the following intervals: pre-shear, shear and post-shear respectively; dotted blue line = hypothetical viscosity that would have been present in the absence of a shear force (pre-shear viscosity).

Looking more specifically via the data table presented in Figure 6.4, the actual time was 61.5 seconds, which was 45.5 seconds following the second high-shear

interval. In contrast, at 37°C 100% viscosity recovery was not successfully reached, with the maximal recovery being ~94% after 100 seconds post-shear.

A **25°C Laponite**

Interval	Time (s)	Viscosity (x 10^5 mPa · s)	Shear Stress (Pa)	% Viscosity Compared To End of 1st Interval)
1st	15.0	3.2	32.0	**100.0**
2nd	15.1	0.0	97.2	**0.3**
	15.5	0.0	60.6	**0.2**
	16.0	0.0	53.9	**0.2**
3rd	16.5	1.2	12.0	**37.5**
	17.5	1.8	17.5	**54.7**
	18.0	1.9	19.3	**60.3**
	18.5	2.1	20.6	**64.4**
	19.0	2.2	21.9	**68.4**
	19.5	2.3	22.9	**71.6**
	21.5	2.6	25.9	**80.9**
	25.5	2.9	28.8	**90.0**
	31.0	3.0	30.4	**95.0**
	60.0	3.2	31.9	**99.7**
	60.5	3.2	31.8	**99.4**
	61.0	3.2	31.9	**99.7**
	61.5	3.2	32.0	**100.0**
	62.0	3.2	31.8	**99.4**
	62.5	3.2	31.9	**100.0**
	63.0	3.2	31.9	**100.0**
	63.5	3.2	31.9	**99.7**
	64.0	3.2	31.9	**99.7**
	64.5	3.2	32.0	**100.0**
	65.0	3.2	31.9	**99.7**
	65.5	3.2	32.0	**100.0**
	66.0	3.2	32.0	**100.3**
	116.0	3.2	32.5	**101.3**

B **37°C Laponite**

Interval	Time (s)	Viscosity (x 10^5 mPa · s)	Shear Stress (Pa)	% Viscosity Compared To End of 1st Interval)
1st	15.0	4.0	40.3	**100.0**
2nd	15.1	0.0	92.6	**0.2**
	15.5	0.0	63.3	**0.2**
	16.0	0.0	57.7	**0.1**
3rd	16.5	1.5	15.2	**37.7**
	17.5	2.5	25.4	**63.0**
	18.0	2.8	27.5	**68.2**
	18.5	2.9	28.9	**71.7**
	19.0	3.0	30.1	**74.7**
	19.5	3.1	30.7	**76.2**
	21.5	3.3	33.1	**82.1**
	25.5	3.5	35.2	**87.3**
	31.0	3.6	36.1	**89.6**
	60.0	3.7	37.2	**92.3**
	60.5	3.7	37.0	**92.1**
	61.0	3.7	37.1	**92.1**
	61.5	3.7	37.1	**92.1**
	62.0	3.7	37.1	**92.1**
	62.5	3.7	37.2	**92.3**
	63.0	3.7	37.1	**92.1**
	63.5	3.7	37.2	**92.3**
	64.0	3.7	37.2	**92.3**
	64.5	3.7	37.1	**92.1**
	65.0	3.7	37.2	**92.3**
	65.5	3.7	37.2	**92.3**
	66.0	3.7	37.2	**92.3**
	116.0	3.8	37.9	**93.8**

Figure 6.4. Selected data values from 3-ITT showing specific time points where the viscosity of Laponite gels recovered back to 70%-100% of its pre-shear viscosity. There were minor differences in the recovery of viscosity between Laponite gels undergoing high shear at 25°C (A) and 37°C (B). The most important difference was that Laponite gels at 37°C did not recover to 100% viscosity after the 116 second duration like 25°C gels; however, this recovery was still greater than 90%. Specific % viscosity values of interest have been highlighted in the following colours: red = ≥70% recovery, green = first time point when 100% recovery was reached (25°C only) and blue = maximal recovery.

Alginate gels also exhibited good thixotropic recovery at both temperatures with ≥70% viscosity restored after 17.5-18.0 seconds during the test (Figure 6.5 and Figure 6.6). This equates to ~2 seconds following the removal of a shear force and was quicker than the ~4 seconds required by Laponite gels (Figure 6.4)

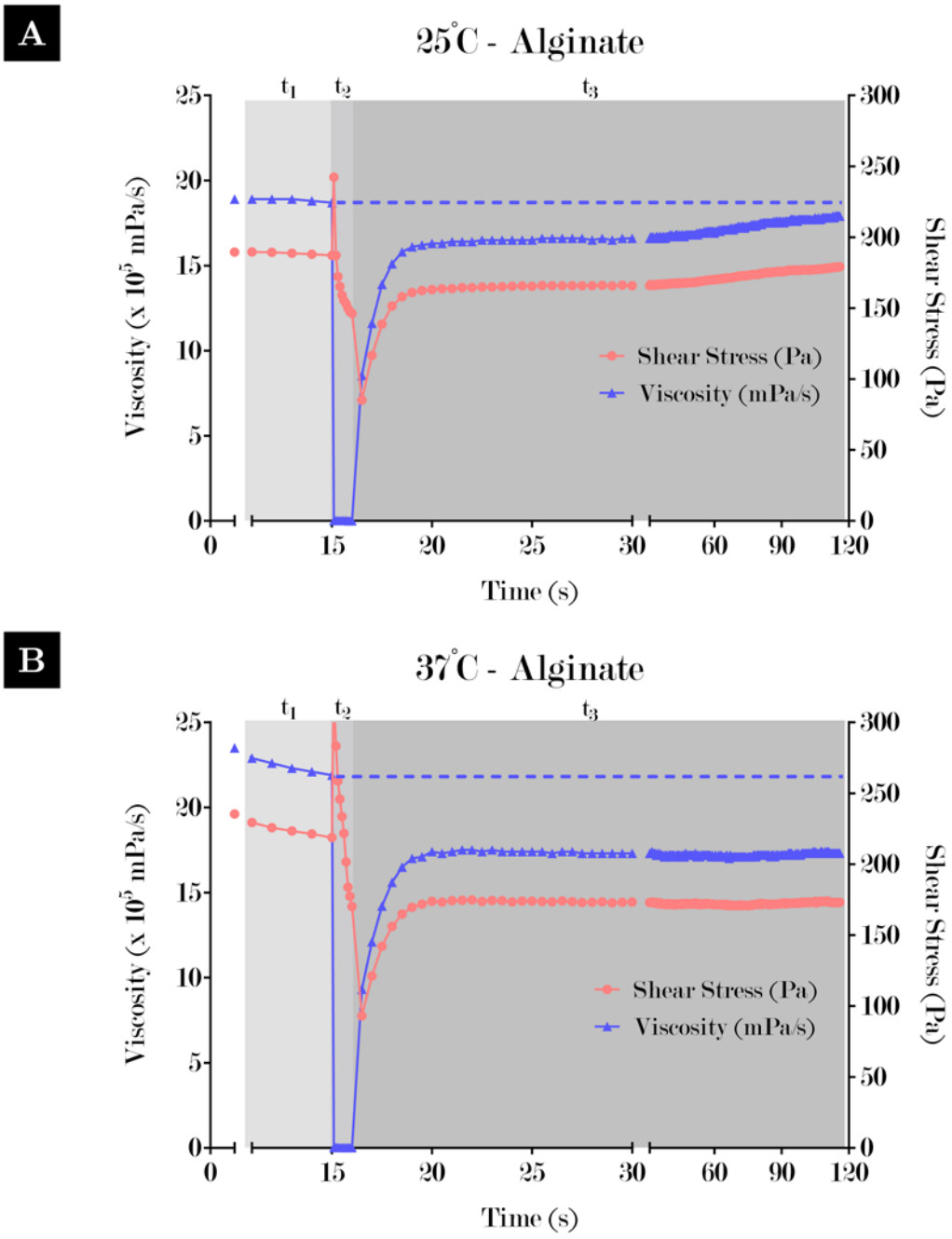

Figure 6.5. 3-interval thixotropy test (3-ITT) of a control gel (1.1% alginate) gels which showed that it exhibited good thixotropic recovery at 25°C (A) and 37°C (B) that was akin to Laponite gels. t_1, t_2 and t_3 denotes the following intervals: pre-shear, shear and post-shear respectively; dotted blue line = hypothetical viscosity that would have been present in the absence of a shear force (pre-shear viscosity).

Unlike Laponite gels, alginate gels at both temperatures did not manage to recover back to 100% viscosity within the 100-second time frame post-shear (Figure 6.5).

A **25°C Alginate**

Interval	Time (s)	Viscosity (x 10^5 mPa · s)	Shear Stress (Pa)	% Viscosity Compared To End of 1st Interval)
1st	15.0	18.7	187.2	**100.0**
2nd	15.1	0.0	242.4	**0.1**
	15.5	0.0	159.1	**0.1**
	16.0	0.0	146.1	**0.1**
3rd	16.5	8.5	85.2	**45.7**
	17.5	13.9	138.8	**74.3**
	18.0	15.1	151.5	**80.7**
	18.5	15.8	158.1	**84.5**
	19.0	16.1	161.0	**86.1**
	19.5	16.2	162.5	**86.6**
	21.5	16.4	164.4	**87.7**
	25.5	16.6	166.0	**88.8**
	31.0	16.6	165.9	**88.8**
	60.0	16.9	169.9	**90.4**
	60.5	17.0	170.3	**90.9**
	61.0	17.0	170.3	**90.9**
	61.5	17.0	170.2	**90.9**
	62.0	17.1	170.5	**91.4**
	62.5	17.0	170.5	**90.9**
	63.0	17.1	170.7	**91.4**
	63.5	17.1	170.8	**91.4**
	64.0	17.1	170.6	**91.4**
	64.5	17.1	170.9	**91.4**
	65.0	17.1	171.0	**91.4**
	65.5	17.1	171.3	**91.4**
	66.0	17.1	171.2	**91.4**
	116.0	17.9	179.0	**95.7**

B **37°C Alginate**

Interval	Time (s)	Viscosity (x 10^5 mPa · s)	Shear Stress (Pa)	% Viscosity Compared To End of 1st Interval)
1st	15.0	21.9	218.8	**100.0**
2nd	15.1	0.0	327.1	**0.1**
	15.5	0.0	233.6	**0.1**
	16.0	0.0	170.1	**0.1**
3rd	16.5	9.3	93.1	**42.6**
	17.5	14.2	142.0	**64.8**
	18.0	15.6	156.1	**71.2**
	18.5	16.5	164.8	**75.3**
	19.0	17.0	169.6	**77.6**
	19.5	17.1	171.8	**78.1**
	21.0	17.4	174.3	**79.5**
	25.5	17.4	173.7	**79.5**
	31.0	17.3	173.1	**79.0**
	60.0	17.1	171.6	**78.1**
	60.5	17.2	171.5	**78.5**
	61.0	17.1	171.5	**78.1**
	61.5	17.1	171.3	**78.1**
	62.0	17.2	171.5	**78.5**
	62.5	17.1	171.5	**78.1**
	63.0	17.2	171.5	**78.5**
	63.5	17.1	171.3	**78.1**
	64.0	17.1	171.7	**78.1**
	64.5	17.1	171.5	**78.1**
	65.0	17.1	170.8	**78.1**
	65.5	17.2	171.5	**78.5**
	66.0	17.1	171.0	**78.1**
	116.0	17.3	173.0	**79.0**

Figure 6.6. 3-ITT data table showing that alginate gel viscosity recovered to ~96% at 25°C (A) and ~79% at 37°C (B) by the end of the post-shear interval. Specific % viscosity values of interest have been highlighted in the following colours: red = ≥70% recovery and blue = maximal recovery.

However, alginate gels at 25°C did recover close to the pre-shear viscosity with a maximal recovery of 95.7% (Figure 6.6 A). In contrast, alginate gels at 37°C did

not reach above 79% of the pre-shear viscosity by the end of the study (Figure 6.6 B).

Although the thixotropy of both gels were similar, there were key difference between their overall viscosities. Alginate gels had greater overall viscosity than Laponite gels at both temperatures as can been seen in Figure 6.7.

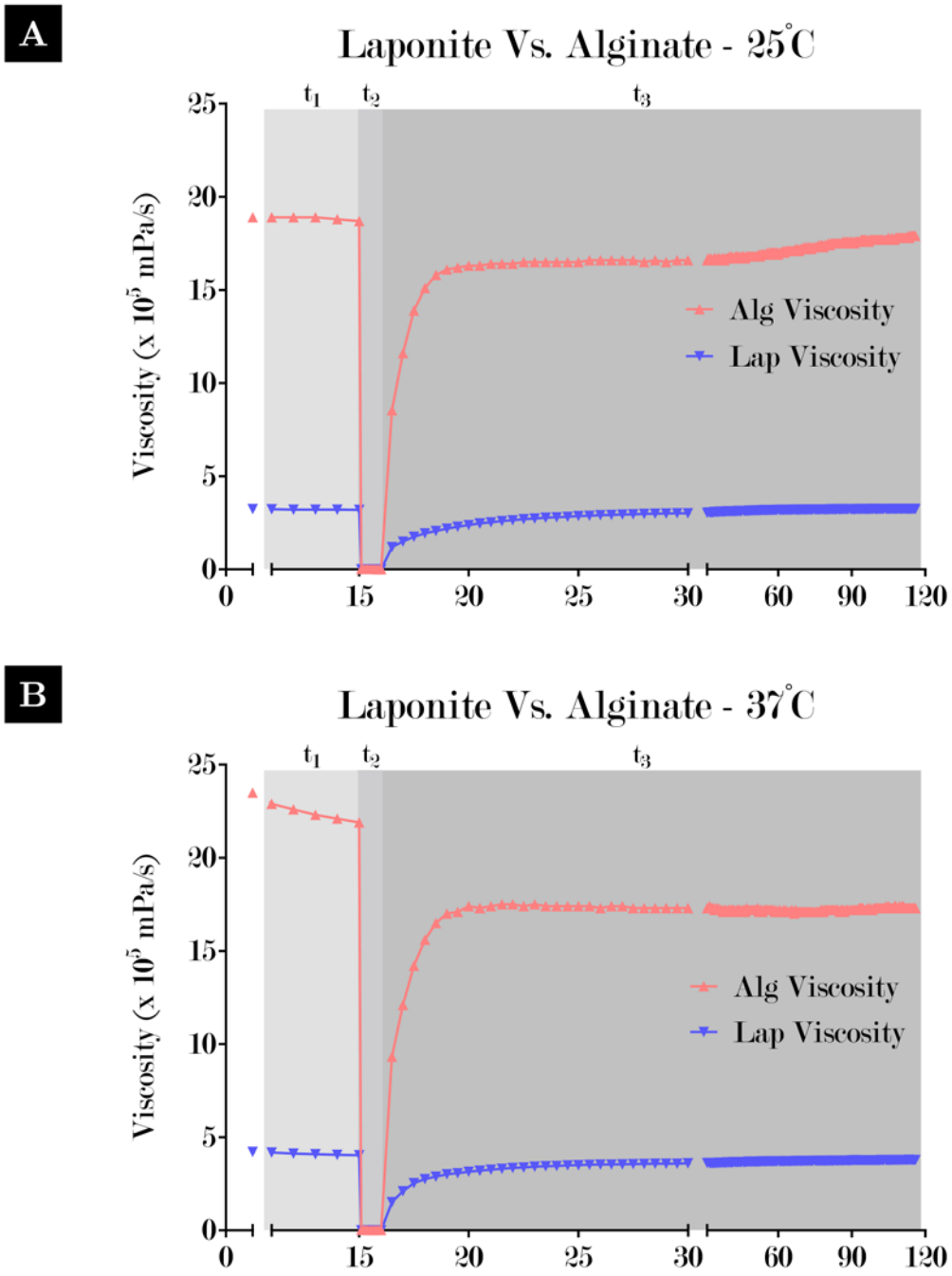

Figure 6.7. Alginate gels exhibited much greater viscosity than Laponite gels before and after the shear interval at 25°C (A) and 37°C (B).

Figure 6.8 shows the differences between pre-shear viscosity of Laponite and alginate gels in more detail. It shows that alginate gels were significantly more viscous than Laponite gels with a difference in viscosity of 1563333 ± 3471 mPa/s (an increase of 486 ± 0.01 %; error = SD; p = <0.0001).

A

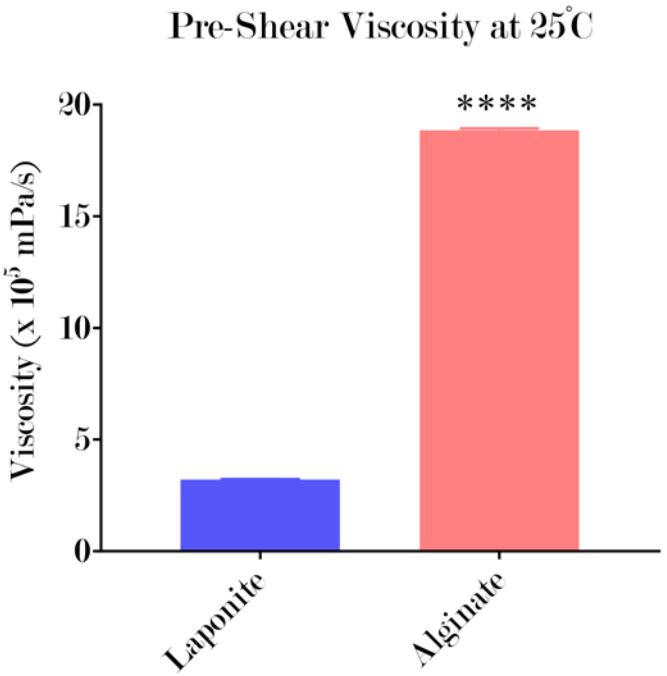

B

Pre-Shear Viscosity Statistics Between Laponite and Alginate Gels at 25°C							
	Viscosity (x 10^5 mPa · s)		Difference Between Means & SD	Mean % Difference & SD	n	p	Sign.
	Laponite	Alginate					
Mean:	3.22	18.85	15.63 ± 0.03	486 ± 0.01	6	<0.0001	****
St.Dev:	0.02	0.08					

Figure 6.8. The pre-shear viscosity of cross-linked alginate gels was significantly greater than Laponite gels at 25°C. (A) Graph showing that alginate gels were significantly more viscous than Laponite gels; **** denotes that p = <0.0001. (B) Table statistics generated from a student's t test of the data from the graph in A; it shows that alginate was 486 ± 0.01 % more viscous.

C.1.1.2 3-ITT Data Tables

C.1.1.2.1 25°C Laponite

Interval	Time (s)	Viscosity (x 10^5 mPa · s)	Shear Stress (Pa)	Viscosity (% diff. from end of 1st Interval)	% Shear Stress Compared To End of 1^{st} Interval)
1^{st}	10.0	3.24	32.43	100.0	100.0
	11.0	3.23	32.30		
	12.0	3.21	32.15		
	13.0	3.21	32.13		
	14.0	3.21	32.07		
	15.0	3.20	32.02		
2^{nd}	15.1	0.01	97.18	0.3	303.5
	15.2	0.01	74.94	0.2	234.1
	15.3	0.01	67.29	0.2	210.1
	15.4	0.01	63.26	0.2	197.6
	15.5	0.01	60.62	0.2	189.3
	15.6	0.01	58.46	0.2	182.6
	15.7	0.01	57.11	0.2	178.4
	15.8	0.01	55.94	0.2	174.7
	15.9	0.01	54.66	0.2	170.7
	16.0	0.01	53.88	0.2	168.3
3^{rd}	16.5	1.20	11.96	37.5	37.3
	17.0	1.49	14.87	46.6	46.4
	17.5	1.75	17.47	54.7	54.6
	18.0	1.93	19.25	60.3	60.1
	18.5	2.06	20.65	64.4	64.5
	19.0	2.19	21.94	68.4	68.5
	19.5	2.29	22.94	71.6	71.6
	20.0	2.38	23.83	74.4	74.4
	20.5	2.47	24.65	77.2	77.0
	21.0	2.53	25.30	79.1	79.0
	21.5	2.59	25.87	80.9	80.8
	22.0	2.64	26.46	82.5	82.6
	22.5	2.69	26.87	84.1	83.9
	23.0	2.73	27.27	85.3	85.2
	23.5	2.77	27.68	86.6	86.5
	24.0	2.80	27.97	87.5	87.3
	24.5	2.82	28.28	88.1	88.3
	25.0	2.86	28.60	89.4	89.3
	25.5	2.88	28.79	90.0	89.9
	26.0	2.91	29.05	90.9	90.7
	26.5	2.92	29.22	91.3	91.3
	27.0	2.95	29.44	92.2	91.9
	27.5	2.96	29.59	92.5	92.4
	28.0	2.98	29.78	93.1	93.0
	28.5	2.99	29.87	93.4	93.3
	29.0	3.00	30.00	93.8	93.7
	29.5	3.01	30.14	94.1	94.1
3^{rd}	30.0	3.01	30.14	94.1	94.1
	30.5	3.02	30.29	94.4	94.6
	31.0	3.04	30.35	95.0	94.8
	31.5	3.04	30.38	95.0	94.9
	32.0	3.06	30.55	95.6	95.4
	32.5	3.05	30.53	95.3	95.4
	33.0	3.06	30.59	95.6	95.5
	33.5	3.06	30.66	95.6	95.8
	34.0	3.08	30.78	96.3	96.1
	34.5	3.08	30.76	96.3	96.1
	35.0	3.08	30.81	96.3	96.2
	35.5	3.08	30.81	96.3	96.2
	36.0	3.09	30.88	96.6	96.5
	36.5	3.10	30.94	96.9	96.6
	37.0	3.09	30.93	96.6	96.6
	37.5	3.09	30.97	96.6	96.7
	38.0	3.10	31.04	96.9	96.9
	38.5	3.10	31.03	96.9	96.9
	39.0	3.11	31.05	97.2	97.0
	39.5	3.12	31.13	97.5	97.2
	40.0	3.12	31.10	97.5	97.1
	40.5	3.11	31.14	97.2	97.2
	41.0	3.12	31.19	97.5	97.4
	41.5	3.11	31.15	97.2	97.3
	42.0	3.12	31.22	97.5	97.5
	42.5	3.12	31.25	97.5	97.6
	43.0	3.13	31.26	97.8	97.6
	43.5	3.13	31.30	97.8	97.8
	44.0	3.14	31.37	98.1	98.0
	44.5	3.12	31.28	97.5	97.7
	45.0	3.14	31.37	98.1	98.0
	45.5	3.14	31.41	98.1	98.1
	46.0	3.14	31.37	98.1	98.0
	46.5	3.14	31.45	98.1	98.2
	47.0	3.14	31.45	98.1	98.2
	47.5	3.14	31.43	98.1	98.2
	48.0	3.15	31.50	98.4	98.4
	48.5	3.15	31.53	98.4	98.5
	49.0	3.15	31.50	98.4	98.4
	49.5	3.16	31.61	98.8	98.7
	50.0	3.16	31.60	98.8	98.7
	50.5	3.16	31.55	98.8	98.5
	51.0	3.16	31.61	98.8	98.7
	51.5	3.16	31.61	98.8	98.7
	52.0	3.16	31.59	98.8	98.7
	52.5	3.17	31.69	99.1	99.0
	53.0	3.17	31.65	99.1	98.8
	53.5	3.17	31.67	99.1	98.9
	54.0	3.18	31.78	99.4	99.2

3rd	54.5	3.17	31.67	99.1	98.9
	55.0	3.17	31.71	99.1	99.0
	55.5	3.18	31.80	99.4	99.3
	56.0	3.17	31.67	99.1	98.9
	56.5	3.18	31.77	99.4	99.2
	57.0	3.18	31.78	99.4	99.3
	57.5	3.18	31.75	99.4	99.1
	58.0	3.18	31.81	99.4	99.3
	58.5	3.18	31.84	99.4	99.4
	59.0	3.18	31.82	99.4	99.4
	59.5	3.19	31.85	99.7	99.5
	60.0	3.19	31.88	99.7	99.6
	60.5	3.18	31.84	99.4	99.4
	61.0	3.19	31.90	99.7	99.6
	61.5	3.20	31.96	100.0	99.8
	62.0	3.18	31.82	99.4	99.4
	62.5	3.20	31.91	100.0	99.6
	63.0	3.20	31.94	100.0	99.8
	63.5	3.19	31.89	99.7	99.6
	64.0	3.19	31.95	99.7	99.8
	64.5	3.20	32.01	100.0	100.0
	65.0	3.19	31.93	99.7	99.7
	65.5	3.20	32.02	100.0	100.0
	66.0	3.21	32.05	100.3	100.1
	66.5	3.21	32.04	100.3	100.1
	67.0	3.21	32.12	100.3	100.3
	67.5	3.20	32.04	100.0	100.1
	68.0	3.20	31.97	100.0	99.9
	68.5	3.20	32.05	100.0	100.1
	69.0	3.21	32.02	100.3	100.0
	69.5	3.21	32.05	100.3	100.1
	70.0	3.21	32.12	100.3	100.3
	70.5	3.21	32.08	100.3	100.2
	71.0	3.20	32.05	100.0	100.1
	71.5	3.21	32.16	100.3	100.4
	72.0	3.21	32.11	100.3	100.3
	72.5	3.21	32.11	100.3	100.3
	73.0	3.22	32.19	100.6	100.5
	73.5	3.20	32.08	100.0	100.2
	74.0	3.21	32.08	100.3	100.2
	74.5	3.22	32.17	100.6	100.5
	75.0	3.21	32.10	100.3	100.3
	75.5	3.22	32.13	100.6	100.3
	76.0	3.21	32.14	100.3	100.4
	76.5	3.21	32.13	100.3	100.3
	77.0	3.22	32.17	100.6	100.5
	77.5	3.22	32.22	100.6	100.6
	78.0	3.22	32.17	100.6	100.5
	78.5	3.22	32.21	100.6	100.6
	79.0	3.22	32.23	100.6	100.7
	79.5	3.21	32.14	100.3	100.4
	80.0	3.22	32.23	100.6	100.7
	80.5	3.22	32.21	100.6	100.6
	81.0	3.22	32.17	100.6	100.5
	81.5	3.23	32.25	100.9	100.7
	82.0	3.23	32.26	100.9	100.8

3rd	82.5	3.22	32.22	100.6	100.6
	83.0	3.22	32.29	100.6	100.9
	83.5	3.22	32.23	100.6	100.6
	84.0	3.23	32.24	100.9	100.7
	84.5	3.24	32.36	101.3	101.1
	85.0	3.22	32.25	100.6	100.7
	85.5	3.22	32.22	100.6	100.6
	86.0	3.24	32.35	101.3	101.0
	86.5	3.23	32.25	100.9	100.7
	87.0	3.23	32.27	100.9	100.8
	87.5	3.23	32.34	100.9	101.0
	88.0	3.23	32.26	100.9	100.8
	88.5	3.23	32.29	100.9	100.8
	89.0	3.24	32.35	101.3	101.0
	89.5	3.23	32.28	100.9	100.8
	90.0	3.23	32.30	100.9	100.9
	90.5	3.23	32.37	100.9	101.1
	91.0	3.22	32.24	100.6	100.7
	91.5	3.23	32.31	100.9	100.9
	92.0	3.24	32.36	101.3	101.1
	92.5	3.23	32.31	100.9	100.9
	93.0	3.24	32.36	101.3	101.1
	93.5	3.23	32.35	100.9	101.0
	94.0	3.24	32.34	101.3	101.0
	94.5	3.24	32.37	101.3	101.1
	95.0	3.23	32.33	100.9	101.0
	95.5	3.24	32.33	101.3	101.0
	96.0	3.23	32.39	100.9	101.1
	96.5	3.23	32.37	100.9	101.1
	97.0	3.23	32.36	100.9	101.1
	97.5	3.24	32.41	101.3	101.2
	98.0	3.24	32.38	101.3	101.1
	98.5	3.24	32.35	101.3	101.0
	99.0	3.25	32.42	101.6	101.3
	99.5	3.24	32.38	101.3	101.1
	100.0	3.23	32.34	100.9	101.0
	100.5	3.24	32.43	101.3	101.3
	101.0	3.24	32.38	101.3	101.1
	101.5	3.24	32.38	101.3	101.1
	102.0	3.24	32.43	101.3	101.3
	102.5	3.24	32.35	101.3	101.0
	103.0	3.24	32.43	101.3	101.3
	103.5	3.24	32.45	101.3	101.3
	104.0	3.24	32.37	101.3	101.1
	104.5	3.24	32.38	101.3	101.1
	105.0	3.24	32.42	101.3	101.2
	105.5	3.24	32.42	101.3	101.3
	106.0	3.24	32.43	101.3	101.3
	106.5	3.25	32.46	101.6	101.4
	107.0	3.24	32.37	101.3	101.1
	107.5	3.24	32.43	101.3	101.3
	108.0	3.24	32.43	101.3	101.3
	108.5	3.24	32.38	101.3	101.1
	109.0	3.25	32.48	101.6	101.4
	109.5	3.25	32.47	101.6	101.4
	110.0	3.24	32.36	101.3	101.1

3rd	110.5	3.24	32.46	101.3	101.4
	111.0	3.25	32.45	101.6	101.3
	111.5	3.24	32.41	101.3	101.2
	112.0	3.25	32.49	101.6	101.5
	112.5	3.24	32.43	101.3	101.3
	113.0	3.24	32.42	101.3	101.2
	113.5	3.24	32.46	101.3	101.4
	114.0	3.24	32.43	101.3	101.3
	114.5	3.24	32.43	101.3	101.3
	115.0	3.25	32.45	101.6	101.4
	115.5	3.25	32.45	101.6	101.3
	116.0	3.24	32.46	101.3	101.4

Table 6.22. 3-ITT raw data values for 25°C Laponite gels.

C.1.1.2.2 37°C Laponite

Interval	Time (s)	Viscosity (x 10^5 mPa · s)	Shear Stress (Pa)	% Viscosity Compared To End of 1^{st} Interval)	% Shear Stress Compared To End of 1^{st} Interval)
1^{st}	10.0	4.22	42.25	100.0	100.0
	11.0	4.18	41.75		
	12.0	4.12	41.23		
	13.0	4.09	40.88		
	14.0	4.06	40.64		
	15.0	4.03	40.34		
2^{nd}	15.1	0.01	92.57	0.2	229.4
	15.2	0.01	75.29	0.2	186.6
	15.3	0.01	69.14	0.2	171.4
	15.4	0.01	65.26	0.2	161.8
	15.5	0.01	63.27	0.2	156.8
	15.6	0.01	61.70	0.2	152.9
	15.7	0.01	60.27	0.1	149.4
	15.8	0.01	59.43	0.1	147.3
	15.9	0.01	58.54	0.1	145.1
	16.0	0.01	57.65	0.1	142.9
3^{rd}	16.5	1.52	15.20	37.7	37.7
	17.0	2.11	21.09	52.4	52.3
	17.5	2.54	25.40	63.0	63.0
	18.0	2.75	27.52	68.2	68.2
	18.5	2.89	28.88	71.7	71.6
	19.0	3.01	30.08	74.7	74.6
	19.5	3.07	30.72	76.2	76.1
	20.0	3.15	31.49	78.2	78.1
	20.5	3.21	32.14	79.7	79.7
	21.0	3.26	32.61	80.9	80.8
	21.5	3.31	33.11	82.1	82.1
	22.0	3.35	33.52	83.1	83.1
	22.5	3.38	33.82	83.9	83.8
	23.0	3.42	34.17	84.9	84.7
	23.5	3.44	34.39	85.4	85.3
	24.0	3.46	34.59	85.9	85.7
	24.5	3.49	34.86	86.6	86.4
	25.0	3.50	35.02	86.8	86.8
	25.5	3.52	35.22	87.3	87.3
	26.0	3.54	35.39	87.8	87.7
	26.5	3.54	35.44	87.8	87.8
	27.0	3.55	35.50	88.1	88.0
	27.5	3.56	35.64	88.3	88.3
	28.0	3.57	35.71	88.6	88.5
	28.5	3.58	35.74	88.8	88.6
	29.0	3.58	35.85	88.8	88.9
	29.5	3.58	35.87	88.8	88.9
	30.0	3.60	35.96	89.3	89.1
	30.5	3.61	36.09	89.6	89.5
	31.0	3.61	36.07	89.6	89.4
	31.5	3.61	36.06	89.6	89.4
	32.0	3.62	36.16	89.8	89.6
	32.5	3.61	36.19	89.6	89.7
	33.0	3.61	36.12	89.6	89.5
	33.5	3.62	36.22	89.8	89.8
	34.0	3.62	36.21	89.8	89.7
	34.5	3.62	36.23	89.8	89.8
	35.0	3.63	36.30	90.1	90.0
	35.5	3.63	36.28	90.1	89.9
	36.0	3.63	36.34	90.1	90.1
	36.5	3.64	36.38	90.3	90.2
	37.0	3.64	36.36	90.3	90.1
	37.5	3.64	36.38	90.3	90.2
	38.0	3.64	36.42	90.3	90.3
	38.5	3.63	36.33	90.1	90.1
	39.0	3.65	36.47	90.6	90.4
	39.5	3.64	36.48	90.3	90.4
	40.0	3.65	36.44	90.6	90.3
	40.5	3.65	36.45	90.6	90.4
	41.0	3.64	36.47	90.3	90.4
	41.5	3.66	36.54	90.8	90.6
3^{rd}	42.0	3.67	36.70	91.1	91.0
	42.5	3.66	36.60	90.8	90.7
	43.0	3.66	36.64	90.8	90.8
	43.5	3.66	36.65	90.8	90.8
	44.0	3.67	36.65	91.1	90.8
	44.5	3.66	36.61	90.8	90.7
	45.0	3.66	36.63	90.8	90.8
	45.5	3.66	36.58	90.8	90.7
	46.0	3.65	36.59	90.6	90.7
	46.5	3.67	36.68	91.1	90.9
	47.0	3.67	36.67	91.1	90.9
	47.5	3.68	36.81	91.3	91.2
	48.0	3.69	36.88	91.6	91.4
	48.5	3.68	36.83	91.3	91.3
	49.0	3.67	36.78	91.1	91.2
	49.5	3.69	36.90	91.6	91.5
	50.0	3.68	36.87	91.3	91.4
	50.5	3.68	36.85	91.3	91.3
	51.0	3.68	36.84	91.3	91.3
	51.5	3.68	36.83	91.3	91.3
	52.0	3.68	36.84	91.3	91.3
	52.5	3.68	36.84	91.3	91.3
	53.0	3.70	36.98	91.8	91.7
	53.5	3.70	36.96	91.8	91.6
	54.0	3.69	36.94	91.6	91.6

3rd	54.5	3.69	36.92	91.6	91.5
	55.0	3.70	37.00	91.8	91.7
	55.5	3.70	37.02	91.8	91.8
	56.0	3.70	37.00	91.8	91.7
	56.5	3.71	37.02	92.1	91.8
	57.0	3.70	36.99	91.8	91.7
	57.5	3.69	36.93	91.6	91.5
	58.0	3.70	36.96	91.8	91.6
	58.5	3.71	37.07	92.1	91.9
	59.0	3.70	36.96	91.8	91.6
	59.5	3.71	37.13	92.1	92.0
	60.0	3.72	37.15	92.3	92.1
	60.5	3.71	37.05	92.1	91.8
	61.0	3.71	37.13	92.1	92.0
	61.5	3.71	37.15	92.1	92.1
	62.0	3.71	37.05	92.1	91.8
	62.5	3.72	37.15	92.3	92.1
	63.0	3.71	37.13	92.1	92.0
	63.5	3.72	37.16	92.3	92.1
	64.0	3.72	37.19	92.3	92.2
	64.5	3.71	37.13	92.1	92.0
	65.0	3.72	37.24	92.3	92.3
	65.5	3.72	37.15	92.3	92.1
	66.0	3.72	37.24	92.3	92.3
	66.5	3.72	37.22	92.3	92.3
	67.0	3.73	37.24	92.6	92.3
	67.5	3.72	37.19	92.3	92.2
	68.0	3.73	37.26	92.6	92.4
	68.5	3.73	37.26	92.6	92.4
	69.0	3.72	37.30	92.3	92.5
	69.5	3.73	37.27	92.6	92.4
	70.0	3.72	37.22	92.3	92.3
	70.5	3.73	37.27	92.6	92.4
	71.0	3.73	37.30	92.6	92.4
	71.5	3.73	37.29	92.6	92.4
	72.0	3.73	37.36	92.6	92.6
	72.5	3.74	37.37	92.8	92.6
	73.0	3.73	37.33	92.6	92.5
	73.5	3.73	37.26	92.6	92.4
	74.0	3.73	37.31	92.6	92.5
	74.5	3.74	37.35	92.8	92.6
	75.0	3.74	37.39	92.8	92.7
	75.5	3.74	37.41	92.8	92.7
	76.0	3.73	37.32	92.6	92.5
	76.5	3.73	37.30	92.6	92.5
	77.0	3.74	37.38	92.8	92.7
	77.5	3.74	37.33	92.8	92.5
	78.0	3.73	37.36	92.6	92.6
	78.5	3.74	37.37	92.8	92.6
	79.0	3.73	37.34	92.6	92.5
	79.5	3.73	37.30	92.6	92.4
	80.0	3.74	37.36	92.8	92.6
	80.5	3.74	37.45	92.8	92.8
	81.0	3.73	37.37	92.6	92.6
	81.5	3.75	37.51	93.1	93.0
	82.0	3.73	37.30	92.6	92.5

3rd	82.5	3.74	37.38	92.8	92.6
	83.0	3.75	37.54	93.1	93.0
	83.5	3.75	37.47	93.1	92.9
	84.0	3.74	37.42	92.8	92.7
	84.5	3.74	37.39	92.8	92.7
	85.0	3.75	37.49	93.1	92.9
	85.5	3.75	37.46	93.1	92.9
	86.0	3.74	37.38	92.8	92.7
	86.5	3.75	37.51	93.1	93.0
	87.0	3.75	37.47	93.1	92.9
	87.5	3.75	37.52	93.1	93.0
	88.0	3.75	37.44	93.1	92.8
	88.5	3.75	37.52	93.1	93.0
	89.0	3.74	37.43	92.8	92.8
	89.5	3.75	37.51	93.1	93.0
	90.0	3.76	37.52	93.3	93.0
	90.5	3.76	37.61	93.3	93.2
	91.0	3.76	37.55	93.3	93.1
	91.5	3.77	37.68	93.5	93.4
	92.0	3.76	37.58	93.3	93.1
	92.5	3.76	37.60	93.3	93.2
	93.0	3.76	37.62	93.3	93.3
	93.5	3.76	37.60	93.3	93.2
	94.0	3.76	37.65	93.3	93.3
	94.5	3.76	37.66	93.3	93.4
	95.0	3.76	37.61	93.3	93.2
	95.5	3.76	37.59	93.3	93.2
	96.0	3.76	37.64	93.3	93.3
	96.5	3.76	37.63	93.3	93.3
	97.0	3.76	37.58	93.3	93.1
	97.5	3.76	37.63	93.3	93.3
	98.0	3.76	37.54	93.3	93.1
	98.5	3.76	37.63	93.3	93.3
	99.0	3.76	37.65	93.3	93.3
	99.5	3.76	37.60	93.3	93.2
	100.0	3.76	37.62	93.3	93.3
	100.5	3.76	37.64	93.3	93.3
	101.0	3.76	37.64	93.3	93.3
	101.5	3.76	37.62	93.3	93.3
	102.0	3.78	37.75	93.8	93.6
	102.5	3.76	37.61	93.3	93.2
	103.0	3.77	37.70	93.5	93.4
	103.5	3.76	37.62	93.3	93.3
	104.0	3.76	37.62	93.3	93.2
	104.5	3.77	37.68	93.5	93.4
	105.0	3.76	37.64	93.3	93.3
	105.5	3.77	37.70	93.5	93.4
	106.0	3.77	37.72	93.5	93.5
	106.5	3.77	37.71	93.5	93.5
	107.0	3.77	37.70	93.5	93.4
	107.5	3.79	37.81	94.0	93.7
	108.0	3.77	37.73	93.5	93.5
	108.5	3.77	37.70	93.5	93.4
	109.0	3.78	37.83	93.8	93.8
	109.5	3.77	37.77	93.5	93.6
	110.0	3.78	37.75	93.8	93.6

3rd	110.5	3.78	37.81	93.8	93.7
	111.0	3.78	37.79	93.8	93.7
	111.5	3.78	37.79	93.8	93.7
	112.0	3.79	37.91	94.0	94.0
	112.5	3.78	37.85	93.8	93.8
	113.0	3.78	37.79	93.8	93.7
	113.5	3.80	37.97	94.3	94.1
	114.0	3.78	37.82	93.8	93.7
	114.5	3.79	37.86	94.0	93.9
	115.0	3.79	37.88	94.0	93.9
	115.5	3.78	37.83	93.8	93.8
	116.0	3.78	37.85	93.8	93.8

Table 6.23. 3-ITT raw data values for 37°C Laponite gels.

C.1.1.2.3 25°C Alginate

Interval	Time (s)	Viscosity (x 10^5 mPa · s)	Shear Stress (Pa)	% Viscosity Compared To End of 1st Interval)	% Shear Stress Compared To End of 1st Interval)
1st	10.0	18.90	189.44	100.0	100.0
	11.0	18.90	189.56		
	12.0	18.90	189.35		
	13.0	18.90	188.73		
	14.0	18.80	188.05		
	15.0	18.70	187.24		
2nd	15.1	0.02	242.38	0.1	129.4
	15.2	0.02	187.13	0.1	99.9
	15.3	0.02	172.14	0.1	91.9
	15.4	0.02	165.22	0.1	88.2
	15.5	0.02	159.10	0.1	85.0
	15.6	0.02	155.43	0.1	83.0
	15.7	0.02	153.07	0.1	81.8
	15.8	0.01	149.83	0.1	80.0
	15.9	0.01	147.39	0.1	78.7
	16.0	0.01	146.12	0.1	78.0
3rd	16.5	8.54	85.24	45.7	45.5
	17.0	11.60	116.66	62.0	62.3
	17.5	13.90	138.75	74.3	74.1
	18.0	15.10	151.50	80.7	80.9
	18.5	15.80	158.05	84.5	84.4
	19.0	16.10	161.02	86.1	86.0
	19.5	16.20	162.46	86.6	86.8
	20.0	16.30	163.04	87.2	87.1
	20.5	16.30	163.63	87.2	87.4
	21.0	16.40	163.82	87.7	87.5
	21.5	16.40	164.39	87.7	87.8
	22.0	16.40	164.42	87.7	87.8
	22.5	16.50	164.88	88.2	88.1
	23.0	16.50	164.91	88.2	88.1
	23.5	16.50	165.14	88.2	88.2
	24.0	16.50	165.39	88.2	88.3
	24.5	16.50	165.60	88.2	88.4
	25.0	16.50	165.40	88.2	88.3
	25.5	16.60	165.95	88.8	88.6
	26.0	16.60	165.83	88.8	88.6
	26.5	16.60	165.81	88.8	88.6
	27.0	16.60	165.84	88.8	88.6
	27.5	16.60	165.81	88.8	88.6
	28.0	16.50	165.75	88.2	88.5
	28.5	16.60	166.04	88.8	88.7
	29.0	16.50	165.70	88.2	88.5
	29.5	16.60	166.24	88.8	88.8
	30.0	16.60	165.86	88.8	88.6
	30.5	16.60	166.07	88.8	88.7
	31.0	16.60	165.90	88.8	88.6
	31.5	16.70	166.76	89.3	89.1
	32.0	16.60	166.11	88.8	88.7
	32.5	16.70	166.45	89.3	88.9
	33.0	16.60	166.35	88.8	88.8
	33.5	16.60	166.06	88.8	88.7
	34.0	16.70	166.62	89.3	89.0
	34.5	16.70	166.69	89.3	89.0
	35.0	16.60	166.49	88.8	88.9
	35.5	16.70	166.71	89.3	89.0
	36.0	16.70	166.98	89.3	89.2
	36.5	16.60	166.50	88.8	88.9
	37.0	16.70	167.06	89.3	89.2
	37.5	16.70	166.76	89.3	89.1
	38.0	16.60	166.87	88.8	89.1
	38.5	16.70	166.93	89.3	89.2
	39.0	16.70	167.17	89.3	89.3
	39.5	16.70	167.09	89.3	89.2
	40.0	16.80	167.48	89.8	89.4
	40.5	16.70	167.37	89.3	89.4
	41.0	16.80	167.36	89.8	89.4
	41.5	16.70	167.54	89.3	89.5
	42.0	16.70	167.44	89.3	89.4
	42.5	16.80	167.32	89.8	89.4
	43.0	16.80	167.71	89.8	89.6
	43.5	16.80	167.34	89.8	89.4
	44.0	16.70	167.41	89.3	89.4
	44.5	16.80	167.73	89.8	89.6
	45.0	16.70	167.45	89.3	89.4
	45.5	16.80	167.62	89.8	89.5
	46.0	16.80	167.83	89.8	89.6
	46.5	16.70	167.68	89.3	89.6
	47.0	16.80	167.85	89.8	89.6
	47.5	16.80	167.98	89.8	89.7
	48.0	16.80	167.73	89.8	89.6
	48.5	16.80	168.00	89.8	89.7
	49.0	16.80	167.99	89.8	89.7
	49.5	16.80	167.96	89.8	89.7
	50.0	16.80	168.07	89.8	89.8
	50.5	16.80	168.19	89.8	89.8
	51.0	16.80	168.02	89.8	89.7
	51.5	16.80	168.33	89.8	89.9
	52.0	16.90	168.49	90.4	90.0
	52.5	16.80	168.53	89.8	90.0
	53.0	16.90	168.79	90.4	90.1
	53.5	16.90	168.71	90.4	90.1
	54.0	16.90	169.02	90.4	90.3

	54.5	16.90	169.09	90.4	90.3
	55.0	16.90	169.11	90.4	90.3
	55.5	17.00	169.31	90.9	90.4
	56.0	16.90	169.45	90.4	90.5
	56.5	17.00	169.48	90.9	90.5
	57.0	17.00	169.75	90.9	90.7
	57.5	17.00	169.70	90.9	90.6
	58.0	17.00	169.80	90.9	90.7
	58.5	17.00	169.69	90.9	90.6
	59.0	17.00	170.03	90.9	90.8
	59.5	17.00	169.98	90.9	90.8
	60.0	16.90	169.86	90.4	90.7
	60.5	17.00	170.33	90.9	91.0
	61.0	17.00	170.33	90.9	91.0
	61.5	17.00	170.15	90.9	90.9
	62.0	17.10	170.53	91.4	91.1
	62.5	17.00	170.46	90.9	91.0
	63.0	17.10	170.68	91.4	91.2
	63.5	17.10	170.77	91.4	91.2
	64.0	17.10	170.59	91.4	91.1
	64.5	17.10	170.92	91.4	91.3
	65.0	17.10	170.96	91.4	91.3
	65.5	17.10	171.26	91.4	91.5
	66.0	17.10	171.18	91.4	91.4
	66.5	17.10	171.23	91.4	91.4
	67.0	17.20	171.24	92.0	91.5
	67.5	17.10	171.27	91.4	91.5
3rd	68.0	17.20	171.50	92.0	91.6
	68.5	17.10	171.67	91.4	91.7
	69.0	17.20	171.84	92.0	91.8
	69.5	17.20	171.96	92.0	91.8
	70.0	17.20	172.18	92.0	92.0
	70.5	17.30	172.32	92.5	92.0
	71.0	17.20	172.40	92.0	92.1
	71.5	17.30	172.49	92.5	92.1
	72.0	17.20	172.75	92.0	92.3
	72.5	17.30	172.77	92.5	92.3
	73.0	17.30	172.54	92.5	92.1
	73.5	17.20	172.62	92.0	92.2
	74.0	17.30	172.87	92.5	92.3
	74.5	17.30	172.88	92.5	92.3
	75.0	17.30	172.99	92.5	92.4
	75.5	17.30	173.21	92.5	92.5
	76.0	17.30	173.10	92.5	92.4
	76.5	17.40	173.40	93.0	92.6
	77.0	17.30	173.51	92.5	92.7
	77.5	17.40	173.62	93.0	92.7
	78.0	17.40	173.75	93.0	92.8
	78.5	17.30	173.58	92.5	92.7
	79.0	17.40	173.56	93.0	92.7
	79.5	17.40	173.75	93.0	92.8
	80.0	17.40	173.91	93.0	92.9
	80.5	17.50	174.32	93.6	93.1
	81.0	17.40	174.22	93.0	93.0
	81.5	17.50	174.43	93.6	93.2
	82.0	17.50	174.80	93.6	93.4

	82.5	17.50	174.74	93.6	93.3
	83.0	17.50	174.86	93.6	93.4
	83.5	17.50	175.07	93.6	93.5
	84.0	17.50	175.25	93.6	93.6
	84.5	17.50	174.75	93.6	93.3
	85.0	17.50	174.99	93.6	93.5
	85.5	17.50	175.13	93.6	93.5
	86.0	17.50	175.11	93.6	93.5
	86.5	17.60	175.49	94.1	93.7
	87.0	17.50	175.42	93.6	93.7
	87.5	17.60	175.49	94.1	93.7
	88.0	17.60	175.66	94.1	93.8
	88.5	17.50	175.68	93.6	93.8
	89.0	17.60	175.75	94.1	93.9
	89.5	17.60	175.90	94.1	93.9
	90.0	17.50	175.50	93.6	93.7
	90.5	17.60	175.79	94.1	93.9
	91.0	17.50	175.65	93.6	93.8
	91.5	17.60	175.92	94.1	94.0
	92.0	17.60	176.14	94.1	94.1
	92.5	17.60	176.36	94.1	94.2
	93.0	17.60	176.22	94.1	94.1
	93.5	17.60	176.73	94.1	94.4
	94.0	17.70	176.39	94.7	94.2
	94.5	17.70	176.67	94.7	94.4
	95.0	17.70	176.81	94.7	94.4
	95.5	17.70	176.67	94.7	94.4
3rd	96.0	17.60	176.36	94.1	94.2
	96.5	17.70	176.66	94.7	94.3
	97.0	17.60	176.44	94.1	94.2
	97.5	17.70	176.49	94.7	94.3
	98.0	17.70	176.84	94.7	94.4
	98.5	17.70	176.58	94.7	94.3
	99.0	17.70	176.70	94.7	94.4
	99.5	17.70	176.93	94.7	94.5
	100.0	17.70	176.98	94.7	94.5
	100.5	17.70	176.89	94.7	94.5
	101.0	17.70	176.87	94.7	94.5
	101.5	17.70	176.76	94.7	94.4
	102.0	17.70	176.85	94.7	94.5
	102.5	17.70	176.67	94.7	94.4
	103.0	17.70	176.97	94.7	94.5
	103.5	17.70	177.08	94.7	94.6
	104.0	17.70	176.90	94.7	94.5
	104.5	17.70	176.97	94.7	94.5
	105.0	17.80	177.19	95.2	94.6
	105.5	17.70	177.10	94.7	94.6
	106.0	17.70	177.34	94.7	94.7
	106.5	17.80	177.37	95.2	94.7
	107.0	17.70	177.42	94.7	94.8
	107.5	17.70	177.34	94.7	94.7
	108.0	17.80	177.66	95.2	94.9
	108.5	17.80	177.58	95.2	94.8
	109.0	17.80	177.68	95.2	94.9
	109.5	17.80	177.89	95.2	95.0
	110.0	17.80	177.73	95.2	94.9

3rd	110.5	17.80	178.02	95.2	95.1
	111.0	17.80	178.15	95.2	95.1
	111.5	17.80	178.10	95.2	95.1
	112.0	17.80	178.20	95.2	95.2
	112.5	17.80	178.45	95.2	95.3
	113.0	17.90	178.42	95.7	95.3
	113.5	17.80	178.77	95.2	95.5
	114.0	17.90	178.69	95.7	95.4
	114.5	17.90	178.62	95.7	95.4
	115.0	17.90	178.75	95.7	95.5
	115.5	17.90	178.88	95.7	95.5
	116.0	17.90	178.99	95.7	95.6

Table 6.24. 3-ITT raw data values for 25°C alginate gels.

C.1.1.2.4 37°C Alginate

Interval	Time (s)	Viscosity (x 10^5 mPa · s)	Shear Stress (Pa)	% Viscosity Compared To End of 1^{st} Interval)	% Shear Stress Compared To End of 1^{st} Interval)
1^{st}	10.0	23.50	235.34	100.0	100.0
	11.0	22.90	229.36		
	12.0	22.60	225.78		
	13.0	22.30	223.45		
	14.0	22.10	221.35		
	15.0	21.90	218.76		
2^{nd}	15.1	0.03	327.05	0.1	149.5
	15.2	0.03	283.29	0.1	129.5
	15.3	0.03	258.62	0.1	118.2
	15.4	0.02	245.90	0.1	112.4
	15.5	0.02	233.55	0.1	106.8
	15.6	0.02	221.74	0.1	101.4
	15.7	0.02	201.59	0.1	92.2
	15.8	0.02	183.77	0.1	84.0
	15.9	0.02	177.31	0.1	81.1
	16.0	0.02	170.11	0.1	77.8
3^{rd}	16.5	9.32	93.13	42.6	42.6
	17.0	12.10	121.18	55.3	55.4
	17.5	14.20	142.04	64.8	64.9
	18.0	15.60	156.12	71.2	71.4
	18.5	16.50	164.81	75.3	75.3
	19.0	17.00	169.55	77.6	77.5
	19.5	17.10	171.82	78.1	78.5
	20.0	17.40	173.81	79.5	79.5
	20.5	17.30	173.34	79.0	79.2
	21.0	17.40	174.27	79.5	79.7
	21.5	17.50	174.48	79.9	79.8
	22.0	17.50	174.72	79.9	79.9
	22.5	17.40	173.70	79.5	79.4
	23.0	17.50	174.38	79.9	79.7
	23.5	17.40	174.24	79.5	79.6
	24.0	17.40	173.46	79.5	79.3
	24.5	17.40	174.01	79.5	79.5
	25.0	17.40	174.03	79.5	79.6
	25.5	17.40	173.74	79.5	79.4
	26.0	17.30	173.36	79.0	79.2
	26.5	17.40	174.12	79.5	79.6
	27.0	17.40	173.50	79.5	79.3
	27.5	17.30	173.04	79.0	79.1
	28.0	17.30	173.14	79.0	79.1
	28.5	17.30	173.43	79.0	79.3
	29.0	17.30	172.70	79.0	78.9
	29.5	17.30	173.12	79.0	79.1
3^{rd}	30.0	17.30	173.29	79.0	79.2
	30.5	17.30	172.50	79.0	78.9
	31.0	17.30	173.05	79.0	79.1
	31.5	17.30	172.89	79.0	79.0
	32.0	17.40	173.23	79.5	79.2
	32.5	17.30	172.76	79.0	79.0
	33.0	17.30	172.82	79.0	79.0
	33.5	17.30	173.17	79.0	79.2
	34.0	17.20	172.39	78.5	78.8
	34.5	17.30	172.62	79.0	78.9
	35.0	17.20	172.06	78.5	78.7
	35.5	17.30	172.89	79.0	79.0
	36.0	17.20	171.89	78.5	78.6
	36.5	17.20	172.30	78.5	78.8
	37.0	17.20	171.88	78.5	78.6
	37.5	17.10	171.70	78.1	78.5
	38.0	17.20	171.70	78.5	78.5
	38.5	17.20	172.05	78.5	78.6
	39.0	17.10	171.45	78.1	78.4
	39.5	17.20	172.14	78.5	78.7
	40.0	17.20	171.95	78.5	78.6
	40.5	17.20	171.48	78.5	78.4
	41.0	17.20	171.98	78.5	78.6
	41.5	17.20	171.93	78.5	78.6
	42.0	17.20	171.31	78.5	78.3
	42.5	17.10	171.79	78.1	78.5
	43.0	17.20	171.98	78.5	78.6
	43.5	17.20	171.58	78.5	78.4
	44.0	17.20	171.78	78.5	78.5
	44.5	17.20	172.09	78.5	78.7
	45.0	17.10	171.65	78.1	78.5
	45.5	17.20	171.92	78.5	78.6
	46.0	17.20	172.21	78.5	78.7
	46.5	17.10	171.70	78.1	78.5
	47.0	17.30	172.40	79.0	78.8
	47.5	17.20	171.94	78.5	78.6
	48.0	17.20	172.19	78.5	78.7
	48.5	17.20	172.08	78.5	78.7
	49.0	17.20	171.82	78.5	78.5
	49.5	17.20	172.17	78.5	78.7
	50.0	17.20	171.82	78.5	78.5
	50.5	17.20	172.31	78.5	78.8
	51.0	17.20	172.12	78.5	78.7
	51.5	17.30	172.64	79.0	78.9
	52.0	17.10	171.65	78.1	78.5
	52.5	17.20	171.97	78.5	78.6
	53.0	17.20	172.17	78.5	78.7
	53.5	17.10	171.41	78.1	78.4
	54.0	17.20	172.02	78.5	78.6

3rd	54.5	17.20	172.02	78.5	78.6
	55.0	17.20	171.66	78.5	78.5
	55.5	17.20	171.93	78.5	78.6
	56.0	17.20	172.14	78.5	78.7
	56.5	17.20	171.85	78.5	78.6
	57.0	17.20	172.16	78.5	78.7
	57.5	17.20	172.10	78.5	78.7
	58.0	17.20	171.93	78.5	78.6
	58.5	17.10	171.60	78.1	78.4
	59.0	17.20	171.87	78.5	78.6
	59.5	17.10	171.46	78.1	78.4
	60.0	17.10	171.57	78.1	78.4
	60.5	17.20	171.50	78.5	78.4
	61.0	17.10	171.46	78.1	78.4
	61.5	17.10	171.32	78.1	78.3
	62.0	17.20	171.47	78.5	78.4
	62.5	17.10	171.52	78.1	78.4
	63.0	17.20	171.46	78.5	78.4
	63.5	17.10	171.28	78.1	78.3
	64.0	17.10	171.69	78.1	78.5
	64.5	17.10	171.48	78.1	78.4
	65.0	17.10	170.79	78.1	78.1
	65.5	17.20	171.52	78.5	78.4
	66.0	17.10	170.98	78.1	78.2
	66.5	17.00	170.65	77.6	78.0
	67.0	17.20	171.23	78.5	78.3
	67.5	17.10	170.98	78.1	78.2
	68.0	17.10	170.87	78.1	78.1
	68.5	17.10	170.98	78.1	78.2
	69.0	17.10	170.82	78.1	78.1
	69.5	17.10	170.74	78.1	78.0
	70.0	17.10	171.00	78.1	78.2
	70.5	17.10	170.99	78.1	78.2
	71.0	17.10	170.76	78.1	78.1
	71.5	17.10	171.29	78.1	78.3
	72.0	17.10	170.92	78.1	78.1
	72.5	17.10	171.04	78.1	78.2
	73.0	17.10	170.90	78.1	78.1
	73.5	17.10	170.81	78.1	78.1
	74.0	17.10	170.87	78.1	78.1
	74.5	17.10	171.12	78.1	78.2
	75.0	17.10	170.70	78.1	78.0
	75.5	17.10	171.03	78.1	78.2
	76.0	17.10	171.17	78.1	78.2
	76.5	17.10	170.86	78.1	78.1
	77.0	17.10	171.18	78.1	78.3
	77.5	17.20	171.49	78.5	78.4
	78.0	17.20	171.45	78.5	78.4
	78.5	17.10	171.42	78.1	78.4
	79.0	17.20	171.89	78.5	78.6
	79.5	17.20	171.64	78.5	78.5
	80.0	17.20	171.73	78.5	78.5
	80.5	17.20	172.22	78.5	78.7
	81.0	17.20	171.39	78.5	78.3
	81.5	17.20	172.21	78.5	78.7
	82.0	17.20	172.07	78.5	78.7

3rd	82.5	17.20	172.03	78.5	78.6
	83.0	17.20	171.75	78.5	78.5
	83.5	17.20	171.83	78.5	78.5
	84.0	17.20	171.77	78.5	78.5
	84.5	17.20	171.43	78.5	78.4
	85.0	17.10	171.69	78.1	78.5
	85.5	17.20	171.45	78.5	78.4
	86.0	17.20	171.51	78.5	78.4
	86.5	17.20	171.75	78.5	78.5
	87.0	17.10	171.66	78.1	78.5
	87.5	17.20	171.82	78.5	78.5
	88.0	17.20	171.78	78.5	78.5
	88.5	17.20	171.82	78.5	78.5
	89.0	17.20	172.29	78.5	78.8
	89.5	17.20	172.13	78.5	78.7
	90.0	17.20	172.22	78.5	78.7
	90.5	17.20	172.39	78.5	78.8
	91.0	17.20	172.44	78.5	78.8
	91.5	17.20	171.83	78.5	78.5
	92.0	17.20	172.56	78.5	78.9
	92.5	17.20	172.20	78.5	78.7
	93.0	17.30	172.40	79.0	78.8
	93.5	17.30	172.19	79.0	78.7
	94.0	17.30	172.38	79.0	78.8
	94.5	17.30	172.42	79.0	78.8
	95.0	17.20	172.31	78.5	78.8
	95.5	17.20	172.45	78.5	78.8
	96.0	17.20	172.49	78.5	78.8
	96.5	17.30	172.74	79.0	79.0
	97.0	17.20	172.37	78.5	78.8
	97.5	17.30	172.63	79.0	78.9
	98.0	17.20	172.44	78.5	78.8
	98.5	17.20	172.57	78.5	78.9
	99.0	17.30	173.09	79.0	79.1
	99.5	17.30	172.55	79.0	78.9
	100.0	17.30	172.89	79.0	79.0
	100.5	17.30	173.12	79.0	79.1
	101.0	17.30	172.88	79.0	79.0
	101.5	17.30	172.81	79.0	79.0
	102.0	17.30	173.24	79.0	79.2
	102.5	17.30	172.94	79.0	79.1
	103.0	17.30	173.03	79.0	79.1
	103.5	17.30	173.13	79.0	79.1
	104.0	17.40	173.05	79.5	79.1
	104.5	17.30	172.88	79.0	79.0
	105.0	17.40	173.70	79.5	79.4
	105.5	17.30	172.66	79.0	78.9
	106.0	17.30	173.46	79.0	79.3
	106.5	17.30	173.37	79.0	79.3
	107.0	17.30	173.24	79.0	79.2
	107.5	17.40	173.85	79.5	79.5
	108.0	17.40	173.59	79.5	79.4
	108.5	17.30	173.41	79.0	79.3
	109.0	17.30	173.57	79.0	79.3
	109.5	17.40	173.70	79.5	79.4
	110.0	17.30	173.36	79.0	79.2

3rd	110.5	17.40	173.90	79.5	79.5
	111.0	17.40	173.44	79.5	79.3
	111.5	17.30	173.00	79.0	79.1
	112.0	17.30	173.06	79.0	79.1
	112.5	17.30	173.02	79.0	79.1
	113.0	17.30	172.79	79.0	79.0
	113.5	17.30	173.06	79.0	79.1
	114.0	17.30	172.91	79.0	79.0
	114.5	17.30	172.74	79.0	79.0
	115.0	17.30	172.83	79.0	79.0
	115.5	17.30	172.71	79.0	78.9
	116.0	17.30	172.96	79.0	79.1

Table 6.25. 3-ITT raw data values for 37°C alginate gels.

C.2 Wound Closure Data Tables Measured in Healthy Mice

Descriptive Statistics												
Statistics of Wound Closure Rates Treated with Laponite ± VEGF												
Day	**0.0 µg/ml**				**0.1 µg/ml**				**1.0 µg/ml**			
	Mean & SD (%)			***n***	**Mean & SD (%)**			***n***	**Mean & SD (%)**			***n***
1	79.0	±	18.5	12	81.6	±	15.4	12	84.9	±	16.4	12
5	61.4	±	16.8	12	56.3	±	20.1	12	59.6	±	17.1	12
7	45.9	±	15.7	11	47.5	±	22.5	10	36.5	±	8.1	9
11	13.0	±	4.9	8	13.6	±	9.4	5	16.3	±	7.8	7

Table 6.26. Statistics of Wound Closure Rates Treated with Laponite ± VEGF.

Descriptive Statistics				
Differences Between Laponite-VEGF Treatment Groups				
Day	**VEGF Concentration (µg/ml)**	**Mean Diff. & SE (%)**	**95% CI (%)**	***p***
1	1.0 vs. 0.1	3.4 ± 5.8	-13.65 to 13.65	0.8301
	1.0 vs. 0.0	6.0 ± 5.8	-13.65 to 13.65	0.5577
	0.1 vs. 0.0	2.6 ± 5.8	-13.65 to 13.65	0.8943
5	1.0 vs. 0.1	3.2 ± 5.8	-10.3 to 17.01	0.8398
	1.0 vs. 0.0	-1.9 ± 5.8	-7.703 to 19.61	0.9429
	0.1 vs. 0.0	-5.1 ± 5.8	-11.06 to 16.25	0.6475
7	1.0 vs. 0.1	-11.0 ± 6.5	-10.41 to 16.9	0.2087
	1.0 vs. 0.0	-9.4 ± 6.3	-15.54 to 11.77	0.3046
	0.1 vs. 0.0	1.7 ± 6.2	-18.79 to 8.524	0.9613
11	1.0 vs. 0.1	2.7 ± 8.3	-26.4 to 4.336	0.9430
	1.0 vs. 0.0	3.2 ± 7.3	-24.41 to 5.653	0.8973
	0.1 vs. 0.0	0.5 ± 8.1	-12.96 to 16.26	0.9975

Table 6.27. Differences Between Laponite-VEGF Treatment Groups.

C.3 Weights & Blood Glucose Measurement Tables

C.3.1 Weights

Descriptive Statistics				
Statistics of C57BL/6 Mice Weight				
Day	***n***	**Mean & SD (g)**		
0	14	23.9	±	1.8
1	11	22.4	±	1.8
5	5	22.4	±	1.3
7	5	22.7	±	1.1
11	5	24.0	±	0.5

Table 6.28. Statistics of mean C57BL/6 weights overtime.

C.3.2 Blood Glucose

Descriptive Statistics				
Statistics of C57BL/6 Mice Blood Glucose Levels				
Day	***n***	**Mean & SD (mmol/l)**		
0	14	8.0	±	1.4
1	11	9.2	±	2.6
5	5	8.3	±	1.7
7	5	11.1	±	2.8
11	5	10.0	±	2.4

Table 6.29. Statistics of mean C57BL/6 weights overtime

C.4 Mean Contraction Rates Measured using Histological Sections

Descriptive Statistics									
Statistics of wound contraction rates treated with Laponite ± VEGF in healthy mice									
Day	**0.0 µg/ml**			**0.1 µg/ml**			**1.0 µg/ml**		
	Mean & SD (%)		***n***	**Mean & SD (%)**		***n***	**Mean & SD (%)**		***n***
5	76.7	± 11.4	3	66.1	± 7.2	3	77.1	± 15.3	3
7	65.8	± 0.1	2	79.6	± 20.8	2	70.9	± 2.7	2
11	32.6	± 6.7	3	42.6	± 17.2	3	36.1	± 22.9	3

Table 6.30. Statistics of wound contraction rates treated with Laponite ± VEGF in healthy mice.

Descriptive Statistics				
Differences between wound contraction rates treated with Laponite ±				
Day	**VEGF Concentration (µg/ml)**	**Mean Diff. & SE (%)**	**95% CI (%)**	***p***
5	1.0 vs. 0.1	10.6 ± 9.8	-14.03 to 35.14	0.5352
	1.0 vs. 0.0	-0.5 ± 9.8	-25.08 to 24.09	0.9986
	0.1 vs. 0.0	-11.1 ± 9.8	-35.64 to 13.53	0.5049
7	1.0 vs. 0.1	-13.8 ± 12.0	-43.9 to 16.32	0.4926
	1.0 vs. 0.0	-5.1 ± 12.0	-35.25 to 24.97	0.9034
	0.1 vs. 0.0	8.6 ± 12.0	-21.46 to 38.76	0.7523
11	1.0 vs. 0.1	-10.0 ± 9.8	-34.54 to 14.63	0.5724
	1.0 vs. 0.0	-3.4 ± 9.8	-28.01 to 21.16	0.9346
	0.1 vs. 0.0	6.5 ± 9.8	-18.05 to 31.12	0.7833

Table 6.31. Differences between wound contraction rates treated with Laponite ± VEGF in healthy mice.

C.5 Mean Re-epithelialisation Rates Measured using Histological Sections

Descriptive Statistics									
Statistics of wound re-epithelialisation rates treated with Laponite ± VEGF in healthy mice									
Day	**0.0 µg/ml**			**0.1 µg/ml**			**1.0 µg/ml**		
	Mean & SD (%)		***n***	**Mean & SD (%)**		***n***	**Mean & SD (%)**		***n***
5	6.1	± 3.6	3	14.7	± 4.4	3	13.1	± 11.9	3
7	18.0	± 0.1	2	9.6	± 4.2	2	3.9	± 5.5	2
11	73.8	± 27.9	3	68.2	± 28.6	3	66.7	± 57.7	3

Table 6.32. Statistics of wound re-epithelialisation rates treated with Laponite ± VEGF in healthy mice.

Descriptive Statistics				
Differences between wound re-epithelialisation rates treated with Laponite ± VEGF in healthy mice				
Day	**VEGF Concentration (µg/ml)**	**Mean Diff. & SE (%)**	**95% CI (%)**	***p***
5	1.0 vs. 0.1	-8.6 ± 18.0	-54.05 to 36.89	0.8835
	1.0 vs. 0.0	-7.1 ± 18.0	-52.52 to 38.42	0.9195
	0.1 vs. 0.0	1.5 ± 18.0	-43.94 to 47	0.9961
7	1.0 vs. 0.1	8.5 ± 22.1	-47.2 to 64.18	0.9221
	1.0 vs. 0.0	14.2 ± 22.1	-41.5 to 69.88	0.7987
	0.1 vs. 0.0	5.7 ± 22.1	-49.99 to 61.39	0.9641
11	1.0 vs. 0.1	5.6 ± 18.0	-39.88 to 51.06	0.9486
	1.0 vs. 0.0	7.2 ± 18.0	-38.31 to 52.63	0.9172
	0.1 vs. 0.0	1.6 ± 18.0	-43.9 to 47.04	0.9958

Table 6.33. Differences between wound re-epithelialisation rates treated with Laponite ± VEGF in healthy mice.

C.6 Mean Chalkley Counts of Wounds Treated with Laponite ±VEGF

Descriptive Statistics									
Statistics of Chalkley counts with wounds treated with Laponite ± VEGF in healthy mice									
Day	**0.0 µg/ml**			**0.1 µg/ml**			**1.0 µg/ml**		
	Mean & SD (Chalkley Count)		***n***	**Mean & SD (Chalkley Count)**		***n***	**Mean & SD (Chalkley Count)**		***n***
5	7.4	± 3.5	5	5.3	± 1.2	3	7.8	± 1.1	3
7	6.2	± 0.1	2	6.2	± 4.5	2	7.0	± 1.4	2
11	8.0	± 1.0	5	7.2	± 1.6	3	7.0	± 2.1	3

Table 6.34. Statistics of Chalkley counts with wounds treated with Laponite ± VEGF in healthy mice.

Descriptive Statistics				
Differences between Chalkley counts with wounds treated with Laponite ± VEGF in healthy mice				
Day	**VEGF Concentration (µg/ml)**	**Mean Diff. & SE (Chalkley Count)**	**95% CI (Chalkley Count)**	***p***
5	1.0 vs. 0.1	2.1 ± 1.6	-2.005 to 6.245	0.4093
	1.0 vs. 0.0	-0.3 ± 1.6	-4.471 to 3.778	0.9752
	0.1 vs. 0.0	-2.5 ± 1.8	-7.078 to 2.145	0.3815
7	1.0 vs. 0.1	0.1 ± 2.2	-5.598 to 5.698	0.9997
	1.0 vs. 0.0	-0.8 ± 2.2	-6.448 to 4.848	0.9314
	0.1 vs. 0.0	-0.9 ± 2.2	-6.498 to 4.798	0.9229
11	1.0 vs. 0.1	0.8 ± 1.6	-3.331 to 4.918	0.8775
	1.0 vs. 0.0	0.9 ± 1.6	-3.198 to 5.051	0.8371
	0.1 vs. 0.0	0.1 ± 1.8	-4.478 to 4.745	0.9970

Table 6.35. Differences between Chalkley counts with wounds treated with Laponite ± VEGF in healthy mice.

C.7 Data Tables of Angiogenic Blinded Scores of Harvested Subcutaneous Laponite Gels ± VEGF in Healthy Mice

C.7.1 Individual Volunteer Scores

Descriptive Statistics

Statistics of mean individual volunteer angiogenic blinded scores of harvested subcutaneous Laponite gels ± VEGF in healthy mice

Volunteer Number	Day	0 µg/ml		1 µg/ml		10 µg/ml		40 µg/ml	
		Mean & SD (Angiogenic Score)	n	Mean & SD (Angiogenic Score)	n	Mean & SD (Angiogenic Score)	n	Mean & SD (Angiogenic Score)	n
1	7	2.0 ± 1.2	4	2.3 ± 0.6	3	2.0 ± 0.0	3	3.0 ± 1.7	3
	14	1.8 ± 1.1	5	2.7 ± 1.5	3	2.3 ± 1.2	3	1.0 ± 0.0	3
	21	1.8 ± 1.6	13	2.7 ± 1.4	11	4.5 ± 1.5	8	4.4 ± 2.0	11
2	7	1.3 ± 0.5	4	2.3 ± 0.6	3	1.7 ± 1.2	3	2.7 ± 2.5	3
	14	1.4 ± 0.5	5	1.0 ± 1.0	3	2.0 ± 1.7	3	2.3 ± 0.6	3
	21	1.4 ± 0.9	13	1.5 ± 1.4	11	3.3 ± 1.4	8	4.4 ± 1.3	11
3	7	0.8 ± 0.5	4	1.0 ± 0.6	3	1.0 ± 1.7	3	2.0 ± 2.0	3
	14	1.0 ± 0.7	5	1.3 ± 1.2	3	1.3 ± 1.5	3	2.0 ± 1.0	3
	21	1.4 ± 1.3	13	3.5 ± 1.0	11	3.5 ± 1.5	8	4.5 ± 1.7	11
4	7	1.5 ± 0.6	4	1.3 ± 0.6	3	2.0 ± 1.0	3	1.7 ± 0.6	3
	14	1.8 ± 0.8	5	2.3 ± 0.6	3	1.3 ± 0.6	3	1.3 ± 0.6	3
	21	2.2 ± 1.0	13	1.7 ± 0.8	11	1.8 ± 0.9	8	1.7 ± 0.6	11
5	7	0.3 ± 0.5	4	2.0 ± 1.0	3	0.7 ± 1.2	3	1.3 ± 0.6	3
	14	0.4 ± 0.5	5	0.3 ± 0.6	3	0.7 ± 1.2	3	0.7 ± 1.2	3
	21	0.8 ± 1.2	13	0.8 ± 1.0	11	3.1 ± 2.3	8	4.7 ± 1.8	11

Table 6.36. Statistics of mean individual volunteer angiogenic blinded scores of harvested subcutaneous Laponite gels ± VEGF in healthy mice.

Descriptive Statistics Statistics of mean individual volunteer angiogenic blinded scores of harvested subcutaneous alginate gels ± VEGF in healthy mice								
Volunteer Number	Day	0 µg/ml		1 µg/ml		10 µg/ml		40 µg/ml	
		Mean & SD (Angiogenic Score)	*n*	Mean & SD (Angiogenic Score)	*n*	Mean & SD (Angiogenic Score)	*n*	Mean & SD (Angiogenic Score)	*n*
1	21	2.2 ± 1.3	5	2.0 ± 2.0	6	2.4 ± 1.7	5	2.5 ± 1.2	6
2		1.0 ± 1.0	5	0.8 ± 0.8	6	1.0 ± 1.4	5	2.2 ± 0.8	6
3		1.0 ± 0.7	5	1.2 ± 1.0	6	0.6 ± 0.9	5	1.8 ± 0.8	6
4		1.2 ± 0.4	5	0.8 ± 0.4	6	1.0 ± 0.0	5	1.0 ± 0.0	6
5		1.4 ± 0.9	5	0.8 ± 0.4	6	2.4 ± 1.5	5	1.2 ± 0.9	5

Table 6.37. Statistics of mean individual volunteer angiogenic blinded scores of harvested subcutaneous alginate gels ± VEGF in healthy mice.

C.7.2 Mean Blinded Scores

Descriptive Statistics Statistics of mean angiogenic blinded scores of harvested subcutaneous Laponite gels ± VEGF in healthy mice								
Day	0 µg/ml		1 µg/ml		10 µg/ml		40 µg/ml	
	Mean & SD (Angiogenic Score)	*n*	Mean & SD (Angiogenic Score)	*n*	Mean & SD (Angiogenic Score)	*n*	Mean & SD (Angiogenic Score)	*n*
7	1.2 ± 0.5	4	1.9 ± 0.5	3	1.5 ± 1.0	3	2.1 ± 1.2	3
14	1.3 ± 0.5	5	1.4 ± 0.9	3	1.5 ± 0.9	3	1.5 ± 0.4	3
21	1.5 ± 0.5	13	1.6 ± 0.7	11	3.2 ± 1.1	8	3.9 ± 1.0	11

Table 6.38. Statistics of mean angiogenic blinded scores of harvested subcutaneous Laponite gels ± VEGF in healthy mice.

Descriptive Statistics				
Differences between mean angiogenic blinded scores of harvested subcutaneous Laponite gels ± VEGF in healthy mice				
Day	**VEGF Concentration (µg/ml)**	**Mean Diff. & SE (Chalkley Count)**	**95% CI (Chalkley Count)**	***p***
7	1 vs 10	0.4 ± 0.6	-1.294 to 2.094	0.9238
	1 vs 40	-0.3 ± 0.6	-1.961 to 1.428	0.9755
	1 vs 0	0.7 ± 0.6	-0.8683 to 2.302	0.6318
	10 vs 40	-0.7 ± 0.6	-2.361 to 1.028	0.7264
	10 vs 0	0.3 ± 0.6	-1.268 to 1.902	0.9518
	40 vs 0	1.0 ± 0.6	-0.6016 to 2.568	0.3641
14	1 vs 10	-0.1 ± 0.6	-1.828 to 1.561	0.9968
	1 vs 40	-0.1 ± 0.6	-1.761 to 1.628	0.9996
	1 vs 0	0.1 ± 0.6	-1.396 to 1.636	0.9967
	10 vs 40	0.1 ± 0.6	-1.628 to 1.761	0.9996
	10 vs 0	0.3 ± 0.6	-1.262 to 1.769	0.9709
	40 vs 0	0.2 ± 0.6	-1.329 to 1.702	0.9879
21	1 vs 10	-1.6 ± 0.4	-2.571 to -0.6426	0.0003
	1 vs 40	-2.3 ± 0.3	-3.212 to -1.442	<0.0001
	1 vs 0	0.1 ± 0.3	-0.7243 to 0.976	0.9794
	10 vs 40	-0.7 ± 0.4	-1.685 to 0.2438	0.2088
	10 vs 0	1.7 ± 0.4	0.8002 to 2.665	<0.0001
	40 vs 0	2.5 ± 0.3	1.603 to 3.303	<0.0001

Table 6.39. Differences between mean angiogenic blinded scores of harvested subcutaneous Laponite gels ± VEGF in healthy mice.

Descriptive Statistics								
Statistics of mean angiogenic blinded scores of harvested subcutaneous Laponite gels ± VEGF in healthy mice after 21 days								
Biomaterial	**0 µg/ml**		**1 µg/ml**		**10 µg/ml**		**40 µg/ml**	
	Mean & SD (Angiogenic Score)	***n***	**Mean & SD (Angiogenic Score)**	***n***	**Mean & SD (Angiogenic Score)**	***n***	**Mean & SD (Angiogenic Score)**	***n***
Laponite	1.5 ± 0.5	13	1.6 ± 0.7	11	3.2 ± 1.1	8	3.9 ± 1.0	11
Alginate	1.4 ± 0.5	5	1.1 ± 0.3	6	1.5 ± 0.5	5	1.7 ± 0.4	6

Table 6.40. Statistics of mean angiogenic blinded scores of harvested subcutaneous Laponite/alginate gels ± VEGF in healthy mice after 21 days.

Descriptive Statistics						
Differences between mean angiogenic score of harvested subcutaneous Laponite gels after 21 days in healthy mice						
Treatment	**Mean Diff. & SE (Angiogenic Score)**			**95% CI (Angiogenic Score)**	***p***	**Significance**
Laponite 1 µg/ml vs. Laponite 10 µg/ml	-1.6	±	0.3	-2.634 to -0.5794	0.0002	***
Laponite 1 µg/ml vs. Laponite 40 µg/ml	-2.3	±	0.3	-3.27 to -1.384	<0.0001	****
Laponite 1 µg/ml vs. Laponite 0 µg/ml	0.1	±	0.3	-0.78 to 1.032	0.9998	ns
Laponite 1 µg/ml vs. Alginate 1 µg/ml	0.5	±	0.4	-0.6374 to 1.607	0.8714	ns
Laponite 1 µg/ml vs. Alginate 10 µg/ml	0.1	±	0.4	-1.054 to 1.331	>0.9999	ns
Laponite 1 µg/ml vs. Alginate 40 µg/ml	-0.1	±	0.4	-1.237 to 1.007	>0.9999	ns
Laponite 1 µg/ml vs. Alginate 0 µg/ml	0.3	±	0.4	-0.9344 to 1.451	0.9972	ns
Laponite 10 µg/ml vs. Laponite 40 µg/ml	-0.7	±	0.3	-1.748 to 0.307	0.3637	ns
Laponite 10 µg/ml vs. Laponite 0 µg/ml	1.7	±	0.3	0.7391 to 2.726	<0.0001	****
Laponite 10 µg/ml vs. Alginate 1 µg/ml	2.1	±	0.4	0.8975 to 3.286	<0.0001	****
Laponite 10 µg/ml vs. Alginate 10 µg/ml	1.7	±	0.4	0.4844 to 3.006	0.0014	**
Laponite 10 µg/ml vs. Alginate 40 µg/ml	1.5	±	0.4	0.2975 to 2.686	0.0053	**
Laponite 10 µg/ml vs. Alginate 0 µg/ml	1.9	±	0.4	0.6044 to 3.126	0.0005	***
Laponite 40 µg/ml vs. Laponite 0 µg/ml	2.5	±	0.3	1.547 to 3.359	<0.0001	****
Laponite 40 µg/ml vs. Alginate 1 µg/ml	2.8	±	0.4	1.69 to 3.934	<0.0001	****
Laponite 40 µg/ml vs. Alginate 10 µg/ml	2.5	±	0.4	1.273 to 3.658	<0.0001	****
Laponite 40 µg/ml vs. Alginate 40 µg/ml	2.2	±	0.4	1.09 to 3.334	<0.0001	****
Laponite 40 µg/ml vs. Alginate 0 µg/ml	2.6	±	0.4	1.393 to 3.778	<0.0001	****
Laponite 0 µg/ml vs. Alginate 1 µg/ml	0.4	±	0.3	-0.7323 to 1.45	0.9669	ns
Laponite 0 µg/ml vs. Alginate 10 µg/ml	0.0	±	0.4	-1.151 to 1.176	>0.9999	ns
Laponite 0 µg/ml vs. Alginate 40 µg/ml	-0.2	±	0.3	-1.332 to 0.8503	0.9968	ns
Laponite 0 µg/ml vs. Alginate 0 µg/ml	0.1	±	0.4	-1.031 to 1.296	>0.9999	ns
Alginate 1 µg/ml vs. Alginate 10 µg/ml	-0.3	±	0.4	-1.686 to 0.9923	0.9916	ns
Alginate 1 µg/ml vs. Alginate 40 µg/ml	-0.6	±	0.4	-1.877 to 0.6766	0.8153	ns
Alginate 1 µg/ml vs. Alginate 0 µg/ml	-0.2	±	0.4	-1.566 to 1.112	0.9994	ns
Alginate 10 µg/ml vs. Alginate 40 µg/ml	-0.3	±	0.4	-1.592 to 1.086	0.9988	ns
Alginate 10 µg/ml vs. Alginate 0 µg/ml	0.1	±	0.4	-1.278 to 1.518	>0.9999	ns
Alginate 40 µg/ml vs. Alginate 0 µg/ml	0.4	±	0.4	-0.9656 to 1.712	0.9870	ns

Table 6.41. Differences between mean angiogenic score of harvested subcutaneous Laponite/alginate gels after 21 days in healthy mice.

C.8 Cellularity Data Tables (Subcutaneous Injection Study)

Descriptive Statistics												
Statistics of mean cellularity data measured from harvested subcutaneous Laponite/alginate gels after 21 days in healthy mice												
Biomaterial	**0 µg/ml**				**1 µg/ml**				**10 µg/ml**				**40 µg/ml**			
	Mean & SD (Cellularity %)			***n***	**Mean & SD (Cellularity %)**			***n***	**Mean & SD (Cellularity %)**			***n***	**Mean & SD (Cellularity %)**			***n***
Laponite	6.5	±	4.7	3	7.4	±	4.2	6	9.2	±	9.0	5	18.4	±	9.7	7
Alginate	1.0	±	0.4	3	1.8	±	0.7	3	1.4	±	0.7	3	2.1	±	0.6	3

Table 6.42. Statistics of mean cellularity data measured from harvested subcutaneous Laponite/alginate gels after 21 days in healthy mice

Descriptive Statistics					
Differences between mean cellularity data measured from harvested subcutaneous Laponite gels after 21 days in healthy mice					
VEGF Concentration (µg/ml)	**Mean & SE (Cellularity %)**			**95% CI (Cellularity %)**	***p***	**Sign.**
0 vs 1	-0.8	±	4.5	-12.41 to 10.71	0.9952	ns
0 vs 10	-2.7	±	4.7	-14.75 to 9.393	0.8954	ns
0 vs 40	-11.9	±	4.4	-23.04 to -0.6853	0.0363	*

Table 6.43. Differences between mean cellularity data measured from harvested subcutaneous Laponite gels after 21 days in healthy mice.

C.9 Chalkley Analysis (Subcutaneous Injection Study)

Descriptive Statistics								
Statistics of mean Chalkley scores of harvested subcutaneous Laponite/alginate gels ± VEGF in healthy mice after 21 days								
Biomaterial	**0 µg/ml**			**1 µg/ml**			**10 µg/ml**			**40 µg/ml**		
	Mean & SD (Angiogenic Score)		***n***	**Mean & SD (Angiogenic Score)**		***n***	**Mean & SD (Angiogenic Score)**		***n***	**Mean & SD (Angiogenic Score)**		***n***
Laponite	4.0	± 0.8	4	2.7	± 1.4	4	4.5	± 4.1	4	8.8	± 1.4	7
Alginate	0.0	± 0.0	3	0.0	± 0.0	3	0.2	± 0.3	3	0.0	± 0.0	3

Table 6.44. Statistics of mean Chalkley scores of harvested subcutaneous Laponite/alginate gels ± VEGF in healthy mice after 21 days.

Descriptive Statistics						
Differences between mean Chalkley scores of harvested subcutaneous Laponite/alginate gels ± VEGF in healthy mice after 21 days						
Treatment	**Mean Diff. & SE (Angiogenic Score)**			**95% CI (Angiogenic Score)**	***p***	**Sign.**
Laponite:Vehicle vs. Laponite:1 µg/ml	1.3	±	1.2	-2.797 to 5.397	0.9599	ns
Laponite:Vehicle vs. Laponite:10 µg/ml	-0.6	±	1.2	-4.647 to 3.547	0.9998	ns
Laponite:Vehicle vs. Laponite:40 µg/ml	-4.9	±	1.1	-8.482 to -1.218	0.0039	**
Laponite:Vehicle vs. Alginate:Vehicle	4.0	±	1.3	-0.4755 to 8.376	0.1041	ns
Laponite:Vehicle vs. Alginate:1 µg/ml	4.0	±	1.3	-0.4755 to 8.376	0.1041	ns
Laponite:Vehicle vs. Alginate:10 µg/ml	3.8	±	1.3	-0.6755 to 8.176	0.1390	ns
Laponite:Vehicle vs. Alginate:40 µg/ml	4.0	±	1.3	-0.4755 to 8.376	0.1041	ns
Laponite:1 µg/ml vs. Laponite:10 µg/ml	-1.9	±	1.2	-5.947 to 2.247	0.7991	ns
Laponite:1 µg/ml vs. Laponite:40 µg/ml	-6.2	±	1.1	-9.782 to -2.518	0.0002	***
Laponite:1 µg/ml vs. Alginate:Vehicle	2.7	±	1.3	-1.776 to 7.076	0.5085	ns
Laponite:1 µg/ml vs. Alginate:1 µg/ml	2.7	±	1.3	-1.776 to 7.076	0.5085	ns
Laponite:1 µg/ml vs. Alginate:10 µg/ml	2.5	±	1.3	-1.976 to 6.876	0.6011	ns
Laponite:1 µg/ml vs. Alginate:40 µg/ml	2.7	±	1.3	-1.776 to 7.076	0.5085	ns
Laponite:10 µg/ml vs. Laponite:40 µg/ml	-4.3	±	1.1	-7.932 to -0.6682	0.0128	*
Laponite:10 µg/ml vs. Alginate:Vehicle	4.5	±	1.3	0.0745 to 8.926	0.0444	*
Laponite:10 µg/ml vs. Alginate:1 µg/ml	4.5	±	1.3	0.0745 to 8.926	0.0444	*
Laponite:10 µg/ml vs. Alginate:10 µg/ml	4.3	±	1.3	-0.1255 to 8.726	0.0610	ns
Laponite:10 µg/ml vs. Alginate:40 µg/ml	4.5	±	1.3	0.0745 to 8.926	0.0444	*
Laponite:40 µg/ml vs. Alginate:Vehicle	8.8	±	1.2	4.802 to 12.8	<0.0001	****
Laponite:40 µg/ml vs. Alginate:1 µg/ml	8.8	±	1.2	4.802 to 12.8	<0.0001	****
Laponite:40 µg/ml vs. Alginate:10 µg/ml	8.6	±	1.2	4.602 to 12.6	<0.0001	****
Laponite:40 µg/ml vs. Alginate:40 µg/ml	8.8	±	1.2	4.802 to 12.8	<0.0001	****
Alginate:Vehicle vs. Alginate:1 µg/ml	0.0	±	1.4	-4.731 to 4.731	>0.9999	ns
Alginate:Vehicle vs. Alginate:10 µg/ml	-0.2	±	1.4	-4.931 to 4.531	>0.9999	ns
Alginate:Vehicle vs. Alginate:40 µg/ml	0.0	±	1.4	-4.731 to 4.731	>0.9999	ns
Alginate:1 µg/ml vs. Alginate:10 µg/ml	-0.2	±	1.4	-4.931 to 4.531	>0.9999	ns
Alginate:1 µg/ml vs. Alginate:40 µg/ml	0.0	±	1.4	-4.731 to 4.731	>0.9999	ns
Alginate:10 µg/ml vs. Alginate:40 µg/ml	0.2	±	1.4	-4.531 to 4.931	>0.9999	ns

Table 6.45. Differences between mean Chalkley scores of harvested subcutaneous Laponite/alginate gels ± VEGF in healthy mice after 21 days.

C.10 Data Values of % VEGF Released from Laponite/alginate Gels Using an ELISA

Descriptive Statistics								
Statistics of mean % of VEGF release from Laponite/alginate gels measured by ELISA analysis								
Day	**PBS + 40 µg/ml VEGF**			**Laponite + 40 µg/ml VEGF**			**Alginate + 40 µg/ml VEGF**	
	Mean & SD (% Release)		***n***	**Mean & SD (% Release)**		***n***	**Mean & SD (% Release)**	***n***
0.5	47.4	± 24.7	3	Data not measured			20.4 ± 2.1	2
1.0	100.0	± 46.7	3	0.8	± 1.5	3	77.5 ± 6.6	3
21.0	68.4	± 15.0	3	0.3	± 0.4	3	45.1 ± 25.8	3

Table 6.46. Statistics of mean % of VEGF release from Laponite/alginate gels measured by ELISA analysis.

Descriptive Statistics				
Differences between mean % of VEGF release from Laponite/alginate gels after 21 days measured by ELISA analysis				
Treatment	**Mean Diff. & SE (%**	**95% CI (% Release)**	***p***	**Significance**
Laponite vs Alginate	-44.8 ± 14.1	-88.07 to -1.596	0.0435	*
Laponite vs PBS	-68.1 ± 14.1	-111.3 to -24.84	0.0069	**
Alginate vs PBS	-23.3 ± 14.1	-66.48 to 19.99	0.2977	ns

Table 6.47. Differences between mean % of VEGF release from Laponite/alginate gels after 21 days measured by ELISA analysis.

Appendix D:

Data Tables & Statistics for

Chapter 5

D.1 Blood Glucose Measurements

D.1.1 Fasted vs Non-Fasted

Descriptive Statistics				
Group Statistics				
Test Group	***n***	**Mean & SD (mmol/l)**	**95% CI (mmol/l)**	
			Lower	**Upper**
Fasted	8	21.6 ± 8.4	14.6	28.7
Non-Fasted	12	23.8 ± 4.6	20.5	27.0

Table 6.48. Data table showing the mean values of fasted vs non-fasted blood glucose measurements in *db/db* mice.

Descriptive Statistics			
Differences Between Fasted and Non-Fasted BG			
Mean & SD (mmol/l)	**95% CI (mmol/l)**	**% Difference**	***p***
2.1 ± 3.1	-4.4 - 8.7	9.9	0.4996

Table 6.49. Mean and % differences between fasted and non-fasted blood glucose levels in *db/db* mice.

D.1.2 Healthy vs Diabetic Mice Blood Glucose Level Data Tables

Descriptive Statistics				
Statistics of C57BL/6 Blood Glucose				
Day	***n***	**Mean & SD (mmol/l)**		
0	14	8.0	±	1.4
1	11	9.2	±	2.6
7	5	11.1	±	2.8
11	5	10.0	±	2.4

Table 6.50. Blood glucose levels of healthy (C57BL/6) mice overtime.

Descriptive Statistics				
Statistics of *db/db* Blood Glucose				
Day	***n***	**Mean & SD (mmol/l)**		
0	34	23.8	±	6.1
1	26	24.7	±	7.8
7	19	27.0	±	4.3
11	9	27.9	±	6.4

Table 6.51. Blood glucose levels of *db/db* mice overtime.

Descriptive Statistics				
Differences Between Healthy and Diabetic BG				
Day	**Mean & SE (mmol/l)**	**95% CI (mmol/l)**	**% Difference**	***p***
0	15.7 ± 1.8	11.3 - 20.2	196.0	<0.0001
1	15.5 ± 2.0	10.5 - 20.6	193.3	<0.0001
7	15.9 ± 2.8	8.8 - 22.9	197.4	<0.0001
11	17.9 ± 3.1	10.1 - 25.8	223.1	<0.0001

Table 6.52. Statistical differences of blood glucose levels between healthy and diabetic mice.

D.2 Weight Measurements

Descriptive Statistics		
Statistics of C57BL/6 Weight		
Day	***n***	**Mean & SD (g)**
0	14	23.9 ± 1.8
1	11	22.4 ± 1.8
7	5	22.7 ± 1.1
11	5	24.0 ± 0.5

Table 6.53. Body weight measurements of healthy (C57BL/6) mice overtime (wound healing study).

Descriptive Statistics		
Statistics of *db/db* Weight		
Day	***n***	**Mean & SD (g)**
0	37	38.3 ± 2.5
1	35	36.9 ± 2.6
7	13	37.5 ± 2.6
11	9	38.5 ± 2.4

Table 6.54. Body weight measurements of *db/db* mice overtime (wound healing study).

Descriptive Statistics				
Differences Between Healthy and Diabetic Weight				
Day	**Mean & SE (g)**	**95% CI (g)**	**% Difference**	***p***
0	14.5 ± 0.7	12.6 - 16.3	60.6	<0.0001
1	14.5 ± 0.8	12.5 - 16.6	60.8	<0.0001
7	14.8 ± 1.2	11.6 - 17.9	61.9	<0.0001
11	14.5 ± 1.3	11.2 - 17.8	60.8	<0.0001

Table 6.55. Statistical difference between body weight of healthy and diabetic mice during wound studies.

D.3 Data Tables of Wound Closure Rates

Descriptive Statistics								
Statistics of wound closure treated with Laponite between healthy and diabetic mice								
Day	**C57BL/6 Mice**				***db/db* Mice**			
	Mean & SD (%)			***n***	**Mean & SD (%)**			***n***
1	79.0	±	18.5	12	104.0	±	11.0	18
7	45.9	±	15.7	11	82.4	±	16.9	16
11	13.0	±	4.9	8	45.2	±	9.2	11

Table 6.56. Statistics of wound closure treated with Laponite between healthy and diabetic mice.

Descriptive Statistics					
Differences between healthy & diabetic wound closure (Laponite-treated)					
Day	**Mean & SE (%)**			**95% CI (%)**	***p***	**Significance**
1	-25.0	±	4.4	-36.16 to -13.86	<0.0001	****
5	-36.5	±	4.6	-48.18 to -24.74	<0.0001	****
11	-32.2	±	5.5	-46.08 to -18.28	<0.0001	****

Table 6.57. Differences between healthy & diabetic wound closure (Laponite-treated).

Descriptive Statistics			
Statistics of wound closure treated with PBS between healthy and diabetic mice after 7 days			
MF1 Mice		***db/db* Mice**	
Mean & SD (%)	***n***	**Mean & SD (%)**	***n***
47.9 ± 14.4	3	64.8 ± 10.5	8

Table 6.58. Statistics of wound closure treated with PBS between healthy and diabetic mice after 7 days.

Descriptive Statistics			
Differences between healthy & diabetic wound closure (Laponite-treated)			
Mean & SE (%)	**95% CI (%)**	***p***	**Significance**
17.0 ± 7.8	-0.6336 to 34.55	0.0571	ns

Table 6.59. Differences between healthy & diabetic wound closure (Laponite-treated).

Descriptive Statistics								
Statistics of wound closure at rostral regions in *db/db* mice								
Day	**Laponite-VEGF**		**Laponite-Vehicle**		**Alginate-VEGF**		**Alginate-Vehicle**	
	Mean & SD (%)	***n***	**Mean & SD (%)**	***n***	**Mean & SD (%)**	***n***	**Mean & SD (%)**	***n***
1	83.2 ± 18.8	6	97.7 ± 17.8	6	88.4 ± 5.9	3	89.4 ± 4.6	3
11	43.4 ± 20.7	6	40.4 ± 15.1	6	33.5 ± 10.0	3	46.1 ± 9.7	3
14	27.4 ± 10.7	6	23.6 ± 4.0	5	13.9 ± 0.6	2	37.3 ± 7.3	3
18	20.2 ± 4.5	3	29.6 ± 7.2	3	16.1 ± 9.5	3	25.4 ± 15.0	3

Table 6.60. Statistics of wound closure at rostral regions in *db/db* mice.

Descriptive Statistics												
Statistics of wound closure at caudal regions in *db/db* mice												
Day	**Laponite-VEGF**				**Laponite-Vehicle**				**Alginate-VEGF**				**Alginate-Vehicle**			
	Mean & SD (%)			***n***	**Mean & SD (%)**			***n***	**Mean & SD (%)**			***n***	**Mean & SD (%)**			***n***
1	89.1	±	16.4	6	97.0	±	12.8	5	87.8	±	9.7	3	110.9	±	7.0	3
11	43.3	±	13.2	6	42.9	±	11.3	5	28.5	±	6.9	3	59.6	±	16.7	3
14	31.5	±	11.7	6	33.6	±	13.8	4	14.5	±	4.4	2	44.0	±	18.1	3
18	21.6	±	7.0	3	23.4	±	4.1	2	21.0	±	9.3	3	33.4	±	18.5	3

Table 6.61. Statistics of wound closure at caudal regions in *db/db* mice.

Descriptive Statistics																				
Statistics of wound closure at in *db/db* mice (rostral & caudal combined means)																				
Day	**Laponite-VEGF**				**Laponite-Vehicle**				**Alginate-VEGF**				**Alginate-Vehicle**				**PBS Control**			
	Mean & SD (%)			***n***	**Mean & SD (%)**			***n***	**Mean & SD (%)**			***n***	**Mean & SD (%)**			***n***	**Mean & SD (%)**			***n***
1	86.1	±	17.1	12	97.4	±	14.9	11	88.1	±	7.2	6	100.1	±	12.9	6	102.3	±	11.0	18
11	43.3	±	16.6	12	41.6	±	12.9	11	31.0	±	8.1	6	52.8	±	14.3	6	46.2	±	12.9	12
14	29.5	±	10.9	12	28.1	±	10.3	9	14.2	±	2.6	4	40.6	±	12.9	6	23.3	±	15.8	12
18	20.9	±	5.3	6	27.1	±	6.5	5	18.5	±	8.8	6	29.4	±	15.7	6	21.5	±	13.8	6

Table 6.62. Statistics of wound closure at in *db/db* mice (rostral & caudal combined means).

Descriptive Statistics

Differences of wound closure rates between Laponite, alginate (± VEGF) and PBS treatments (rostral wounds)

Day	Treatment	Mean Diff & SE (%)	95% CI (%)	*p*	Sign.
1	Laponite-VEGF vs. Laponite Vehicle	-14.5 ± 6.8	-32.51 to 3.513	ns	0.1565
	Laponite-VEGF vs. Alginate-VEGF	-5.2 ± 8.4	-27.3 to 16.83	ns	0.9232
	Laponite-VEGF vs. Alginate Vehicle	-6.2 ± 8.4	-28.24 to 15.88	ns	0.8808
	Laponite Vehicle vs. Alginate-VEGF	9.3 ± 8.4	-12.8 to 31.33	ns	0.6855
	Laponite Vehicle vs. Alginate Vehicle	8.3 ± 8.4	-13.74 to 30.38	ns	0.7523
	Alginate-VEGF vs. Alginate Vehicle	-0.9 ± 9.6	-26.42 to 24.53	ns	0.9997
11	Laponite-VEGF vs. Laponite Vehicle	3.0 ± 6.8	-15.04 to 20.98	ns	0.9721
	Laponite-VEGF vs. Alginate-VEGF	9.9 ± 8.4	-12.16 to 31.96	ns	0.6387
	Laponite-VEGF vs. Alginate Vehicle	-2.7 ± 8.4	-24.76 to 19.36	ns	0.9883
	Laponite Vehicle vs. Alginate-VEGF	6.9 ± 8.4	-15.13 to 28.99	ns	0.8405
	Laponite Vehicle vs. Alginate Vehicle	-5.7 ± 8.4	-27.73 to 16.39	ns	0.9049
	Alginate-VEGF vs. Alginate Vehicle	-12.6 ± 9.6	-38.07 to 12.88	ns	0.563
14	Laponite-VEGF vs. Laponite Vehicle	3.8 ± 7.2	-15.09 to 22.69	ns	0.9512
	Laponite-VEGF vs. Alginate-VEGF	13.5 ± 9.6	-11.95 to 39	ns	0.5029
	Laponite-VEGF vs. Alginate Vehicle	-9.8 ± 8.4	-31.9 to 12.23	ns	0.6435
	Laponite Vehicle vs. Alginate-VEGF	9.7 ± 9.9	-16.38 to 35.83	ns	0.7592
	Laponite Vehicle vs. Alginate Vehicle	-13.6 ± 8.6	-36.42 to 9.148	ns	0.3973
	Alginate-VEGF vs. Alginate Vehicle	-23.4 ± 10.8	-51.85 to 5.118	ns	0.1443
18	Laponite-VEGF vs. Laponite Vehicle	-9.4 ± 9.6	-34.9 to 16.05	ns	0.7633
	Laponite-VEGF vs. Alginate-VEGF	4.1 ± 9.6	-21.4 to 29.55	ns	0.9744
	Laponite-VEGF vs. Alginate Vehicle	-5.2 ± 9.6	-30.67 to 20.28	ns	0.9492
	Laponite Vehicle vs. Alginate-VEGF	13.5 ± 9.6	-11.97 to 38.98	ns	0.5047
	Laponite Vehicle vs. Alginate Vehicle	4.2 ± 9.6	-21.25 to 29.7	ns	0.9717
	Alginate-VEGF vs. Alginate Vehicle	-9.3 ± 9.6	-34.75 to 16.2	ns	0.7717

Table 6.63. Differences of wound closure rates between Laponite, alginate (± VEGF) and PBS treatments (rostral wounds).

Descriptive Statistics

Differences of wound closure rates between Laponite, alginate (± VEGF) and PBS treatments (caudal wounds)

Day	Treatment	Mean Diff & SE (%)	95% CI (%)	*p*	Sign.
1	Laponite-VEGF vs. Laponite Vehicle	-8.0 ± 6.8	-25.98 to 10.06	0.6488	ns
	Laponite-VEGF vs. Alginate-VEGF	1.3 ± 8.0	-19.77 to 22.32	0.9985	ns
	Laponite-VEGF vs. Alginate Vehicle	-21.8 ± 8.0	-42.83 to -0.7378	0.0398	*
	Laponite Vehicle vs. Alginate-VEGF	9.2 ± 8.2	-12.5 to 30.97	0.6760	ns
	Laponite Vehicle vs. Alginate Vehicle	-13.8 ± 8.2	-35.56 to 7.911	0.3419	ns
	Alginate-VEGF vs. Alginate Vehicle	-23.1 ± 9.2	-47.36 to 1.241	0.0688	ns
11	Laponite-VEGF vs. Laponite Vehicle	0.3 ± 6.8	-17.69 to 18.35	>0.9999	ns
	Laponite-VEGF vs. Alginate-VEGF	14.8 ± 8.0	-6.29 to 35.8	0.2587	ns
	Laponite-VEGF vs. Alginate Vehicle	-16.3 ± 8.0	-37.36 to 4.727	0.1815	ns
	Laponite Vehicle vs. Alginate-VEGF	14.4 ± 8.2	-7.308 to 36.16	0.3048	ns
	Laponite Vehicle vs. Alginate Vehicle	-16.7 ± 8.2	-38.38 to 5.089	0.1903	ns
	Alginate-VEGF vs. Alginate Vehicle	-31.1 ± 9.2	-55.37 to -6.772	0.0069	**
14	Laponite-VEGF vs. Laponite Vehicle	-2.0 ± 7.3	-21.25 to 17.17	0.9922	ns
	Laponite-VEGF vs. Alginate-VEGF	17.0 ± 9.2	-7.271 to 41.33	0.2591	ns
	Laponite-VEGF vs. Alginate Vehicle	-12.4 ± 8.0	-33.46 to 8.63	0.4087	ns
	Laponite Vehicle vs. Alginate-VEGF	19.1 ± 9.7	-6.709 to 44.84	0.2162	ns
	Laponite Vehicle vs. Alginate Vehicle	-10.4 ± 8.6	-33.11 to 12.35	0.6242	ns
	Alginate-VEGF vs. Alginate Vehicle	-29.4 ± 10.3	-56.61 to -2.275	0.0287	*
18	Laponite-VEGF vs. Laponite Vehicle	-1.8 ± 10.3	-29.01 to 25.33	0.9979	ns
	Laponite-VEGF vs. Alginate-VEGF	0.5 ± 9.2	-23.75 to 24.84	>0.9999	ns
	Laponite-VEGF vs. Alginate Vehicle	-11.9 ± 9.2	-36.15 to 12.45	0.5725	ns
	Laponite Vehicle vs. Alginate-VEGF	2.4 ± 10.3	-24.78 to 29.55	0.9955	ns
	Laponite Vehicle vs. Alginate Vehicle	-10.0 ± 10.3	-37.18 to 17.16	0.7642	ns
	Alginate-VEGF vs. Alginate Vehicle	-12.4 ± 9.2	-36.7 to 11.9	0.5355	ns

Table 6.64. Differences of wound closure rates between Laponite, alginate (± VEGF) and PBS treatments (caudal wounds).

D.4 Epithelial Thickness Data Tables

Descriptive Statistics								
Statistics of re-epithelialisation rates treated with vehicle Laponite gels in *db/db* mice								
Day	**Rostral**				**Caudal**			
	Mean & SD (µm)			***n***	**Mean & SD (µm)**			***n***
14	76.2	±	14.6	3	60.7	±	14.9	3
18	56.5	±	28.9	3	70.6	±	23.0	3

Table 6.65. Statistics of epithelial thickness measured from wounds treated with vehicle Laponite gels/PBS in *db/db* mice (rostral & caudal combined means).

Descriptive Statistics							
Statistics of re-epithelialisation rates treated with in *db/db* mice							
Day	**Rostral**				**Caudal**		
	Mean & SD (µm)			***n***	**Mean & SD (µm)**		
14	32.6	±	9.0	3	40.4	±	29.0
18	46.0	±	10.0	3	67.1	±	17.9

Table 6.66. Differences of epithelial thickness between rostral and caudal regions treated with vehicle Laponite gels.

Descriptive Statistics

Differences of epithelial thickness between rostral and caudal regions treated with vehicle Laponite gels

Day	Mean Diff & SE(µm)	95% CI (µm)	*p*	Sign.
14	15.4 ± 17.3	-32.04 to 62.91	0.6382	ns
18	-14.0 ± 17.3	-61.51 to 33.44	0.6874	ns

Table 6.67. Differences of epithelial thickness between rostral and caudal regions treated with Laponite gels.

Descriptive Statistics

Differences of epithelial thickness between rostral and caudal regions treated with PBS

Day	Mean Diff & SE(µm)	95% CI (µm)	*p*	Sign.
14	-7.7 ± 15.0	-48.77 to 33.3	0.8550	ns
18	-21.1 ± 15.0	-62.14 to 19.94	0.3537	ns

Table 6.68. Differences of epithelial thickness between rostral and caudal regions treated with PBS.

Descriptive Statistics

Statistics of re-epithelialisation rates treated with vehicle Laponite gels/PBS in db/db mice (rostral & caudal combined means)

Day	Rostral		Caudal	
	Mean & SD (µm)	*n*	Mean & SD (µm)	*n*
14	68.5 ± 15.7	6	36.5 ± 19.7	6
18	63.6 ± 24.6	6	56.6 ± 17.4	6

Table 6.69. Differences of epithelial thickness between Laponite gels and PBS (rostral & caudal combined means)

Descriptive Statistics

Differences of epithelial thickness between Laponite & PBS treatments (rostral and caudal combined means)

Day	Mean Diff & SE(µm)	95% CI (µm)	*p*	Sign.
14	32.0 ± 11.3	4.587 to 59.31	0.0209	*
18	7.0 ± 11.3	-20.4 to 34.33	0.7932	ns

Table 6.70. Statistical differences of epithelial thickness between Laponite gels and PBS (rostral & caudal combined means).

D.5 Rates of Re-epithelialisation Data Tables

Descriptive Statistics

Statistics of re-epithelialisation rates at rostral regions in *db/db* mice

Day	Laponite-Vehicle		PBS	
	Mean & SD (%)	*n*	Mean & SD (%)	*n*
7	30.5 ± 16.8	2	16.9 ± 13.2	2
14	90.7 ± 16.2	3	80.0 ± 34.7	3
18	100.0 ± 0.0	3	47.0 ± 23.4	3

Table 6.71. Statistics of re-epithelialisation rates at rostral regions in *db/db* mice.

Descriptive Statistics								
Statistics of re-epithelialisation rates at caudal regions in *db/db* mice								
Day	**Laponite-Vehicle**				**PBS**			
	Mean & SD (%)			***n***	**Mean & SD (%)**			***n***
7	6.4	±	6.2	2	18.1	±	8.4	2
14	59.2	±	20.6	3	60.0	±	34.6	3
18	100.0	±	0.0	3	48.9	±	27.2	3

Table 6.72. Statistics of re-epithelialisation rates at caudal regions in *db/db* mice.

Descriptive Statistics					
Differences of re-epithelialisation rates between Laponite and PBS treatments (rostral & caudal wounds)					
Day	**Treatment**	**Mean Diff & SE (%)**	**95% CI (%)**	***p***	**Sign.**
7	3% Laponite (R) vs. PBS (R)	13.7 ± 19.7	-40.69 to 67.99	0.8988	ns
	3% Laponite (R) vs. 3% Laponite (C)	24.2 ± 19.7	-30.19 to 78.49	0.6169	ns
	3% Laponite (R) vs. PBS (C)	12.5 ± 19.7	-41.89 to 66.79	0.9207	ns
	PBS (R) vs. 3% Laponite (C)	10.5 ± 19.7	-43.84 to 64.84	0.9501	ns
	PBS (R) vs. PBS (C)	-1.2 ± 19.7	-55.54 to 53.14	>0.9999	ns
	3% Laponite (C) vs. PBS (C)	-11.7 ± 19.7	-66.04 to 42.64	0.9329	ns
14	3% Laponite (R) vs. PBS (R)	10.7 ± 16.1	-33.67 to 55.07	0.9091	ns
	3% Laponite (R) vs. 3% Laponite (C)	31.5 ± 16.1	-12.9 to 75.83	0.2322	ns
	3% Laponite (R) vs. PBS (C)	30.6 ± 16.1	-13.73 to 75	0.2527	ns
	PBS (R) vs. 3% Laponite (C)	20.8 ± 16.1	-23.6 to 65.13	0.5772	ns
	PBS (R) vs. PBS (C)	19.9 ± 16.1	-24.43 to 64.3	0.6088	ns
	3% Laponite (C) vs. PBS (C)	-0.8 ± 16.1	-45.2 to 43.53	>0.9999	ns
18	3% Laponite (R) vs. PBS (R)	53.0 ± 16.1	8.666 to 97.4	0.0150	*
	3% Laponite (R) vs. 3% Laponite (C)	0.0 ± 16.1	-44.37 to 44.37	>0.9999	ns
	3% Laponite (R) vs. PBS (C)	51.1 ± 16.1	6.7 to 95.43	0.0199	*
	PBS (R) vs. 3% Laponite (C)	-53.0 ± 16.1	-97.4 to -8.666	0.0150	*
	PBS (R) vs. PBS (C)	-2.0 ± 16.1	-46.33 to 42.4	0.9993	ns
	3% Laponite (C) vs. PBS (C)	51.1 ± 16.1	6.7 to 95.43	0.0199	*

Table 6.73. Differences of re-epithelialisation rates between Laponite and PBS treatments (rostral & caudal wounds).

Descriptive Statistics						
Differences of re-epithelialisation rates between Laponite and PBS treatments (rostral & caudal combined means)						
Day	**Mean Diff & SE (%)**			**95% CI (%)**	***p***	**Sign.**
7	1.0	±	13.7	-35.14 to 37.09	>0.9999	ns
14	4.9	±	11.2	-24.55 to 34.42	0.9869	ns
18	52.1	±	11.2	22.57 to 81.53	0.0002	***

Table 6.74. Differences of re-epithelialisation rates between Laponite and PBS treatments (rostral & caudal combined means).

D.6 Epithelial Thickness in *db/db* mice treated with Laponite ± VEGF

Descriptive Statistics								
Statistics of epithelial thickness treated Laponite ± VEGF in *db/db* mice (rostral & caudal combined means)								
Day	**VEGF**				**Vehicle**			
	Mean & SD (µm)			***n***	**Mean & SD (µm)**			***n***
14	43.8	±	16.9	6	62.1	±	28.3	5
18	57.6	±	21.0	6	48.2	±	23.0	6

Table 6.75. Statistics of epithelial thickness treated Laponite ± VEGF in *db/db* mice (rostral & caudal combined means).

Descriptive Statistics								
Statistics of epithelial thickness treated with Laponite-VEGF/alginate-VEGF in *db/db* mice (rostral & caudal combined means)								
Day	**VEGF**				**Vehicle**			
	Mean & SD (µm)			***n***	**Mean & SD (µm)**			***n***
14	57.6	±	21.0	6	48.2	±	23.0	6
18	44.1	±	25.0	3	59.6	±	14.7	3

Table 6.76. Statistics of epithelial thickness treated with Laponite-VEGF/alginate-VEGF in *db/db* mice (rostral & caudal combined means).

Descriptive Statistics					
Epithelial thickness differences between Laponite gels ± VEGF					
Day	**Mean Diff & SE(µm)**			**95% CI (µm)**	***p***	**Sign.**
14	-18.4	±	13.5	-51.21 to 14.47	0.3446	ns
18	9.5	±	12.9	-21.83 to 40.79	0.7204	ns

Table 6.77. Epithelial thickness differences between Laponite gels ± VEGF.

Descriptive Statistics

Epithelial thickness differences between Laponite-VEGF and alginate-VEGF

Day	Mean Diff & SE(µm)	95% CI (µm)	*p*	Sign.
14	9.5 ± 9.5	-21.75 to 40.72	0.7083	ns
18	-15.5 ± -15.5	-59.7 to 28.64	0.6323	ns

Table 6.78. Epithelial thickness differences between Laponite-VEGF and alginate-VEGF.

Descriptive Statistics

Statistics of re-epithelialisation rates in wounds treated with Laponite gels ± VEGF in *db/db* mice

Day	VEGF		Vehicle	
	Mean & SD (%)	*n*	Mean & SD (%)	*n*
14	86.6 ± 32.9	6	75.7 ± 33.5	5
18	95.0 ± 12.4	6	100.0 ± 0.0	6

Table 6.79. Statistics of re-epithelialisation rates in wounds treated with Laponite gels ± VEGF in *db/db* mice.

Descriptive Statistics								
Statistics of re-epithelialisation rates in wounds treated with Laponite ± VEGF and alginate ± VEGF in *db/db* mice after 18 days								
Day	**VEGF**				**Vehicle**			
	Mean & SD (%)			***n***	**Mean & SD (%)**			***n***
Laponite	95.0	±	12.4	6	100.0	±	0.0	6
Alginate	75.7	±	36.5	5	31.1	±	14.2	5

Table 6.80. Statistics of re-epithelialisation rates in wounds treated with Laponite ± VEGF and alginate ± VEGF in *db/db* mice after 18 days.

Descriptive Statistics				
Differences of re-epithelialisation rates between Laponite ± VEGF and alginate ± VEGF (rostral & caudal combined means) after 18 days				
Treatment	**Mean Diff & SE (%)**	**95% CI (%)**	***p***	**Sign.**
Laponite:VEGF vs. Laponite:Vehicle	-5.1 ± 11.3	-36.99 to 26.89	0.9694	ns
Laponite:VEGF vs. Alginate:VEGF	19.3 ± 11.9	-14.22 to 52.76	0.3897	ns
Laponite:VEGF vs. Alginate:Vehicle	63.9 ± 11.9	30.4 to 97.38	0.0002	***
Laponite:Vehicle vs. Alginate:VEGF	24.3 ± 11.9	-9.175 to 57.81	0.2064	ns
Laponite:Vehicle vs. Alginate:Vehicle	68.9 ± 11.9	35.45 to 102.4	<0.0001	****
Alginate:VEGF vs. Alginate:Vehicle	44.6 ± 12.4	9.636 to 79.6	0.0099	**

Table 6.81. Differences of re-epithelialisation rates between Laponite ± VEGF and alginate ± VEGF (rostral & caudal combined means) after 18 days.

Descriptive Statistics					
Differences of re-epithelialisation rates between Laponite ± VEGF (rostral & caudal combined means)					
Day	**Mean Diff & SE (%)**		**95% CI (%)**	***p***	**Sign.**
14	10.8 ± 11.6		-18.59 to 40.25	0.7364	ns
18	-5.1 ± 11.1		-33.1 to 23	0.9577	ns

Table 6.82. Differences of re-epithelialisation rates between Laponite ± VEGF (rostral & caudal combined means).

D.7 Wound Cellularity Data Tables in *db/db* Mice

Descriptive Statistics								
Statistics of mean cellularity data measured from harvested wounds treated with Laponite gels ± VEGF in *db/db* mice								
Day	**VEGF**				**Vehicle**			
	Mean & SD (Cellularity %)			***n***	**Mean & SD (Cellularity %)**			***n***
14	43.1	±	14.8	6	32.9	±	19.9	5
18	11.7	±	8.8	6	19.3	±	8.0	10

Table 6.83. Statistics of mean cellularity data measured from harvested wounds treated with Laponite gels ± VEGF in *db/db* mice.

Descriptive Statistics

Differences between mean cellularity data measured from harvested wounds treated with Laponite gels ± VEGF in *db/db* mice

Day	Mean Diff. & SE (Cellularity %)	95% CI (Cellularity %)	*p*	Significance
14	10.2 ± 7.6	-9.39 to 29.8	0.4746	ns
18	-7.6 ± 6.5	-24.32 to 9.099	0.5831	ns

Table 6.84. Differences between mean cellularity data measured from harvested wounds treated with Laponite gels ± VEGF in *db/db* mice.

Appendix E:

List of Publications & Attended Conferences

E.1 List of Potential Journal Paper Publications

All major findings presented in Chapter 3: Delivery of Bioactive Factors Using Laponite Hydrogels: An *In Vitro* Approach and*Chapter 3:* formed the basis of a proposed novel journal paper to be submitted for publication in the 'Journal of Controlled Release'.

At the time of thesis submission this proposed paper had a working title of 'Injectable clay gels for delivering angiogenic microenvironments'.

E.2 List of Attended Conferences

Find below in the two subchapters a list of all attended conferences (including abstract publications) and poster sessions presenting relevant findings documented in this thesis.

E.2.1 Oral Presentations

Page DJ, Dawson JI, Mani R, Oreffo ROC, Clarkin CE, Evans ND (2015). Novel clay gels as regenerative microenvironments for the treatment of diabetic foot ulcers. **Advances in Regenerative Medicine: the road to translation: 3rd South West Regional Regenerative Medicine Meeting.** 22nd & 23rd September 2015. Cadbury House - Doubletree by Hilton, Congresbury, Bristol. Oral Presentation.

Page DJ, Dawson JI, Mani R, Clarkin CE, Evans ND (2016). VEGF-associated clay gels promotes *in vitro* angiogenesis: potential tissue engineering application

for chronic wounds. **Faculty of Medicine Research Conference 2016, 23rd June 2016.** University Hospital Southampton, Southampton, UK. Oral Presentation.

Page DJ, Dawson JI, Mani R, Clarkin CE, Evans ND. Novel Delivery of Proangiogenic VEGF Using Clay Biomaterial to Augment the Recovery of Chronic Skin Wounds. **Future Investigators of Regenerative Medicine (FIRM) Symposium 2016.** 27th September 2016. Hotel Cap Roig, Platja d'aro, Costa Brava, Spain. Oral Presentation.

E.2.2 Poster Presentations

Page DJ, Dawson JI, Gibbs DM, Mani R, Clarkin CE, Oreffo ROC, Evans ND (2015). Novel Clay Gels As Regenerative Microenvironments For The Treatment of Diabetic Foot Ulcers (DFUs). **Institute for Life Sciences Poster Session: Life Technologies. 6th March 2015.** University of Southampton, Southampton, United Kingdom. Poster Presentation.

Page DJ, Dawson JI, Gibbs DM, Mani R, Clarkin CE, Oreffo ROC, Evans ND (2015). Novel Clay Gels As Regenerative Microenvironments For The Treatment of Diabetic Foot Ulcers (DFUs). **Set For Britain Exhibition. 9th March 2015.** House of Commons, London, United Kingdom. Poster Presentation.

Page DJ, Dawson JI, Mani R, Oreffo ROC, Clarkin CE, Evans ND (2015). Novel clay gels as regenerative microenvironments for the treatment of diabetic foot ulcers. **Tissue & Cell Engineering Society (TCES) Annual Conference 2015. 19th July – 21st July 2015. Published: 2015.** Grand Harbour Hotel, Southampton, United Kingdom. Poster Presentation. Abstract published in eCM

Journal Vol 29 Suppl 3, 2015, p87, http://www.ecmjournal.org/journal/supplements/vol029supp03/vol029supp03tm**.**

Page DJ, Dawson JI, Mani R, Oreffo ROC, Clarkin CE, Evans ND (2015). Novel clay gels as regenerative microenvironments for the treatment of diabetic foot ulcers. **Post Graduate Faculty of Engineering & The Environment 2015 Annual Conference. 4th November 2015.** Grand Harbour Hotel, Southampton, United Kingdom. Poster Presentation.

Page DJ, Dawson JI, Mani R, Clarkin CE, Evans ND (2016). VEGF-associated clay gels promotes *in vitro* angiogenesis: potential tissue engineering application for chronic wounds. **European Chapter Meeting of the Tissue Engineering and Regenerative Medicine International Society (TERMIS) 2016. 28th June – 1st July 2016.** Uppsala Concert and Congress (UKK), Uppsala, Sweden. Poster Presentation. **Abstract published in eCM Journal Vol 31 Suppl 1, 2016, p334,** http://www.ecmjournal.org/journal/supplements/vol031supp01/vol031supp01_P.htm**.**

Page DJ, Dawson JI, Mani R, Oreffo ROC, Clarkin CE, Evans ND (2016). Novel growth factor delivery using clay gels for the treatment of diabetic foot ulcers. **Tissue & Cell Engineering Society (TCES) Annual Conference 2016. 4th-6th July 2016**. University College London (UCL), London, UK. **Poster Presentation. Abstract published in eCM Journal Vol 32 Suppl 4, 2016, p334,**

http://www.ecmjournal.org/journal/supplements/vol032supp04/vol032supp04.htm**.**

Page DJ, Dawson JI, Mani R, Clarkin CE, Evans ND (2016). Delivery of proangiogenic VEGF using clay to promote diabetic foot ulcer healing. **Skin Deep – 20 Years of Research, British Skin Foundation Research Conference. 13th October 2016.** Royal College of Physicians, London, UK. Poster Presentation. **Abstract published in British Journal of Dermatology (2016) 175 (Suppl. S2), p41,** http://onlinelibrary.wiley.com/doi/10.1111/bjd.14911/epdf.

Page DJ, Dawson JI, Mani R, Clarkin CE, Evans ND (2017). VEGF-associated clay gels promotes angiogenesis in an *in vitro* and a murine-based model: possible treatment for chronic diabetic ulcers. **16th International Clay Conference: Clays, From The Oceans To Space.** 17th-21st July 2017, Granada, Spain. Poster Presentation.

Bibliography

[1] K. Järbrink, G. Ni, H. Sönnergren, A. Schmidtchen, C. Pang, R. Bajpai, J. Car, The humanistic and economic burden of chronic wounds: a protocol for a systematic review, Systematic Reviews, 6 (2017) 15.
[2] R.E. Pecoraro, G.E. Reiber, E.M. Burgess, Pathways to diabetic limb amputation. Basis for prevention, Diabetes care, 13 (1990) 513-521.
[3] D.R. Bickers, H.W. Lim, D. Margolis, M.A. Weinstock, C. Goodman, E. Faulkner, C. Gould, E. Gemmen, T. Dall, A. American Academy of Dermatology, D. Society for Investigative, The burden of skin diseases: 2004 a joint project of the American Academy of Dermatology Association and the Society for Investigative Dermatology, Journal of the American Academy of Dermatology, 55 (2006) 490-500.
[4] J.R. Beard, A.M. Officer, A.K. Cassels, The World Report on Ageing and Health, Gerontologist, 56 Suppl 2 (2016) S163-166.
[5] L. Gould, P. Abadir, H. Brem, M. Carter, T. Conner-Kerr, J. Davidson, L. DiPietro, V. Falanga, C. Fife, S. Gardner, E. Grice, J. Harmon, W.R. Hazzard, K.P. High, P. Houghton, N. Jacobson, R.S. Kirsner, E.J. Kovacs, D. Margolis, F. McFarland Horne, M.J. Reed, D.H. Sullivan, S. Thom, M. Tomic-Canic, J. Walston, J.A. Whitney, J. Williams, S. Zieman, K. Schmader, Chronic wound repair and healing in older adults: current status and future research, J Am Geriatr Soc, 63 (2015) 427-438.
[6] W.T. Cefalu, R.E. Ratner, The Diabetes Control and Complications Trial/Epidemiology of Diabetes Interventions and Complications Study at 30 Years: The "Gift" That Keeps on Giving!, Diabetes care, 37 (2014) 5-7.
[7] N.C. Schaper, Diabetic foot ulcer classification system for research purposes: a progress report on criteria for including patients in research studies, Diabetes/metabolism research and reviews, 20 Suppl 1 (2004) S90-95.
[8] M.A. Fonder, G.S. Lazarus, D.A. Cowan, B. Aronson-Cook, A.R. Kohli, A.J. Mamelak, Treating the chronic wound: A practical approach to the care of nonhealing wounds and wound care dressings, Journal of the American Academy of Dermatology, 58 (2008) 185-206.
[9] E. Caló, V.V. Khutoryanskiy, Biomedical applications of hydrogels: A review of patents and commercial products, European Polymer Journal, 65 (2015) 252-267.
[10] G. Gainza, S. Villullas, J.L. Pedraz, R.M. Hernandez, M. Igartua, Advances in drug delivery systems (DDSs) to release growth factors for wound healing and skin regeneration, Nanomedicine, 11 (2015) 1551-1573.
[11] M. Kokabi, M. Sirousazar, Z.M. Hassan, PVA–clay nanocomposite hydrogels for wound dressing, European Polymer Journal, 43 (2007) 773-781.
[12] K.-T. Huang, C.-J. Huang, Novel Zwitterionic Nanocomposite Hydrogel as Effective Chronic Wound Healing Dressings, in: F.-C. Su, S.-H. Wang, M.-L. Yeh (Eds.) 1st Global Conference on Biomedical Engineering & 9th Asian-Pacific Conference on Medical and Biological Engineering: October 9-12, 2014, Tainan, Taiwan, Springer International Publishing, Cham, 2015, pp. 35-38.

[13] H. Tomás, C.S. Alves, J. Rodrigues, Laponite®: A key nanoplatform for biomedical applications?, Nanomedicine: Nanotechnology, Biology and Medicine, (2017).
[14] J.I. Dawson, R.O. Oreffo, Clay: new opportunities for tissue regeneration and biomaterial design, Advanced materials, 25 (2013) 4069-4086.
[15] N. Devi, J. Dutta, Preparation and characterization of chitosan-bentonite nanocomposite films for wound healing application, Int J Biol Macromol, (2017).
[16] K.-T. Huang, Y.-L. Fang, P.-S. Hsieh, C.-C. Li, N.-T. Dai, C.-J. Huang, Zwitterionic nanocomposite hydrogels as effective wound dressings, J. Mater. Chem. B, 4 (2016) 4206-4215.
[17] W.H. Organization, Global report on diabetes, World Health Organization2016.
[18] D. UK, Facts and Stats (October 2016), 2016.
[19] N. Holman, N.G. Forouhi, E. Goyder, S.H. Wild, The Association of Public Health Observatories (APHO) Diabetes Prevalence Model: estimates of total diabetes prevalence for England, 2010-2030, Diabetic medicine : a journal of the British Diabetic Association, 28 (2011) 575-582.
[20] A. American Diabetes, Diagnosis and classification of diabetes mellitus, Diabetes care, 31 Suppl 1 (2008) S55-60.
[21] World Health Organization. Office of Health Communications and Public Relations., Diabetes, World Health Organization, Geneva, 2012.
[22] D. Expert Committee on the, M. Classification of Diabetes, Report of the expert committee on the diagnosis and classification of diabetes mellitus, Diabetes care, 26 Suppl 1 (2003) S5-20.
[23] M. Wallberg, A. Cooke, Immune mechanisms in type 1 diabetes, Trends in immunology, (2013).
[24] J.C. Barrett, D.G. Clayton, P. Concannon, B. Akolkar, J.D. Cooper, H.A. Erlich, C. Julier, G. Morahan, J. Nerup, C. Nierras, V. Plagnol, F. Pociot, H. Schuilenburg, D.J. Smyth, H. Stevens, J.A. Todd, N.M. Walker, S.S. Rich, C. Type 1 Diabetes Genetics, Genome-wide association study and meta-analysis find that over 40 loci affect risk of type 1 diabetes, Nature genetics, 41 (2009) 703-707.
[25] F. Pociot, B. Akolkar, P. Concannon, H.A. Erlich, C. Julier, G. Morahan, C.R. Nierras, J.A. Todd, S.S. Rich, J. Nerup, Genetics of type 1 diabetes: what's next?, Diabetes, 59 (2010) 1561-1571.
[26] A.K. Imkampe, M.C. Gulliford, Trends in Type 1 diabetes incidence in the UK in 0- to 14-year-olds and in 15- to 34-year-olds, 1991-2008, Diabetic medicine : a journal of the British Diabetic Association, 28 (2011) 811-814.
[27] W.E. Barbeau, What is the key environmental trigger in type 1 diabetes - Is it viruses, or wheat gluten, or both?, Autoimmun Rev, 12 (2012) 295-299.
[28] L. Rosenfeld, Insulin: Discovery and Controversy, Clinical Chemistry, 48 (2002) 2270-2288.
[29] D.T. Karamitsos, The story of insulin discovery, Diabetes Research and Clinical Practice, 93 (2011) S2-S8.

[30] R.G. Miller, A.M. Secrest, R.K. Sharma, T.J. Songer, T.J. Orchard, Improvements in the life expectancy of type 1 diabetes: the Pittsburgh Epidemiology of Diabetes Complications study cohort, Diabetes, 61 (2012) 2987-2992.
[31] R.I.G. Holt, N.A. Hanley, B. Dawson, Essential endocrinology and diabetes, 6th ed., Wiley-Blackwell, Chichester, 2012.
[32] P. Marchetti, F. Dotta, D. Lauro, F. Purrello, An overview of pancreatic beta-cell defects in human type 2 diabetes: implications for treatment, Regulatory peptides, 146 (2008) 4-11.
[33] R. Lupi, S. Del Prato, beta-cell apoptosis in type 2 diabetes: Quantitative and functional consequences, Diabetes Metab, 34 (2008) S56-S64.
[34] R. Sladek, G. Rocheleau, J. Rung, C. Dina, L. Shen, D. Serre, P. Boutin, D. Vincent, A. Belisle, S. Hadjadj, B. Balkau, B. Heude, G. Charpentier, T.J. Hudson, A. Montpetit, A.V. Pshezhetsky, M. Prentki, B.I. Posner, D.J. Balding, D. Meyre, C. Polychronakos, P. Froguel, A genome-wide association study identifies novel risk loci for type 2 diabetes, Nature, 445 (2007) 881-885.
[35] R.H. Ahmed, H.Z. Huri, Z. Al-Hamodi, S.D. Salem, B. Al-Absi, S. Muniandy, Association of DPP4 Gene Polymorphisms with Type 2 Diabetes Mellitus in Malaysian Subjects, PloS one, 11 (2016) e0154369.
[36] WHO, IDF, Definition and Diagnosis of diabetes Mellitus and Intermediate Hyperglycemia, WHO, 2006, pp. 3, 10-15.
[37] R. Aubert, Diabetes in America, DIANE Publishing Company1995.
[38] J.M. Forbes, M.E. Cooper, Mechanisms of diabetic complications, Physiological reviews, 93 (2013) 137-188.
[39] V. Falanga, Wound healing and its impairment in the diabetic foot, Lancet, 366 (2005) 1736-1743.
[40] M. Brownlee, Biochemistry and molecular cell biology of diabetic complications, Nature, 414 (2001) 813-820.
[41] K.H. Gabbay, L.O. Merola, R.A. Field, Sorbitol pathway: presence in nerve and cord with substrate accumulation in diabetes, Science, 151 (1966) 209-210.
[42] S. Yamagishi, S. Maeda, T. Matsui, S. Ueda, K. Fukami, S. Okuda, Role of advanced glycation end products (AGEs) and oxidative stress in vascular complications in diabetes, Biochimica et biophysica acta, 1820 (2012) 663-671.
[43] P. Geraldes, G.L. King, Activation of protein kinase C isoforms and its impact on diabetic complications, Circulation research, 106 (2010) 1319-1331.
[44] L. Prompers, M. Huijberts, J. Apelqvist, E. Jude, A. Piaggesi, K. Bakker, M. Edmonds, P. Holstein, A. Jirkovska, D. Mauricio, G. Ragnarson Tennvall, H. Reike, M. Spraul, L. Uccioli, V. Urbancic, K. Van Acker, J. van Baal, F. van Merode, N. Schaper, High prevalence of ischaemia, infection and serious comorbidity in patients with diabetic foot disease in Europe. Baseline results from the Eurodiale study, Diabetologia, 50 (2007) 18-25.
[45] N. Katsilambros, Atlas of the diabetic foot, 2nd ed., Wiley-Blackwell, Chichester, 2010.

[46] C.A. Abbott, A.P. Garrow, A.L. Carrington, J. Morris, E.R. Van Ross, A.J. Boulton, s. North-West diabetes foot care, Foot ulcer risk is lower in South-Asian and african-Caribbean compared with European diabetic patients in the U.K.: the North-West diabetes foot care study, Diabetes care, 28 (2005) 1869-1875.
[47] A.J.M. Boulton, The diabetic foot, Medicine, 38 (2010) 644-648.
[48] A.J. Boulton, The diabetic foot: from art to science. The 18th Camillo Golgi lecture, Diabetologia, 47 (2004) 1343-1353.
[49] T. Mustoe, Understanding chronic wounds: a unifying hypothesis on their pathogenesis and implications for therapy, American journal of surgery, 187 (2004) 65s-70s.
[50] A.R. Young, S.L. Walker, UV radiation, vitamin D and human health: an unfolding controversy introduction, Photochem Photobiol, 81 (2005) 1243-1245.
[51] J.L. Monaco, W.T. Lawrence, Acute wound healing an overview, Clinics in plastic surgery, 30 (2003) 1-12.
[52] A. Zarbock, R.K. Polanowska-Grabowska, K. Ley, Platelet-neutrophil-interactions: linking hemostasis and inflammation, Blood reviews, 21 (2007) 99-111.
[53] E.W. Davie, K. Fujikawa, W. Kisiel, The coagulation cascade: initiation, maintenance, and regulation, Biochemistry, 30 (1991) 10363-10370.
[54] N. Laurens, P. Koolwijk, M.P. de Maat, Fibrin structure and wound healing, Journal of thrombosis and haemostasis : JTH, 4 (2006) 932-939.
[55] M.C. Heng, Wound healing in adult skin: aiming for perfect regeneration, International journal of dermatology, 50 (2011) 1058-1066.
[56] S. Mine, T. Fujisaki, M. Suematsu, Y. Tanaka, Activated platelets and endothelial cell interaction with neutrophils under flow conditions, Internal medicine, 40 (2001) 1085-1092.
[57] H.O. Rennekampff, J.F. Hansbrough, V. Kiessig, C. Dore, M. Sticherling, J.M. Schroder, Bioactive interleukin-8 is expressed in wounds and enhances wound healing, The Journal of surgical research, 93 (2000) 41-54.
[58] G. Broughton, 2nd, J.E. Janis, C.E. Attinger, The basic science of wound healing, Plastic and reconstructive surgery, 117 (2006) 12S-34S.
[59] M.H. Kim, W. Liu, D.L. Borjesson, F.R. Curry, L.S. Miller, A.L. Cheung, F.T. Liu, R.R. Isseroff, S.I. Simon, Dynamics of neutrophil infiltration during cutaneous wound healing and infection using fluorescence imaging, The Journal of investigative dermatology, 128 (2008) 1812-1820.
[60] A. Young, C.-E. McNaught, The physiology of wound healing, Surgery (Oxford), 29 (2011) 475-479.
[61] S.J. Leibovich, R. Ross, The role of the macrophage in wound repair. A study with hydrocortisone and antimacrophage serum, The American journal of pathology, 78 (1975) 71-100.
[62] T.J. Koh, L.A. DiPietro, Inflammation and wound healing: the role of the macrophage, Expert reviews in molecular medicine, 13 (2011) e23.

[63] T. Velnar, T. Bailey, V. Smrkolj, The wound healing process: an overview of the cellular and molecular mechanisms, The Journal of international medical research, 37 (2009) 1528-1542.
[64] G.S. Schultz, A. Wysocki, Interactions between extracellular matrix and growth factors in wound healing, Wound Repair and Regeneration, 17 (2009) 153-162.
[65] C. Frantz, K.M. Stewart, V.M. Weaver, The extracellular matrix at a glance, Journal of cell science, 123 (2010) 4195-4200.
[66] M.C. Robson, D.L. Steed, M.G. Franz, Wound healing: biologic features and approaches to maximize healing trajectories, Current problems in surgery, 38 (2001) 72-140.
[67] H.N. Lovvorn Iii, D.T. Cheung, M.E. Nimni, N. Perelman, J.M. Estes, N.S. Adzick, Relative distribution and crosslinking of collagen distinguish fetal from adult sheep wound repair, Journal of Pediatric Surgery, 34 (1999) 218-223.
[68] J.W. Madden, E.E. Peacock, Jr., Studies on the biology of collagen during wound healing. 3. Dynamic metabolism of scar collagen and remodeling of dermal wounds, Annals of surgery, 174 (1971) 511-520.
[69] A.B. Roberts, M.B. Sporn, R.K. Assoian, J.M. Smith, N.S. Roche, L.M. Wakefield, U.I. Heine, L.A. Liotta, V. Falanga, J.H. Kehrl, et al., Transforming growth factor type beta: rapid induction of fibrosis and angiogenesis in vivo and stimulation of collagen formation in vitro, Proceedings of the National Academy of Sciences of the United States of America, 83 (1986) 4167-4171.
[70] E.J. Battegay, J. Rupp, L. Iruela-Arispe, E.H. Sage, M. Pech, PDGF-BB modulates endothelial proliferation and angiogenesis in vitro via PDGF beta-receptors, The Journal of cell biology, 125 (1994) 917-928.
[71] R.C. Sainson, D.A. Johnston, H.C. Chu, M.T. Holderfield, M.N. Nakatsu, S.P. Crampton, J. Davis, E. Conn, C.C. Hughes, TNF primes endothelial cells for angiogenic sprouting by inducing a tip cell phenotype, Blood, 111 (2008) 4997-5007.
[72] M.S. Pepper, Transforming growth factor-beta: vasculogenesis, angiogenesis, and vessel wall integrity, Cytokine & growth factor reviews, 8 (1997) 21-43.
[73] L.F. Brown, K.T. Yeo, B. Berse, T.K. Yeo, D.R. Senger, H.F. Dvorak, L. van de Water, Expression of vascular permeability factor (vascular endothelial growth factor) by epidermal keratinocytes during wound healing, The Journal of experimental medicine, 176 (1992) 1375-1379.
[74] A. Hoeben, B. Landuyt, M.S. Highley, H. Wildiers, A.T. Van Oosterom, E.A. De Bruijn, Vascular endothelial growth factor and angiogenesis, Pharmacological reviews, 56 (2004) 549-580.
[75] J.H. Distler, A. Hirth, M. Kurowska-Stolarska, R.E. Gay, S. Gay, O. Distler, Angiogenic and angiostatic factors in the molecular control of angiogenesis, The quarterly journal of nuclear medicine : official publication of the Italian Association of Nuclear Medicine, 47 (2003) 149-161.
[76] P. Carmeliet, Angiogenesis in health and disease, Nature medicine, 9 (2003) 653-660.

[77] P. Kumar, S. Kumar, E.P. Udupa, U. Kumar, P. Rao, T. Honnegowda, Role of angiogenesis and angiogenic factors in acute and chronic wound healing, Plastic and Aesthetic Research, 2 (2015).
[78] M. Murakami, L.T. Nguyen, Z.W. Zhuang, K.L. Moodie, P. Carmeliet, R.V. Stan, M. Simons, The FGF system has a key role in regulating vascular integrity, The Journal of clinical investigation, 118 (2008) 3355-3366.
[79] P. Bao, A. Kodra, M. Tomic-Canic, M.S. Golinko, H.P. Ehrlich, H. Brem, The role of vascular endothelial growth factor in wound healing, The Journal of surgical research, 153 (2009) 347-358.
[80] L. Lamalice, F. Le Boeuf, J. Huot, Endothelial cell migration during angiogenesis, Circulation research, 100 (2007) 782-794.
[81] G. Gabbiani, The myofibroblast in wound healing and fibrocontractive diseases, J Pathol, 200 (2003) 500-503.
[82] S.J. Miller, E.M. Burke, M.D. Rader, P.A. Coulombe, R.M. Lavker, Re-epithelialization of porcine skin by the sweat apparatus, The Journal of investigative dermatology, 110 (1998) 13-19.
[83] J.M. Davidson, Wound repair, Journal of Hand Therapy, 11 (1998) 80-94.
[84] K.I. Anderson, Y.L. Wang, J.V. Small, Coordination of protrusion and translocation of the keratocyte involves rolling of the cell body, The Journal of cell biology, 134 (1996) 1209-1218.
[85] J. Li, J. Chen, R. Kirsner, Pathophysiology of acute wound healing, Clinics in dermatology, 25 (2007) 9-18.
[86] M.L. Usui, R.A. Underwood, J.N. Mansbridge, L.A. Muffley, W.G. Carter, J.E. Olerud, Morphological evidence for the role of suprabasal keratinocytes in wound reepithelialization, Wound repair and regeneration : official publication of the Wound Healing Society [and] the European Tissue Repair Society, 13 (2005) 468-479.
[87] K. Safferling, T. Sutterlin, K. Westphal, C. Ernst, K. Breuhahn, M. James, D. Jager, N. Halama, N. Grabe, Wound healing revised: a novel reepithelialization mechanism revealed by in vitro and in silico models, The Journal of cell biology, 203 (2013) 691-709.
[88] S. Guo, L.A. Dipietro, Factors affecting wound healing, J Dent Res, 89 (2010) 219-229.
[89] S.M. Levenson, E.F. Geever, L.V. Crowley, J.F. Oates, 3rd, C.W. Berard, H. Rosen, The Healing of Rat Skin Wounds, Annals of surgery, 161 (1965) 293-308.
[90] B.K. Sun, Z. Siprashvili, P.A. Khavari, Advances in skin grafting and treatment of cutaneous wounds, Science, 346 (2014) 941-945.
[91] H. Galkowska, U. Wojewodzka, W.L. Olszewski, Chemokines, cytokines, and growth factors in keratinocytes and dermal endothelial cells in the margin of chronic diabetic foot ulcers, Wound repair and regeneration : official publication of the Wound Healing Society [and] the European Tissue Repair Society, 14 (2006) 558-565.
[92] F. Tecilazich, T. Dinh, L. Pradhan-Nabzdyk, E. Leal, A. Tellechea, A. Kafanas, C. Gnardellis, M.L. Magargee, A. Dejam, V. Toxavidis, J.C. Tigges, E. Carvalho, T.E.

Lyons, A. Veves, Role of endothelial progenitor cells and inflammatory cytokines in healing of diabetic foot ulcers, PloS one, 8 (2013) e83314.
[93] M. Miao, Y. Niu, T. Xie, B. Yuan, C. Qing, S. Lu, Diabetes-impaired wound healing and altered macrophage activation: a possible pathophysiologic correlation, Wound repair and regeneration : official publication of the Wound Healing Society [and] the European Tissue Repair Society, 20 (2012) 203-213.
[94] K. Maruyama, J. Asai, M. Li, T. Thorne, D.W. Losordo, P.A. D'Amore, Decreased macrophage number and activation lead to reduced lymphatic vessel formation and contribute to impaired diabetic wound healing, American Journal of Pathology, 170 (2007) 1178-1191.
[95] P. Martin, R. Nunan, Cellular and molecular mechanisms of repair in acute and chronic wound healing, Br J Dermatol, 173 (2015) 370-378.
[96] R. Serra, R. Grande, G. Buffone, V. Molinari, P. Perri, A. Perri, B. Amato, M. Colosimo, S. de Franciscis, Extracellular matrix assessment of infected chronic venous leg ulcers: role of metalloproteinases and inflammatory cytokines, Int Wound J, 13 (2016) 53-58.
[97] R. Lobmann, A. Ambrosch, G. Schultz, K. Waldmann, S. Schiweck, H. Lehnert, Expression of matrix-metalloproteinases and their inhibitors in the wounds of diabetic and non-diabetic patients, Diabetologia, 45 (2002) 1011-1016.
[98] B.C. Nwomeh, H.X. Liang, I.K. Cohen, D.R. Yager, MMP-8 is the predominant collagenase in healing wounds and nonhealing ulcers, Journal of Surgical Research, 81 (1999) 189-195.
[99] D.R. Yager, S.M. Chen, S.I. Ward, O.O. Olutoye, R.F. Diegelmann, I. Kelman Cohen, Ability of chronic wound fluids to degrade peptide growth factors is associated with increased levels of elastase activity and diminished levels of proteinase inhibitors, Wound Repair and Regeneration, 5 (1997) 23-32.
[100] H. Li, X. Zhang, X. Guan, X. Cui, Y. Wang, H. Chu, M. Cheng, Advanced glycation end products impair the migration, adhesion and secretion potentials of late endothelial progenitor cells, Cardiovascular diabetology, 11 (2012) 46.
[101] S. Frank, G. Hubner, G. Breier, M.T. Longaker, D.G. Greenhalgh, S. Werner, Regulation of vascular endothelial growth factor expression in cultured keratinocytes. Implications for normal and impaired wound healing, The Journal of biological chemistry, 270 (1995) 12607-12613.
[102] D.L. Doxey, M.C. Ng, R.E. Dill, A.M. Iacopino, Platelet-derived growth factor levels in wounds of diabetic rats, Life sciences, 57 (1995) 1111-1123.
[103] D.G. Greenhalgh, K.H. Sprugel, M.J. Murray, R. Ross, PDGF and FGF stimulate wound healing in the genetically diabetic mouse, The American journal of pathology, 136 (1990) 1235-1246.
[104] S. Balaji, M. LeSaint, S.S. Bhattacharya, C. Moles, Y. Dhamija, M. Kidd, L.D. Le, A. King, A. Shaaban, T.M. Crombleholme, P. Bollyky, S.G. Keswani, Adenoviral-mediated gene transfer of insulin-like growth factor 1 enhances wound healing and induces angiogenesis, The Journal of surgical research, 190 (2014) 367-377.

[105] M. Afshari, B. Larijani, M. Fadayee, A. Ghahary, M. Pajouhi, M.-H. Bastanhagh, R. Baradar-Jalili, A.-R. Vassigh, F. Darvishzadeh, Efficacy of topical epidermal growth factor in healing diabetic foot ulcers, Clinical Practice, 2 (2005) 759.
[106] B.S. Pukstad, L. Ryan, T.H. Flo, J. Stenvik, R. Moseley, K. Harding, D.W. Thomas, T. Espevik, Non-healing is associated with persistent stimulation of the innate immune response in chronic venous leg ulcers, J Dermatol Sci, 59 (2010) 115-122.
[107] G. Lauer, S. Sollberg, M. Cole, I. Flamme, J. Sturzebecher, K. Mann, T. Krieg, S.A. Eming, Expression and proteolysis of vascular endothelial growth factor is increased in chronic wounds, Journal of Investigative Dermatology, 115 (2000) 12-18.
[108] D. Telgenhoff, B. Shroot, Cellular senescence mechanisms in chronic wound healing, Cell death and differentiation, 12 (2005) 695-698.
[109] DCCT, The effect of intensive treatment of diabetes on the development and progression of long-term complications in insulin-dependent diabetes mellitus. The Diabetes Control and Complications Trial Research Group, The New England journal of medicine, 329 (1993) 977-986.
[110] G.P. Leese, D. Stang, J.A. Mcknight, S.D.F.A. Group, A national strategic approach to diabetic foot disease in Scotland: changing a culture, The British Journal of Diabetes & Vascular Disease, 11 (2011) 69-73.
[111] T.P.I.C.a.C.F.f.D.F.C. (TRIEPodD-UK), Podiatry competency framework for integrated diabetic foot care: a user's guide, in: J. McCardle, Chadwick, P, Leese, G, McInnes, A.D., Stang, D, Stuart , L. and Young, M. (Ed.), SB Communications Group, London, 2012, pp. 7-8.
[112] K. Bakker, J. Apelqvist, N.C. Schaper, B. International Working Group on Diabetic Foot Editorial, Practical guidelines on the management and prevention of the diabetic foot 2011, Diabetes/metabolism research and reviews, 28 Suppl 1 (2012) 225-231.
[113] S. Baranoski, E.A. Ayello, I. Ovid Technologies, Wound care essentials: practice principles, 2nd ed., Lippincott Williams & Wilkins, Ambler, PA ; London, 2008.
[114] G.D. Mulder, J.S. Vande Berg, Cellular senescence and matrix metalloproteinase activity in chronic wounds. Relevance to debridement and new technologies, Journal of the American Podiatric Medical Association, 92 (2002) 34-37.
[115] K. Alexiadou, J. Doupis, Management of diabetic foot ulcers, Diabetes therapy : research, treatment and education of diabetes and related disorders, 3 (2012) 4.
[116] S.K. Kota, S.K. Kota, L.K. Meher, S. Sahoo, S. Mohapatra, K.D. Modi, Surgical revascularization techniques for diabetic foot, Journal of cardiovascular disease research, 4 (2013) 79-83.
[117] P.L. Faries, V.J. Teodorescu, N.J. Morrissey, L.H. Hollier, M.L. Marin, The role of surgical revascularization in the management of diabetic foot wounds, American journal of surgery, 187 (2004) 34S-37S.
[118] D. UK, Putting feet first: Diabetes UK position on preventing amputations and improving foot care for people with diabetes, (2013).
[119] G.D. Winter, Formation of the scab and the rate of epithelization of superficial wounds in the skin of the young domestic pig, Nature, 193 (1962) 293-294.

[120] C.D. Hinman, H. Maibach, Effect of Air Exposure and Occlusion on Experimental Human Skin Wounds, Nature, 200 (1963) 377-378.
[121] W.H. Eaglstein, Moist wound healing with occlusive dressings: a clinical focus, Dermatologic surgery : official publication for American Society for Dermatologic Surgery [et al.], 27 (2001) 175-181.
[122] J.R. Hilton, D.T. Williams, B. Beuker, D.R. Miller, K.G. Harding, Wound dressings in diabetic foot disease, Clinical infectious diseases : an official publication of the Infectious Diseases Society of America, 39 Suppl 2 (2004) S100-103.
[123] P. Martin, Wound healing--aiming for perfect skin regeneration, Science, 276 (1997) 75-81.
[124] T. Tumbar, G. Guasch, V. Greco, C. Blanpain, W.E. Lowry, M. Rendl, E. Fuchs, Defining the epithelial stem cell niche in skin, Science, 303 (2004) 359-363.
[125] P.A. Zuk, M. Zhu, P. Ashjian, D.A. De Ugarte, J.I. Huang, H. Mizuno, Z.C. Alfonso, J.K. Fraser, P. Benhaim, M.H. Hedrick, Human adipose tissue is a source of multipotent stem cells, Molecular biology of the cell, 13 (2002) 4279-4295.
[126] J.G. Toma, M. Akhavan, K.J. Fernandes, F. Barnabe-Heider, A. Sadikot, D.R. Kaplan, F.D. Miller, Isolation of multipotent adult stem cells from the dermis of mammalian skin, Nature cell biology, 3 (2001) 778-784.
[127] T.A. Mustoe, G.F. Pierce, C. Morishima, T.F. Deuel, Growth Factor-Induced Acceleration of Tissue-Repair through Direct and Inductive Activities in a Rabbit Dermal Ulcer Model, Journal of Clinical Investigation, 87 (1991) 694-703.
[128] G.F. Pierce, T.A. Mustoe, R.M. Senior, J. Reed, G.L. Griffin, A. Thomason, T.F. Deuel, In vivo incisional wound healing augmented by platelet-derived growth factor and recombinant c-sis gene homodimeric proteins, The Journal of experimental medicine, 167 (1988) 974-987.
[129] K.G. Harding, H.L. Morris, G.K. Patel, Science, medicine and the future: healing chronic wounds, Bmj, 324 (2002) 160-163.
[130] C.H. Heldin, B. Westermark, Mechanism of action and in vivo role of platelet-derived growth factor, Physiological reviews, 79 (1999) 1283-1316.
[131] T.J. Wieman, Clinical efficacy of becaplermin (rhPDGF-BB) gel. Becaplermin Gel Studies Group, American journal of surgery, 176 (1998) 74S-79S.
[132] D.L. Steed, Clinical evaluation of recombinant human platelet-derived growth factor for the treatment of lower extremity diabetic ulcers. Diabetic Ulcer Study Group, Journal of vascular surgery, 21 (1995) 71-78; discussion 79-81.
[133] M.C. Robson, W.G. Payne, W.L. Garner, Integrating the results of phase IV (postmarketing) clinical trial with four previous trials reinforces the position that Regranex (becaplermin) Gel 0.01% is an effective adjunct to the treatment of diabetic foot ulcers, J Appl Res, 5 (2005) 35-45.
[134] T.J. Wieman, J.M. Smiell, Y. Su, Efficacy and safety of a topical gel formulation of recombinant human platelet-derived growth factor-BB (becaplermin) in patients with chronic neuropathic diabetic ulcers. A phase III randomized placebo-controlled double-blind study, Diabetes care, 21 (1998) 822-827.

[135] K. Lee, E.A. Silva, D.J. Mooney, Growth factor delivery-based tissue engineering: general approaches and a review of recent developments, Journal of the Royal Society, Interface / the Royal Society, 8 (2011) 153-170.
[136] J.L. Whyte, A.A. Smith, B. Liu, W.R. Manzano, N.D. Evans, G.R. Dhamdhere, M.Y. Fang, H.Y. Chang, A.E. Oro, J.A. Helms, Augmenting endogenous Wnt signaling improves skin wound healing, PloS one, 8 (2013) e76883.
[137] S. Hiratsuka, O. Minowa, J. Kuno, T. Noda, M. Shibuya, Flt-1 lacking the tyrosine kinase domain is sufficient for normal development and angiogenesis in mice, Proceedings of the National Academy of Sciences of the United States of America, 95 (1998) 9349-9354.
[138] D.G. Nowak, J. Woolard, E.M. Amin, O. Konopatskaya, M.A. Saleem, A.J. Churchill, M.R. Ladomery, S.J. Harper, D.O. Bates, Expression of pro- and anti-angiogenic isoforms of VEGF is differentially regulated by splicing and growth factors, Journal of cell science, 121 (2008) 3487-3495.
[139] M.N. Nakatsu, R.C. Sainson, S. Perez-del-Pulgar, J.N. Aoto, M. Aitkenhead, K.L. Taylor, P.M. Carpenter, C.C. Hughes, VEGF(121) and VEGF(165) regulate blood vessel diameter through vascular endothelial growth factor receptor 2 in an in vitro angiogenesis model, Laboratory investigation; a journal of technical methods and pathology, 83 (2003) 1873-1885.
[140] S. Romano Di Peppe, A. Mangoni, G. Zambruno, G. Spinetti, G. Melillo, M. Napolitano, M.C. Capogrossi, Adenovirus-mediated VEGF(165) gene transfer enhances wound healing by promoting angiogenesis in CD1 diabetic mice, Gene therapy, 9 (2002) 1271-1277.
[141] C. Cai, M.C. Bottcher, J.A. Werner, R. Mandic, Differential expression of VEGF121, VEGF165 and VEGF189 in angiomas and squamous cell carcinoma cell lines of the head and neck, Anticancer research, 30 (2010) 805-810.
[142] F.S. Grunewald, A.E. Prota, A. Giese, K. Ballmer-Hofer, Structure-function analysis of VEGF receptor activation and the role of coreceptors in angiogenic signaling, Biochimica et biophysica acta, 1804 (2010) 567-580.
[143] I. Stalmans, Y.S. Ng, R. Rohan, M. Fruttiger, A. Bouche, A. Yuce, H. Fujisawa, B. Hermans, M. Shani, S. Jansen, D. Hicklin, D.J. Anderson, T. Gardiner, H.P. Hammes, L. Moons, M. Dewerchin, D. Collen, P. Carmeliet, P.A. D'Amore, Arteriolar and venular patterning in retinas of mice selectively expressing VEGF isoforms, The Journal of clinical investigation, 109 (2002) 327-336.
[144] P. Carmeliet, Y.S. Ng, D. Nuyens, G. Theilmeier, K. Brusselmans, I. Cornelissen, E. Ehler, V.V. Kakkar, I. Stalmans, V. Mattot, J.C. Perriard, M. Dewerchin, W. Flameng, A. Nagy, F. Lupu, L. Moons, D. Collen, P.A. D'Amore, D.T. Shima, Impaired myocardial angiogenesis and ischemic cardiomyopathy in mice lacking the vascular endothelial growth factor isoforms VEGF164 and VEGF188, Nature medicine, 5 (1999) 495-502.
[145] D. Lambrechts, P. Carmeliet, Genetics in Zebrafish, Mice, and Humans to Dissect Congenital Heart Disease: Insights in the Role of VEGF, in: P.S. Gerald (Ed.) Current Topics in Developmental Biology, Academic Press2004, pp. 189-224.

[146] R.D. Galiano, O.M. Tepper, C.R. Pelo, K.A. Bhatt, M. Callaghan, N. Bastidas, S. Bunting, H.G. Steinmetz, G.C. Gurtner, Topical vascular endothelial growth factor accelerates diabetic wound healing through increased angiogenesis and by mobilizing and recruiting bone marrow-derived cells, The American journal of pathology, 164 (2004) 1935-1947.
[147] S.M. Eppler, D.L. Combs, T.D. Henry, J.J. Lopez, S.G. Ellis, J.H. Yi, B.H. Annex, E.R. McCluskey, T.F. Zioncheck, A target-mediated model to describe the pharmacokinetics and hemodynamic effects of recombinant human vascular endothelial growth factor in humans, Clinical pharmacology and therapeutics, 72 (2002) 20-32.
[148] C. Niehrs, The complex world of WNT receptor signalling, Nature reviews. Molecular cell biology, 13 (2012) 767-779.
[149] R. Nusse, Wnt signaling, Cold Spring Harbor perspectives in biology, 4 (2012).
[150] H. Clevers, Wnt/beta-catenin signaling in development and disease, Cell, 127 (2006) 469-480.
[151] J. Behrens, Everything You Would Like to Know About Wnt Signaling, Sci. Signal., 6 (2013) pe17-.
[152] X. Lim, S.H. Tan, W.L. Koh, R.M. Chau, K.S. Yan, C.J. Kuo, R. van Amerongen, A.M. Klein, R. Nusse, Interfollicular epidermal stem cells self-renew via autocrine Wnt signaling, Science, 342 (2013) 1226-1230.
[153] H. Nguyen, B.J. Merrill, L. Polak, M. Nikolova, M. Rendl, T.M. Shaver, H.A. Pasolli, E. Fuchs, Tcf3 and Tcf4 are essential for long-term homeostasis of skin epithelia, Nature genetics, 41 (2009) 1068-1075.
[154] M. Ito, Z. Yang, T. Andl, C. Cui, N. Kim, S.E. Millar, G. Cotsarelis, Wnt-dependent de novo hair follicle regeneration in adult mouse skin after wounding, Nature, 447 (2007) 316-320.
[155] V. Levy, C. Lindon, Y. Zheng, B.D. Harfe, B.A. Morgan, Epidermal stem cells arise from the hair follicle after wounding, FASEB journal : official publication of the Federation of American Societies for Experimental Biology, 21 (2007) 1358-1366.
[156] O. Wichterle, D. Lim, Hydrophilic Gels for Biological Use, Nature, 185 (1960) 117-118.
[157] Q. Chai, Y. Jiao, X. Yu, Hydrogels for Biomedical Applications: Their Characteristics and the Mechanisms behind Them, Gels, 3 (2017) 6.
[158] W.E. Hennink, C.F. van Nostrum, Novel crosslinking methods to design hydrogels, Advanced Drug Delivery Reviews, 64 (2012) 223-236.
[159] P. Nathan, B.G. Macmillan, I.A. Holder, Effect of a Synthetic Dressing Formed on a Burn Wound in Rats: a Comparison of Allografts, Collagen Sheets, and Polyhydroxyethylmethacrylate in the Control of Wound Infection, Applied Microbiology, 28 (1974) 465-468.
[160] P. Nathan, E.J. Law, B.G. MacMillan, D.F. Murphy, S.H. Ronel, M.J. D'Andrea, R.A. Abrahams, A new biomaterial for the control of infection in the burn wound, Transactions - American Society for Artificial Internal Organs, 22 (1976) 30-41.
[161] J.M. Anderson, D.F. Gibbons, The New Generation of Biomedical Polymers, Biomaterials, Medical Devices, and Artificial Organs, 2 (2009) 235-248.

[162] A.C. Brown, T.H. Barker, Fibrin-based biomaterials: modulation of macroscopic properties through rational design at the molecular level, Acta Biomater, 10 (2014) 1502-1514.
[163] R. Judith, M. Nithya, C. Rose, A.B. Mandal, Application of a PDGF-containing novel gel for cutaneous wound healing, Life sciences, 87 (2010) 1-8.
[164] P. Sikareepaisan, U. Ruktanonchai, P. Supaphol, Preparation and characterization of asiaticoside-loaded alginate films and their potential for use as effectual wound dressings, Carbohydrate Polymers, 83 (2011) 1457-1469.
[165] C. Alemdaroglu, Z. Degim, N. Celebi, F. Zor, S. Ozturk, D. Erdogan, An investigation on burn wound healing in rats with chitosan gel formulation containing epidermal growth factor, Burns, 32 (2006) 319-327.
[166] J.S. Calnan, J.J. Pflug, A.S. Chhabra, N. Raghupati, Clinical and experimental studies of polyhydroxyethylmethacrylate gel ("hydron") for reconstructive surgery, British Journal of Plastic Surgery, 24 (1971) 113-124.
[167] G. Duncan, S. Andrews, W. McCulloch, Issues in clinical practice: Dressings, Primary Intention: The Australian Journal of Wound Management, 10 (2002) 29.
[168] J.C. Dumville, S. Deshpande, S. O'Meara, K. Speak, Hydrocolloid dressings for healing diabetic foot ulcers, The Cochrane database of systematic reviews, (2012) Cd009099.
[169] A. Nakayama, A. Kakugo, J.P. Gong, Y. Osada, M. Takai, T. Erata, S. Kawano, High Mechanical Strength Double-Network Hydrogel with Bacterial Cellulose, Advanced Functional Materials, 14 (2004) 1124-1128.
[170] Q. Xing, K. Yates, C. Vogt, Z. Qian, M.C. Frost, F. Zhao, Increasing mechanical strength of gelatin hydrogels by divalent metal ion removal, Sci Rep, 4 (2014) 4706.
[171] L.L. Chiu, M. Radisic, Controlled release of thymosin beta4 using collagen-chitosan composite hydrogels promotes epicardial cell migration and angiogenesis, J Control Release, 155 (2011) 376-385.
[172] S. Brahim, A. Narinesingh D Fau - Guiseppi-Elie, A. Guiseppi-Elie, Release characteristics of novel pH-sensitive p(HEMA-DMAEMA) hydrogels containing 3-(trimethoxy-silyl) propyl methacrylate, (2003).
[173] J. Chen, H. Park, K. Park, Synthesis of superporous hydrogels: hydrogels with fast swelling and superabsorbent properties, Journal of biomedical materials research, 44 (1999) 53-62.
[174] C. Xu, J. Kopeček, Self-Assembling Hydrogels, Polymer Bulletin, 58 (2006) 53-63.
[175] K. Haraguchi, T. Takehisa, Nanocomposite Hydrogels: A Unique Organic–Inorganic Network Structure with Extraordinary Mechanical, Optical, and Swelling/De-swelling Properties, Advanced materials, 14 (2002) 1120-1124.
[176] Q. Wang, J.L. Mynar, M. Yoshida, E. Lee, M. Lee, K. Okuro, K. Kinbara, T. Aida, High-water-content mouldable hydrogels by mixing clay and a dendritic molecular binder, Nature, 463 (2010) 339-343.
[177] H. Takeno, Y. Kimura, W. Nakamura, Mechanical, Swelling, and Structural Properties of Mechanically Tough Clay-Sodium Polyacrylate Blend Hydrogels, Gels, 3 (2017).

[178] D. Yang, S. Peng, M.R. Hartman, T. Gupton-Campolongo, E.J. Rice, A.K. Chang, Z. Gu, G.Q. Lu, D. Luo, Enhanced transcription and translation in clay hydrogel and implications for early life evolution, Sci Rep, 3 (2013) 3165.
[179] P. Burey, B.R. Bhandari, T. Howes, M.J. Gidley, Hydrocolloid gel particles: formation, characterization, and application, Crit Rev Food Sci Nutr, 48 (2008) 361-377.
[180] R.J. Sengwa, S. Choudhary, S. Sankhla, Dielectric properties of montmorillonite clay filled poly(vinyl alcohol)/poly(ethylene oxide) blend nanocomposites, Composites Science and Technology, 70 (2010) 1621-1627.
[181] E. De Giglio, S. Cometa, C. Satriano, L. Sabbatini, P.G. Zambonin, Electrosynthesis of hydrogel films on metal substrates for the development of coatings with tunable drug delivery performances, Journal of Biomedical Materials Research Part A, 88A (2009) 1048-1057.
[182] M.T. Poldervaart, H. Wang, J. van der Stok, H. Weinans, S.C. Leeuwenburgh, F.C. Oner, W.J. Dhert, J. Alblas, Sustained release of BMP-2 in bioprinted alginate for osteogenicity in mice and rats, PloS one, 8 (2013) e72610.
[183] K. Saha, B.S. Butola, M. Joshi, Drug-loaded polyurethane/clay nanocomposite nanofibers for topical drug-delivery application, Journal of Applied Polymer Science, 131 (2014) n/a-n/a.
[184] J.L. Cleland, A. Daugherty, R. Mrsny, Emerging protein delivery methods, Current Opinion in Biotechnology, 12 (2001) 212-219.
[185] Z.S. Haidar, R.C. Hamdy, M. Tabrizian, Delivery of recombinant bone morphogenetic proteins for bone regeneration and repair. Part A: Current challenges in BMP delivery, Biotechnology Letters, 31 (2009) 1817.
[186] Y. Liang, M.D. Nikolić, R.R. Bélanger, H. Gong, A. Song, Silicon in agriculture : from theory to practice, 2015.
[187] S. Guggenheim, R.T. Martin, Definition of Clay and Clay Mineral - Joint Report of the Aipea Nomenclature and Cms Nomenclature Committees, Clay Clay Miner, 43 (1995) 255-256.
[188] M. Carretero, C. Gomes, F. Tateo, Clays and human health, Handbook of clay science. Elsevier, Amsterdam, (2006) 717-741.
[189] M.J. Wilson, Clay mineralogical and related characteristics of geophagic materials, Journal of chemical ecology, 29 (2003) 1525-1547.
[190] C. Viseras, C. Aguzzi, P. Cerezo, A. Lopez-Galindo, Uses of clay minerals in semisolid health care and therapeutic products, Appl Clay Sci, 36 (2007) 37-50.
[191] S.E. Haydel, C.M. Remenih, L.B. Williams, Broad-spectrum in vitro antibacterial activities of clay minerals against antibiotic-susceptible and antibiotic-resistant bacterial pathogens, The Journal of antimicrobial chemotherapy, 61 (2008) 353-361.
[192] D. Zhang, C.H. Zhou, C.X. Lin, D.S. Tong, W.H. Yu, Synthesis of clay minerals, Appl Clay Sci, 50 (2010) 1-11.
[193] A. Meunier, N. Fradin, Clays, Springer-Verlag, Berlin ; Heidelberg, 2004.
[194] G. Lagaly, Chapter 5 Colloid Clay Science, in: B.K.G.T. Faïza Bergaya, L. Gerhard (Eds.) Developments in Clay Science, Elsevier2006, pp. 141-245.

[195] P.D. Kaviratna, T.J. Pinnavaia, P.A. Schroeder, Dielectric properties of smectite clays, J Phys Chem Solids, 57 (1996) 1897-1906.
[196] R.T. Martin, S.W. Bailey, D.D. Eberl, D.S. Fanning, S. Guggenheim, H. Kodama, D.R. Pevear, J. Srodon, F.J. Wicks, Report of the Clay-Minerals-Society Nomenclature Committee - Revised Classification of Clay Materials, Clay Clay Miner, 39 (1991) 333-335.
[197] A. Meunier, SpringerLink, Clays [electronic resource], 1st ed., Springer, Berlin ; New York, 2005.
[198] M. Dijkstra, J.P. Hansen, P.A. Madden, Gelation of a clay colloid suspension, Physical review letters, 75 (1995) 2236-2239.
[199] E.M. Ahmed, Hydrogel: Preparation, characterization, and applications: A review, Journal of Advanced Research, 6 (2015) 105-121.
[200] J. Zhu, Bioactive modification of poly(ethylene glycol) hydrogels for tissue engineering, Biomaterials, 31 (2010) 4639-4656.
[201] A.S. Sawhney, C.P. Pathak, J.A. Hubbell, Bioerodible hydrogels based on photopolymerized poly (ethylene glycol)-co-poly (. alpha.-hydroxy acid) diacrylate macromers, Macromolecules, 26 (1993) 581-587.
[202] W.-G. Koh, A. Revzin, M.V. Pishko, Poly (ethylene glycol) hydrogel microstructures encapsulating living cells, Langmuir, 18 (2002) 2459-2462.
[203] N.A. Peppas, K.B. Keys, M. Torres-Lugo, A.M. Lowman, Poly(ethylene glycol)-containing hydrogels in drug delivery, J Control Release, 62 (1999) 81-87.
[204] S. Zhu, S. Li, H. Escuin-Ordinas, R. Dimatteo, W. Xi, A. Ribas, T. Segura, Accelerated wound healing by injectable star poly(ethylene glycol)-b-poly(propylene sulfide) scaffolds loaded with poorly water-soluble drugs, J Control Release, (2018).
[205] D.R. Griffin, W.M. Weaver, P.O. Scumpia, D. Di Carlo, T. Segura, Accelerated wound healing by injectable microporous gel scaffolds assembled from annealed building blocks, Nat Mater, 14 (2015) 737-744.
[206] P.-Y. Lee, Z. Li, L. Huang, Thermosensitive Hydrogel as a Tgf-β1 Gene Delivery Vehicle Enhances Diabetic Wound Healing, Pharmaceutical Research, 20 (2003) 1995-2000.
[207] K.K. Chereddy, G. Vandermeulen, V. Preat, PLGA based drug delivery systems: Promising carriers for wound healing activity, Wound repair and regeneration : official publication of the Wound Healing Society [and] the European Tissue Repair Society, 24 (2016) 223-236.
[208] E.A. Kamoun, X. Chen, M.S. Mohy Eldin, E.-R.S. Kenawy, Crosslinked poly(vinyl alcohol) hydrogels for wound dressing applications: A review of remarkably blended polymers, Arabian Journal of Chemistry, 8 (2015) 1-14.
[209] Y. Jiang, J. Chen, C. Deng, E.J. Suuronen, Z. Zhong, Click hydrogels, microgels and nanogels: emerging platforms for drug delivery and tissue engineering, Biomaterials, 35 (2014) 4969-4985.
[210] D. Wallace, Collagen gel systems for sustained delivery and tissue engineering, Advanced Drug Delivery Reviews, 55 (2003) 1631-1649.

[211] P. Applications, Biomedical Applications of Blood Vessels, Blood Vessels, 22 (2003) 350-365.
[212] I. Ono, T. Tateshita, M. Inoue, Effects of a collagen matrix containing basic fibroblast growth factor on wound contraction, Journal of biomedical materials research, 48 (1999) 621-630.
[213] S. Chrissouli, H. Pratsinis, V. Velissariou, A. Anastasiou, D. Kletsas, Human amniotic fluid stimulates the proliferation of human fetal and adult skin fibroblasts: the roles of bFGF and PDGF and of the ERK and Akt signaling pathways, Wound repair and regeneration : official publication of the Wound Healing Society [and] the European Tissue Repair Society, 18 (2010) 643-654.
[214] S. Ortega, M. Ittmann, S.H. Tsang, M. Ehrlich, C. Basilico, Neuronal defects and delayed wound healing in mice lacking fibroblast growth factor 2, Proceedings of the National Academy of Sciences of the United States of America, 95 (1998) 5672-5677.
[215] P. Losi, E. Briganti, C. Errico, A. Lisella, E. Sanguinetti, F. Chiellini, G. Soldani, Fibrin-based scaffold incorporating VEGF- and bFGF-loaded nanoparticles stimulates wound healing in diabetic mice, Acta Biomater, 9 (2013) 7814-7821.
[216] H.X. Shi, C. Lin, B.B. Lin, Z.G. Wang, H.Y. Zhang, F.Z. Wu, Y. Cheng, L.J. Xiang, D.J. Guo, X. Luo, G.Y. Zhang, X.B. Fu, S. Bellusci, X.K. Li, J. Xiao, The anti-scar effects of basic fibroblast growth factor on the wound repair in vitro and in vivo, PloS one, 8 (2013) e59966.
[217] I. Ono, L.-J. Zhou, T. Tateshita, Effects of a collagen matrix containing prostaglandin E1 on wound contraction, Journal of Dermatological Science, 25 (2001) 106-115.
[218] K. Kawai, S. Suzuki, Y. Tabata, Y. Ikada, Y. Nishimura, Accelerated tissue regeneration through incorporation of basic fibroblast growth factor-impregnated gelatin microspheres into artificial dermis, Biomaterials, 21 (2000) 489-499.
[219] K.V. Harish Prashanth, R.N. Tharanathan, Chitin/chitosan: modifications and their unlimited application potential-an overview, Trends in Food Science and Technology, 18 (2007) 117-131.
[220] B.K. Park, M.M. Kim, Applications of chitin and its derivatives in biological medicine, International Journal of Molecular Sciences, 11 (2010) 5152-5164.
[221] M. Rinaudo, Chitin and chitosan: Properties and applications, Progress in Polymer Science (Oxford), 31 (2006) 603-632.
[222] L.L. Balassa, Use of chitin for promoting wound healing, (1972) 1-6.
[223] L.L. Balassa, Chitin and chitin derivatives for promoting wound healing, (1975) 2-5.
[224] O. Somorin, N. Nishi, S. Tokura, J. Noguchi, Studies on Chitin. II. Preparation of Benzyl and Benzoylchitins, Polym J, 11 (1979) 391-396.
[225] Y. Shigemasa, S. Minami, Applications of Chitin and Chitosan for Biomaterials, Biotechnology and Genetic Engineering Reviews, 13 (1996) 383-420.
[226] Y.W. Cho, Y.N. Cho, S.H. Chung, G. Yoo, S.W. Ko, Water-soluble chitin as a wound healing accelerator, Biomaterials, 20 (1999) 2139-2145.

[227] K. Ono, Y. Saito, H. Yura, K. Ishikawa, A. Kurita, T. Akaike, M. Ishihara, Photocrosslinkable chitosan as a biological adhesive, Journal of biomedical materials research, 49 (2000) 289-295.
[228] M. Ishihara, K. Nakanishi, K. Ono, M. Sato, M. Kikuchi, Y. Saito, H. Yura, T. Matsui, H. Hattori, M. Uenoyama, A. Kurita, Photocrosslinkable chitosan as a dressing for wound occlusion and accelerator in healing process, Biomaterials, 23 (2002) 833-840.
[229] O. Smidsrod, G. Skjak-Braek, Alginate as immobilization matrix for cells, Trends in biotechnology, 8 (1990) 71-78.
[230] J. Sun, H. Tan, Alginate-Based Biomaterials for Regenerative Medicine Applications, 2013.
[231] K.Y. Lee, D.J. Mooney, Alginate: properties and biomedical applications, Prog Polym Sci, 37 (2012) 106-126.
[232] P. Agulhon, M. Robitzer, J.-P. Habas, F. Quignard, Influence of both cation and alginate nature on the rheological behavior of transition metal alginate gels, Carbohydrate Polymers, 112 (2014) 525-531.
[233] G.T. Grant, E.R. Morris, D.A. Rees, P.J.C. Smith, D. Thom, Biological interactions between polysaccharides and divalent cations: The egg-box model, FEBS letters, 32 (1973) 195-198.
[234] A. Tellechea, E.A. Silva, J. Min, E.C. Leal, M.E. Auster, L. Pradhan-Nabzdyk, W. Shih, D.J. Mooney, A. Veves, Alginate and DNA Gels Are Suitable Delivery Systems for Diabetic Wound Healing, The international journal of lower extremity wounds, 14 (2015) 146-153.
[235] J.I. Dawson, J.M. Kanczler, X.B. Yang, G.S. Attard, R.O. Oreffo, Clay gels for the delivery of regenerative microenvironments, Advanced materials, 23 (2011) 3304-3308.
[236] S.C. Lee, I.K. Kwon, K. Park, Hydrogels for Delivery of Bioactive Agents: A Historical Perspective, Advanced drug delivery reviews, 65 (2013) 17-20.
[237] P. Ince, F.L. Game, W.J. Jeffcoate, Rate of Healing of Neuropathic Ulcers of the Foot in Diabetes and Its Relationship to Ulcer Duration and Ulcer Area, Diabetes care, 30 (2007) 660-663.
[238] Q. Liu, Y.C. Huang, Y. Lan, Q.H. Zuo, C.H. Li, Y. Zhang, R. Guo, W. Xue, Acceleration of skin regeneration in full-thickness burns by incorporation of bFGF-loaded alginate microspheres into a CMCS-PVA hydrogel, Journal of Tissue Engineering and Regenerative Medicine, 11 (2017) 1562-1573.
[239] A. Kumar, M. Jaiswal, Design and in vitro investigation of nanocomposite hydrogel based in situ spray dressing for chronic wounds and synthesis of silver nanoparticles using green chemistry, Journal of Applied Polymer Science, 133 (2016).
[240] N. Golafshan, R. Rezahasani, M. Tarkesh Esfahani, M. Kharaziha, S.N. Khorasani, Nanohybrid hydrogels of laponite: PVA-Alginate as a potential wound healing material, Carbohydrate Polymers, 176 (2017) 392-401.
[241] M. Ul-Islam, T. Khan, W.A. Khattak, J.K. Park, Bacterial cellulose-MMTs nanoreinforced composite films: novel wound dressing material with antibacterial properties, Cellulose, 20 (2012) 589-596.

[242] G.M. Dario, G.G. da Silva, D.L. Goncalves, P. Silveira, A.T. Junior, E. Angioletto, A.M. Bernardin, Evaluation of the healing activity of therapeutic clay in rat skin wounds, Mater Sci Eng C Mater Biol Appl, 43 (2014) 109-116.
[243] C. Aguzzi, G. Sandri, C. Bonferoni, P. Cerezo, S. Rossi, F. Ferrari, C. Caramella, C. Viseras, Solid state characterisation of silver sulfadiazine loaded on montmorillonite/chitosan nanocomposite for wound healing, Colloids and Surfaces B: Biointerfaces, 113 (2014) 152-157.
[244] B.A. Instruments, Laponite: Technical Information B-RI 21, 2014.
[245] B. Ruzicka, E. Zaccarelli, A fresh look at the Laponite phase diagram, Soft Matter, 7 (2011) 1268-1286.
[246] S. Wang, Y. Wu, R. Guo, Y. Huang, S. Wen, M. Shen, J. Wang, X. Shi, Laponite nanodisks as an efficient platform for Doxorubicin delivery to cancer cells, Langmuir, 29 (2013) 5030-5036.
[247] S. Xiao, R. Castro, D. Maciel, M. Goncalves, X. Shi, J. Rodrigues, H. Tomas, Fine tuning of the pH-sensitivity of laponite-doxorubicin nanohybrids by polyelectrolyte multilayer coating, Mater Sci Eng C Mater Biol Appl, 60 (2016) 348-356.
[248] M. Goncalves, P. Figueira, D. Maciel, J. Rodrigues, X. Qu, C. Liu, H. Tomas, Y. Li, pH-sensitive Laponite((R))/doxorubicin/alginate nanohybrids with improved anticancer efficacy, Acta Biomater, 10 (2014) 300-307.
[249] M. Ghadiri, W. Chrzanowski, W.H. Lee, R. Rohanizadeh, Layered silicate clay functionalized with amino acids: wound healing application, Rsc Adv, 4 (2014) 35332.
[250] R.H. Demling, Nutrition, Anabolism, and the Wound Healing Process: An Overview, Eplasty, 9 (2009) e9.
[251] M. Ghadiri, W. Chrzanowski, R. Rohanizadeh, Antibiotic eluting clay mineral (Laponite) for wound healing application: an in vitro study, Journal of materials science. Materials in medicine, (2014).
[252] E.A. Jaffe, R.L. Nachman, C.G. Becker, C.R. Minick, Culture of human endothelial cells derived from umbilical veins. Identification by morphologic and immunologic criteria, The Journal of clinical investigation, 52 (1973) 2745-2756.
[253] NCBI, 6-Bromoindirubin-3-oxime (BIO) Compound Summary (CID=91895618), National Center for Biotechnology Information, PubChem Compound Database; https://pubchem.ncbi.nlm.nih.gov/compound/91895618 (accessed May 15, 2018).
[254] A.-S. Tseng, F.B. Engel, Mark T. Keating, The GSK-3 Inhibitor BIO Promotes Proliferation in Mammalian Cardiomyocytes, Chemistry & Biology, 13 (2006) 957-963.
[255] N.C.f.B.I.N. a, 6-bromoindirubin-3'-oxime PubChem Compound Summary, 2014.
[256] H.W. Chalkley, J. Cornfield, H. Park, A Method for Estimating Volume-Surface Ratios, Science, 110 (1949) 295-297.
[257] S. Hansen, D.A. Grabau, F.B. Sørensen, M. Bak, W. Vach, C. Rose, The Prognostic Value of Angiogenesis by Chalkley Counting in a Confirmatory Study Design on 836 Breast Cancer Patients, Clinical Cancer Research, 6 (2000) 139-146.
[258] P.B. Vermeulen, G. Gasparini, S.B. Fox, C. Colpaert, L.P. Marson, M. Gion, J.A.M. Beliën, R.M.W. de Waal, E. Van Marck, E. Magnani, N. Weidner, A.L. Harris,

L.Y. Dirix, Second international consensus on the methodology and criteria of evaluation of angiogenesis quantification in solid human tumours, European Journal of Cancer, 38 (2002) 1564-1579.
[259] Y. Karslıoğlu, N. Yiğit, Ö. Öngürü, Chalkley method in the angiogenesis research and its automation via computer simulation, Pathology - Research and Practice, 210 (2014) 161-168.
[260] T.R. Hoare, D.S. Kohane, Hydrogels in drug delivery: Progress and challenges, Polymer, 49 (2008) 1993-2007.
[261] M. Gou, X. Li, M. Dai, C. Gong, X. Wang, Y. Xie, H. Deng, L. Chen, X. Zhao, Z. Qian, Y. Wei, A novel injectable local hydrophobic drug delivery system: Biodegradable nanoparticles in thermo-sensitive hydrogel, International Journal of Pharmaceutics, 359 (2008) 228-233.
[262] N.K. Singh, D.S. Lee, In situ gelling pH- and temperature-sensitive biodegradable block copolymer hydrogels for drug delivery, Journal of Controlled Release, 193 (2014) 214-227.
[263] R.C. Fang, R.D. Galiano, A review of becaplermin gel in the treatment of diabetic neuropathic foot ulcers, Biologics : targets & therapy, 2 (2008) 1-12.
[264] L.I. Moura, A.M. Dias, E. Carvalho, H.C. de Sousa, Recent advances on the development of wound dressings for diabetic foot ulcer treatment--a review, Acta Biomater, 9 (2013) 7093-7114.
[265] M.I. Carretero, M. Pozo, Clay and non-clay minerals in the pharmaceutical industry, Appl Clay Sci, 46 (2009) 73-80.
[266] C. Fathke, L. Wilson, K. Shah, B. Kim, A. Hocking, R. Moon, F. Isik, Wnt signaling induces epithelial differentiation during cutaneous wound healing, BMC cell biology, 7 (2006) 4.
[267] J.E. Mealy, C.B. Rodell, J.A. Burdick, Sustained Small Molecule Delivery from Injectable Hyaluronic Acid Hydrogels through Host-Guest Mediated Retention, Journal of materials chemistry. B, Materials for biology and medicine, 3 (2015) 8010-8019.
[268] Q. Zhang, M.B. Major, S. Takanashi, N.D. Camp, N. Nishiya, E.C. Peters, M.H. Ginsberg, X. Jian, P.A. Randazzo, P.G. Schultz, R.T. Moon, S. Ding, Small-molecule synergist of the Wnt/beta-catenin signaling pathway, Proceedings of the National Academy of Sciences of the United States of America, 104 (2007) 7444-7448.
[269] D.L. Steed, D. Donohoe, M.W. Webster, L. Lindsley, Effect of extensive debridement and treatment on the healing of diabetic foot ulcers. Diabetic Ulcer Study Group, Journal of the American College of Surgeons, 183 (1996) 61-64.
[270] A. Buxboim, K. Rajagopal, A.E. Brown, D.E. Discher, How deeply cells feel: methods for thin gels, J Phys Condens Matter, 22 (2010) 194116.
[271] J. Kleinheinz, K. Jung S Fau - Wermker, C. Wermker K Fau - Fischer, U. Fischer C Fau - Joos, U. Joos, Release kinetics of VEGF165 from a collagen matrix and structural matrix changes in a circulation model, (2010).
[272] K. Vougogiannopoulou, Y. Ferandin, K. Bettayeb, V. Myrianthopoulos, O. Lozach, Y. Fan, C.H. Johnson, P. Magiatis, A.-L. Skaltsounis, E. Mikros, L. Meijer, Soluble 3′, 6-substituted indirubins with enhanced selectivity towards glycogen

synthase kinase -3 alter circadian period, Journal of medicinal chemistry, 51 (2008) 6421-6431.
[273] F.M. Chen, M. Zhang, Z.F. Wu, Toward delivery of multiple growth factors in tissue engineering, Biomaterials, 31 (2010) 6279-6308.
[274] A.R. Patel, K. Dewettinck, Comparative evaluation of structured oil systems: Shellac oleogel, HPMC oleogel, and HIPE gel, European Journal of Lipid Science and Technology, 117 (2015) 1772-1781.
[275] C. Wang, F. Zhu, Y. Cui, H. Ren, Y. Xie, A. Li, L. Ji, X. Qu, D. Qiu, Z. Yang, An easy-to-use wound dressing gelatin-bioactive nanoparticle gel and its preliminary in vivo study, Journal of Materials Science: Materials in Medicine, 28 (2016) 10.
[276] N.Q. Tran, Y.K. Joung, E. Lih, K.D. Park, In situ forming and rutin-releasing chitosan hydrogels as injectable dressings for dermal wound healing, Biomacromolecules, 12 (2011) 2872-2880.
[277] H.H. Tonnesen, J. Karlsen, Alginate in drug delivery systems, Drug Dev Ind Pharm, 28 (2002) 621-630.
[278] L. Chen, R. Mirza, Y. Kwon, L.A. DiPietro, T.J. Koh, The murine excisional wound model: Contraction revisited, Wound repair and regeneration : official publication of the Wound Healing Society [and] the European Tissue Repair Society, 23 (2015) 874-877.
[279] M. Ghadiri, W. Chrzanowski, R. Rohanizadeh, Biomedical applications of cationic clay minerals, Rsc Adv, 5 (2015) 29467-29481.
[280] E.J. Carragee, E.L. Hurwitz, B.K. Weiner, A critical review of recombinant human bone morphogenetic protein-2 trials in spinal surgery: emerging safety concerns and lessons learned, Spine J, 11 (2011) 471-491.
[281] S. Barrientos, H. Brem, O. Stojadinovic, M. Tomic-Canic, Clinical application of growth factors and cytokines in wound healing, Wound repair and regeneration : official publication of the Wound Healing Society [and] the European Tissue Repair Society, 22 (2014) 569-578.
[282] S. Dhall, João P. Silva, Y. Liu, M. Hrynyk, M. Garcia, A. Chan, J. Lyubovitsky, Ronald J. Neufeld, M. Martins-Green, Release of insulin from PLGA–alginate dressing stimulates regenerative healing of burn wounds in rats, Clinical science, 129 (2015) 1115-1129.
[283] K.Y. Lee, M.C. Peters, D.J. Mooney, Comparison of vascular endothelial growth factor and basic fibroblast growth factor on angiogenesis in SCID mice, Journal of Controlled Release, 87 (2003) 49-56.
[284] A.U.C. Ferreira, A.L. Poli, F. Gessner, M.G. Neumann, C.C.S. Cavalheiro, Interaction of Auramine O with montmorillonite clays, J Lumin, 136 (2013) 63-67.
[285] G. Oster, Y. Nishijima, Fluorescence and Internal Rotation: Their Dependence on Viscosity of the Medium1, Journal of the American Chemical Society, 78 (1956) 1581-1584.
[286] S.A. Park, J. Covert, L. Teixeira, M.J. Motta, S.L. DeRemer, N.L. Abbott, R. Dubielzig, M. Schurr, R.R. Isseroff, J.F. McAnulty, C.J. Murphy, Importance of defining experimental conditions in a mouse excisional wound model, Wound repair and

regeneration : official publication of the Wound Healing Society [and] the European Tissue Repair Society, 23 (2015) 251-261.
[287] D.M. Ansell, L. Campbell, H.A. Thomason, A. Brass, M.J. Hardman, A statistical analysis of murine incisional and excisional acute wound models, Wound repair and regeneration : official publication of the Wound Healing Society [and] the European Tissue Repair Society, 22 (2014) 281-287.
[288] W.M.S. Russell, R.L. Burch, The principles of humane experimental technique, Methuen, London,, 1959.
[289] G. Demers, G. Griffin, G. De Vroey, J.R. Haywood, J. Zurlo, M. Bedard, Harmonization of animal care and use guidance, Science, 312 (2006) 700-701.
[290] B.G. Han, C.M. Hao, E.E. Tchekneva, Y.Y. Wang, C.A. Lee, B. Ebrahim, R.C. Harris, T.S. Kern, D.H. Wasserman, M.D. Breyer, Z. Qi, Markers of glycemic control in the mouse: comparisons of 6-h- and overnight-fasted blood glucoses to Hb A1c, American journal of physiology. Endocrinology and metabolism, 295 (2008) E981-986.
[291] A. Nauta, C. Seidel, L. Deveza, D. Montoro, M. Grova, S.H. Ko, J. Hyun, G.C. Gurtner, M.T. Longaker, F. Yang, Adipose-derived stromal cells overexpressing vascular endothelial growth factor accelerate mouse excisional wound healing, Mol Ther, 21 (2013) 445-455.
[292] X.C. Ding, J. Gao, Z.G. Wang, H. Awada, Y.D. Wang, A shear-thinning hydrogel that extends in vivo bioactivity of FGF2, Biomaterials, 111 (2016) 80-89.
[293] S. Wohl-Bruhn, M. Badar, A. Bertz, B. Tiersch, J. Koetz, H. Menzel, P.P. Mueller, H. Bunjes, Comparison of in vitro and in vivo protein release from hydrogel systems, J Control Release, 162 (2012) 127-133.
[294] N. Artzi, N. Oliva, C. Puron, S. Shitreet, S. Artzi, A.B. Ramos, A. Groothuis, G. Sahagian, E.R. Edelman, In vivo and in vitro tracking of erosion in biodegradable materials using non-invasive fluorescence imaging (vol 10, pg 704, 2011), Nature Materials, 10 (2011) 896-896.
[295] A.J.F. King, The use of animal models in diabetes research, British Journal of Pharmacology, 166 (2012) 877-894.
[296] J.t. Michaels, S.S. Churgin, K.M. Blechman, M.R. Greives, S. Aarabi, R.D. Galiano, G.C. Gurtner, db/db mice exhibit severe wound-healing impairments compared with other murine diabetic strains in a silicone-splinted excisional wound model, Wound repair and regeneration : official publication of the Wound Healing Society [and] the European Tissue Repair Society, 15 (2007) 665-670.
[297] S.R. Sullivan, R.A. Underwood, N.S. Gibran, R.O. Sigle, M.L. Usui, W.G. Carter, J.E. Olerud, Validation of a model for the study of multiple wounds in the diabetic mouse (db/db), Plastic and reconstructive surgery, 113 (2004) 953-960.
[298] H. Chen, O. Charlat, L.A. Tartaglia, E.A. Woolf, X. Weng, S.J. Ellis, N.D. Lakey, J. Culpepper, K.J. More, R.E. Breitbart, G.M. Duyk, R.I. Tepper, J.P. Morgenstern, Evidence That the Diabetes Gene Encodes the Leptin Receptor: Identification of a Mutation in the Leptin Receptor Gene in db/db Mice, Cell, 84 (1996) 491-495.

[299] M.D. Klok, S. Jakobsdottir, M.L. Drent, The role of leptin and ghrelin in the regulation of food intake and body weight in humans: a review, Obesity Reviews, 8 (2007) 21-34.
[300] K. Kobayashi, T.M. Forte, S. Taniguchi, B.Y. Ishida, K. Oka, L. Chan, The db/db mouse, a model for diabetic dyslipidemia: Molecular characterization and effects of western diet feeding, Metabolism, 49 (2000) 22-31.
[301] D.A. Fontaine, D.B. Davis, Attention to Background Strain Is Essential for Metabolic Research: C57BL/6 and the International Knockout Mouse Consortium, Diabetes, 65 (2016) 25-33.
[302] J.E. Ayala, V.T. Samuel, G.J. Morton, S. Obici, C.M. Croniger, G.I. Shulman, D.H. Wasserman, O.P. McGuinness, Standard operating procedures for describing and performing metabolic tests of glucose homeostasis in mice, Disease Models & Mechanisms, 3 (2010) 525-534.
[303] S.A. Park, L.B. Teixeira, V.K. Raghunathan, J. Covert, R.R. Dubielzig, R.R. Isseroff, M. Schurr, N.L. Abbott, J. McAnulty, C.J. Murphy, Full-thickness splinted skin wound healing models in db/db and heterozygous mice: implications for wound healing impairment, Wound repair and regeneration : official publication of the Wound Healing Society [and] the European Tissue Repair Society, 22 (2014) 368-380.
[304] M. Martson, J. Viljanto, P. Laippala, P. Saukko, Cranio-caudal differences in granulation tissue formation: an experimental study in the rat, Wound repair and regeneration : official publication of the Wound Healing Society [and] the European Tissue Repair Society, 7 (1999) 119-126.
[305] N. Alizadeh, M.S. Pepper, A. Modarressi, K. Alfo, K. Schlaudraff, D. Montandon, G. Gabbiani, M.-L. Bochaton-Piallat, B. Pittet, Persistent ischemia impairs myofibroblast development in wound granulation tissue: A new model of delayed wound healing, Wound Repair and Regeneration, 15 (2007) 809-816.
[306] I.A. Darby, B. Laverdet, F. Bonté, A. Desmoulière, Fibroblasts and myofibroblasts in wound healing, Clinical, Cosmetic and Investigational Dermatology, 7 (2014) 301-311.
[307] G. Zhao, P.C. Hochwalt, M.L. Usui, R.A. Underwood, P.K. Singh, G.A. James, P.S. Stewart, P. Fleckman, J.E. Olerud, Delayed Wound Healing in Diabetic (db/db) Mice with Pseudomonas aeruginosa Biofilm Challenge – A Model for the Study of Chronic Wounds, Wound repair and regeneration : official publication of the Wound Healing Society [and] the European Tissue Repair Society, 18 (2010) 467-477.
[308] R. Zhao, H. Liang, E. Clarke, C. Jackson, M. Xue, Inflammation in Chronic Wounds, International Journal of Molecular Sciences, 17 (2016) 2085.
[309] Y. Liu, D. Min, T. Bolton, V. Nubé, S.M. Twigg, D.K. Yue, S.V. McLennan, Increased Matrix Metalloproteinase-9 Predicts Poor Wound Healing in Diabetic Foot Ulcers, Diabetes care, 32 (2009) 117-119.
[310] J.C. McDaniel, S. Roy, T.A. Wilgus, Neutrophil activity in chronic venous leg ulcers—A target for therapy?, Wound repair and regeneration : official publication of the Wound Healing Society [and] the European Tissue Repair Society, 21 (2013) 339-351.

[311] J.M.Y. Shah, E. Omar, D.R. Pai, S. Sood, Cellular events and biomarkers of wound healing, Indian Journal of Plastic Surgery : Official Publication of the Association of Plastic Surgeons of India, 45 (2012) 220-228.
[312] S. Muller-Rover, B. Handjiski, C. van der Veen, S. Eichmuller, K. Foitzik, I.A. McKay, K.S. Stenn, R. Paus, A comprehensive guide for the accurate classification of murine hair follicles in distinct hair cycle stages, The Journal of investigative dermatology, 117 (2001) 3-15.
[313] L. Alonso, E. Fuchs, The hair cycle, Journal of cell science, 119 (2006) 391-393.
[314] K. Datta, A.T. Singh, A. Mukherjee, B. Bhat, B. Ramesh, A.C. Burman, Eclipta alba extract with potential for hair growth promoting activity, J Ethnopharmacol, 124 (2009) 450-456.
[315] V. Todorović, P. Peško, M. Micev, M. Bjelović, M. Budeč, M. Mićić, D. Brašanac, O. Ilić-Stojanović, Insulin-like growth factor-I in wound healing of rat skin, Regulatory peptides, 150 (2008) 7-13.
[316] P.K. Bos, G.J.V.M. van Osch, D.A. Frenz, J.A.N. Verhaar, H.L. Verwoerd-Verhoef, Growth factor expression in cartilage wound healing: temporal and spatial immunolocalization in a rabbit auricular cartilage wound model, Osteoarthritis and Cartilage, 9 (2001) 382-389.
[317] M.P. Philpott, D.A. Sanders, T. Kealey, Effects of Insulin and Insulin-Like Growth Factors on Cultured Human Hair Follicles: IGF-I at Physiologic Concentrations Is an Important Regulator of Hair Follicle Growth In Vitro, Journal of Investigative Dermatology, 102 (1994) 857-861.
[318] L. Tang, O. Bernardo, C. Bolduc, H. Lui, S. Madani, J. Shapiro, The expression of insulin-like growth factor 1 in follicular dermal papillae correlates with therapeutic efficacy of finasteride in androgenetic alopecia, Journal of the American Academy of Dermatology, 49 (2003) 229-233.
[319] S.Y. Ahn, L.Q. Pi, S.T. Hwang, W.S. Lee, Effect of IGF-I on Hair Growth Is Related to the Anti-Apoptotic Effect of IGF-I and Up-Regulation of PDGF-A and PDGF-B, Ann Dermatol, 24 (2012) 26-31.
[320] G.C. Keustermans, S.B. Hoeks, J.M. Meerding, B.J. Prakken, W. de Jager, Cytokine assays: an assessment of the preparation and treatment of blood and tissue samples, Methods, 61 (2013) 10-17.
[321] N. Gupta, S. Mansoor, A. Sharma, A. Sapkal, J. Sheth, P. Falatoonzadeh, B. Kuppermann, M. Kenney, Diabetic retinopathy and VEGF, Open Ophthalmol J, 7 (2013) 4-10.
[322] K. Gupta, J. Zhang, Angiogenesis: a curse or cure?, Postgraduate Medical Journal, 81 (2005) 236-242.
[323] A.A. Farooqi, Z.H. Siddik, Platelet-derived growth factor (PDGF) signalling in cancer: rapidly emerging signalling landscape, Cell biochemistry and function, 33 (2015) 257-265.
[324] D. Papanas, E. Maltezos, Benefit-Risk Assessment of Becaplermin in the Treatment of Diabetic Foot Ulcers, Drug Safety, 33 (2010) 455-461.

[325] J.N. Clore, I.K. Cohen, R.F. Diegelmann, Quantitation of collagen types I and III during wound healing in rat skin, Proceedings of the Society for Experimental Biology and Medicine. Society for Experimental Biology and Medicine (New York, N.Y.), 161 (1979) 337-340.
[326] L. Cuttle, M. Nataatmadja, J.F. Fraser, M. Kempf, R.M. Kimble, M.T. Hayes, Collagen in the scarless fetal skin wound: detection with picrosirius-polarization, Wound repair and regeneration : official publication of the Wound Healing Society [and] the European Tissue Repair Society, 13 (2005) 198-204.
[327] A. Andreoli, M.-T. Ruf, G.E. Sopoh, P. Schmid, G. Pluschke, Immunohistochemical Monitoring of Wound Healing in Antibiotic Treated Buruli Ulcer Patients, PLOS Neglected Tropical Diseases, 8 (2014) e2809.
[328] F.G. Rocha, C.A. Sundback, N.J. Krebs, J.K. Leach, D.J. Mooney, S.W. Ashley, J.P. Vacanti, E.E. Whang, The effect of sustained delivery of vascular endothelial growth factor on angiogenesis in tissue-engineered intestine, Biomaterials, 29 (2008) 2884-2890.
[329] N.N. Nissen, P.J. Polverini, A.E. Koch, M.V. Volin, R.L. Gamelli, L.A. DiPietro, Vascular endothelial growth factor mediates angiogenic activity during the proliferative phase of wound healing, The American journal of pathology, 152 (1998) 1445-1452.
[330] J. Kishimoto, R. Ehama, Y. Ge, T. Kobayashi, T. Nishiyama, M. Detmar, R.E. Burgeson, In Vivo Detection of Human Vascular Endothelial Growth Factor Promoter Activity in Transgenic Mouse Skin, The American journal of pathology, 157 (2000) 103-110.
[331] M. Jafarbeglou, M. Abdouss, A.M. Shoushtari, M. Jafarbeglou, Clay nanocomposites as engineered drug delivery systems, RSC Adv., 6 (2016) 50002-50016.
[332] E.L. Snyder, B.C. Calhoun, Topical platelet growth factor therapy: of lotions and potions, Transfusion, 41 (2001) 1186-1189.
[333] A.L. Laiva, F.J. O'Brien, M.B. Keogh, Innovations in gene and growth factor delivery systems for diabetic wound healing, Journal of Tissue Engineering and Regenerative Medicine, (2017) n/a-n/a.
[334] K.A. Whitehead, J. Matthews, P.H. Chang, F. Niroui, J.R. Dorkin, M. Severgnini, D.G. Anderson, In vitro-in vivo translation of lipid nanoparticles for hepatocellular siRNA delivery, ACS Nano, 6 (2012) 6922-6929.
[335] D. Bonn, H. Kellay, H. Tanaka, G. Wegdam, J. Meunier, Laponite: What is the difference between a gel and a glass?, Langmuir, 15 (1999) 7534-7536.
[336] C. Aguzzi, P. Cerezo, C. Viseras, C. Caramella, Use of clays as drug delivery systems: Possibilities and limitations, Appl Clay Sci, 36 (2007) 22-36.
[337] B.S. Kheirabadi, J.E. Mace, I.B. Terrazas, C.G. Fedyk, J.S. Estep, M.A. Dubick, L.H. Blackbourne, Safety evaluation of new hemostatic agents, smectite granules, and kaolin-coated gauze in a vascular injury wound model in swine, The Journal of trauma, 68 (2010) 269-278.
[338] Y.J. Zhang, B. Gao, X.W. Liu, Topical and effective hemostatic medicines in the battlefield, International journal of clinical and experimental medicine, 8 (2015) 10-19.

[339] A. Thomas, K.G. Harding, K. Moore, Alginates from wound dressings activate human macrophages to secrete tumour necrosis factor-alpha, Biomaterials, 21 (2000) 1797-1802.
[340] J.G. Powers, L.M. Morton, T.J. Phillips, Dressings for chronic wounds, Dermatologic therapy, 26 (2013) 197-206.
[341] J.C. Dumville, R.J. Hinchliffe, N. Cullum, F. Game, N. Stubbs, M. Sweeting, F. Peinemann, Negative pressure wound therapy for treating foot wounds in people with diabetes mellitus, The Cochrane database of systematic reviews, (2013) Cd010318.
[342] M. Pasparakis, I. Haase, F.O. Nestle, Mechanisms regulating skin immunity and inflammation, Nat Rev Immunol, 14 (2014) 289-301.
[343] K. Wojciechowicz, K. Gledhill, C.A. Ambler, C.B. Manning, C.A. Jahoda, Development of the mouse dermal adipose layer occurs independently of subcutaneous adipose tissue and is marked by restricted early expression of FABP4, PloS one, 8 (2013) e59811.
[344] J.M. Davidson, F. Yu, S.R. Opalenik, Splinting Strategies to Overcome Confounding Wound Contraction in Experimental Animal Models, Advances in Wound Care, 2 (2013) 142-148.
[345] V. Moulin, F.A. Auger, D. Garrel, L. Germain, Role of wound healing myofibroblasts on re-epithelialization of human skin, Burns, 26 (2000) 3-12.
[346] R.D. Galiano, J.t. Michaels, M. Dobryansky, J.P. Levine, G.C. Gurtner, Quantitative and reproducible murine model of excisional wound healing, Wound repair and regeneration : official publication of the Wound Healing Society [and] the European Tissue Repair Society, 12 (2004) 485-492.
[347] J.J. Mendes, C.I. Leandro, D.P. Bonaparte, A.L. Pinto, A Rat Model of Diabetic Wound Infection for the Evaluation of Topical Antimicrobial Therapies, Comparative Medicine, 62 (2012) 37-48.
[348] T. Dalton, S.E. Dowd, R.D. Wolcott, Y. Sun, C. Watters, J.A. Griswold, K.P. Rumbaugh, An In Vivo Polymicrobial Biofilm Wound Infection Model to Study Interspecies Interactions, PloS one, 6 (2011) e27317.
[349] A. Abdullahi, S. Amini-Nik, M.G. Jeschke, Animal Models in Burn Research, Cellular and molecular life sciences : CMLS, 71 (2014) 3241-3255.
[350] R. Nunan, K.G. Harding, P. Martin, Clinical challenges of chronic wounds: searching for an optimal animal model to recapitulate their complexity, Disease Models & Mechanisms, 7 (2014) 1205-1213.
[351] B. Behm, P. Babilas, M. Landthaler, S. Schreml, Cytokines, chemokines and growth factors in wound healing, Journal of the European Academy of Dermatology and Venereology, 26 (2012) 812-820.
[352] H.R. Gatla, B. Singha, V. Persaud, I. Vancurova, Evaluating cytoplasmic and nuclear levels of inflammatory cytokines in cancer cells by western blotting, Methods in molecular biology (Clifton, N.J.), 1172 (2014) 271-283.
[353] A. Dawn, T. Shiraki, H. Ichikawa, A. Takada, Y. Takahashi, Y. Tsuchiya, L.T.N. Lien, S. Shinkai, Stereochemistry-Dependent, Mechanoresponsive Supramolecular Host

Assemblies for Fullerenes: A Guest-Induced Enhancement of Thixotropy, Journal of the American Chemical Society, 134 (2012) 2161-2171.
[354] Y. Ohsedo, M. Oono, K. Saruhashi, H. Watanabe, N. Miyamoto, A new composite thixotropic hydrogel composed of a low-molecular-weight hydrogelator and a nanosheet, Rsc Adv, 4 (2014) 44837-44840.
[355] O.S. Toker, S. Karasu, M.T. Yilmaz, S. Karaman, Three interval thixotropy test (3ITT) in food applications: A novel technique to determine structural regeneration of mayonnaise under different shear conditions, Food Research International, 70 (2015) 125-133.